

THE UNIVERSITY OF HULL

Deposit of thesis in the University Library

Name: Mustafa Alyassiry

Department / Programme: Chemistry / PhD

Degree: PhD

I do hereby give consent that appropriate copies of my thesis

**Synthesis of components to form linked multi-metal constructs: potential MRI/optical contrast agents.** (title)

if accepted for the degree of PhD (e.g. PhD, MPhil) in the University of Hull and thereafter deposited in the University Library and the University's digital repository will be made available for University and public access as follows:

1. the paper copy shall be available for consultation, interlibrary loan and photocopying;
2. the electronic copy shall be made available for access by any person or institution via the world wide web. Please provide a copy of the final, examined version, on CD-Rom.

I do not require my thesis to be withheld from general access

Signature: \_\_\_\_\_



Date: 09/12/2015

-----  
If in special circumstances, the author wishes to withhold this consent for *a period of not more than five years* from the date of the degree being awarded, and if for similar reasons he or she does not wish details of the thesis to be presented via the University Library's catalogues or repository or forwarded to any indexing or abstracting organisation, he or she should complete and **sign sections (1) and/or (2)** below, as appropriate.

(1) I wish access to my thesis to be withheld until \_\_\_\_\_ for the following reason \_\_\_\_\_

Signature: \_\_\_\_\_ Date: \_\_\_\_\_

(2) I further wish that full details of the title and subject of my thesis are not to be presented via the University Library's catalogue or repository or forwarded to any indexing or abstracting organisation until \_\_\_\_\_ for the following reason \_\_\_\_\_

Signature: \_\_\_\_\_ Date: \_\_\_\_\_

PROPER PROCESSING OF THE THESIS FOR ITS LONG-TERM MANAGEMENT CANNOT TAKE PLACE UNTIL THIS FORM HAS BEEN COMPLETED AND RETURNED. IF NO FORM IS RETURNED TO THE GRADUATE SCHOOL WITHIN 2 MONTHS OF SUBMITTING THE THESIS, IT WILL BE ASSUMED THAT THE AUTHOR CONSENTS TO THE THESIS BEING MADE AVAILABLE

THE UNIVERSITY OF HULL

**Synthesis of components to form linked multi-metal constructs:  
potential MRI/optical contrast agents**

Being a thesis submitted for the degree of  
Doctor of Philosophy in the University of Hull

by

Mustafa M.A. Al-Yassiry B.Sc. M.Sc.

December 2015

## Abstract

Azamacrocyclic chelators with coordinating pendant arms can form complexes with lanthanide(III) ions offering a high level of kinetic and thermodynamic stability. There are many potentially useful applications of these complexes in areas such as magnetic resonance imaging (MRI) contrast agents, or luminescent imaging agents dependent on the incorporated metal centre (possible examples include gadolinium(III), europium(III) or terbium(III)).

The synthesis and characterisation of multi-metallic metal complexes as potential imaging agents have been carried out. A series of novel chelators designed to coordinate lanthanide ions ( $Gd^{3+}$ ,  $Eu^{3+}$ ,  $Tb^{3+}$ ,  $Y^{3+}$ ) based on the known DO3A chelator have been synthesised bearing various heterocyclic pendent arms (pyridine, pyrazine, pyrimidine), which can act as chromophore groups or as linking units to form multi-metallic species. NMR and potentiometric titrations of the ligands and the lanthanide complexes have been investigated to determine the protonation states across a pH range. The relaxometric properties have been studied for gadolinium(III) complexes of the synthesised chelators showing high relaxivity rates for both  $T_1$  (up to  $51.8 \text{ mM}^{-1} \text{ s}^{-1}$ ) and  $T_2$  (up to  $21.6 \text{ mM}^{-1} \text{ s}^{-1}$ ).

## **Risk Assessment**

All experiments were carried out in accordance with the University of Hull's Health and Safety guidelines. A full COSHH and risk assessment was carried out for each new experiment, signed by the undertaking student, supervisor (Prof S.J. Archibald) and the departmental safety officer (Dr T. McCreedy) before any practical work started. The COSHH forms carry the reference numbers M.A1-M.A28.

## **Acknowledgements**

First of all I would like to thank my God for His mercies and blessings, thank you for opening the door when I least expected it and for helping me along the way. Glory is to your name for all that you have done in my life and thanks to your prophet Mohammad (Peace Be Upon Him and his family) for showing us the way to that light.

I would like to thank my dear wife (Farah Aloraibi) for her patience, support, and encouragement, from the first day of our meeting up to the present day, without you none of this would have been achieved, and thanks a lot for my awosom sons Ahmad, Alhorr, Kaseem and my beautiful duoghter Mishkat for always supporting me throughout my years.

Many thanks to my supervisor, Professor Stephen J. Archibald and Dr. Benjamin P. Burke for their advice, discussions, encouragement, patience, and enthusiasm throughout my PhD studies.

I would like also to thank all the friends that I have made and everyone who helped me in the lab, in no particular order: Shubhanshi (best friend), Ali, Boon-Uma, Bassim, Neazar, Hayley, Seraj, Beckie, Zainab, Juozas, Rhiannon and Alicja.

Finally and most importantly I would like to thank my parents and my family in Iraq. For supporting me not only by their blessing and prayers for me throughout my PhD but for all the different types of support that they have given me and the ever present encouragement over all the years of my life. You are very much appreciated.

## **Declaration**

Except where specific reference is made to other sources, the work presented in this thesis is the work of the author. It has not been submitted, whole or part, for any other degree.

Mustafa M.A. Al-Yassiry

## Abbreviations

AIBN	Azobisisobutyronitrile
3D	Three dimensional
$\tau$	Emission lifetime
$\tau_m$	Residency time (inner sphere)
$\tau_m'$	Residency time (outer sphere)
$\tau_R$	Tumbling correlation rate
$B_0$	Magnetic field direction
Bipy	2, 2'-Bipyridine
BFC	Bifunctional chelator
BODIPY	Boron dipyrromethene
CT	Computed tomography
DCM	Dichloromethane
DMA	Dimethylacetamide
$K_{ML}$	Stability constant
TACN	1,4,7-triazacyclononane
DOPA	3,4-Dihydroxyphenylalanine
DOTA	1,4,7,10-Tetraazacyclododecane-1,4,7,10-tetraacetic acid
DOTP	1,4,7,10-Tetraazacyclododecane-1,4,7,10 tetra(methylenephosphonic acid)
DO3A	1,4,7-Tris( <i>tert</i> -butoxycarbonylmethyl)-1,4,7,10-tetraazacyclododecane
DTPA	Diethylene triamine pentaacetic acid
EDTA	Ethylenediamine tetraacetic acid
ESI	Electrospray ionization
HPLC	High performance liquid chromatography
HRMS	High resolution mass spectrometry
ICP	Inductively coupled plasma
ICP-OES	Inductively coupled plasma optical emission spectroscopy
JT	Jahn-Teller
MALDI	Matrix-assisted laser desorption/ionisation
MRI	Magnetic resonance imaging
MS	Mass spectrometry

M <sub>0</sub>	Net Magnetization
MLCT	Metal ligand charge transfer
LMCT	Ligand metal charge transfer
NIR	Near-infrared
NMR	Nuclear magnetic resonance
NMV	Net magnetisation vector
NOTA	1,4,7-Triazacyclononane-1,4,7-triacetic acid
NTA	Nanoparticle tracking analysis
NBS	N-Bromosuccinimide
PET	Positron emission tomography
Pyr	Pyridine
Pym	Pyrimidine
pyz	Pyrazine
ppm	Parts per million
r	Gd-H distance (inner sphere)
r'	Gd-H distance (outer sphere)
rf	Radio frequency
RT	Room temperature
R	Heterocycles with reactive halide
S	spin ground state
S <sub>1</sub>	Excited singlet state
SaOH <sub>2</sub>	Salicyladoxime
T <sub>1</sub>	Triplet state
T <sub>1</sub>	Longitudinal or spin-lattice relaxation
T <sub>2</sub>	Transverse or spin-spin relaxation
TACN	1,4,7-Triazacyclononane
<sup>t</sup> Bu-DO3A	1,4,7-Tris( <i>tert</i> -butoxycarbonylmethyl)-1,4,7,10-tetraazacyclododecane
TEA	Triethylamine
THF	Tetrahydrofuran
TETA	2-[4-nitrobenzyl]-1, 4, 8, 11-tetraazacyclotetradecane N,N',N'',N'''-tetraacetic acid
TLC	Thin layer chromatography

TM	Transition metals
TCCA	Trichloroisocyanuric acid
UV	Ultra-violet
$\omega_0$	Larmors frequency

## Table of contents

Abstract.....	ii
Risk Assessment.....	iii
Acknowledgements.....	iv
Declaration.....	v
Abbreviations.....	vi
Table of Figures.....	ix
Table of Schemes.....	xviii
1. Introduction.....	xix
1.1 Macrocyclic chelators.....	1
1.1.2 The chelate and macrocycle effect.....	2
1.1.3 Macrocyclic systems incorporating pendent arms.....	3
1.2 Molecular imaging.....	5
1.2.1 Magnetic resonance imaging (MRI).....	6
1.2.2 Optical.....	16
1.2.3 Radiopharmaceuticals.....	22
Synthesis of heterocycle functionalised tetraazamacrocyclic chelators.....	24
2.1 Aims.....	25
2.2 Heterocyclic pendent arms.....	26
2.2.1 Methods for alkyl halide heterocycle synthesis.....	27
2.2.2 Synthesis of alkyl halide terminating heterocycles – summary.....	31
2.3 Synthesis of macrocyclic chelators.....	32
2.3.1 Synthetic methodology to form functionalised DO3A derivatives.....	32
2.3.2 Synthesis of 1,4,7-tris(tert-butoxycarbonylmethyl)-1,4,7,10-tetraazacyclododecane ( <i>t</i> Bu-DO3A).....	34
2.3.3 Synthesis of heterocyclic functionalised tBu-DO3A derivatives.....	35
2.3.4 Deprotection to form heterocycle functionalised DO3A derivatives.....	37
2.3.5 Synthesis of macrocyclic chelators – summary.....	39
2.4 <sup>1</sup> H NMR and titration pH speciation studies.....	40
2.4.1 <sup>1</sup> H NMR and pH speciation studies of pyridyl DO3A ( <b>10</b> ).....	41

2.4.2 <sup>1</sup> H NMR and speciation pH studies of pyrimidine DO3A chelator ( <b>11</b> ) .....	45
2.4.3 <sup>1</sup> H NMR and speciation pH studies on pyrazine DO3A chelator ( <b>12</b> ).....	49
2.5 Conclusions.....	53
Synthesis and characterisation of lanthanide(III) tetraazamacrocyclic complexes.....	54
3.1 Introduction.....	55
3.2 Synthesis of lanthanide(III) complexes. ....	57
3.2.1 Preparation of lanthanide(III) complexes of 1,4,7-tris(carboxymethyl)-10-(methyl[pyr][pyz][pym])tetraazacyclododecane.....	57
3.2.2 <sup>1</sup> H NMR/ potentiometric titration studies for lanthanide(III) complexes. ....	63
3.2.3 T <sub>1</sub> relaxation studies for Gd(III) complexes. ....	75
3.3 Conclusions.....	79
Towards the synthesis of multi-metallic species for potential use as imaging agents .....	80
4.1 Aims.....	81
4.2 Bimetallic and multi-metallic species.....	83
4.2.1 Gadolinium chelate based contrast agents .....	84
4.3 Synthesis and characterisation of Ln-Re bimetallic species.....	89
4.3.1 Rhenium chromophore synthesis.....	90
4.3.2 Formation of combined Re-Ln(III) complexes via heterocyclic linkers. ....	101
4.4 Multi-metallic systems .....	108
4.4.1 Formation of multi manganese(III) systems.....	110
4.4.2 Combination of Fe(III) with heterocycle arms.....	119
4.5 Conclusions.....	126
Concluding Remarks and Future Directions .....	130
5.1. Conclusions.....	131
5.2. Future directions .....	137
5.2.1 Macrocycles functional chelators – Vary metal ion, vary application.....	137
5.2.2 Bearing of lanthanide(III) and rhenium complexes future work.....	137
5.2.3 Substitution of N-donor (pyridine) future work.....	138
5.2.4 Substitution of N-donor (pyrimidine, pyrazine) future work.....	138

Experimental.....	139
6.1 General notes.....	140
6.2 Materials.....	140
6.3 Instrumentation.....	140
6.3.1. NMR spectroscopy.....	140
6.3.2 MS.....	140
6.3.3 CHN.....	141
6.3.4 ICP-OES.....	141
6.3.5 Potentiometric titrations.....	141
6.3.6 X-ray crystallography.....	141
6.4 Synthesis of heterocycle functionalised tetraazamacrocyclic chelators.....	143
6.4.1 Attempted synthesis of 4-(bromomethyl) pyrimidine.....	143
6.4.2 Attempted synthesis of 2-(bromomethyl) pyrazine.....	144
6.4.3 Synthesis of 4-chloromethyl pyrimidine.....	145
6.4.4 Synthesis 2-chloromethyl pyrazine.....	146
6.4.5 Synthesis of 1, 4, 7-tris (tert-butoxycarbonylmethyl)-1, 4, 7, 10-tetraazacyclododecane hydrobromide.....	147
6.4.6 Synthesis of 1, 4, 7-Tris (tert-butoxycarbonylmethyl)-1, 4, 7, 10-tetraazacyclododecane ( <i>t</i> Bu-DO3A).....	148
6.4.7 Synthesis of tri- <i>tert</i> -butyl 2, 2, 2-10-(4-methylpyridyl) 14,7,10 tetraazacyclododecane-1, 4, 7-triyl) triacetate.....	149
6.4.8 Synthesis of tri- <i>tert</i> -butyl 2, 2', 2''-(10(4-methyl pyrimidyl)-1, 4, 7, 10-tetraazacyclododecane-1, 4, 7-triyl) triacetate.....	150
6.4.9 Synthesis of tri- <i>tert</i> -butyl 2, 2', 2''-(10-(2-methyl pyrazine)-1, 4, 7, 10-tetraazacyclododecane-1, 4, 7-triyl) triacetate.....	151
6.4.10 (10-(4-methyl pyridyl)-1, 4, 7, 10-tetraazacyclododecane-1, 4, 7-triyl) triacetic acid.....	152
6.4.11 Synthesis of 2,2',2''-(10-(4-methyl pyrimidyl)-1,4,7,10-tetraazacyclododecane-1,4,7-triyl)triacetic acid.....	154
6.4.12 Synthesis of 1, 4, 7-tris (tert-butoxycarboxymethyl)-10-(2-methylpyrazine) tetraazadodecane.....	155
6.4.13 Attempted method of synthesis metal(III) complexes of 1, 4, 7-tris (tert-butoxycarboxymethyl)-10-[pyr, pyz, pym] tetraazadodecane.....	156

6.4.14 synthesis of metal(III) complex of 1, 4, 7-tris (tert-butoxycarboxymethyl)-10-(4-methylpyridyl) tetraazadodecane. ....	157
6.4.15 Synthesis of gadolinium (III) complex of 1, 4, 7-tris (tert-butoxycarboxymethyl)-10-(4-methylpyridyl)tetraazadodecane. (Gd10) .....	157
6.4.16 Synthesis of europium(III) complex of 1, 4, 7-tris (tert-butoxycarboxymethyl)-10-(4-methylpyridyl) tetraazadodecane. (Eu10) .....	157
6.4.17 Synthesis of terbium(III) complex of 1, 4, 7-tris (tert-butoxycarboxymethyl)-10-(4-methylpyridyl) tetraazadodecane. (Tb10).....	157
6.4.18 Synthesis of yttrium(III) complex of 1, 4, 7-tris (tert-butoxycarboxymethyl)-10-(4-methylpyridyl) tetraazadodecane. (Y10) .....	158
6.4.19 Synthesis of metal(III) complexes of 1, 4, 7-tris (tert-butoxycarboxymethyl)-10-(4-methylpyrimidyl) tetraazadodecane. ....	159
6.4.20 Synthesis of gadolinium(III) complexes of 1, 4, 7-tris (tert-butoxycarboxymethyl)-10-(4-methylpyrimidyl)tetraazadodecane. (Gd11).....	159
6.4.21 Synthesis of europium(III) complex of 1, 4, 7-tris (tert-butoxycarboxymethyl)-10-(4-methylpyrimidyl)tetraazadodecane. (Eu11) .....	159
6.4.22 Synthesis of terbium(III) complex of 1, 4, 7-tris (tert-butoxycarboxymethyl)-10-(4-methylpyrimidyl) tetraazadodecane. (Tb11).....	159
6.4.23 Synthesis of yttrium (III) complex of 1, 4, 7-tris (tert-butoxycarboxymethyl)-10-(4-methylpyrimidyl) tetraazadodecane. (Y11).....	160
6.4.24 Synthesis of metal (III) complex of 1, 4, 7-tris (tert-butoxycarboxymethyl)-10-(2-methylpyrazine) tetraazadodecane.....	161
6.4.25 Synthesis of gadolinium(III) complex of 1, 4, 7-tris (tert-butoxycarboxymethyl)-10-(2-methylpyrazine) tetraazadodecane. (Gd11).....	161
6.4.26 Synthesis of europium(III) complex of 1, 4, 7-tris (tert-butoxycarboxymethyl)-10-(2-methylpyrazine)tetraazadodecane. (Eu11) .....	161
6.4.27 Synthesis of terbium(III) complex of 1, 4, 7-tris (tert-butoxycarboxymethyl)-10-(2-methylpyrazine)tetraazadodecane. (Tb11) .....	161
6.4.28 Synthesis of yttrium(III) complex of 1, 4, 7-tris(tert-butoxycarboxymethyl)-10-(2-methylpyrazine)tetraazadodecane. (Y11) .....	162
6.5 Synthesis of Multi-metallic species .....	163
6.5.1 <i>fac</i> -chlorotricarbonyl (bipyridine) rhenium(I). ....	163
6.5.2 <i>fac</i> -(acetonitrile) tricarbonyl (2, 2'-bipyridine) rhenium (I) triflate.....	164
6.5.3 Combined complexes (rhenium-lanthanide).....	165
6.5.4 Combined complexes (rhenium-lanthanide). (Pyridyl linker) .....	166

6.5.5 Combined complexes (rhenium-lanthanide). (Pyrimidyl linker) .....	167
6.5.6 Combined complexes (rhenium-lanthanide). (Pyrazine linker) .....	168
6.5.7 Oxime synthesis: Et-saoH <sub>2</sub> .....	170
6.5.8 Synthesis manganese (III) triangle ( <b>19</b> ) .....	171
6.6 Single crystal X-ray diffractometer data .....	172
6.6.1 Data for <b>15</b> .....	172
6.6.2 Data for <b>16</b> .....	176
6.6.3 Data for <b>17</b> .....	180
6.6.4 Data for <b>20</b> .....	184
6.6.5 Data for <b>21</b> .....	190
6.6.6 Data for <b>22</b> .....	196
6.6.7 Data for <b>23</b> .....	199

## List of Figures

Figure 1 – Some examples of macrocyclic chelators.....	1
Figure 2 – Curtis’s macrocycle; 5,7,7,12,14,14-hexamethyl- 1,4,8,11-tetraazacyclotetradeca-4,11-diene. ....	2
Figure 3 – DO3A chelator with a phenylamino acetic acid pendent arm. ....	3
Figure 4 – DO3A chelator with nitroaminoresorcinol pendent arm. ....	4
Figure 5 – DO3A chelator with quinoline pendent arm. ....	4
Figure 6 – Characteristics of the medical imaging modalities. ....	5
Figure 7 – An example of a MRI scanner. <sup>10</sup> .....	6
Figure 8 – A positively charged nucleus which produces a magnetic field (the magnetic vector) when the nucleus has spin. ....	7
Figure 9 – Diagram to show the effect of an applied magnetic field ( $B_0$ ) on the set of individual protons in fluid or tissue. ....	8
Figure 10 – Showing a proton precessing about the magnetic field direction. The precessional axis is parallel to the main magnetic field $B_0$ in the z direction, with a frequency of $\omega_0$ , and a net magnetization of $M$ . ....	8
Figure 11 – Diagram to show the effect of a $90^\circ$ excitation pulse. ....	9
Figure 12 – Schematic of energy transfer from/to a gadolinium(III) based contrast agent leading to an increase in relaxivity. ....	12
Figure 13 – Chemical structures of $[GdDOTA(H_2O)]^{2-}$ ( $L^4$ ) and $[GdDTPA(H_2O)]^{1-}$ ( $L^5$ ). ....	12
Figure 14 – Common MRI contrast agents used in clinics. ....	13
Figure 15 – Some contrast agents with a gadolinium(III) centre that are licensed for clinical use macrocyclic (left), linear (right). ....	14
Figure 16 – A diagram of the transmetallation between gadolinium(III) and endogenous cations such as zinc ( $Zn^{2+}$ ). The zinc replaces the gadolinium(III) of the chelate and is eliminated from the body in urine as zinc chelate. The gadolinium(III) combines with endogenous anions and is deposited in tissues. ....	15
Figure 17 – Chemical structures of commonly used organic dyes BODIPY and rhodamine. ...	16
Figure 18 – Schematic to show the energy transfer processes to sensitise emission. ....	17
Figure 19 – Luminescence emission processes of a europium chelate. ....	19
Figure 20 – Rhenium (I) bipyridine chromophore ( $L^{12}$ ). ....	20
Figure 21 – Lanthanide complexes based DO3A with rhenium bipyridine chromophore attracted ( $L^{13}$ ). ....	21
Figure 22 – Schematic illustration of the interaction of the three major disciplines. <sup>45</sup> .....	22
Figure 23 – Schematic design of a PET radiopharmaceutical and its interaction with the target site. <sup>45</sup> .....	23
Figure 24 – Radiopharmaceutical chelator based on DO3A. ....	23
Figure 25 – Proposed schemes for the synthesis of heterocyclic substituted DO3A derivatives. ....	25
Figure 26 - Annotated molecular structure of heterocycles (pyridine, pyrimidine, and pyrazine). ....	26

Figure 27 – Chemical structures of 4-chloromethyl pyrimidine ( <b>3</b> ) and 2-chloromethyl pyrazine ( <b>4</b> ) precursors with purchased unit (4-bromomethylpyridine hydrobromide). .....	31
Figure 28 - Library of chelators prepared for lanthanides complexation. ....	39
Figure 29 - <sup>1</sup> H NMR spectrum of chelator ligand <b>10</b> shown the effect of pD on aromatic protons. ....	41
Figure 30 – The pH effect on the 4-methylpyridine arm in chelator ligand <b>10</b> . ....	41
Figure 31 - Protonation patterns of pyridine DO3A ( <b>10</b> ).....	42
Figure 32 - Speciation diagram of pyridine DO3A ( <b>10</b> ) .....	44
Figure 33 - <sup>1</sup> H NMR spectrum of chelator ligand <b>11</b> shown the effect of pD on aromatic protons. ....	45
Figure 34 - The pH effect on the 4-methylpyridine arm in chelator ligand <b>11</b> . ....	45
Figure 35 - Protonation patterns of pyrimidine DO3A ( <b>11</b> ). ....	46
Figure 36 - Speciation diagram of pyrimidine DO3A ( <b>11</b> ). ....	47
Figure 37 - <sup>1</sup> H NMR spectra of chelator <b>12</b> shown the effect of pD on aromatic protons. ....	49
Figure 38 - The pH effect on the 2-methylpyrazine arm in chelator ( <b>12</b> ). ....	49
Figure 39 - Protonation patterns of pyrazine DO3A ( <b>11</b> ). ....	50
Figure 40 - Speciation diagram of pyrazine DO3A ( <b>12</b> ). ....	51
Figure 41 - The three synthesised chelators ( <b>10</b> , <b>11</b> , and <b>12</b> ) with three heterocyclic arms (pyr, pym, and pyz).....	53
Figure 42 - <sup>1</sup> H NMR spectrum of chelator ligand <b>Y10</b> shown the effect of pD on the aromatic region. ....	63
Figure 43 - The pH effect on the 4-methylpyridine arm in <b>Y10</b> complex. ....	64
Figure 44 - Speciation diagram of <b>Gd10</b> , <b>Eu10</b> , and <b>Y10</b> . ....	66
Figure 45 - <sup>1</sup> H NMR spectrum of chelator ligand <b>Y11</b> shown the effect of pD on aromatic protons .....	68
Figure 46 – Protons positions of 4-methylpyridine arm in chelator ligand ( <b>Y11</b> ). ....	68
Figure 47 - Speciation diagram of <b>Gd11</b> , <b>Eu11</b> , and <b>Y11</b> . ....	70
Figure 48 - <sup>1</sup> H NMR spectrum of chelator ligand <b>Y12</b> shown the effect of pD on aromatic protons .....	71
Figure 49 - Protons positions of 2-methylpyrazine arm in chelator ligand ( <b>Y12</b> ). ....	71
Figure 50 - Speciation diagram of <b>Gd12</b> , <b>Eu12</b> , and <b>Y12</b> . ....	73
Figure 51 -Graph to show concentration vs. 1/T at pH 7 for <b>Gd11</b> .....	76
Figure 52 –Plot of concentration vs. 1/T for <b>Gd12</b> .....	77
Figure 53 - Lanthanide complexes of (pyridine, pyrimidine, and pyrazine) containing tetraazamacrocycles synthesised. ....	79
Figure 54 - Schematic representation of the combination of Ln(III) complexes with monometallic species (rhenium or iron) through the heterocyclic bridge. ....	81
Figure 55 - Schematic representation of the combination of Ln(III) complexes with multi-metallic manganese species through the heterocyclic bridge. ....	82
Figure 56 - Schematic representation of multi-imetallic species. ....	83
Figure 57 - Heterocyclic based GdDO3A agents. ....	84

Figure 58 - Schematic representation for MRI and optical combination of different contrast agents.....	86
Figure 59 – Example of linking trimer Gd complexes (f-block) with chromophore based Ti metal (d-block). ....	87
Figure 60 - Literature example for linking Gd complexes (f-block) with chromophore based Re metal (d-block). ....	87
Figure 61 - Literature example for linking trimer Gd complexes (f-block) with two chromophore based on Ru metal (d-block). ....	88
Figure 62 - Literature example for linking Gd complexes (f-block) with multimetallic species (silicone nanoparticle) included to Ru metals molecules (d-block). ....	88
Figure 63 - Schematic representation the combination of Ln(III) complexes with monometallic species (rhenium bipyridine complex) throughout the heterocycles bridge. ....	89
Figure 64 - Synthesis steps to produce Re-Ln compounds <b>M24</b> , <b>M25</b> , and <b>M26</b> . ....	90
Figure 65 - Molecular structure and X-ray image of $[\text{Re}_2(\text{bipy})_2(\text{CO})_6(\text{CF}_3\text{SO}_3^-)]$ ( <b>15</b> ) dimer. ....	93
Figure 66 - $[\text{Re}_2(\text{bipy})_2(\text{CO})_6(\mu\text{-H})(\text{Cl})]$ dimer attached via hydrido bridge ( $L^{24}$ ). <sup>101</sup> ....	94
Figure 67 - Crystal structure and X-ray image of rhenium bipyridine complex coordinate ethyl acetate solvent with triflate anion.....	95
Figure 68 - <i>Fac</i> - $\text{Re}(\text{bipy})(\text{CO})_3\text{COOMe}$ example from literature ( $L^{25}$ ). <sup>104</sup> ....	95
Figure 69 - Crystal structure and X-ray image of rhenium bipyridine complex coordinate ethylacetate solvent with THF ring and triflate anion .....	97
Figure 70 - Rhenium bipyridine complex contain THF ring ( $L^{26}$ ) from literature. <sup>105</sup> .....	98
Figure 71 - Synthesised rhenium complex <b>14</b> and crystallised rhenium bipyridine complexes <b>15</b> , <b>16</b> and <b>17</b> . ....	100
Figure 72 - Representing example from the literature ( $L^{27}$ ), of the combining of Ln(III) complexes with rhenium bipyridine complexes through pyridine ring. ....	103
Figure 73 - Lanthanide macrocyclic complex linked with triazolophthalazene chromophore ( $L^{28}$ ). <sup>19</sup> .....	105
Figure 74 - Rhenium –lanthanide building blocks from the literature ( $L^{29}$ ). <sup>106</sup> .....	106
Figure 75 - Three novel combined products <b>M24</b> , <b>M25</b> , and <b>M26</b> .....	107
Figure 76 - Schematic representation of the combination of Gd(III) complexes with multimetallic species throughout the heterocyclic bridge. Colour code: Mn(III) (purple), O (red), N (blue) C (grey). ....	108
Figure 77 - Multimetallic species of Mn triangle and the positions of oxime ligands ( <b>18</b> ). ...	110
Figure 78 - Schematic representation the proposed combination of <b>M10</b> complexes with Mn triangle ( <b>19</b> ) throughout the heterocycle bridge (pyr). ....	114
Figure 79 - Multimetallic molecule of Mn triangle attached to picoline Colour code: Mn(III) (purple), O (red), N (blue) C (yellow) Cl (green). ( $L^{30}$ ).....	115
Figure 80 - X-ray crystal structure of penta-manganese <b>21</b> .....	116
Figure 81 - The molecular structure of literature penta-manganese complex, colour code: Mn(III) = red, Mn(IV) = purple, O = green, N = blue, C = yellow, Val = grey. <sup>120,121</sup> .....	117

Figure 82 - The novel multimetallic (Mn triangle) with bromomethylpyridine ring attached (20), and formed Mn pentamer (21).....	118
Figure 83 - Schematic representation of lanthanide(III) complexes proposed linking via iron. ....	119
Figure 84 – Proposed linking of two lanthanide complexes via the iron and the heterocycle linker (pyrazine). ....	120
Figure 85 - Crystal structure of $[Fe(II)(H_2O)_4(trans-pyr)_2][O_2CCH_3]_2$ from literature ( $L^{32}$ , eft). <sup>122</sup> Synthesised crystal <b>22</b> (right). ....	121
Figure 86. Unit cell of the crystal structure of <b>22</b> .....	122
Figure 87 - Proposed combination of four lanthanide(III) complexes via iron linker. ....	124
Figure 88 - crystal structure of $[Fe(II) (trans-py)_4Cl_2]$ from literature ( $L^{33}$ ,left). <sup>123</sup> Synthesised crystal <b>23</b> (right). ....	124
Figure 89 - three novel bimetallic building block of Re bipyridine complex with lanthanide complexes based DO3A macrocycles through three different heterocycles bridges (pyridine, pyrazine, and pyrimidine). ....	126
Figure 90 - Three novel Re bipyridine complex with triflate anions; Re dimer ( <b>15</b> ), Re bipyridine ethyl acetate ( <b>16</b> ) and Re bipyridine ethyl acetate/THF ( <b>17</b> ). ....	127
Figure 91 - Novel crystal of combination of Mn(III) triangle with pyridine heterocycle ( <b>20</b> ). ....	128
Figure 92 - Novel penta manganese single molecule magnets ( <b>21</b> ). ....	128
Figure 93 - Two novel mono metallic species (iron) attached to N-donors pyrazine ( <b>22</b> ) top & pyrimidine ( <b>23</b> ) bottom. ....	129
Figure 94 - Novel alkyl halide of pyrazine ( <b>3</b> ).....	132
Figure 95 - Three novel chelators have been synthesised in this work .....	132
Figure 96 –Novel lanthanide(III) complexes in this work .....	133
Figure 97 -Three combined system <b>M24</b> , <b>M25</b> , <b>M26</b> have been synthesised in this work. ...	134
Figure 98 - Substituted of N-heterocycles with iron.....	135
Figure 99 - Novel formation of rhenium bipyridine crystals .....	135
Figure 100 - Manganese(III) triangle & pyridine groups.....	136

## List of Schemes

<i>Scheme 1 – Attempted bromination reactions of 4-methylpyrimidine &amp; 2-methylpyrazine to form 1 and 2 respectively.</i>	27
<i>Scheme 2 - Proposed self-reaction of heterocycles making dimers or trimers, etc.</i>	28
<i>Scheme 3 – Attempted conversion of 4-hydroxymethylpyrimidine and 2-hydroxymethylpyrazine to 4-chloromethylpyrimidine (3) and 2-chloromethylpyrazine (4) respectively.</i>	29
<i>Scheme 4 – Substitution reactions of 4-methylpyrimidine and 2-methylpyrazine to form 4-chloromethylpyrimidine (3) and 2-chloromethylpyrazine (4) respectively.</i>	30
<i>Scheme 5 – Two synthetic methods to produce N functionalised <sup>t</sup>Bu-DO3A derivatives.</i>	32
<i>Scheme 6 - Alternative synthetic route to form <sup>t</sup>Bu-DO3A (6).</i>	34
<i>Scheme 7 - Proposed synthetic routes to form N-functionalised <sup>t</sup>Bu-DO3A derivatives with 4-bromomethyl pyridine hydrobromide, 3 and 4.</i>	35
<i>Scheme 8 - Formation of pyridine, pyrimidine, and pyrazine DO3A triacid derivatives by hydrolysis.</i>	37
<i>Scheme 9 - Lanthanide complex formation based on synthesised 10, 11, and 12.</i>	55
<i>Scheme 10 – Synthetic method of lanthanide complexation.</i>	57
<i>Scheme 11 – Ln(III) complexes formed with 10</i>	59
<i>Scheme 12 - Ln(III) complexes formed with 11.</i>	61
<i>Scheme 13 – Lanthanide(III) complexes formed with 12.</i>	62
<i>Scheme 14 - Pyridine protonation constants of Gd10, Eu10, and Y10.</i>	65
<i>Scheme 15 - Pyrimidine protonation constants of Gd11, Eu11, and Y11.</i>	69
<i>Scheme 16 - Pyrimidine protonation constants of Gd12, Eu12, and Y12.</i>	72
<i>Scheme 17 - Synthesis methods to produce a rhenium chloride complex 13 which is used in this work to attach a chromophore.</i>	91
<i>Scheme 18 - Synthesis methods to produce the acetonitrile rhenium (I) complex 14 (chromophore) from the rhenium chloride complex 13.</i>	92
<i>Scheme 19 – General reaction scheme to form M24, M25, and M26</i>	101
<i>Scheme 20. Reaction scheme to synthesise M24</i>	103
<i>Scheme 21 - Reaction scheme of synthesis of M25</i>	104
<i>Scheme 22 - Reaction scheme for the synthesis of M26</i>	105
<i>Scheme 23 - Synthetic route to form oxime 18</i>	111
<i>Scheme 24 - Schematic representation of combining oxime ligand (18) with Mn(II) precursor to form a Mn(III) triangle (multimetallic species)(19).</i>	112
<i>Scheme 25 - Schematic representation the reaction of Mn(III) triangle with pyridine (heterocycle).</i>	113
<i>Scheme 26- preparation reaction of crystal structure [Fe(II)(H<sub>2</sub>O)<sub>4</sub>(2methylpyrazine)<sub>2</sub>(CH<sub>3</sub>)<sub>2</sub>Br<sub>2</sub>](22)</i>	120
<i>Scheme 27 - preparation reaction of crystal structure of [Fe(II) (4-methyl-pym)<sub>4</sub>](Br)<sub>2</sub>(23)</i>	123

# **Introduction**

## **Chapter 1**

## 1. Introduction

### 1.1 Macrocyclic chelators

Macrocyclic ligands are polydentate ligands which contain donor atoms as part of a cyclic backbone. Usually, macrocyclic ligands have a minimum of nine atoms in the ring, with at least three donor atoms. The type of donor atoms and the macrocycle size can be tailored for binding different metal ions such as lanthanide or transition metal ions. Many different chelating ligands have been synthesised in recent years and used to modify and control the properties of metal ions in biological systems. The acetate pendent arms are compatible with both lanthanide ions and transition metals, providing a strong binding interaction.<sup>1</sup>

Azamacrocyclic chelators, such as DOTA, NOTA, TETA, and DO3A, see Figure 1, offer a high level of kinetic and thermodynamic stability with advantages over acyclic systems in the functionalisation pattern and the more organised spatial arrangement of donor atoms with the potential to encapsulate the metal ion.

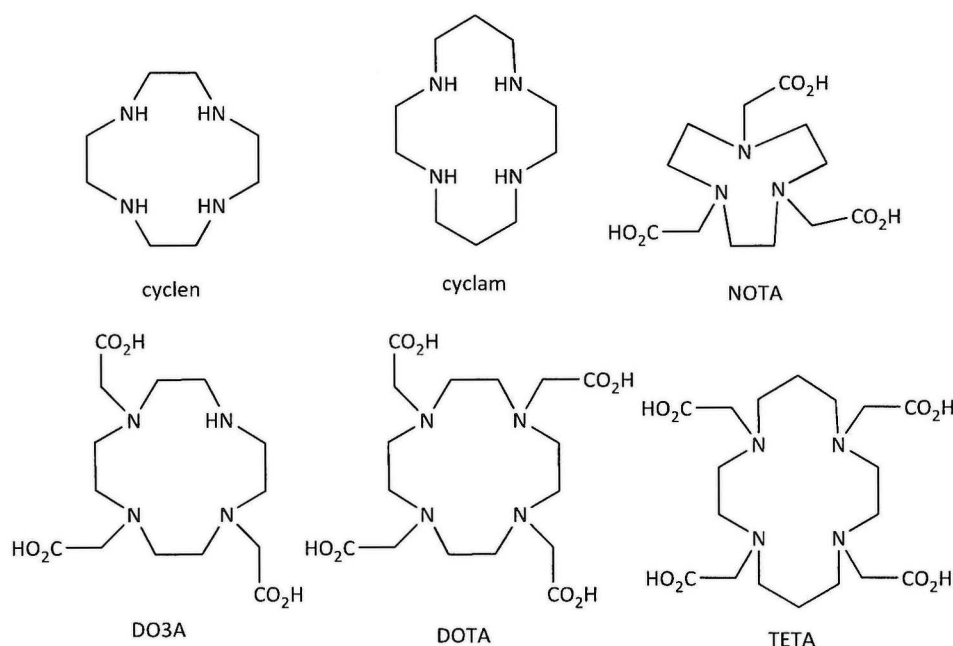


*Figure 1 – Some examples of macrocyclic chelators.*

Macrocyclic chelators can be utilised as a basis for many contrast agents for imaging biological systems or bifunctional (BFCs) chelators for attaching radiometals to protein targeting groups. Chelators based on cyclen or cyclam are commonly utilised.<sup>1</sup>

### 1.1.2 The chelate and macrocycle effect

The enhanced stability of the complex containing polydentate ligands over similar monodentate ligands can be explained via the chelate effect. When the bidentate or polydentate ligands bind to a metal ion, there is a free energy gain compared to the same number of unidentate ligands and the result is the formation of more stable complexes.

A similar concept underpins the macrocyclic effect. Cabbiness and Margerum first described the macrocyclic effect in 1969. They exemplified this by the detected stability enhancement in the Nickel (II) complex when coordinated with Curtis's macrocycle, see Figure 2, in comparison to non-cyclic tetramine ligands.<sup>2,3</sup>

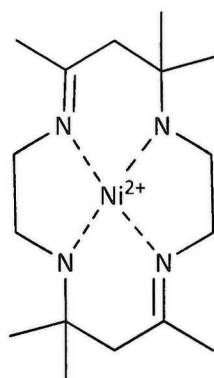


*Figure 2 – Curtis's macrocycle; 5,7,7,12,14,14-hexamethyl- 1,4,8,11-tetraazacyclotetradeca-4,11-diene.*

Macrocycles are designed to offer a pre-organised environment that is maintained in the absence of a metal ion. Therefore, the enthalpic energy cost of the metal-chelator binding will be minimised when the metal binds to the macrocycle. Although one potential drawback is that the macrocycles often have the unfavourable property of slow metal formation kinetics. However the advantage is seen in the decomplexation process where ligand may require rearrangement before allowing any metal dissociation to occur. Overall, this is identified as the macrocyclic effect. Hence, a macrocyclic chelator, such as cyclen, is more stable than its open chain analogues.<sup>4,5</sup>

### 1.1.3 Macrocyclic systems incorporating pendent arms

A number of fundamental biological processes involve macrocyclic ligands, such as mammalian oxygen transport and photosynthetic pathways. Macrocyclic complexes have been investigated to mimic these systems. Macrocyclic complexes have also been prepared for diagnostic and therapeutic applications. There are many potentially useful applications of these complexes in areas such as magnetic resonance imaging (MRI) as contrast agents, radiopharmaceutical agents and, with the inclusion of a sensitising chromophore, luminescent sensors.

Pendent arms can be attached to macrocyclic back bones for particular reasons. Firstly, the additional donor atoms provided by pendent arms can coordinate to the metal centre to increase stability; secondly, there is the possibility of using the pendent arm as a linker group, allowing the attachment of further moieties to the metal complex; thirdly, the pendent arms can alter the coordination sphere of the metal centre and effect the physical properties (i.e. redox potentials). Many examples have been reported in the literature for DO3A macrocycles incorporating various types of pendent arms; some of them are shown in Figures 3-6 ( $L^1$ ,  $L^2$ , and  $L^3$ ).

$L^1$  is a DO3A chelator with a phenylamino acetic acid pendent arm (see Figure 3). It is utilised in zinc(II) sensing by MRI with the relaxivity for the gadolinium(III) complex increased over 100% in the presence of zinc(II). The acetate pendent arms are required to give a saturated coordination environment for the gadolinium(III) centre in the absence of zinc(II).<sup>5,6</sup>

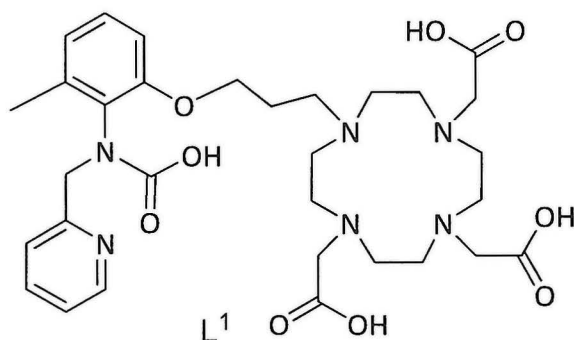


*Figure 3 – DO3A chelator with a phenylamino acetic acid pendent arm.*

Other examples of activated MR contrast agents are known, for example, with nitroresorcinol pendent arms that have sensitivity to calcium(II) binding,  $L^2$  (see Figure 4). It has lower affinity

for the calcium than previously investigated sensors to allow the probe to be responsive when calcium concentration changes rapidly, similar to the previous example, an up to 100% increase in relaxivity is observed. The physical response could be improved by investigation of the influence of anion binding.<sup>7</sup>

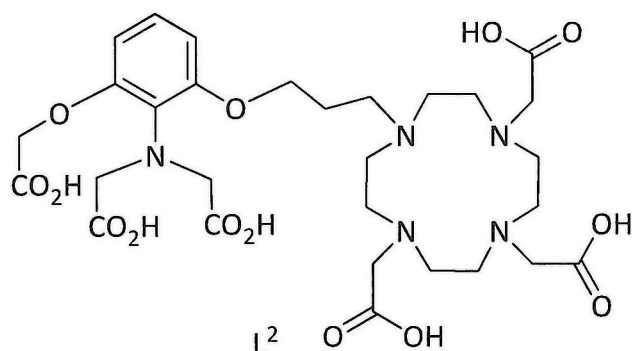


Figure 4 – DO3A chelator with nitroaminoresorcinol pendent arm.

Wei-Sheng Li, synthesised a new macrocyclic chelator (L<sup>3</sup>), where DO3A was functionalised with a quinoline pendent arm, see Figure 5, which exhibited a higher efficiency in terms of relaxivity compared to the clinically used Gd-DTPA (7.18 mM<sup>-1</sup> s<sup>-1</sup> at 400 MHz) and the ability to form a multimetallic species with three gadolinium(III) complexes around an aluminium centre coordinated to the three pendent arms (one from each chelate). There were additional interesting photophysical properties for the L<sup>3</sup> chelator with bright-green luminescence centred at 510 nm, hence it is a potential bimodal MRI/optical imaging agent that could be used in tracing and diagnosis in biological systems.<sup>1,8</sup>

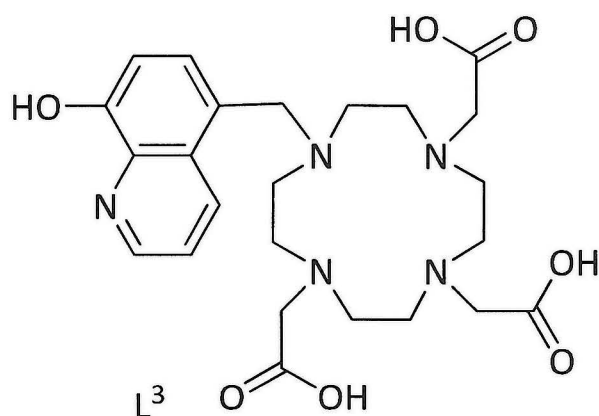


Figure 5 – DO3A chelator with quinoline pendent arm.

## 1.2 Molecular imaging

Molecular imaging can be broadly defined as the measurement and the characterization of biological processes in vivo at the cellular and molecular level. Imaging research is often focussed on understanding the molecular and cellular mechanisms of diseases with non-invasive protocols that provide high resolution images. Molecular imaging is considered a growing research discipline as targeted imaging of specific molecular pathways in vivo to test and develop novel tools is developed. Pathways that are believed to be key in developing disease processes are of high interest.

Various modalities can be used for molecular imaging, such as single-photon emission computed tomography (SPECT) and positron emission tomography (PET), which are nuclear medicine techniques involving radioisotopes. Structural techniques such as magnetic resonance imaging (MRI) and computed tomography (CT) are used on their own or in combination with PET and SPECT. Other imaging modalities, such as optical and ultrasound are also used in some applications. Optical imaging is limited by tissue penetration but does allow parts of the human body to be imaged a few centimetres from the surface.

Each technique has specific characteristic advantages and disadvantages (see Figure 6). Most of them are clinically used and can be translated from animals to humans in the drug development process.<sup>9,10</sup>

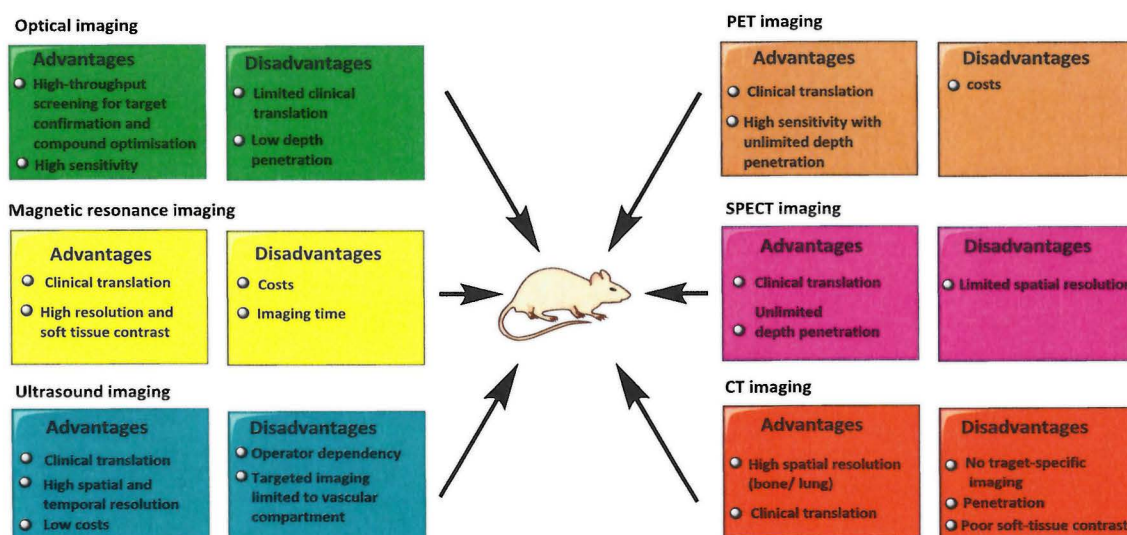


Figure 6 – Characteristics of the medical imaging modalities.

### 1.2.1 Magnetic resonance imaging (MRI)

Magnetic resonance imaging (MRI), an effective medical imaging modality for functional and anatomical imaging of body structures. It can be routinely used for the detection and characterisation of tumour or diseased tissues at an early stage (see Figure 7).

MRI has some advantages over other medical techniques such as positron emission tomography (PET) or single-photo emission tomography (SPECT), as it can provide three-dimensional penetration with no ionising radiation and high contrast and spatial resolution. It has the ability to differentiate between soft tissues, unlike the X-ray technique.

Proton relaxation time ( $T_1$  and  $T_2$ ) of water molecules in tissues is one of the main parameters in the production of an MR image. However, when small variations in relaxation times between healthy and pathological regions lead to poor contrast, contrast enhancing agents are essential to alter the relaxation times of water protons within these tissues and improve the image.<sup>11,12</sup>

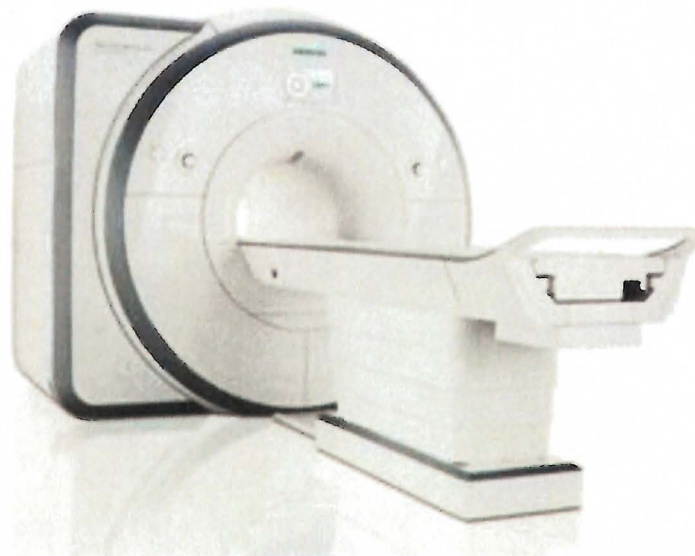


*Figure 7 – An example of a MRI scanner.<sup>10</sup>*

The principles of MRI rely on the spinning motion of specific nuclei present in biological tissues. This kind of spin comes from the individual spins of neutrons and protons within the nucleus. In nuclei that have an even mass number (the number of protons equals the number of neutrons), this nucleus cannot show any net spin because the half spins in one direction

and half spins in the other cancel each other out. In nuclei with an odd number, the number of neutrons is slightly higher or lower than the number of protons, so the spin direction is not equal and is positive. In this situation the nucleus itself has a net spin or angular momentum, and this kind of nucleus is called an MR-active nucleus, such as  $^1\text{H}$ ,  $^{13}\text{C}$  or  $^{19}\text{F}$ .

These nuclei show a tendency to align their axis of rotation to an applied magnetic field. This occurs because they have an angular momentum or spin, and, as they contain protons with a positive charge (i.e. they possess electrical charge). Three individual forces (magnetism, charge, motion) are the main components for electromagnetic induction. When two of these forces are present, then the third is automatically induced. Where MR active nuclei contain a net magnetization (charge) and are spinning (motion), magnetic momentum automatically develops, which can align with an applied magnetic field <sup>13</sup> (see Figure 8).

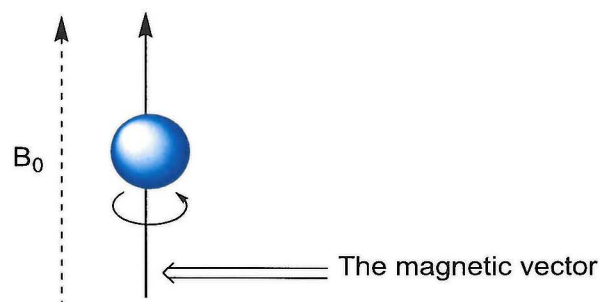


*Figure 8 – A positively charged nucleus which produces a magnetic field (the magnetic vector) when the nucleus has spin.*

MRI involves the net magnetisation of the human body which occurs naturally when applying an external magnetic field. This causes human body protons to align in the same direction as the magnetic field ( $B_0$ ) through net magnetisation. This applies to any atoms that have nuclear spin, and hydrogen ( $^1\text{H}$ ) is one of the atoms that is commonly used to probe the body.

Protons are present in both water and fat in most human body tissues, and, by relying on their relaxation time, the MRI signal can be produced. Due to the fact that protons have spin and the nucleus is positively charged, it acts as a small magnet; therefore, it has a local magnetic field. And will show the same magnitude and orientation properties exactly as the magnetic bar to this magnetic field (i.e. south and north pole), which is called in terms of vector.<sup>5,14</sup> Similar spins are involved in MR measurements. The spin vectors are oriented randomly in the tissue when there is no magnetic field applied, the spin vectors will align themselves

during application of an externally strong field in the parallel direction  $B_0$ , and thus tissue will be considered as a weak magnet (see Figure 9).

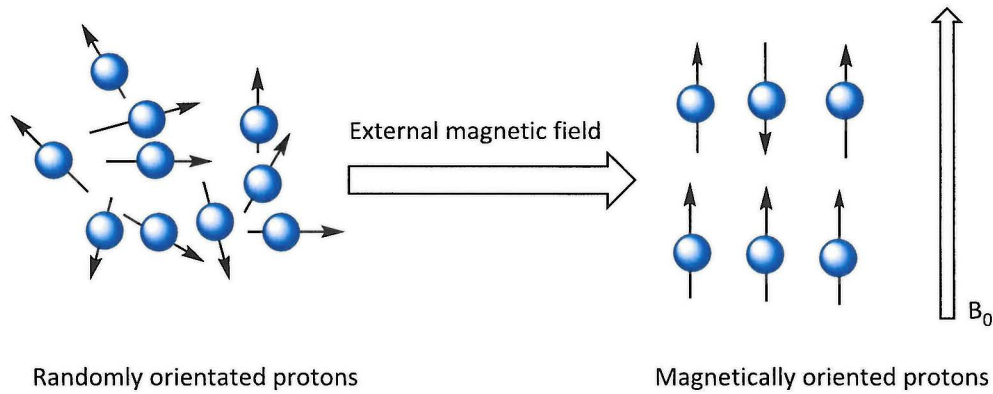


*Figure 9 – Diagram to show the effect of an applied magnetic field ( $B_0$ ) on the set of individual protons in fluid or tissue.*

As the protons of the water molecules are not fixed in one position, and these protons in the presence of a magnetic field rotate about that field slightly away from the magnetic field axis (this proton rotation is called precession), the position of that precession is always parallel to  $B_0$  and in the direction of z axis (see Figure 10). Additionally, the speed of precession, called the precessional frequency, can be understood according to the Larmors equation  $\omega_0 = B_0 \times \gamma$ , where it is proportional to the strength of the magnetic field, and the precessional frequency that can be obtained through this equation decides the energy of the radio frequency (rf) used.<sup>7,15</sup>

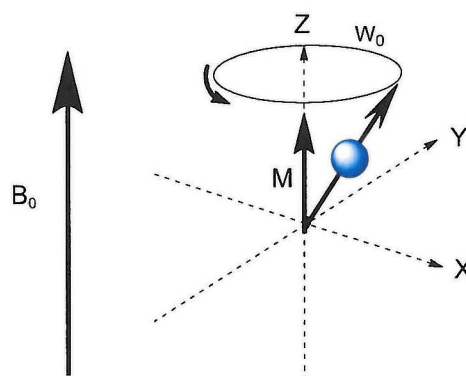


*Figure 10 – Showing a proton precessing about the magnetic field direction. The precessional axis is parallel to the main magnetic field  $B_0$  in the z direction, with a frequency of  $\omega_0$ , and a net magnetization of  $M$ .*

There are two orientations of the spins in the z component: spin up (parallel) and spin down (anti-parallel). Protons can simply swap between these two orientations by losing (spinning down) or gaining (spinning up) energy, and the difference in the energy of the two spins is directly proportional to the strength of the applied magnetic field. The protons in the equilibrium state are all out of phase with each other, which means they are either spin up or spin down relative to the magnetic field ( $B_0$ ). The net magnetisation ( $M_0$ ) is represented by the vector sum which is aligned in the same direction of the external magnetic field ( $B_0$ ).<sup>16</sup>

The basis of the MRI experiment depends on the manipulation of this M value by moving it from the longitudinal plane to the transverse plane component, and then getting it to relax back to equilibrium state. As the MRI processes involve a short pulse of radio frequency (rf) energy, which has a particular frequency ( $\omega_0$ ), the protons can absorb and resonate with it at precession frequency through this radio frequency (rf) pulse. That absorbed frequency is proportional to  $B_0$  ( $\omega_0 = B_0 \times \gamma$ ), causing M to move out of  $B_0$  alignment and to rotate from the z plane (longitudinal) into the xy plane ( $M_1$ , transverse), and the absorption usually occurs at a  $90^\circ$  angle to the  $B_0$ <sup>17</sup> (see Figure 11).

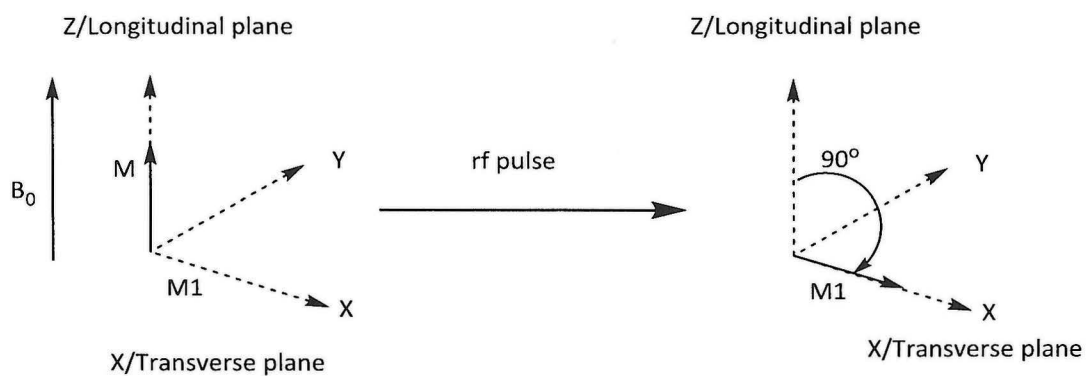


*Figure 11 – Diagram to show the effect of a  $90^\circ$  excitation pulse.*

When that rf pulse stops, the realignment of the protons will start from  $M_1$  and return them to their equilibrium form. That change in the field leads to energy emission at frequency  $\omega_0$ , consequently producing the signal of the MRI. That process of returning the net magnetisation to the z plane or protons to equilibrium is associated with energy loss and is known as relaxation.<sup>16</sup>

MRI has two important relaxation times,  $T_1$  and  $T_2$ .  $T_1$  relaxation can be used to provide the mechanism of the protons as they release their energy to the surrounding lattice to return to the equilibrium state of the protons. In that type of relaxation no energy transfer can occur between the excited protons, with the other spin causing an increase in the longitudinal magnetisation, so the  $T_1$  relaxation might be known as spin-lattice relaxation or longitudinal relaxation time.  $T_2$  relaxation can be identified as the process of the energy transfer from one proton to the neighbouring proton and keeps the absorbed energy which contributes to the overall spin. Therefore  $T_2$  can be also be called a spin-spin relaxation or transverse relaxation time.

Water and fat both have protons, with both  $T_1$  and  $T_2$  relaxation times, but they both occur more rapidly in fat than in water. As a result of that, protons of the fat have short  $T_1$  relaxation times, which means they will appear bright compared to the protons of the water or the tumour, which have long  $T_1$  relaxation times and will appear dark, and that is because of the fat protons' reduced ability to release energy to the lattice and their high mobility. A  $T_1$  contrast agent makes the  $T_1$  relaxation time of the bulk water protons shorter and then makes them appear brighter.<sup>16,17</sup>

### 1.2.1.1 MRI contrast agents

MRI contrast agents (CA), are biocompatible magnetic materials that have the ability to alter the relaxation rates  $T_1$  and  $T_2$  of the surrounding water protons leading to a contrast enhancement of the image of the tissues of interest. The developments in producing effective and safe MRI contrast agents have played a significant role in the improvement of image quality and increased the contrast of the MRI image between the healthy and the diseased tissue when there is poor or weak contrast between them because of the small difference in relaxation times.

Generally, MRI contrast agents are classified according to their relaxation mechanism and magnetic properties into  $T_1$  and  $T_2$  contrast agents.<sup>16</sup>

### 1.2.1.2 $T_1$ contrast agents

Gadolinium(III) chelators are commonly used as effective  $T_1$  contrast agents for increasing the  $T_1$  relaxation rate ( $1/T_1$ ) and generate positive image contrast.

Gadolinium(III) has interesting properties which make it an ideal choice for MR imaging; for instance, gadolinium(III) is a highly paramagnetic metal (seven unpaired electrons) and its symmetric S-state results in slow electronic relaxation, all lead to a reduction in the longitudinal relaxation time for bulk water molecules. Therefore, this is very useful for rapid exchange and application to medical diagnosis.

Gadolinium(III) also acts as a  $T_1$  contrast agent by increasing the signal observed, and therefore, in a  $T_1$  weighted image, tissues with short  $T_1$  times (fat) appear bright and water and tumour tissues with long  $T_1$  times appear dark.

Gadolinium(III) contrast agents should have at least one bound water molecule (see Figure 12), which leads to rapid relaxation, and the bulk water molecules will exchange very rapidly.<sup>18</sup> The relaxation can also be affected by other factors such as Gd-H inner distance ( $r$ ), residency time ( $\tau_m$ ), number of inner-sphere water molecules ( $q$ ) and Gd-H outer distance ( $r'$ ), with a tumbling correlation rate ( $\tau_R$ ).

Gadolinium(III) complexes prepared with the ability to accommodate a larger number of water molecules ( $q$ ) have a slower tumbling rate ( $\tau_R$ ) and optimally short water residence ( $\tau_m$ ), which should all lead to an increase in the relaxivity of the contrast agents.

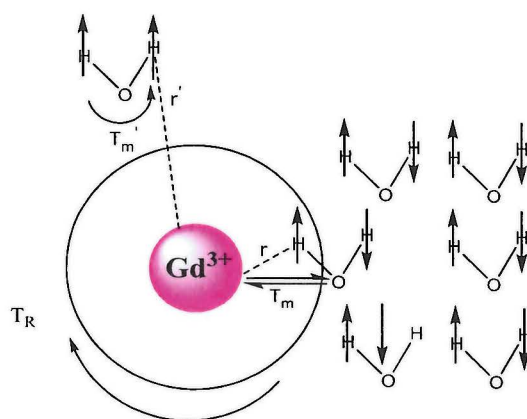


Figure 12 – Schematic of energy transfer from/to a gadolinium(III) based contrast agent leading to an increase in relaxivity.

Decrease in the proton relaxation time in the solution is obtained by the addition of paramagnetic agents. The preferred element in the periodic table is Gd because of its seven unpaired electrons and symmetric electronic state. Despite these ideal properties, gadolinium cannot be used as free ions due to the high level of toxicity that comes from the free Gd(III) ions; therefore organic ligands always need to be tightly bound to the single gadolinium ion to prevent toxicity.<sup>12</sup>

Most gadolinium(III)-based imaging contrast agents are based on the cyclic or macrocyclic ligands such as  $L^4$  or  $L^5$  respectively (see Figure 13), which contain eight donor atoms, allowing one water molecule to interact directly with the nine-coordinate gadolinium.<sup>12,19</sup>

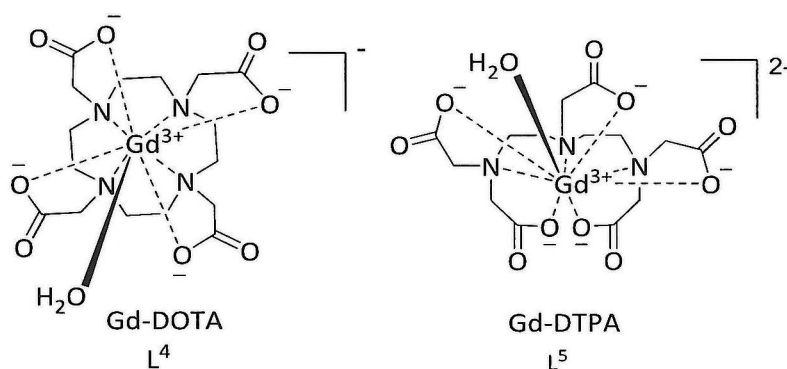


Figure 13 – Chemical structures of  $[GdDOTA(H_2O)]^{2-}$  ( $L^4$ ) and  $[GdDTPA(H_2O)]^{1-}$  ( $L^5$ ).

A different MRI contrast agent which is also clinically approved is Gd-HP-DO3A (ProHance) ( $L^6$ ), this complex has seven donors from the macrocyclic gadolinium(III) non-ionic complex, with two coordination sites available for the water binding. Gd-DOTA ( $L^4$ ) and Gd-HP-DO3A both show greater stability compared with Gd-DTPA-BMA ( $L^7$ ) due to their macrocyclic effect (see Figure 14); therefore, the chances of releasing the free toxic gadolinium(III) ion are reduced.<sup>20-22</sup>

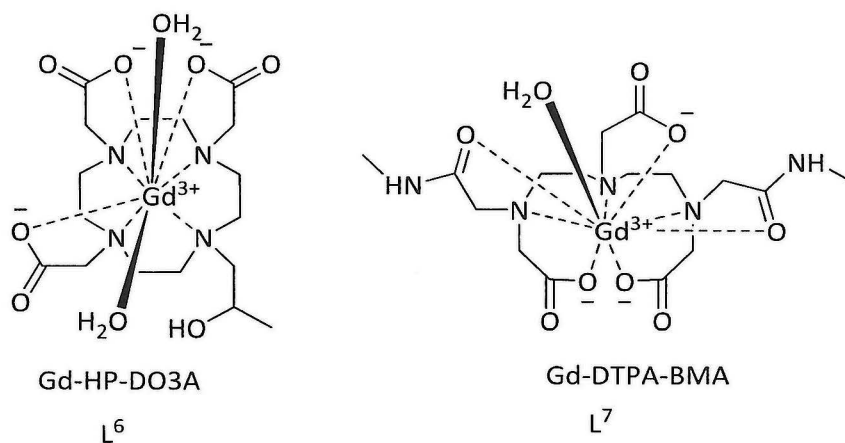


Figure 14 – Common MRI contrast agents used in clinics.

### 1.2.1.3 Stability of Gd complexes

Most of the chelates that are commonly designed are based on macrocyclic or linear units, with chelators such as DOTA and DTPA. They both show high stability of lanthanide complexes, for the dissociation rates under acidic conditions.<sup>23,24</sup> The dissociation rate of the linear chelates can be defined as acid-catalysed behaviour, and thus rates should become considerably slower at neutral pH; the monoprotection and the deprotonation are the first steps. The dissociation in macrocyclic ligands is initiated by protonation at one of the acetate arms, and, when the nitrogen(s) becomes protonated, the gadolinium(III) cannot occupy the macrocyclic cavity, which will offer a good chance of complete dissociation from the ligand.<sup>25</sup> The gadolinium contrast agents can be made charged or neutral by the mixed use of carboxyl groups (negatively charged groups) and non-ionic groups such as amides or alcohols. The neutral Gd-DO3A based ( $L^8$ ) example related to the stable ionic-macrocyclic chelators is stable, while the gadoversetamide ( $L^9$ ) example on the non-ionic linear chelates is the least stable agent (Figure 15). Nephrogenic systemic fibrosis (NSF) can be initiated by using low stability Gd-CAs which are likely to undergo transmetallation and will lead to the release of free gadolinium(III) ions and their deposition inside the tissue and thus attract circulating fibrocytes, causing the process of fibrosis to start.<sup>26</sup>

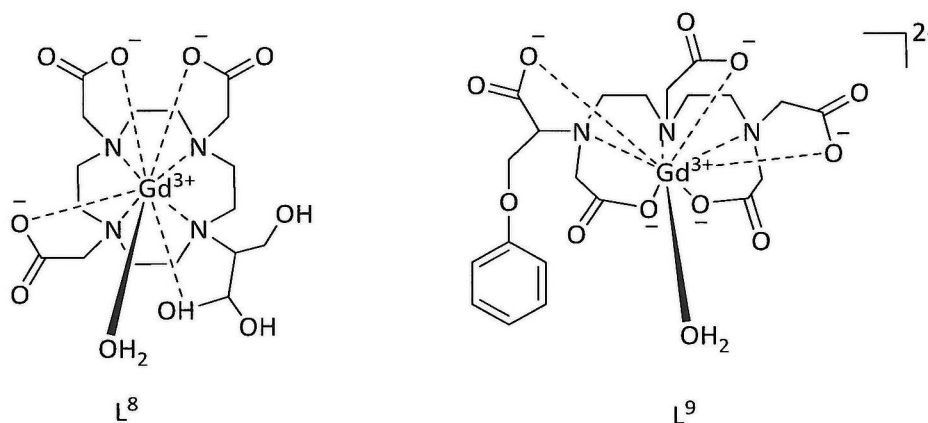


Figure 15 – Some contrast agents with a gadolinium(III) centre that are licensed for clinical use macrocyclic (left), linear (right).

Chelation can be defined as the binding between the ligand and metal ion, and these ligands work by modifying and controlling the properties of the metal ions in biological systems.<sup>27</sup> As mentioned previously, the high toxicity of the free gadolinium(III) and the reason behind toxicity is the ability of the gadolinium ion to be dislocated with calcium ions which exist in

many peptides and enzymes in the body, resulting in disabling their functionality. Therefore, most of the gadolinium(III) complexes (contrast agents) based on macrocyclic or linear ligands should have high levels of thermodynamic stability and kinetic inertness to be clinically approved. Once the contrast agents are injected into the blood stream, the zinc ion which is present in high concentrations in the blood will compete with gadolinium, leading to the release of gadolinium(III) ions from this process in small doses. These will attach to endogenous anions such as carbonate, phosphate, hydroxide and citrate and will then be deposited in tissues and initiate NSF issues,<sup>12</sup> while the zinc(II) chelate will be excreted with the urine, and the patients with renal clearance will be at risk of NSF leading to thickening of the skin and destruction of most vital organs, such as kidneys, heart, liver and lungs.<sup>28</sup>

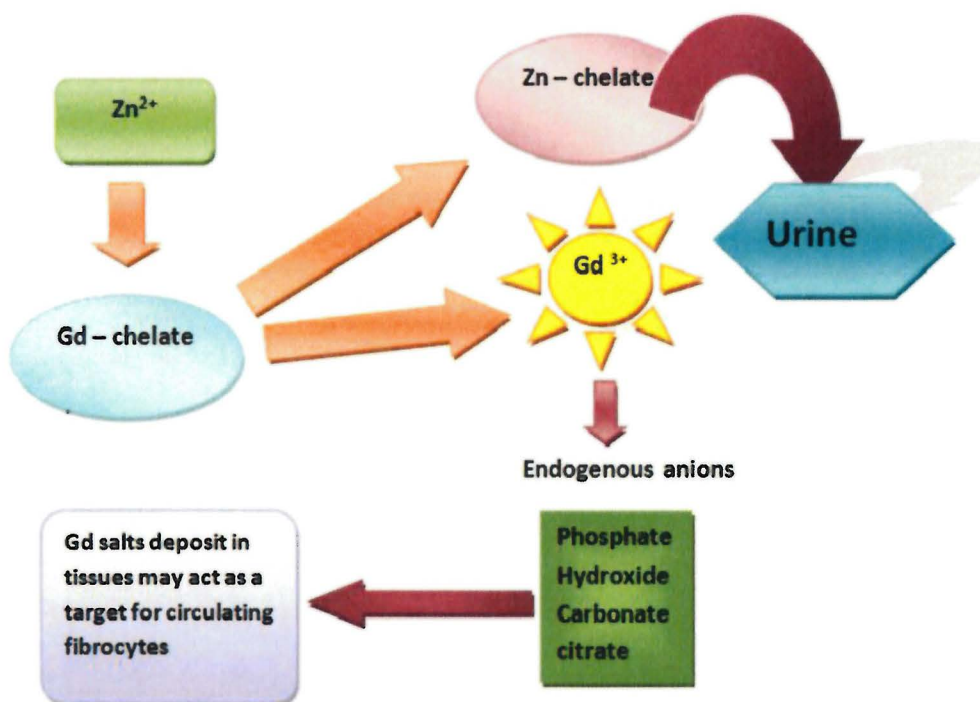


Figure 16 – A diagram of the transmetallation between gadolinium(III) and endogenous cations such as zinc (Zn<sup>2+</sup>). The zinc replaces the gadolinium(III) of the chelate and is eliminated from the body in urine as zinc chelate. The gadolinium(III) combines with endogenous anions and is deposited in tissues.

## 1.2.2 Optical

For many years, optical imaging has been widely used for biomedical research, to study mammalian biology in depth and to make the cellular processes easy to see inside living subjects. However, the utility of optical imaging is still limited in clinical use, because of limitations of light penetration of mammalian tissue; therefore, it is usually reserved for the study of small animals. Optical imaging of the small molecules can be categorised into two groups: lanthanide luminescence and optical dyes.<sup>29,30</sup>

### 1.2.2.1 Optical dyes

The molecules which absorb light convert the excitation of these molecules from a lower to a higher energy state are called optical fluorescent or luminescent dyes, and after that the molecule will return to the ground state, causing emission of light. The excitation energy is higher than the emission energy because of the energy lost during the process of luminescence/fluorescence (absorption-to-emission), which is also different from the emitted wavelength. This process will be repeated many times in the same molecules catalytically, and then, through the effect of photobleaching, the molecule will degrade.<sup>31</sup>

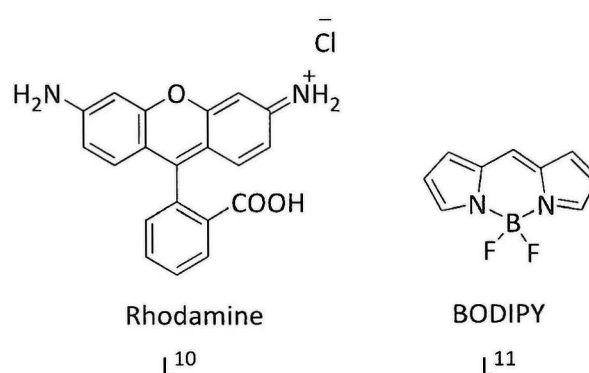


*Figure 17 – Chemical structures of commonly used organic dyes BODIPY and rhodamine.*

In many biological applications there are common dyes that have been used, such as rhodamine (L<sup>10</sup>) and boron dipyrromethenes (BODIPY) (L<sup>11</sup>), see Figure 17. This type of dye has some advantages in these applications, for example they are known to be taken up into cells, and the rhodamine agents are used to target mitochondrial function as hydrophobic cation agents which give apoptotic information using confocal microscopy.<sup>32,33</sup>

### 1.2.2.2 Lanthanide luminescence

Lanthanide cations can be characterised by a low absorption coefficient leading to the low efficiency of the emitting levels of the metal centre via direct excitation. However, the coordination between the lanthanide ions and the solvents could lead to non-radiative pathways for return to the ground state.

These problems can be resolved by coordinating the lanthanide cations to a suitable chromophore antenna, where the chromophore will absorb the light energy and form excited states in the ligand centre. Through the energy transfer the emitting levels of the cation centre can then become populated.

The ideal ligand would be polydentate and include eight or nine donor atoms to make sure that the metal ion has a full first coordination sphere. This will help to limit solvent molecules binding to the metal and cause quenching of luminescence.<sup>34</sup> Therefore, the chromophore will absorb the excitation photons, which is followed by energy transfer to the metal centre, and in the end the metal centre will sensitise the lanthanide luminescence (see Figure 18).

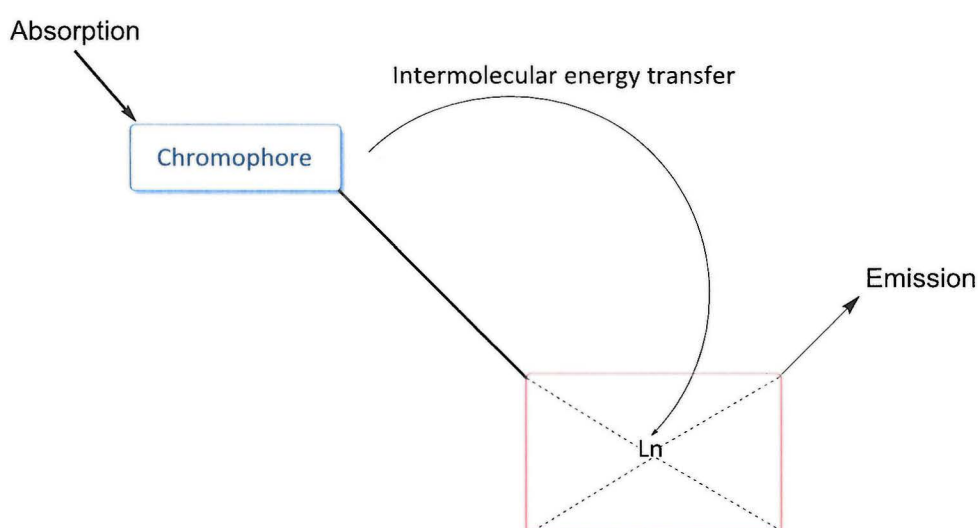


*Figure 18 – Schematic to show the energy transfer processes to sensitise emission.*

The excitation wavelength is known as the wavelength that the molecule absorbs energy at. This wavelength is dependent on the attached chromophore with molecules, while the emission wavelength is known as the wavelength of the energy released from the molecule.<sup>35</sup>

The Stokes shift is represented by the difference between the excitation and emission wavelength. Usually, the absorbed energy of the molecule is lost between the process of absorbing and emitting energy to the metal centre of the complex; therefore, as already mentioned, the emitted energy is always less than the absorbed energy which is required for excitation.

One approach to form an appropriate chelator is attaching the chromophore antenna, which will allow the energy absorbed by ligand to be then transferred to the lanthanide metal centre. In terms of avoiding competition between the biological chromophores and the chromophore antenna in any biological application, the desired chromophore antenna should absorb energy above 300 nm, to contrast with most natural chromophores which absorb energy below 300 nm.<sup>17</sup>

The use of lanthanide complexes has been pursued for use in biological fields because of their large Stokes shift and long fluorescence lifetime. For example, the sensitised europium complex has a luminescence lifetime of about 0.6  $\mu$ s, which is long compared to the 5 ns fluorescence lifetime of BODIPY derivatives. These molecules have the ability to produce fluorescence in background regimes from low to zero, which makes these complexes the perfect choice for use as contrast agents in various biological applications.

Europium(III) and terbium(III) are the most commonly used lanthanides in luminescence experiments because they both have long-lived excited states, and their emission wavelength can be observed in suitable ranges (visible spectrum); europium(III) is emitted in the red and the terbium(III) is emitted in the green region. Generally, an effective luminescence molecule can be built from three important components, which are the macrocycle, the chromophore antenna that is attached to the macrocycle, and the complex with the lanthanide(III) ion; therefore, the formation of lanthanide(III) luminescence must be produced via a process starting with energy absorption via the chromophore antenna and then release to the cation. That process is known as the antenna-to-cation sensitisation process.<sup>17,35,36</sup>

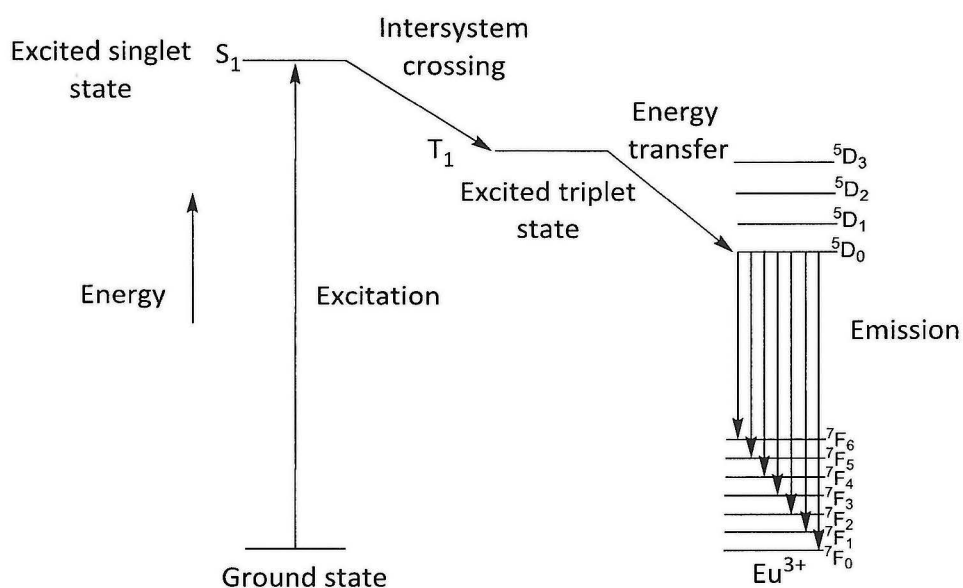


Figure 19 – Luminescence emission processes of a europium chelate.

Basically the emission of the lanthanide via sensitisation can be demonstrated in energy level terms through a Jablonski diagram (see Figure 19). The sensitisation pathway can be initiated when the chromophore antenna absorbs energy in its excited state ( $S_1$ ), which is then transferred to excited triplet state of the chromophore via its intersystem crossing, and then followed by energy transfer to the lanthanide(III) metal ions. Then, when the transition to the ground state of lanthanides(III) metal ions occurs, which will allow metal sensitisation, and the luminescence is initiated. The emission of  $\text{Eu(III)}$  can be seen clearly in Figure 19. The energy will transfer from the triplet state of the antenna to the  ${}^5D_0$  state of the europium(III), and the emission will occur when the internal conversion from europium(III)  ${}^5D_0$  state to ground state  ${}^7F_J$  ( $J = 0-4$ ) happens. This transfer of energy can be quenched by solvents.<sup>37</sup>

### 1.2.2.3 Sensitiser

The most common sensitiser employed are aryl chromophore. The bipyridine derivatives ( $L^{12}$ ) can be considered one of these sensitiser, which have received much attention. This is because of their many applications in medical diagnostic imaging as luminescence labels, as well as their applications in targeted use because of their ability to enhance the solubility of the aqueous media and to couple with biomolecules, as in Figure 20. However, much interest has been recently shown in the use of d-block transition metal (TM) complexes as sensitiser in what are known as d-f hybrid arrays. Rhenium (I) bipyridine complexes can be considered one of the broad range of complexes with very large molar absorption coefficients. In particular the visible part of it leads to intersystem crossing with high yield to the triplet metal ligand charge transfer state ( $^3MLCT$ ) to become the ideal sensitiser with a useful emission level for the lanthanide ions, especially for lanthanide with near IR luminescence. Rhenium showed relatively long luminescence using the  $^3MLCT$  state.<sup>38</sup>

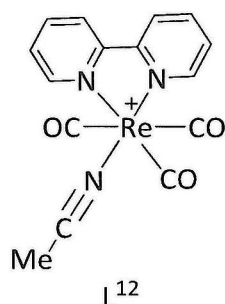


Figure 20 – Rhenium (I) bipyridine chromophore ( $L^{12}$ ).

Typically, there are two ways of the energy transfer process of d-f transition; first, when the Ln(III)-based luminescence causes sensitisation, which can be a clear indication that the energy transfer happened, it makes energy transfer difficult to detect with common detectors that are usually used to measure NIR luminescence because it occurs on a time scale of nanoseconds and these detectors work with a long response, and, second, when the luminescence occurs in the energy donor (d-block) that reduces the luminescence lifetime and results in quantitative information on the energy transfer, which is technically much easier because sensitive, fast detectors are available which are able to work when the energy transfer rises to 100 ns in order to detect the residual luminescence lifetime in the nanosecond timescale.

#### 1.2.2.4 Lanthanide luminescence sensitised by transition metal complexes

A rhenium complex has been used as a chromophore for lanthanide sensitisation in reported research. As is known, the excited state of the transition metal (d-d transition) is Laporte forbidden. A small extinction coefficient ( $\epsilon_{\max}$ ) can be observed to about 20-100  $\text{M}^{-1}\text{cm}^{-1}$ ; however, the outer orbital ligand in the transition metal complexes plays a key role in luminescence or charge transfer of these complexes with a different procedure for this process, called a metal-ligand charge transfer (MLCT) and ligand-metal charge transfer (LMCT). Both ways involve the electron transfer from the outer d orbital of the metal and  $\pi/\pi^*$  orbitals in the ligand. In LMCT, the  $\pi$  electrons from the ligand are transferred to the outer d orbitals of the metal; in MLCT, the outer d electrons of the metal are transferred to the  $\pi^*$  orbitals of the ligand. Both of these transitions are allowed and are very intense, having typical  $\epsilon_{\max}$  values of 1000-50,000  $\text{M}^{-1}\text{cm}^{-1}$ .<sup>39</sup>

When the TM is in a low oxidation state, the d orbitals are low lying in energy.<sup>13</sup> This small energy gap between the metal and ligand orbitals allows electron transfer to occur, and therefore MLCT takes place. The energy gap can be further shortened if the  $\pi^*$  orbital of the ligand has a lower lying energy level, or by introducing  $\pi$ -acceptor ligands such as 2-2'-bipyridine.<sup>40</sup> The accessible MLCT states can either be singlet ( $^1\text{MLCT}$ ) or triplet states ( $^3\text{MLCT}$ ). The latter are more desirable as they are longer lived and therefore exhibit a longer luminescence lifetime.<sup>41</sup> Many researchers<sup>42,43</sup> have reported novel luminescent lanthanide complexes produced by joining a chromophore with macrocycle ligands to a sensitising rhenium bipyridine chromophore with lanthanide DO3A -based complexes ( $\text{L}^{13}$ ),<sup>44</sup> as shown in Figure 21.

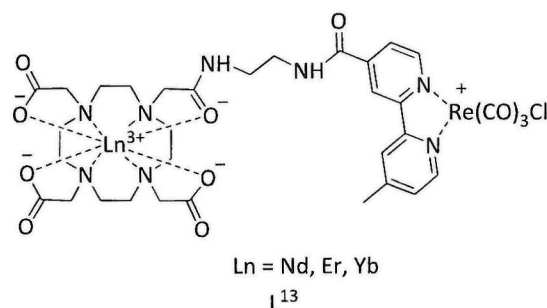
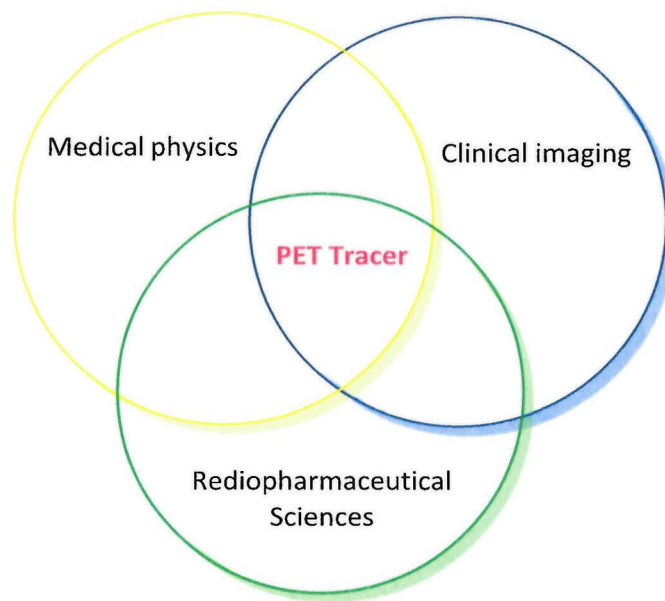


Figure 21 – Lanthanide complexes based DO3A with rhenium bipyridine chromophore attracted ( $\text{L}^{13}$ ).

### 1.2.3 Radiopharmaceuticals

Radiopharmaceuticals can be identified as radiolabel molecules (drugs) and are designed for in vivo application to deliver diagnostic or therapeutic doses of ionising radiation to specific targets, mostly cancer tumours. These type of molecules can be used for the imaging or treatment of cancer cells. Diagnostically, these radiopharmaceuticals can facilitate visualisation of these functional processes in vivo. Any abnormal function produced as a result of pathological change at molecular level can conceivably be visualised with suitably designed radiopharmaceuticals.

Three major disciplines collaborate closely to allow the successful application of radiopharmaceuticals in PET/CT imaging techniques: medical physics, clinical imaging, and radiopharmaceutical science<sup>45,46</sup> (see Figure 22).



*Figure 22 – Schematic illustration of the interaction of the three major disciplines.<sup>45</sup>*

Positron emission tomography (PET) tracers play a role in producing the basis for signal detection via radionuclides, which provide both imaging quality and clinical interpretation. Most of these isotopes used in PET are short lived positron-emitting nuclides and are summarised in Table 1 below.

Nuclide	Half-life	Nuclide	Half-life
F-18 (F <sup>-</sup> )	110 min	O-15	2 min
F-18 (F <sub>2</sub> )	110 min	Ga-68	68 min
C-11	20 min	Rb-82	1.3 min
N-13	10 min		

*Table 1 – Important PET nuclides and their half-lives.*

Basically, PET radiopharmaceuticals consist of two parts, which are a positron-emitting radionuclide and a molecular structure (which can be a ligand for metal radioisotopes). These two components can be connected stably by using a linker (see Figure 23). The vehicle molecules have to offer a high degree of selectivity and specificity in relation to the target area.<sup>45,46</sup>

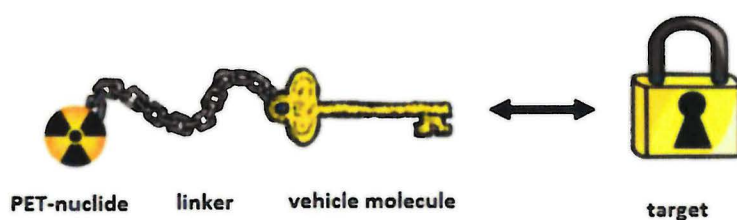


*Figure 23 – Schematic design of a PET radiopharmaceutical and its interaction with the target site.<sup>45</sup>*

The commonly used chelators for metal radioisotopes are DOTA or DTPA, which have been used to form labelled radiopharmaceuticals with useful in vivo kinetics and thermodynamic stability. Mier et al.<sup>47</sup> Synthesised bifunctional chelating agents (BFCAs) based on the DOTA macrocyclic chelator (L<sup>14</sup>) labelled, see Figure 24, and have successfully used them as peptide radiopharmaceuticals for both therapy and diagnosis of tumour disease.

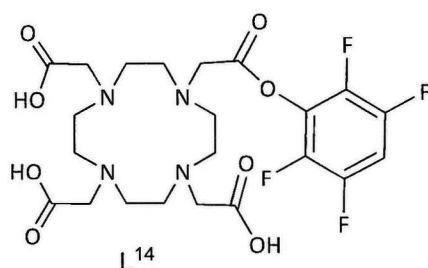


*Figure 24 – Radiopharmaceutical chelator based on DO3A.*

## **Chapter 2**

# **Synthesis of heterocycle functionalised tetraazamacrocyclic chelators**

## 2.1 Aims

This chapter reports the synthesis of functionalised tetraazamacrocycles which have the potential to be used in imaging applications after complexation with various lanthanides (the complex formation reactions are reported in chapter 3), see Figure 25. The first step is the synthesis of the heterocyclic arms based on pyrimidine (pym) and pyrazine (pyz) which contain a reactive halide group, see section 2.2 (step one), and to then prepare the macrocyclic backbone (*t*Bu-DO3A), see section 2.3.2 (step two). The steps of this process are: attachment of the selected heterocyclic arms [pyridine (pyr), pym and pyz], see section 2.3.3, to form DO3A derivatives (step three) and finally deprotection (step four) to reveal the acetate groups for metal ion coordination.

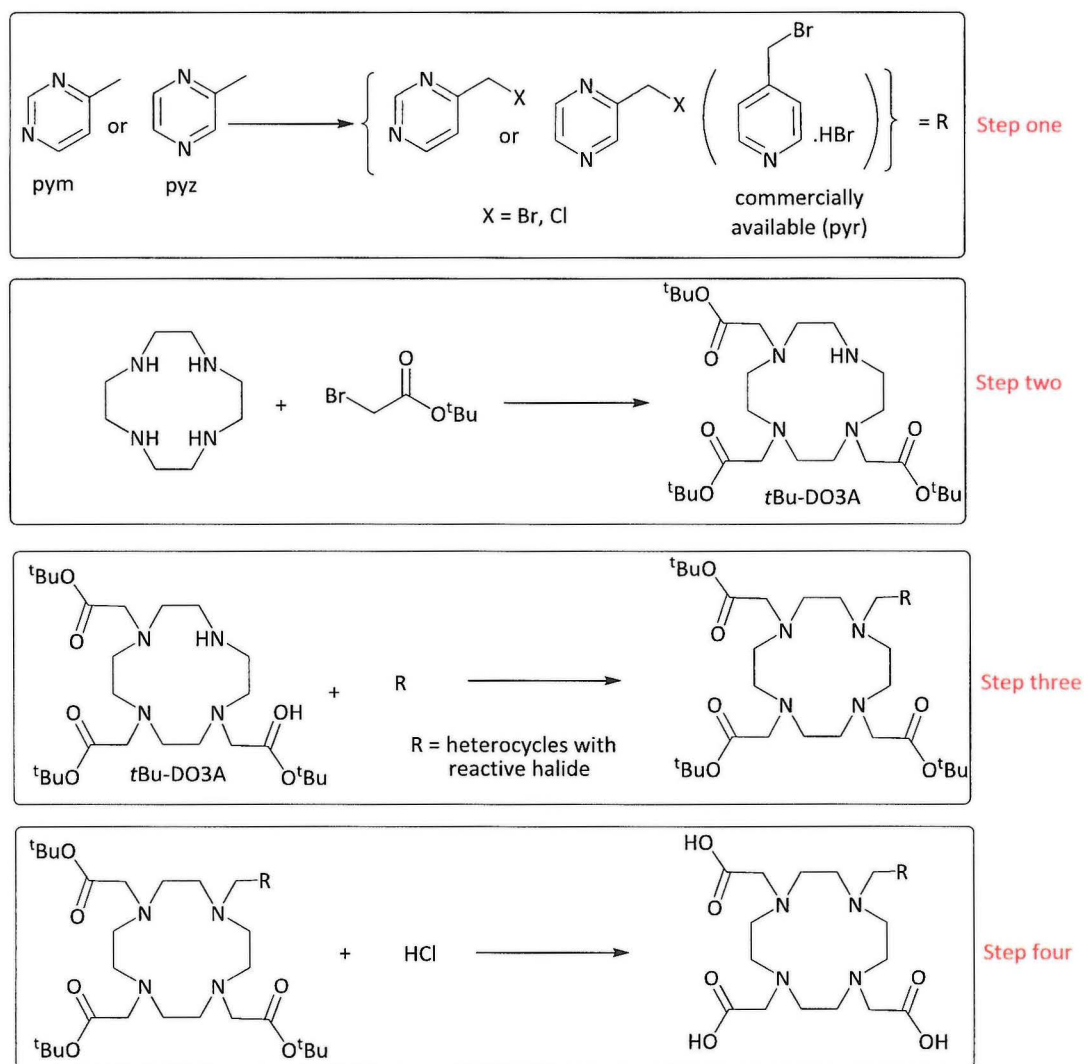


Figure 25 – Proposed schemes for the synthesis of heterocyclic substituted DO3A derivatives.

## 2.2 Heterocyclic pendent arms

This section reports the synthesis of heterocycles (pyrazine and pyrimidine) with alkyl halides as reactive groups for functionalisation. This group of heterocyclic units has been selected because of the following appropriate properties:

1. They contain a nitrogen atom for metal coordination.
2. They can be used as a chromophore, the highly conjugated  $\pi$  system allows energy transfer between the heterocycles via the ligand to metal centre.
3. They include reactive nitrogen atoms which could be functionalised further.

In this work, two heterocyclic alkyl halides (4-chloromethylpyrimidine, 2-chloromethylpyrazine) have been synthesised, while the third heterocycle (4-bromomethylpyridine hydrobromide) used was commercially available, see Figure 26.

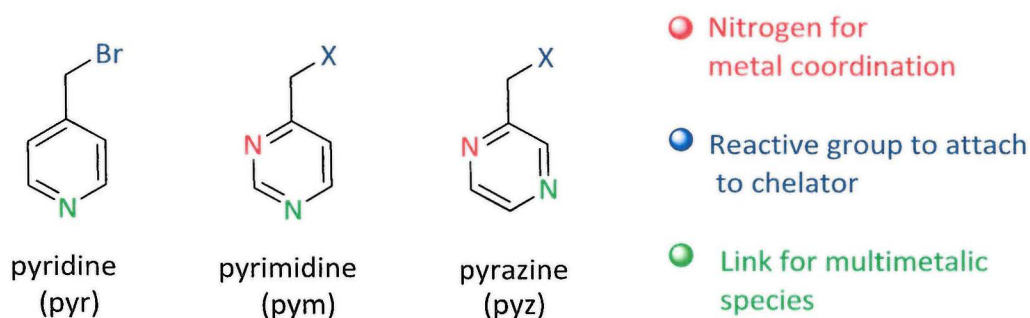


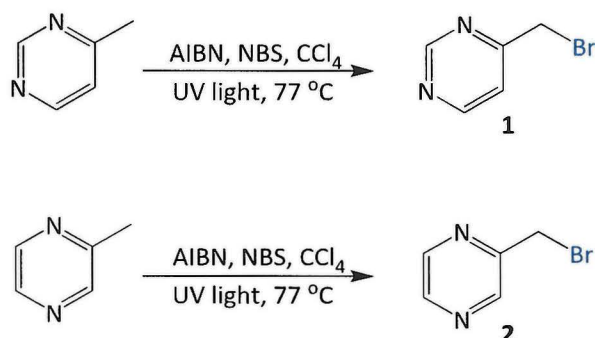
Figure 26 - Annotated molecular structure of heterocycles (pyridine, pyrimidine, and pyrazine).

## 2.2.1 Methods for alkyl halide heterocycle synthesis

N-heterocyclic precursors which terminate with alkyl halides for further reactions with amines on azamacrocycles (<sup>t</sup>Bu-DO3A) were required for this work.

### 2.2.1.1 Bromination reaction of 4-methylpyrimidine or 2-methylpyrazine using N-bromosuccinimide.

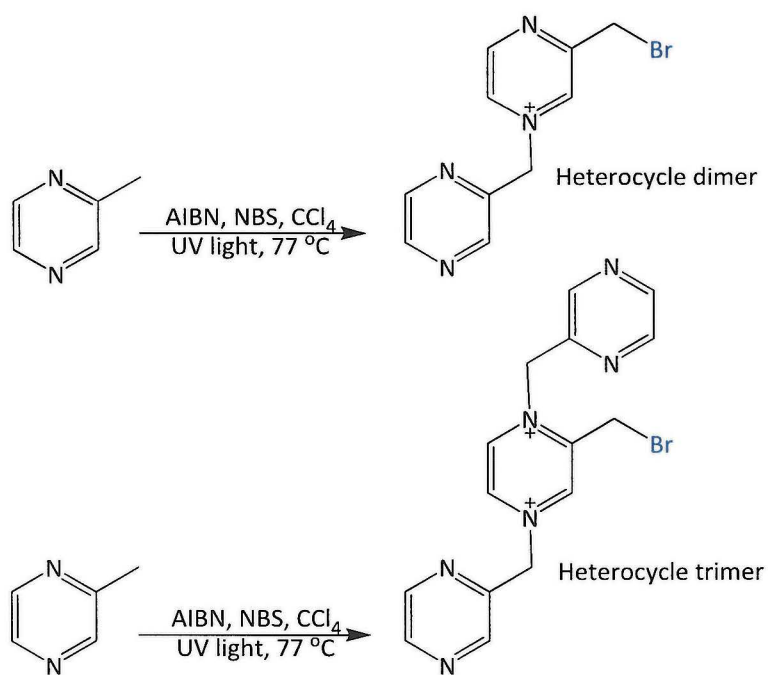
Initially, the formation of an alkyl bromide was attempted to give a good leaving group for nucleophilic substitution. The bromination reactions of heterocycles were carried out using a modified version of the literature method,<sup>48</sup> applied to the bromination of 4-methylpyrimidine and 2-methylpyrazine, see Scheme 1, using equimolar amounts of N-bromosuccinimide (NBS), with azobisisobutyronitrile (AIBN) added as a radical initiator.



*Scheme 1 – Attempted bromination reactions of 4-methylpyrimidine & 2-methylpyrazine to form 1 and 2 respectively.*

The reaction was carried out in carbon tetrachloride under argon with heating to reflux overnight using a UV lamp placed next to the reaction vessel as an initiating light source.<sup>49</sup>

In general, radical initiators such as AIBN are not stable to light, therefore they need to be stored under suitable conditions away from the light and in the refrigerator.<sup>49,50</sup> After heating to reflux, the solvent was evaporated under reduced pressure giving a black oily crude material, the <sup>1</sup>H NMR and mass spectrum both confirmed that the desired product was not produced using this synthetic procedure. It is postulated that due to the high reactivity of bromide group on the heterocycle unit it is more likely to self react with other heterocycle units forming dimers, trimers or larger oligomers, see Scheme 2. It was therefore believed that alkyl bromides may be too reactive and they were not explored further.

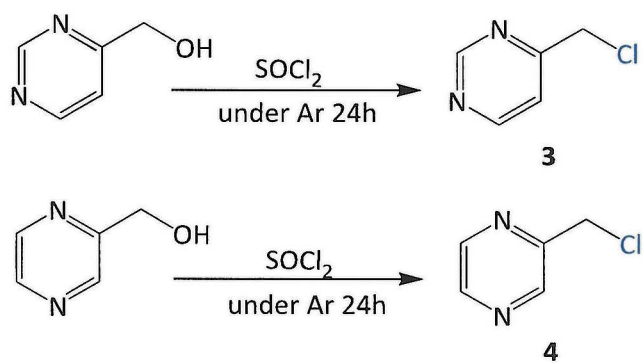


*Scheme 2 - Proposed self-reaction of heterocycles making dimers or trimers, etc.*

### 2.2.1.2 Chlorination reaction of alcohol pyrimidine and pyrazine derivatives with thionyl chloride.

A literature chlorination method was modified for use with these heterocycles,<sup>51</sup> and attempts were carried out to make substitution reactions leading to formation of pyrimidine and pyrazine with alkyl halides. This would give a less reactive halide group (chloro) to prevent the 'self-reaction' from occurring.

The chlorination of a primary alcohol was attempted by treatment with thionyl chloride, the reaction was then stirred for 24 h under argon, see Scheme 3.



*Scheme 3 – Attempted conversion of 4-hydroxymethylpyrimidine and 2-hydroxymethylpyrazine to 4-chloromethylpyrimidine (3) and 2-chloromethylpyrazine (4) respectively.*

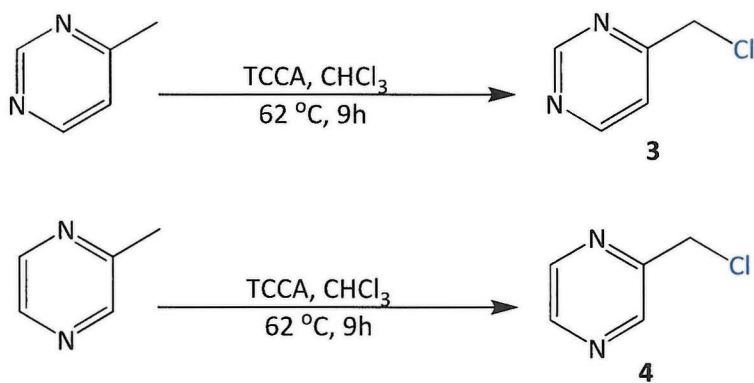
By reaction with thionyl chloride the hydroxyl group was expected to convert to chloride, however the characterisation shows the desired products were not formed by using this synthetic procedure, with the observed peaks in the mass spectrum assigned as fragments of the starting materials, self-reacted heterocycles, and impurities.

### 2.2.1.3 Chlorination reaction of 4-methylpyrimidine or 2-methylpyrazine using trichloroisocyanuric acid.

Subsequently, an alternate chlorination method was sought using cheap commercial reagents and less harsh reaction conditions. A method was found using trichloroisocyanuric acid (TCCA) as the chlorination agent which had been utilised to form 4-chloromethyl pyrimidine previously and this method was followed.<sup>52</sup> This method was then applied to the synthesis of 2-chloromethyl pyrazine.

The synthetic procedure was carried out by using TCCA in this reaction as an effective monochloroisocyanuric agent or electrophilic halogenating agent, which can efficiently work to introduce halogen atoms into electron rich compounds.<sup>53,54</sup>

The reaction was carried out by mixing TCCA in an equal molar ratio of either 4-methylpyrimidine or 2-methylpyrazine in chloroform, see Scheme 4. A non-polar aprotic solvent was used to facilitate the chlorination reaction. The reaction mixture was heated to reflux for 9 h followed by filtration and the solvent was removed *in vacuo*, the crude products were purified by silica gel column chromatography (hexane: ethyl acetate, 2:1).



*Scheme 4 – Substitution reactions of 4-methylpyrimidine and 2-methylpyrazine to form 4-chloromethylpyrimidine (3) and 2-chloromethylpyrazine (4) respectively.*

The <sup>1</sup>H NMR, CHN and the GC-MS analysis showed successful synthesis of the desired products 4-chloromethyl pyrimidine (3) and 2-chloromethyl pyrazine (4) with this method in yields of 48% and 45% respectively. Unexpectedly, the products (3, 4) are air sensitive and they decompose rapidly, therefore it is best to be use them directly after synthesis and purification.

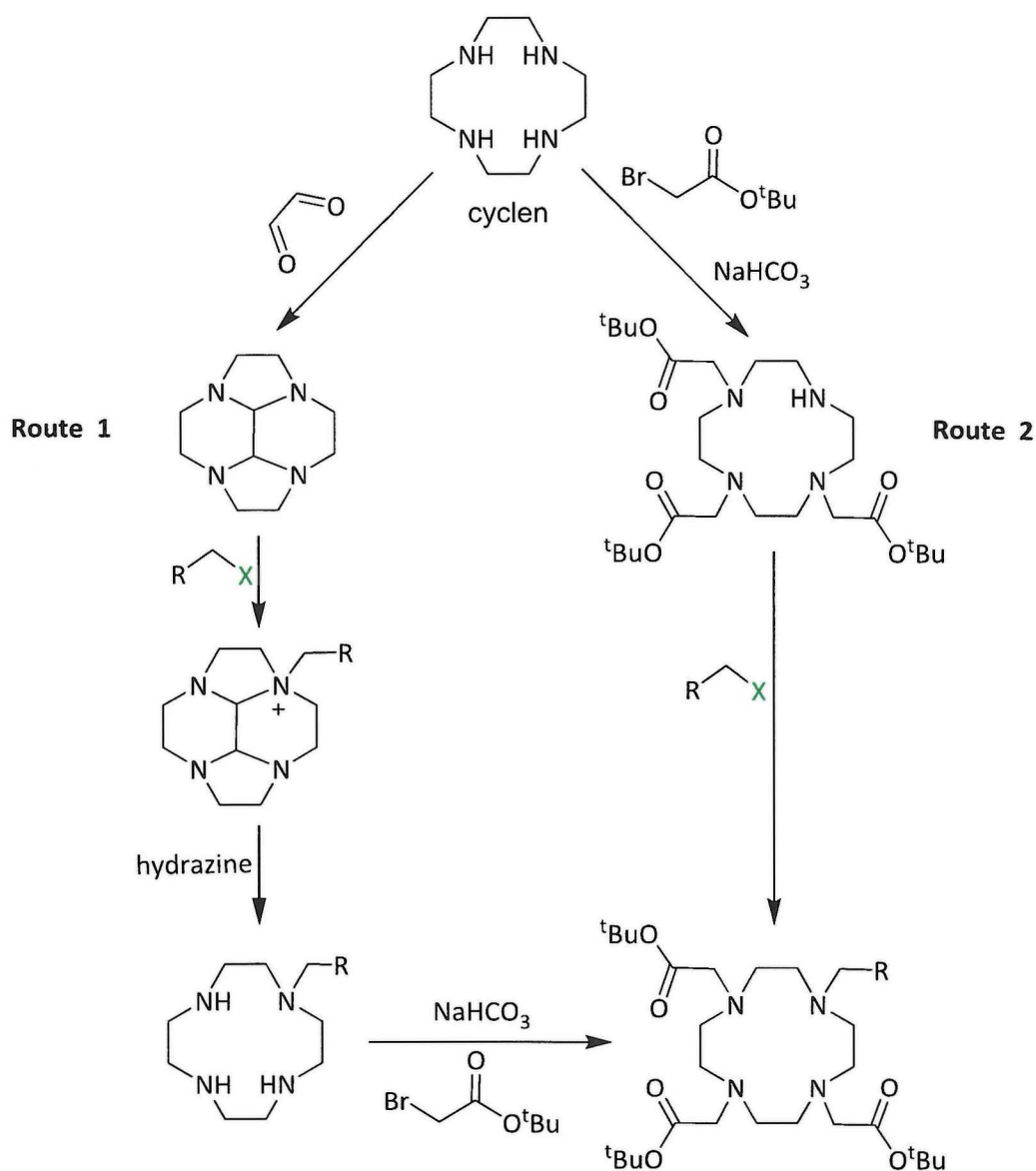


## 2.3 Synthesis of macrocyclic chelators

### 2.3.1 Synthetic methodology to form functionalised DO3A derivatives

1,4,7-Tris(*tert*-butoxycarbonylmethyl)-1,4,7,10-tetraazacyclododecane (*t*Bu-DO3A)

functionalised derivatives are generally synthesised using one of two possible routes, see Scheme 5. Route 1 involves formation of a glyoxal bridge, followed by selective alkylation of a single nitrogen which is favoured due to the folded nature of the bridged cyclen causing only two of the nitrogens to be oriented with the lone pairs pointing out of the formed cavity in a suitable orientation for reaction<sup>55,56</sup>.



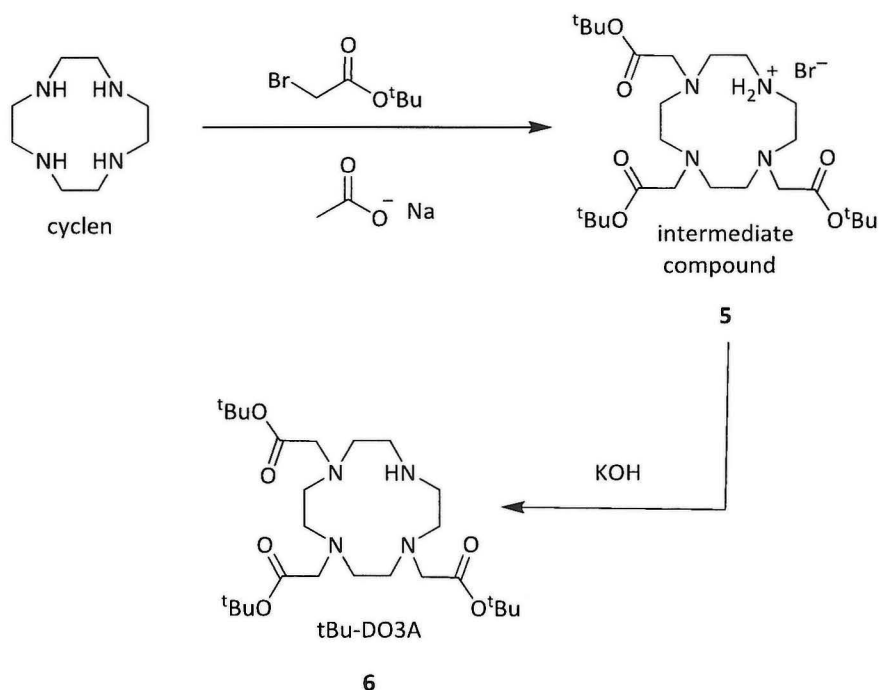
Scheme 5 – Two synthetic methods to produce *N* functionalised *t*Bu-DO3A derivatives.

The appropriate selection of solvent leads the quaternised amino product to precipitate and prevent any further reaction after a single substitution.<sup>57</sup> Hydrazine is used to remove the bridge and expose the remaining secondary amines which can be alkylated to form the desired 3:1 unsymmetrical product.

Route **2** involves selective triple alkylation of the cyclen ring with *tert*-butyl ester protected carboxylic acids, followed by functionalisation of the remaining secondary amine with a different reactive arm to produce the same product as route **1**.

Route **1** has the advantage of giving mono-substituted cyclen in high purity, and so no chromatographic separation is required, but has the disadvantage of low overall yields due to the increased number of steps and the variability in yield dependent on pendant arm selection.<sup>58</sup> While route **2** has the advantage that the synthesis can be done by two easy reaction steps and that will reduce the cyclen losses in the reaction with good overall yields, therefore route **2** was preferred.

### 2.3.2 Synthesis of 1,4,7-tris(tert-butoxycarbonylmethyl)-1,4,7,10-tetraazacyclododecane (*t*Bu-DO3A).



*Scheme 6 - Alternative synthetic route to form *t*Bu-DO3A (6).*

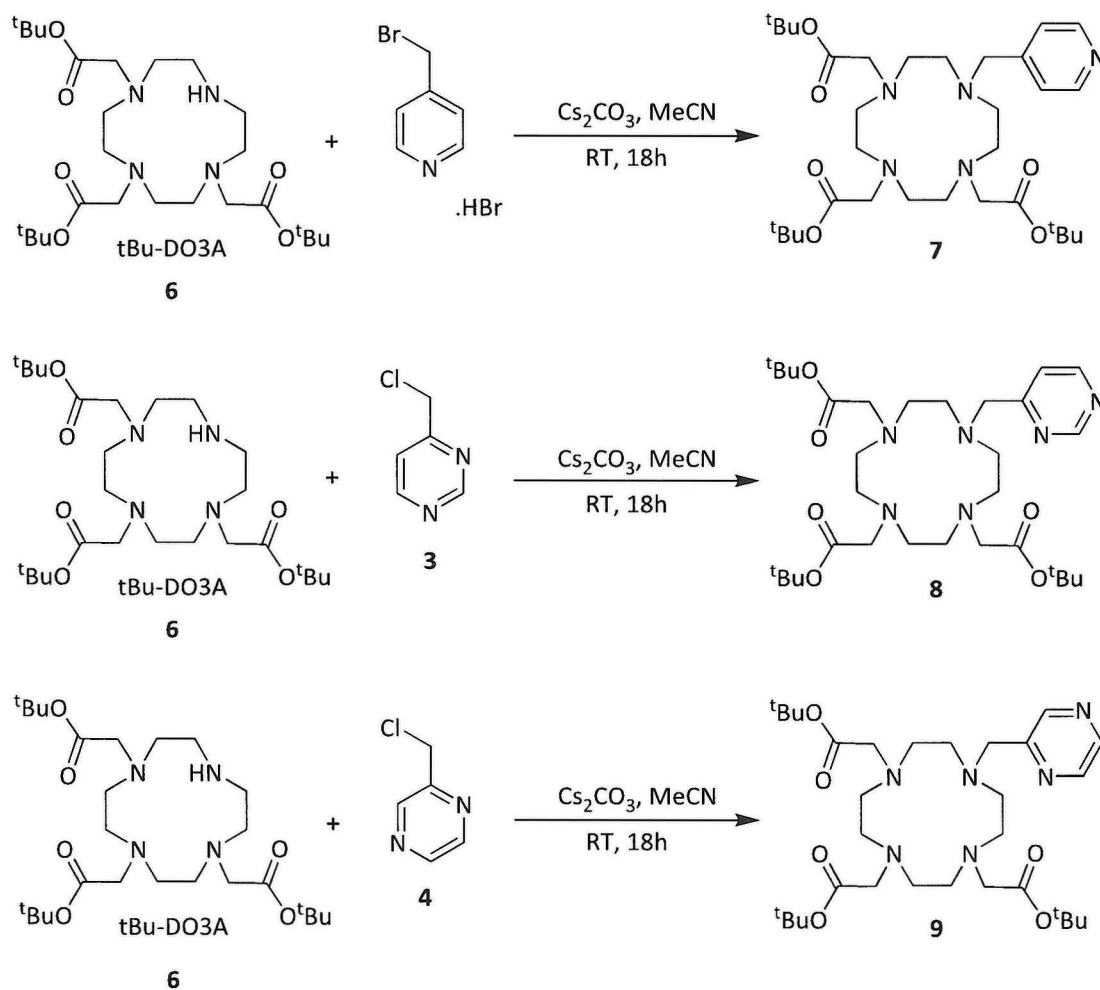
A recently published literature method was used to synthesise *t*Bu-DO3A (6) with no purification methods are needed,<sup>59</sup> which involved a two-step reaction. This was achieved by firstly synthesising an intermediate compound 5 (hydrobromide salt), and secondly proceeding to the desired compound *t*Bu-DO3A (6), see Scheme 6. The reaction conditions to form 5 involved dimethylacetamide (DMA) as the solvent and using sodium acetate as a base, this results in the formation of hydrobromide salt (*t*Bu-DO3A.HBr) (5) after 24 h which, following work up, was isolated in a 77% yield.

The hydrobromide salt (5) is easily converted into *t*Bu-DO3A (6) by dissolving in water at 70°C and adding a 10% aqueous solution of potassium hydroxide in a two-fold excess, which causes 6 to precipitate out in near quantitative yield.<sup>10-12</sup>

The two-step method which goes through a hydrobromide intermediate (5) gives high purity compound as characterised by NMR, CHN and MS in an overall yield of *ca.* 90% yield in 26 h reaction time, without the need for chromatography and has been scaled up to form > 11g of 5.

### 2.3.3 Synthesis of heterocyclic functionalised tBu-DO3A derivatives.

Once tBu-DO3A (**6**) had been synthesised in high enough purity, alkylation of the secondary amine could be performed, in which the two synthesised alkyl halide heterocycles [2-chloromethylpyrazine (**3**) and 4-chloromethylpyrimidine (**4**)] alongside the third heterocycle [4-bromomethylpyridine hydrobromide] are attached to the macrocycle (**6**), see Scheme 7.



*Scheme 7 - Proposed synthetic routes to form N-functionalised tBu-DO3A derivatives with 4-bromomethyl pyridine hydrobromide, 3 and 4.*

This reaction was carried out using a stoichiometric amount of DO3A (**6**) and alkyl halide heterocycles (4-bromomethyl pyridine hydrobromide, **3** and **4**), along with five equivalents of an appropriate base (caesium carbonate) in a large volume of dry acetonitrile to prevent self-reaction that could occur by attaching more than one heterocycle arm together on the ligands (**7**, **8**, **9**), see Scheme 2. Caesium carbonate was used as a base, with caesium(I) being too large

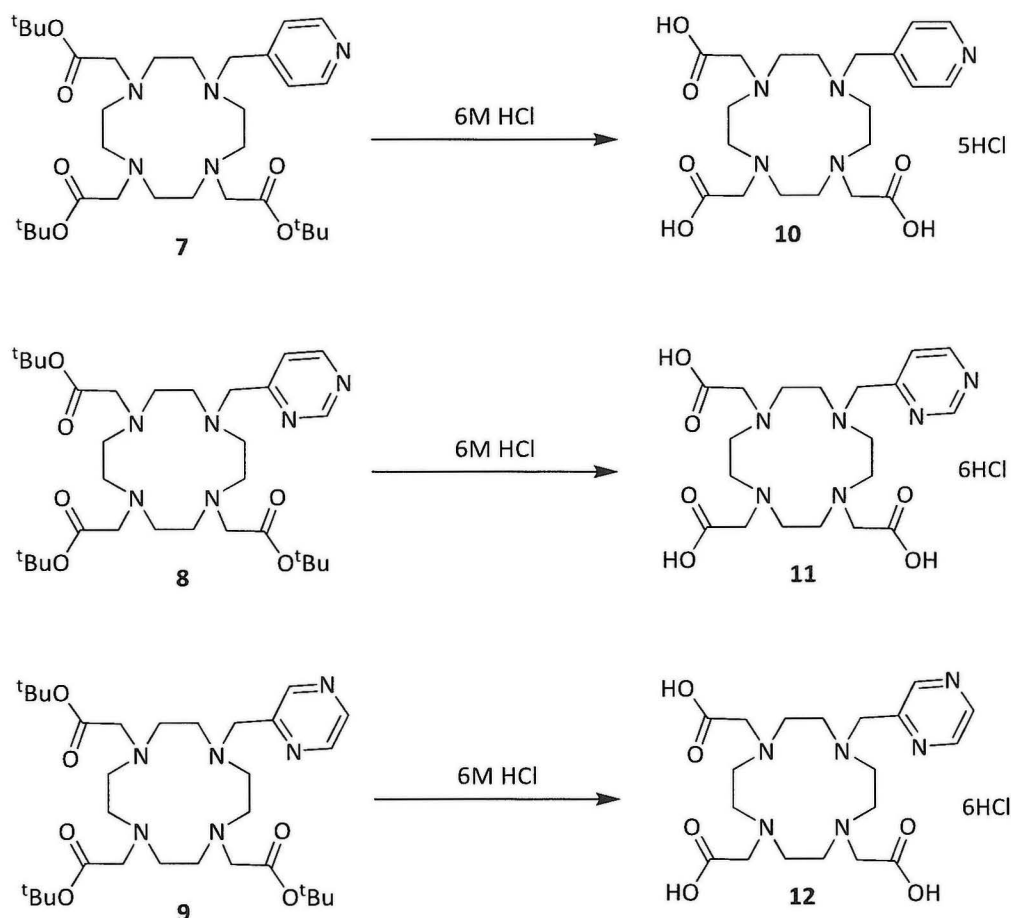
to form complex with the metal ion in the macrocyclic cavity. After the base was added, the reaction mixture was stirred for 24 h under argon at room temperature.  $^1\text{H}$  NMR spectra clearly show the identified peaks of the heterocycles in the aromatic region, while the characteristic peak for the *t*Bu-esters groups in the DO3A (**6**) is at approximately 1.4-1.6 ppm.<sup>58,60,61</sup> All three products (**7**, **8**, and **9**) were fully characterised by NMR and MS analysis with good overall yields of 94%, 92% and 95% respectively.

The most challenging part in these reactions was purifying the products (**7**, **8**, and **9**) before going to next step (deprotection), purifying attempts failed using silica gel or alumina flash column chromatography with several eluent solvents in different gradients. There were difficulties in getting good separation between the crude components as they are very close on the TLC plate. At this stage focus shifted to ensuring the reaction had gone to completion and to avoid chromatography purification. This could be replaced by filtering the products several times to get rid of the base and then directly moving to the deprotection step with aqueous acidic solution, see section 2.3.4.

This worked well as the products (**7**, **8**, and **9**) were also shown to be highly unstable. They are sensitive to the air and decompose very rapidly even under low temperature storage.

### 2.3.4 Deprotection to form heterocycle functionalised DO3A derivatives.

The acid catalysed hydrolysis of esters is a common method used in deprotection of DO3A derivatives and proceeds by heating the reaction mixture to reflux.<sup>62,63</sup> Deprotection of **7**, **8**, and **9**, where the *tert*-butyl ester groups were removed, was initially carried out by dissolving the compounds in 6M HCl and heating the reaction mixture to reflux for 18 h, see Scheme 8. After the water was removed by rotary evaporation, ether was added and decanted multiple times to dissolve and remove any ether soluble impurities.



*Scheme 8 - Formation of pyridine, pyrimidine, and pyrazine DO3A triacid derivatives by hydrolysis.*

The <sup>1</sup>H NMR spectra contained broad and overlapping peaks which makes definitive assignment of these regions difficult, although the peaks that represented the *tert*-butyl groups were no longer present. CHN analysis & high resolution mass spectrometry confirmed the purity and the identity of the products (**10**, **11**, and **12**) with overall yields of 87%, 84% and 82% respectively.

In an attempt to increase the percentage yield of the products and reduce reaction time, the deprotection of the ester groups was achieved more effectively by using a microwave reactor. The desired products were produced by heating the reaction mixture at 130°C with similar purity to overnight reaction product, however in this method the time was reduced from an overnight reaction to 10 minutes reaction and yield was increased for the products (**10**, **11**, and **12**) to be 98%, 96%, and 95% respectively.

This method was the preferred deprotection method for these type of ligands due to the quick synthesis time with high yield.

### 2.3.5 Synthesis of macrocyclic chelators – summary

Heterocyclic (pyr, pym, pyz) functionalised DO3A derivatives with three reactive arms (**10**, **11**, and **12**) have been produced to allow investigation of conditions for complex formation with lanthanide(III) metal ions (chapter 3) to give compounds useful in a variety of biomedical applications, including as contrast agents in MR imaging.<sup>58</sup>

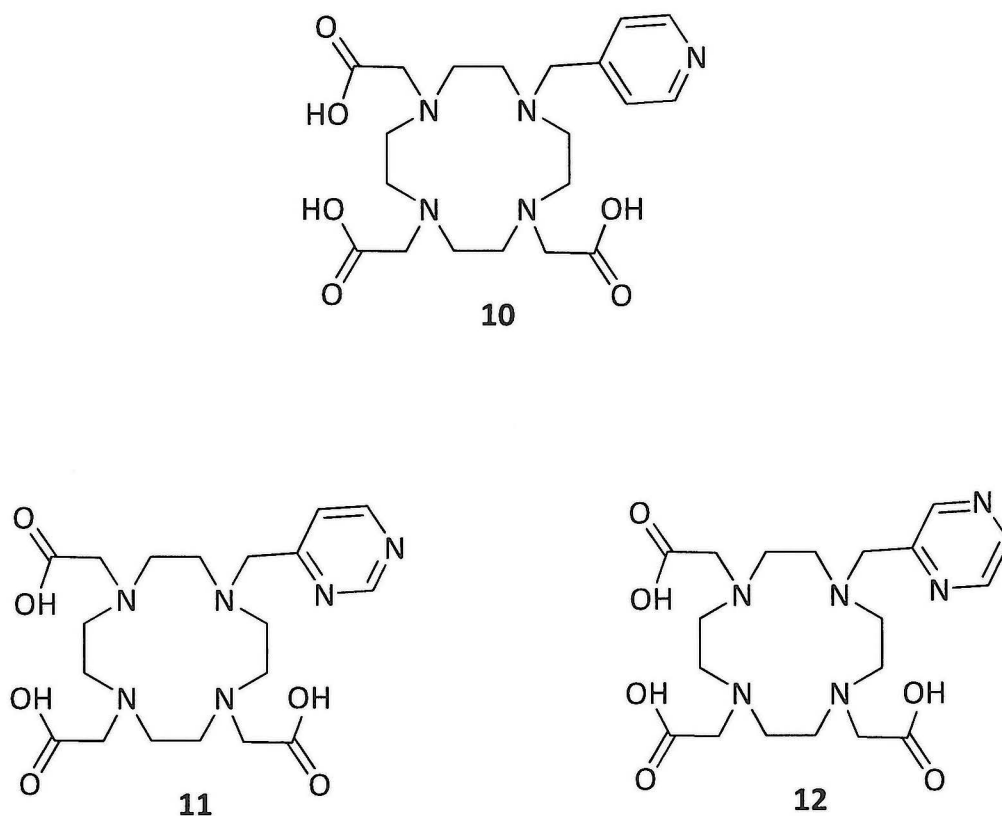


*Figure 28 - Library of chelators prepared for lanthanides complexation.*

The chelators ligands (**10**, **11**, and **12**) have been synthesised in high yields and purity. Two of them are novel (**11**, **12**) and the third one (**10**) is previously described,<sup>64</sup> although synthesized in this work by an alternate method.

The synthesis of the known pyridine chelator (**10**) was repeated because it is needed as comparator for the other two chelators (**11**, **12**) in this research work. **11** and **12** contain different heterocyclic arms (pyrimidine, pyrazine) and the effect of heterocycle N-positions on linked energy transfer processes can be investigated.

## 2.4 $^1\text{H}$ NMR and titration pH speciation studies.

$^1\text{H}$  NMR studies were carried out to determine the effect that pH has on the ligands and the heterocyclic pendent arm by comparing the spectra across a pH range. A good understanding of the nature and the properties of synthesised ligands (**10**, **11**, and **12**) can be also achieved through analysis of the protonation states over a pH range through potentiometric titrations, carried out by titration using tetramethylammonium hydroxide. It is worth considering at what pH the protons in the surrounding environment might start to compete effectively with the lanthanide(III) ions and the N-heterocycle arms (pyridine, pyrimidine, and pyrazine) become protonated, hence are no longer available for coordination. This could be a switch for changing the coordination sphere around the metal ion potentially influencing any energy transfer process or the relaxivity properties at the metal centre.

### 2.4.1 $^1\text{H}$ NMR and pH speciation studies of pyridyl DO3A (**10**)

The  $^1\text{H}$  NMR spectra of **10** were recorded across a range of the pH values from 1.43-12.43 ppm, see Figure 29. In the aryl area there are two doublet peaks regions assigned to protons at the **A**, **B** positions on the pyridyl ring, see Figure 30

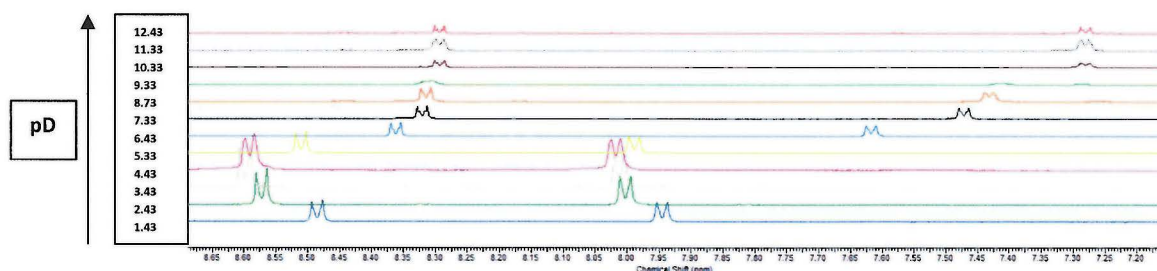


Figure 29 -  $^1\text{H}$  NMR spectrum of chelator ligand **10** shown the effect of pD on aromatic protons.

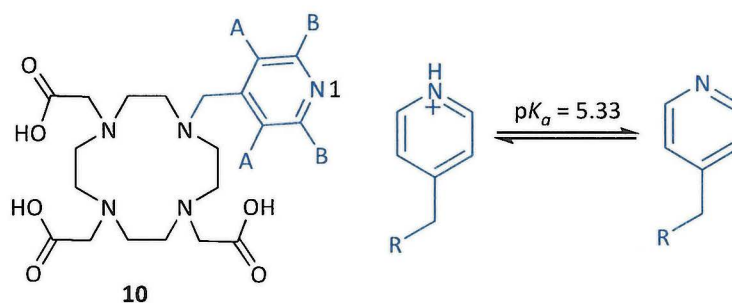


Figure 30 – The pH effect on the 4-methylpyridine arm in chelator ligand **10**.

At pH=1.43 the doublet peak at 7.94-7.95 ppm can be assigned to the protons at position **A**. The second doublet peak at 8.48-8.49 ppm can be assigned to the **B** protons. The doublets integrate to two protons due to the symmetry of the heterocycle.

The substitution position of the pyridine ring means that it cannot coordinate to the metal ion (at least in an intramolecular coordination interaction). The  $^1\text{H}$  NMR peaks show little shift on coordination to a diamagnetic metal centre from the deprotonated form compared to the other chelators (**11**, **12**), because no coordination bonds can be formed from *N*-position of pyridine toward the metal centre.

These doublet peaks show some differences in the peak region associated with varying pH of the sample and can be observed clearly at two different pH values of 2.43 and 5.33. The change was explained as the *N*1-position of pyridine at being protonated pH=2.43. The  $^1\text{H}$  NMR spectra confirmed deprotonation when the sample pH is above 5.33, as the peaks of the

**A** protons that are assigned 7.99-8.01 ppm at the pH = 2.43 move up field to 7.61-7.63 ppm at pH = 6.43.

A similar observation was made for the peaks of the **B** protons at pH=2.43 with a shift from 8.56-8.58 ppm to 8.35-8.37 ppm. The comparison of  $^1\text{H}$  NMR spectra indicates the nitrogen protonation of pyridine was via range of applied pD (1.43 - 5.33) and the deprotonation of the pyridine is observed at pD 5.33 which is corresponded to the protonation constant of the pyridine ring in the literature with a  $pK_a$  of 5.22.<sup>65</sup>

Investigation of the protonation of the pyridine DO3A (**10**) was carried out by potentiometric titration using tetramethylammonium hydroxide as base which determined five protonation constants, see Figure 31.

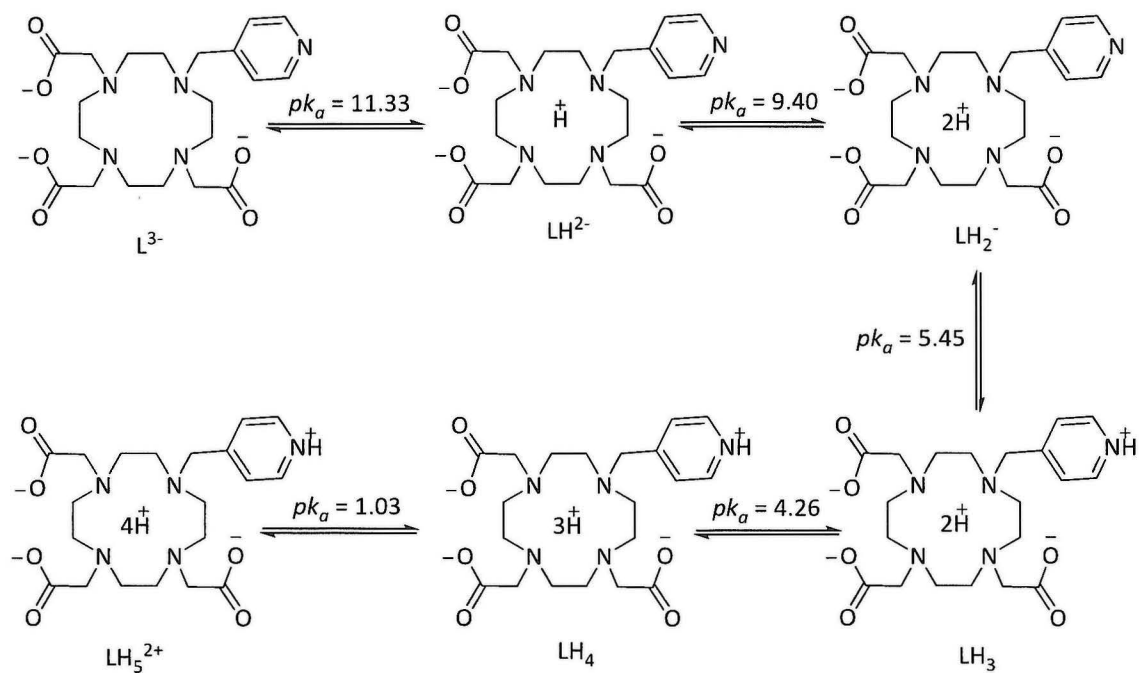


Figure 31 - Protonation patterns of pyridine DO3A (**10**).

The neutral form of **10** is represented at  $LH_3$  and five protonation constants can be determined from potentiometry. The deprotonation of *N*1-pyridine ring determined through speciation studies was correlated with the  $^1\text{H}$  NMR deprotonation studies of **10**. The deprotonation of the pyridyl group (from  $LH_3$  to give  $LH_2^-$ ) occurs at pH 5.45 compared to 5.33 from the NMR studies. This indicates the possibility for this chelator (**10**) to be linked via

coordination of the nitrogen of pyridine at physiological pH or reacted further for other biological applications. The five protonation sites, the pyridyl nitrogen and the cyclen nitrogens. The  $pK_a$  protonation values for pyridine DO3A (**10**) was corresponding compared with N-pyridine derivatives in the literature,<sup>66</sup> see Table 2.

Pyridine DO3A ( <b>10</b> )	$pK_a$	N-pyridine derivatives	$pK_a$
$L^{3-} + H^+ \rightleftharpoons LH^{2-}$	11.3		
$LH^{2-} + H^+ \rightleftharpoons LH_2^-$	9.4		
$LH_2^- + H^+ \rightleftharpoons LH_3$	5.4	AH <sup>+</sup>	5.3
$LH_3 + H^+ \rightleftharpoons LH_4^+$	4.2		
$LH_4^+ + H^+ \rightleftharpoons LH_5^{2+}$	1.0		

*Table 2 - Protonation constants for **10** and literature data for N-pyridine derivative from literature.<sup>66</sup>*

In addition, protonation constants from potentiometric titration can be depicted as a speciation diagram, showing which species are occurring at different pH, see Figure 32. The  $LH_2^-$  protonation state is the major component over a range of pH, including physiological pH. This protonation state has two protonated amines in the cyclen ring with a deprotonated pyridyl chromophore. The completely deprotonated form of **10** is observed with the highest pH value ( $pK_a = 11.33$  for the  $L^{3-}$  form) as would be expected and this is the expected form in complex formation with lanthanide metal ions.

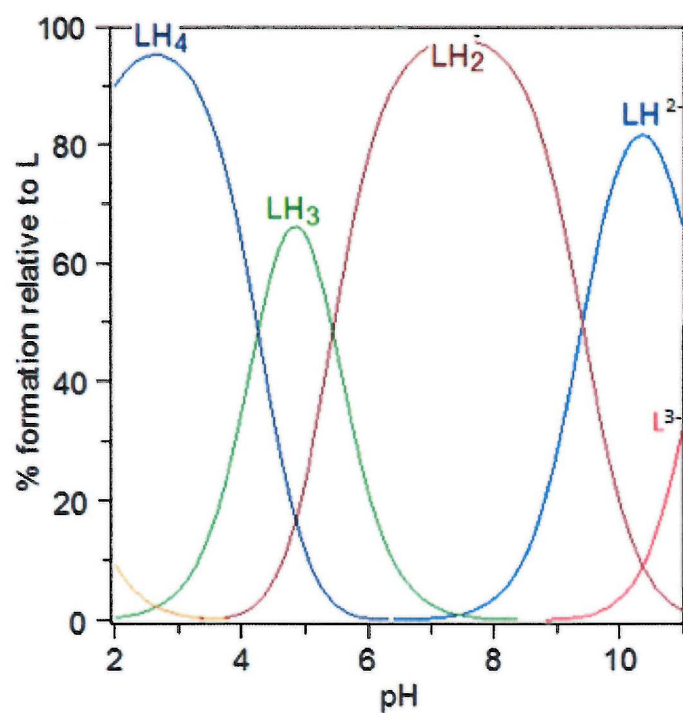


Figure 32 - Speciation diagram of pyridine DO3A (10)

There are literature examples of some different but related N-pyridyl derivative chelators which had shown very interesting properties in several biomedical imaging applications.<sup>62,63</sup> The  $pK_a$  protonation values for the pyridyl DO3A (10) from this work corresponds with N-pyridine derivatives in the literature.<sup>66</sup>

## 2.4.2 $^1\text{H}$ NMR and speciation pH studies of pyrimidine DO3A chelator (**11**).

Analogous NMR and potentiometry studies were carried out on **11** to assess the protonation states.

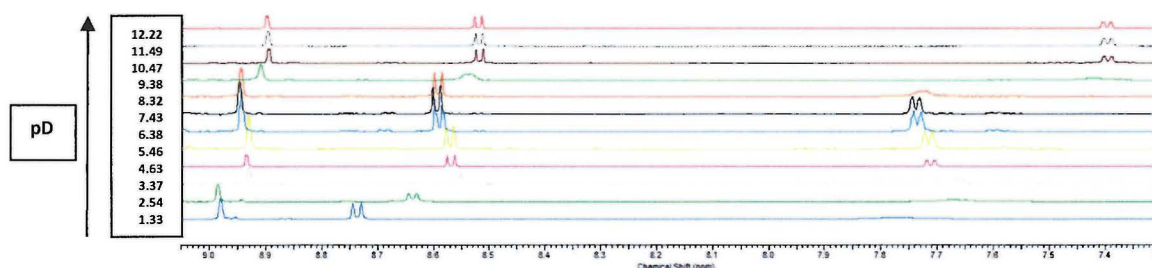


Figure 33 -  $^1\text{H}$  NMR spectrum of chelator ligand **11** shown the effect of pD on aromatic protons.

The  $^1\text{H}$  NMR spectra of **11** were analysed with stepwise increase of the pD values in the range 1.33-12.22 pD, see Figure 33. The group of aryl peaks which appear in  $^1\text{H}$  NMR spectra represent can be assigned to three different protons (**A**, **B**, **C**) on the pyrimidine ring, see Figure 34. The spectra clearly display the two deprotonation stages that can occur at the pyrimidine ring. The positions of these two doublet peaks were significantly shifted at pD = 2.54 to 7.67-7.68 ppm for the **A** protons, and 8.63-8.64 ppm for the **B** protons, indicating the first protonation step of the pyrimidine.

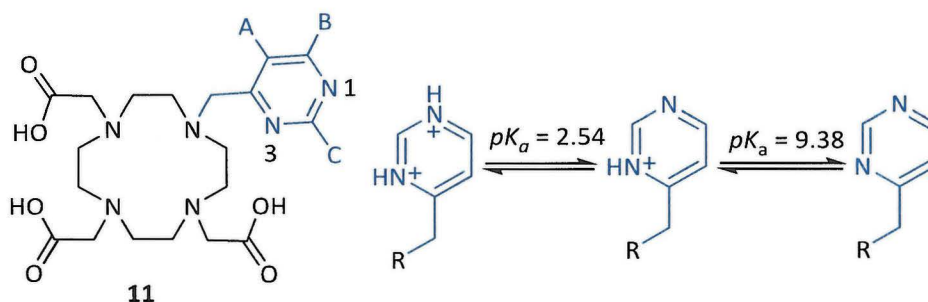


Figure 34 - The pH effect on the 4-methylpyridine arm in chelator ligand **11**.

The second considerable change was at pD = 9.38 in which the **A** and **B** peaks shift to become the two doublet peaks 7.42-7.43 ppm (**A**) and 8.53-8.54 ppm (**B**), while the 8.91 ppm peak assigned as the **C** protons is shifted very slightly to 8.88 ppm. This indicates deprotonation of the second heterocyclic nitrogen. The comparison of  $^1\text{H}$  NMR spectra shows two expected deprotonation stages at the pyrimidine moiety which depends on the pH values of its environment indicating the potential for pH dependent lanthanide luminescence modulation via the sensitisation process from pyrimidine to selected lanthanide(III) metal ions.<sup>67</sup>

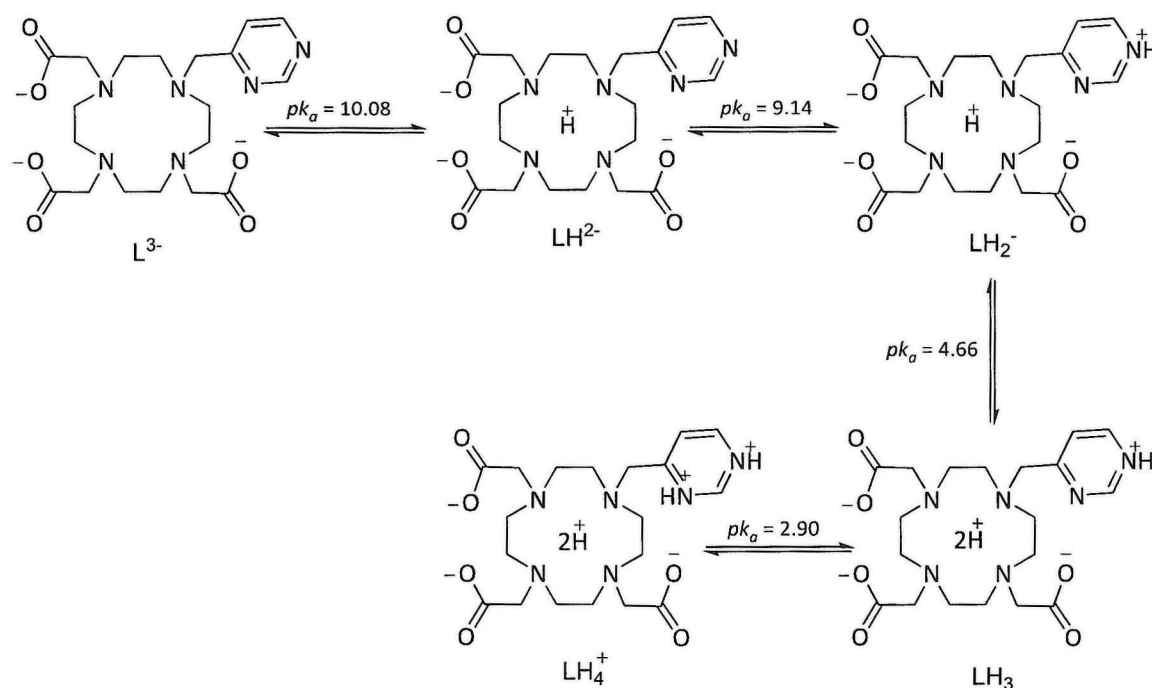


Figure 35 - Protonation patterns of pyrimidine DO3A (**11**).

The  $pK_a$  values for deprotonation *N1* and *N3* of pyrimidine ring were at 2.54 and 9.38 respectively, these results corresponded well to literature results from  $^1\text{H}$  NMR studies for 2,4,6-pyrimidinetriamine reported in the literature by Bernhard *et al.*,<sup>68</sup> where  $pK_a$  values for *N1* and *N3* were 2.53 and 9.43 respectively were determined. Potentiometry studies of this **11** determined four protonation constants, see Figure 35. The ligand and the pyrimidine nitrogen were both protonated at a relatively low  $pK_a$  value and with the second pyrimidine nitrogen protonated at  $pK_a = 2.90$ . This provides an interesting opportunity for this chelator (**11**) to be used in wide range of pH environments (2.90-10.08) for conjugation through its heterocycle linker (pym). The second nitrogen of the pyrimidine ring was deprotonated at  $pK_a = 9.14$  offering the potential for coordination to the metal centre.

Pyrimidine DO3A ( <b>11</b> )	pK <sub>a</sub>	Pyrimidine derivatives	pK <sub>a</sub>
$L^{3-} + H^+ \rightleftharpoons LH^{2-}$	10.8		
$LH^{2-} + H^+ \rightleftharpoons LH_2^-$	9.14	AH <sup>+</sup>	9.80
$LH_2^- + H^+ \rightleftharpoons LH_3$	4.66		
$LH_3 + H^+ \rightleftharpoons LH_4^+$	2.90	AH <sub>2</sub> <sup>+</sup>	2.48

Table 3 - Protonation constants for **11** and literature data for pyrimidine derivatives

The comparison of protonation constants with analogous literature compounds,<sup>68,69</sup> shows two protonation constants for the pyrimidine derivatives corresponded to the results obtained pyrimidine DO3A (**11**), see Table 3.

In addition, the protonation constants from the potentiometric titration data can be depicted as a speciation diagram, showing which species are occurring at different pH values, see

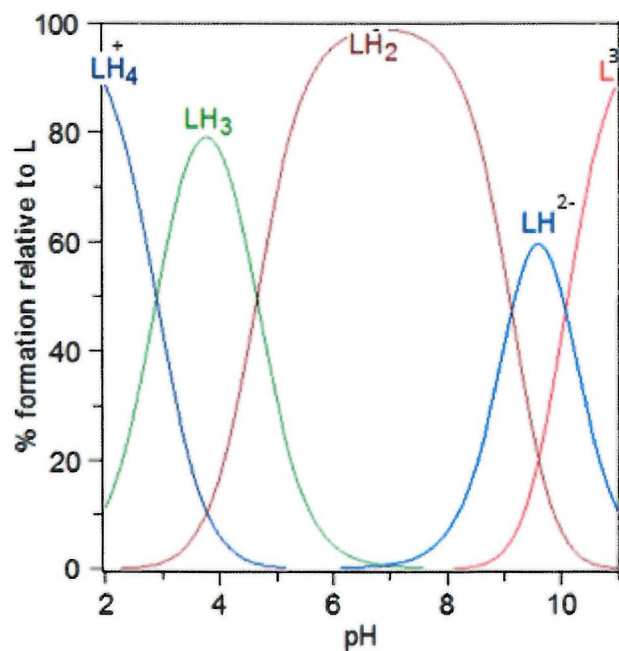


Figure 36 - Speciation diagram of pyrimidine DO3A (**11**).

LH<sub>2</sub><sup>-</sup> is present over a broad pH range (pH 4.66–9.11) with one of the nitrogens in pyrimidine ring protonated. That is will increase the potential for linked species to remain intact under physiological conditions.

The chelator is not fully deprotonated until the  $pK_a = 10.08$  (i.e. all coordinating groups deprotonated). This will be the ligand state that coordinates to the lanthanide(III) ion with the potential for the pyrimidine ring to join the coordination sphere via the *N3*-nitrogen position and/or as a link to a second metal centre through coordination to the *N1*-nitrogen.

### 2.4.3 $^1\text{H}$ NMR and speciation pH studies on pyrazine DO3A chelator (**12**)

The  $^1\text{H}$  NMR study was repeated for chelator **12** to investigate the protonation processes that occur at the pyrazine ring by studying the region of the spectra where the aromatic protons will be present across pD range of 1.43-12.43, see Figure 37.

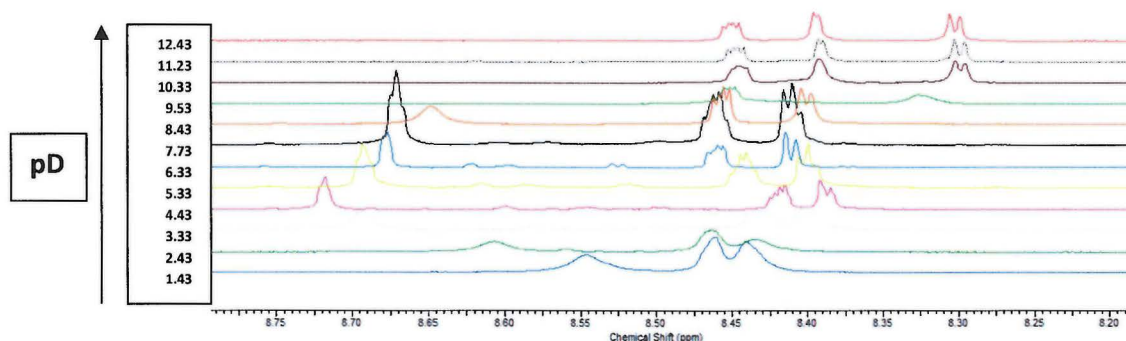


Figure 37 -  $^1\text{H}$  NMR spectra of chelator **12** shown the effect of pD on aromatic protons.

The  $^1\text{H}$  NMR spectra show three peaks regions in the aromatic area representing the three hydrogen atoms (**A**, **B**, **C**) in the pyrazine ring. They appear as two peaks (**A**, **B**) close to each other in chemical shift and the **C** proton peak which shows the greatest change over the pD range, see Figure 38.

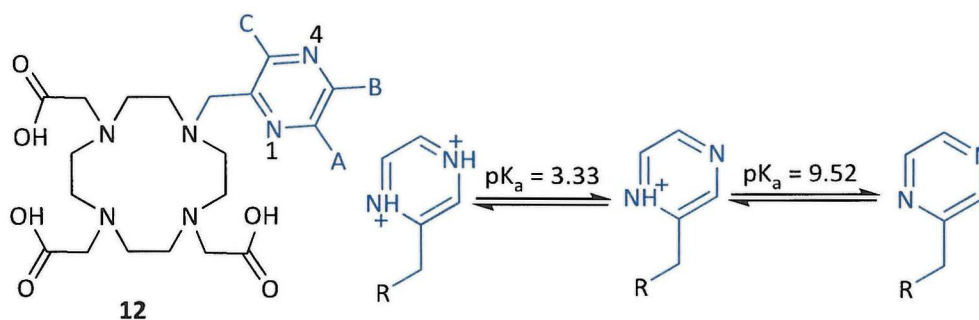


Figure 38 - The pH effect on the 2-methylpyrazine arm in chelator (**12**).

The first deprotonation at one of pyrazine nitrogen atoms is observed at pD = ca. 3.33 with the **A** and **B** proton peaks moving up field from chemical shifts of 8.44 and 8.46 ppm at pD = 1.43 to 8.39 and 8.43 ppm respectively. A more significant shift was seen for the **C** proton with the peak shifting from 8.55 ppm at pD = 1.43 to 8.69 ppm at pD = 3.33. The second deprotonation step at the pyrazine nitrogen atom appears to occur at around pD = 9.53 where both peaks for **A** and **B** protons are shifted up-field. The protonation at the N1-position of the

pyrazine ring would mean that coordination to this nitrogen requires the lanthanide metal centre to compete effectively with the proton and may impact on energy transfer processes for sensitisation of lanthanide luminescence processes. The protonation at the N4-position of pyrazine may disrupt the potential of the linker group (pyrazine) to be further functionalised for any biological targeting applications or to link to another metal containing species via a coordinate bond. Potentiometric titrations, see Figure 39, was carried out for this chelator (**12**) to further understand the effect that changing pH may have on the coordination modes of the chelator and consequences of that on the binding, sensitisation and conjugation of its lanthanide complexes (Chapter 3).<sup>70</sup>

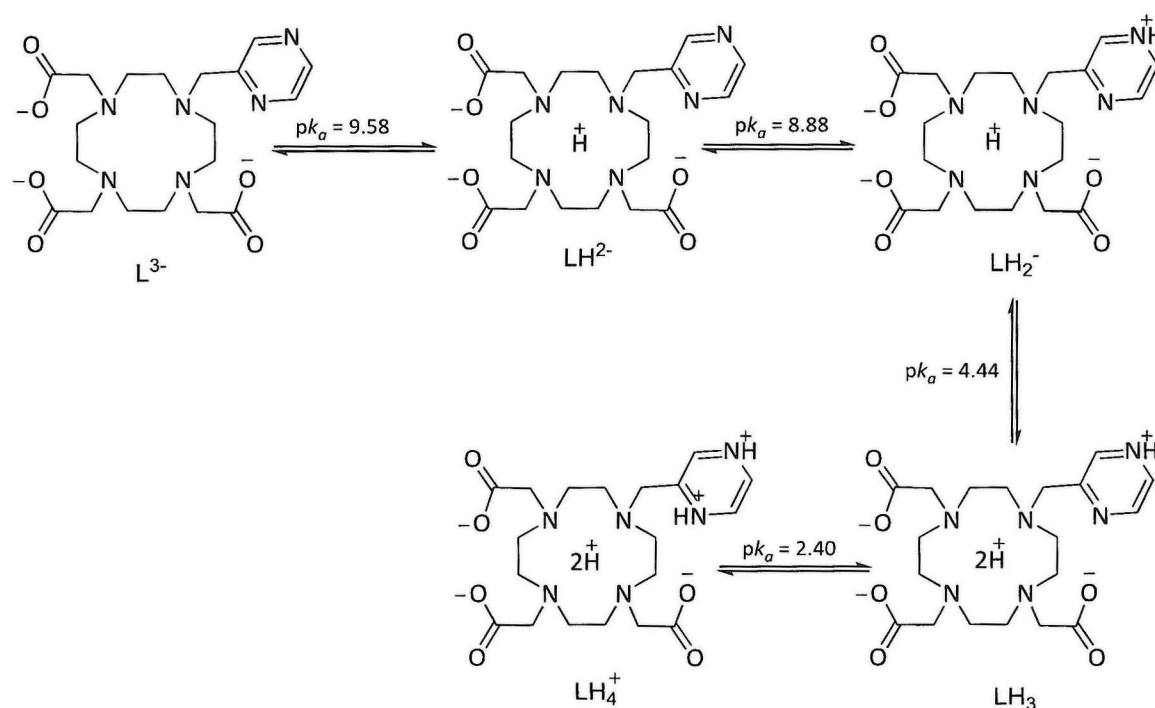


Figure 39 - Protonation patterns of pyrazine DO3A (**11**).

Four protonation constants were determined for **12**, again using tetramethylammonium as base. At a  $pK_a$  of 2.40 the first nitrogen atom of the pyrazine ring is deprotonated, therefore the pyrazine arm (linker) will be available for further functionalization. While the deprotonation process of second nitrogen was starts at  $pK_a = ca. 4.44$  and reaches completion at  $pK_a = 8.88$ . Both of heterocycle deprotonation  $pK_a$  values correspond to literature data for analogous compounds with reported deprotonation of pyrazine derivatives at  $pK_a = 2.72, 8.60$ <sup>71,72</sup> see Table 4.

Pyrazine DO3A ( <b>12</b> )	pK <sub>a</sub>	Pyrazine derivatives	pK <sub>a</sub>
$L^{3-} + H^+ \rightleftharpoons LH^{2-}$	9.58		
$LH^{2-} + H^+ \rightleftharpoons LH_2^{-}$	8.88	AH <sup>+</sup>	8.60
$LH_2^{-} + H^+ \rightleftharpoons LH_3$	4.49		
$LH_3 + H^+ \rightleftharpoons LH_4^+$	2.40	AH <sub>2</sub> <sup>+</sup>	2.72

Table 4 - Protonation constants for **12** and literature examples of pyrazine derivatives.

A speciation diagram was produced for compound **12**, see Figure 40.

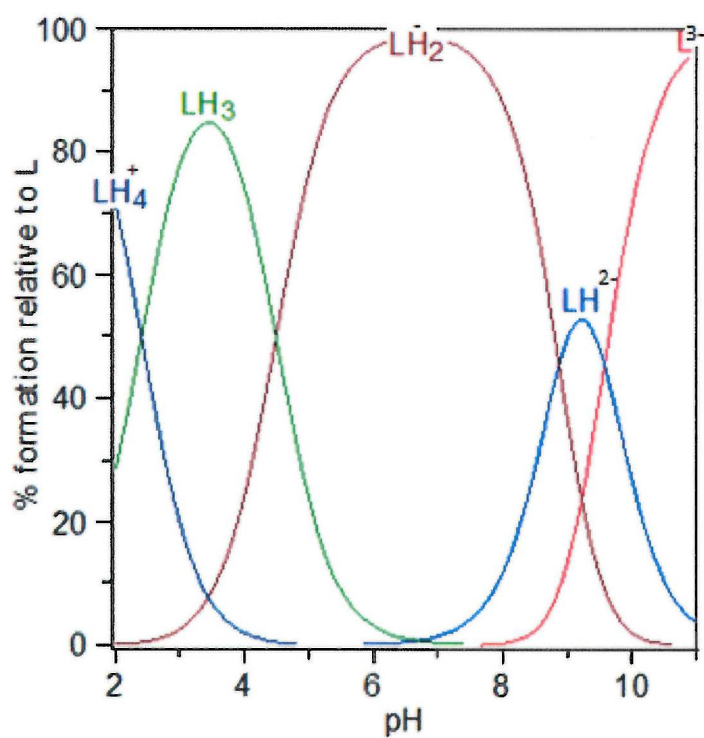


Figure 40 - Speciation diagram of pyrazine DO3A (**12**).

The LH<sub>2</sub> protonation state dominates over a wide pH range (4.49-8.88) of pK<sub>a</sub> values and represents protonation of two nitrogen atoms, one in the macrocyclic cavity and one on the heterocyclic ring.

When comparing **11** and **12**, in **11** the second heterocyclic nitrogen (pyrazine-*N*4) is easier to protonate than the pyrimidine equivalent. On comparing **11** to the pyridyl derivative, the pyrazine known has lower basicity compare to pyridine due to related mesomeric and strong inductive effects to the *N*1 position of the pyridine.<sup>73</sup>

## 2.5 Conclusions

Three novel chelating ligands (**10**, **11**, and **12**), see Figure 41, have been synthesised using three different heterocycles pendent arms (pyridyl, pyrazine, and pyrimidine) respectively, with optimised syntheses developed for the heterocyclic halide precursors.

$^1\text{H}$  NMR and speciation studies were carried out on these three chelators (**10**, **11**, and **12**) to characterise the protonation states of the heterocycles (NMR) and the azamacrocycles (potentiometric titration). This is important as understanding the effect protonation may have on the coordination modes of the chelators and in particular the heterocyclic arms will inform potential applications.

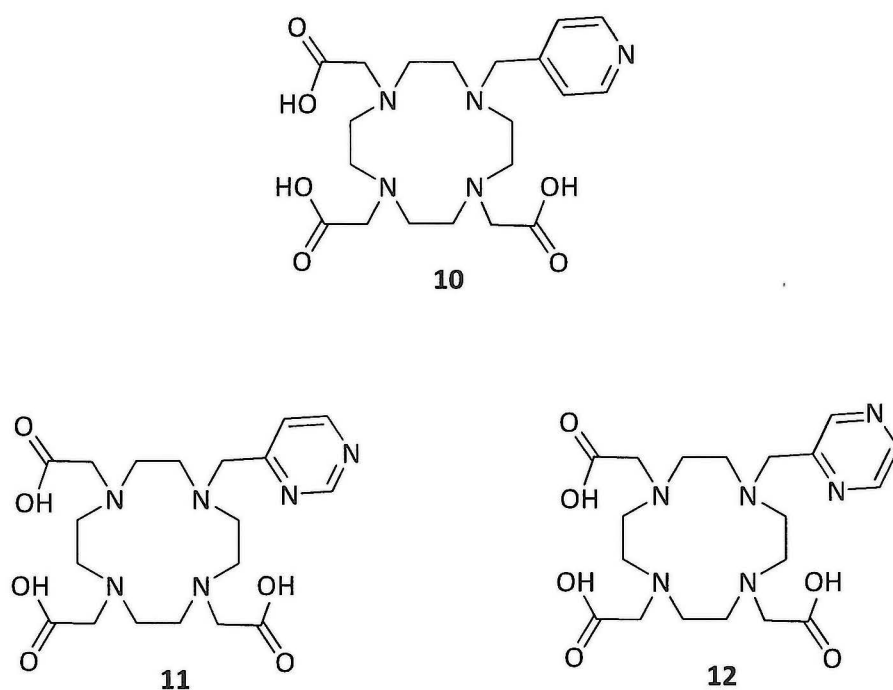


Figure 41 - The three synthesised chelators (**10**, **11**, and **12**) with three heterocyclic arms (pyr, pym, and pyz)

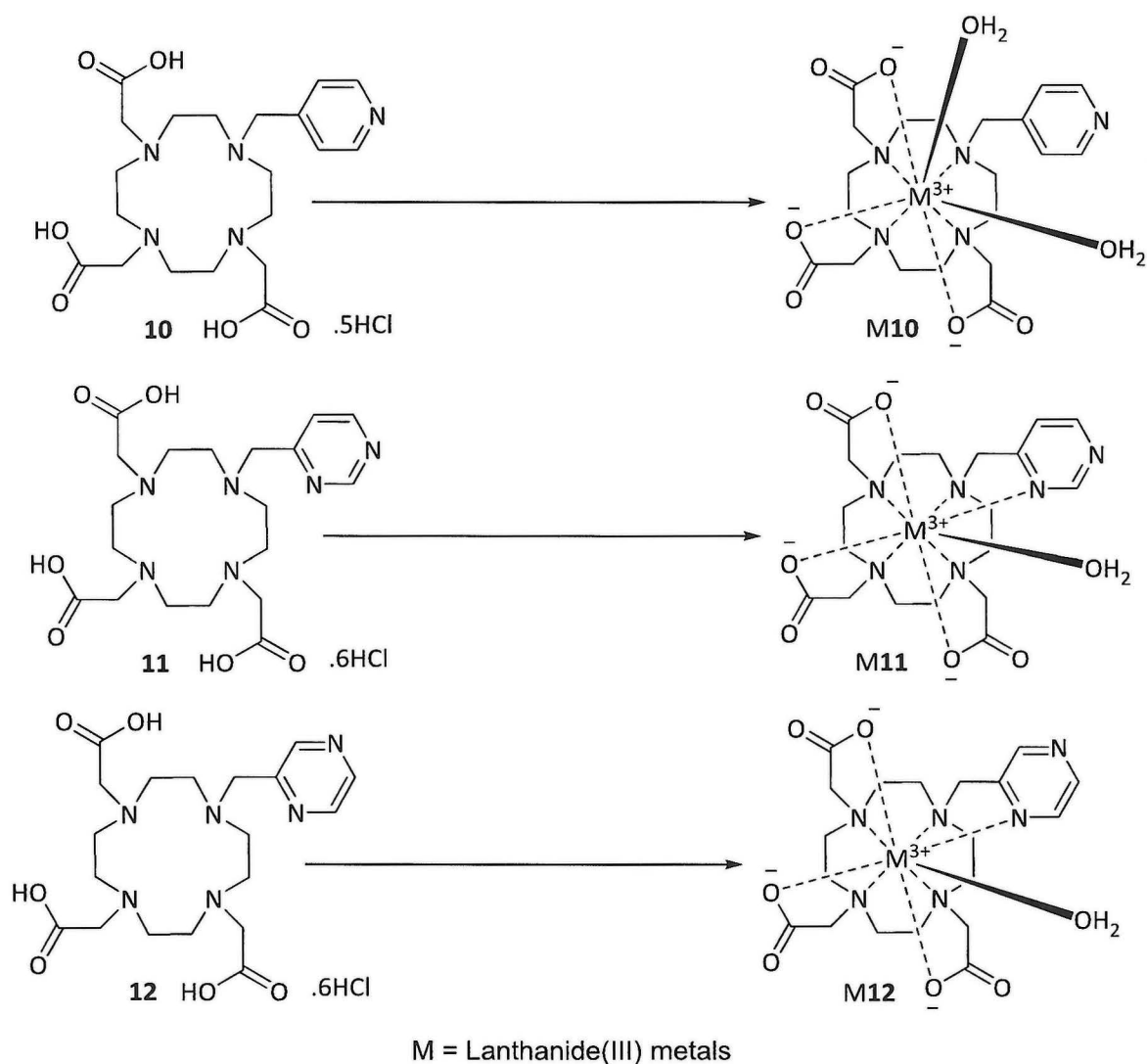
## **Chapter 3**

# **Synthesis and characterisation of lanthanide(III) tetraazamacrocyclic complexes**

### 3.1 Introduction

A goal of this research is to form lanthanide complexes with heterocycle containing ligands that could be used in a variety of biomedical applications, including as contrast agents in MR imaging, in luminescence imaging or for conjugation with biomolecules via the non-coordinated nitrogen atoms.

Complexation reactions of lanthanide(III) metal ions that are reported in this chapter utilise the three synthesised chelate ligands (**10**, **11**, and **12**), see Scheme 9, incorporating heterocyclic (pyr, pym, and pyz) pendant arms (see chapter 2).



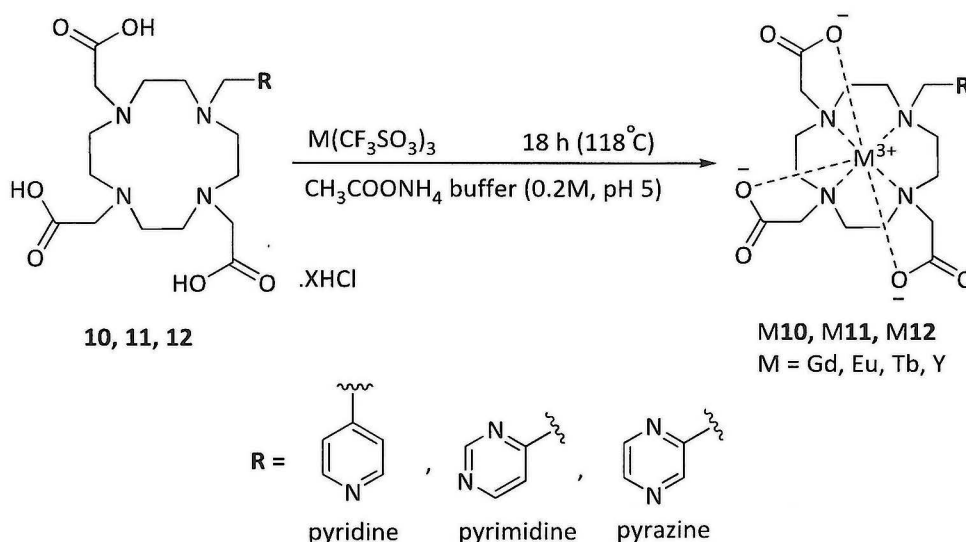
*Scheme 9 - Lanthanide complex formation based on synthesised **10**, **11**, and **12**.*

The coordination modes of the heterocyclic arms (pyr, pym, and pyz) in ligands **10**, **11**, and **12** to the lanthanide ions are of interest as there are few reports of such complexes. The heterocycles (pyr, pym, and pyz) can act as monodentate or bridging ligands, allowing use as a linker group to form further larger molecular arrays.

## 3.2 Synthesis of lanthanide(III) complexes.

### 3.2.1 Preparation of lanthanide(III) complexes of 1,4,7-tris(carboxymethyl)-10-(methyl[pyr][pyz][pym])tetraazacyclododecane.

The synthetic procedure was taken from literature and modified in some cases.<sup>1,62</sup> The preparation of lanthanide(III) complexes utilised the synthesised ligands reported in chapter 2 (**10**, **11**, and **12**). The preferred lanthanide ions were  $\text{Gd}^{3+}$ ,  $\text{Eu}^{3+}$ ,  $\text{Tb}^{3+}$ , and  $\text{Y}^{3+}$ , see Scheme 10.  $\text{Gd}^{3+}$  is of interest due to its attractive paramagnetic properties which can be used as MRI contrast agents (seven unpaired electrons and a symmetric S electronic state).  $\text{Tb}^{3+}$  and  $\text{Eu}^{3+}$  luminesce in the visible spectrum on sensitisation for optical imaging applications.  $\text{Y}^{3+}$  is diamagnetic and facilitates characterisation by NMR spectroscopy to determine the structural arrangement of the chelating ligand in solution on lanthanide(III) complex formation.



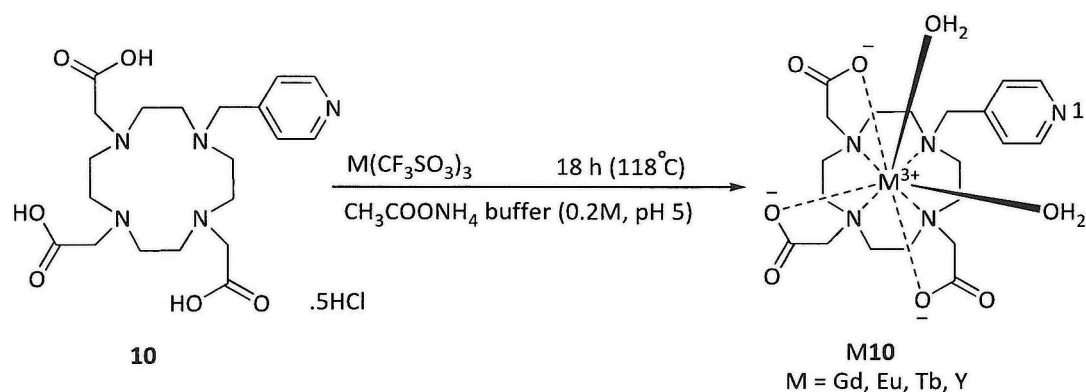
*Scheme 10 – Synthetic method of lanthanide complexation.*

The reactions to form **M10**, **M11**, and **M12** were carried out in ammonium acetate buffer at pH 5.0 and the metal triflate solution was added dropwise to a solution of the chelator, the reactions were then heated to reflux for 18 h in ammonium acetate buffer at pH 5 to avoid the formation of lanthanide hydroxide species which would reduce the overall yield.

The synthesised complexes (**M10**, **M11**, and **M12**) were then purified using ion exchange chromatography (Amberlite XAD16N). A large amount of water (500 ml) was used as the initial

eluent to make sure all of the inorganic salts were removed. In most previous cases reported in the literature, a mixture of water: acetonitrile (9:1) was then used after the pure water to elute the desired product. However in this study, replication of this method was unsuccessful, therefore the solvent to elute the product was changed to use 100 ml of methanol which resulted in isolation of the desired metal complexes.

### 3.2.1.1 Lanthanide(III) complexes of 1, 4, 7-tris (carboxymethyl)-10-(4-methylpyridyl) tetraazadodecane.



*Scheme 11 – Ln(III) complexes formed with 10*

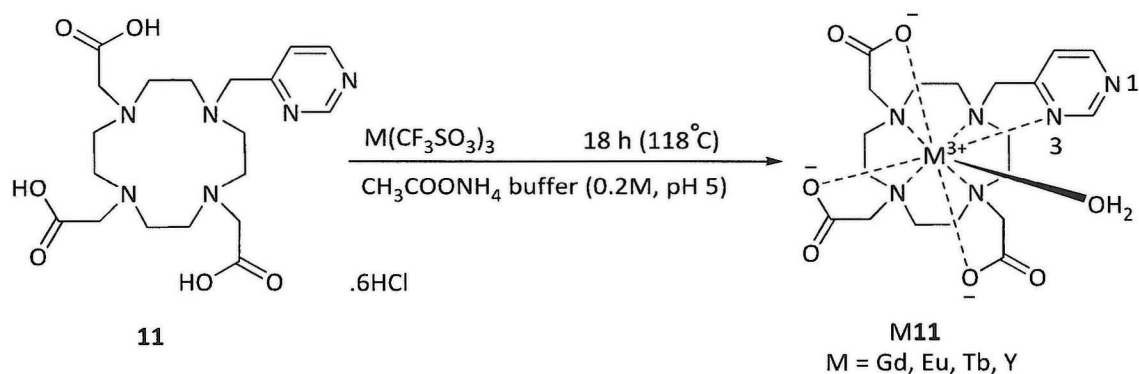
The chelate ligand (10-(pyridin-4-ylmethyl)-1, 4, 7, 10-tetraazacyclododecane-1, 4, 7-triyl) triacetic acid (**10**) has been used to prepare four lanthanide complexes (**M10**) by using M(III) trifluoromethanesulfonate salts in ammonium acetate buffer solution, see Scheme 11.

All **M10** complexes carry the same type of functionalization and it is expected that seven donor atoms will coordinate to the lanthanide ions, excluding the *N1*-nitrogen of pyridine which is not orientated to allow intramolecular coordination. Therefore, the energy transfer from pyridine (acting as a chromophore antenna) to sensitise the lanthanide metals may be less efficient in **M10** complexes as the pyridyl nitrogen is not coordinated. Complex formation is likely to give an unsymmetrical eight coordinate complex, with seven of the donors from the chelate ligand (**10**) and leaving one coordination site available for a water molecule. The formation of these complexes (**M10**) was confirmed by high resolution mass spectrometry and CHN with acceptable level of yield and purity as light yellow solid, and the yields are 39%, 40%, 35%, and 43% for **G10**, **Eu10**, **Tb10**, and **Y10** respectively. Faulkner co-workers research previously reported the same chelate,<sup>74</sup> synthesised by a different method, and the complexation reactions were also carried out using different procedures. They used three lanthanide metal complexes (ytterbium, europium, and gadolinium) but did not provide CHN analysis data.

The motivation for repeating the chelator (**10**) synthesis in this work was to use it for comparison with the other two chelators (**11**, **12**) which contain different heterocyclic arms (pyrimidine, pyrazine) and to be use it as a control (non-coordinating heterocycle) complex.

In addition, the successful preliminary results by the Faulkner group on their pyridine DO3A chelator gave inspiration to this project and indicated that the designed synthesis was feasible, including the combination with a monometallic complex containing a luminescent chromophore (*vide infra*).<sup>74</sup>

### 3.2.1.2 Lanthanide(III) complexes of 1, 4, 7-tris (carboxymethyl)-10-(4-methylpyrimidyl) tetraazadodecane.

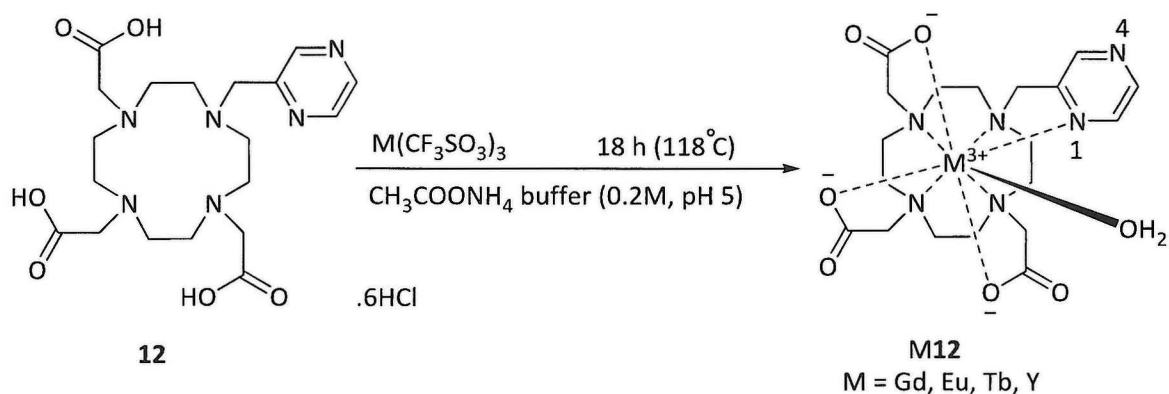


Scheme 12 - Ln(III) complexes formed with 11.

The lanthanide(III) complexes ( $\text{Gd}^{3+}$ ,  $\text{Eu}^{3+}$ ,  $\text{Tb}^{3+}$ ,  $\text{Y}^{3+}$ ) of pyrimidine DO3A chelator (**11**) were synthesised in ammonium acetate buffer at pH 5, see Scheme 12. The N3-position on the pyrimidine ring at **M11** is a potential coordination site for the lanthanide(III) ion bound into the chelator cavity as one of eight coordination bonds formed. Four bonds can be formed with the N donor atoms from the macrocyclic (cyclen) ring, with three other coordination sites from monodentate carboxylate pendant arms. The coordination environment of these complexes may be modified by variation in the pH (*vide infra*). The complexes formed (**M11**) were as isolated as light brown solids with yields of 33%, 34%, 36% and 40% for **Gd11**, **Eu11**, **Tb11**, and **Y11** respectively.

The coordinated N3-position on the pyrimidine ring can facilitate the energy or electron transfer pathway to initiate efficient sensitisation from the heterocycles (chromophore) directly to metal centre. Also, coordination interactions are possible at the N1-position of the pyrimidine and to bridge to other metal containing species to form a multimetallic species.<sup>58,75,76</sup> Faulkner and co-workers produced a range of complexes with different bridging heterocycles which consist of two of or more DO3A macrocycles linked together by aryl groups or heterocycles (m-xyllyl bridging unit,<sup>77</sup> 4,4'-dimethyl-2,2'-bipyridyl group<sup>78</sup> or naphthyl group).<sup>70</sup>

### 3.2.1.3 Synthesis of lanthanide(III) complexes of 1, 4, 7-tris(carboxymethyl)-10-(2-methylpyrazinyl) tetraazadodecane.



*Scheme 13 – Lanthanide(III) complexes formed with 12.*

Lanthanide(III) complexes ( $\text{Gd}^{3+}$ ,  $\text{Eu}^{3+}$ ,  $\text{Tb}^{3+}$ ,  $\text{Y}^{3+}$ ) of the pyrazine DO3A chelator **12** were synthesised using the same set of lanthanide metal ions as used to produce the M11 complexes, see Scheme 13. Similar to the pyrazine system the N1-position can coordinate to the lanthanide(III) metal, whilst the N3-position could be used to coordinate to other metal ions or complexes. As previously, the effect of pH on the coordination modes of the chelator ligand (**12**) and the heterocycle arm was studied. The synthesised complexes M12 were isolated as black solids, in varying yields (30-40%, M= Gd, Eu, Tb or Y).

Parker and co-workers designed related lanthanide(III) complexes with different heterocycles, such as 4-nitropyrimidine, acting as sensitisation antennae that were also based on a DO3A macrocyclic backbone. 4-Nitropyrimidine contributed to the chelation of the lanthanide(III) metal centres to give nine coordinate compounds and stable complexes for testing in biological assays.<sup>79</sup>

### 3.2.2 $^1\text{H}$ NMR/ potentiometric titration studies for lanthanide(III) complexes.

$^1\text{H}$  NMR studies and/or potentiometric titrations were carried out on gadolinium(III), europium(III), and yttrium(III) complexes from M10, M11, and M12 complexes, to investigate the effect that pH has on these complexes and determine the protonated species present under different pH conditions. A key consideration for the potential applications of these complexes is the pH value when the heterocycle nitrogen becomes protonated and can no longer form a coordinate bond with a metal centre. Potentiometric titrations were carried out with 10, 11, and 12 in a 1:1 ratio with the lanthanide(III) salts ( $\text{Gd}^{+3}$ ,  $\text{Eu}^{+3}$ ,  $\text{Y}^{+3}$ ) to determine speciation across a pH range.

#### 3.2.2.1 $^1\text{H}$ NMR and potentiometric titrations for lanthanide(III) complexes of pyridine DO3A. [Gd10, Eu10, Y10].

$^1\text{H}$  NMR spectra were recorded for the yttrium(III) complex (Y10) under basic and acidic conditions to determine approximate  $\text{pK}_a$  values. The study of Y10 was recorded across range of pD values (1.63-12.43), see Figure 42

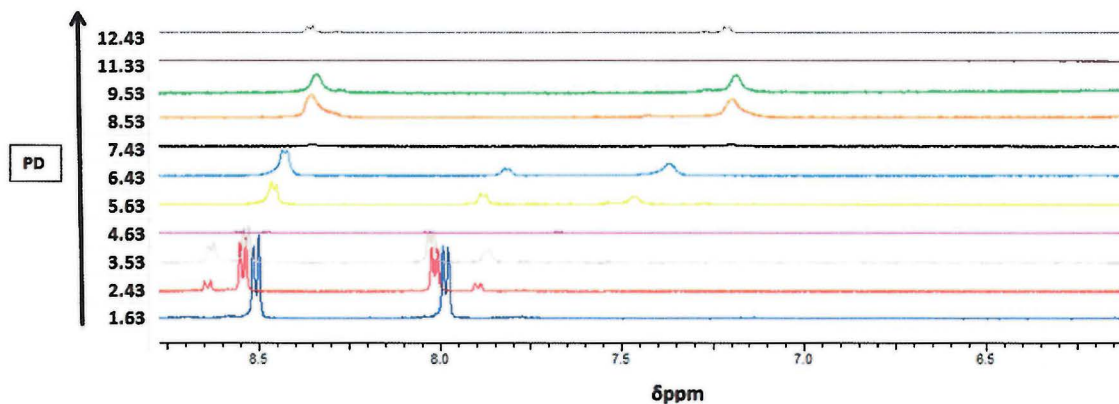
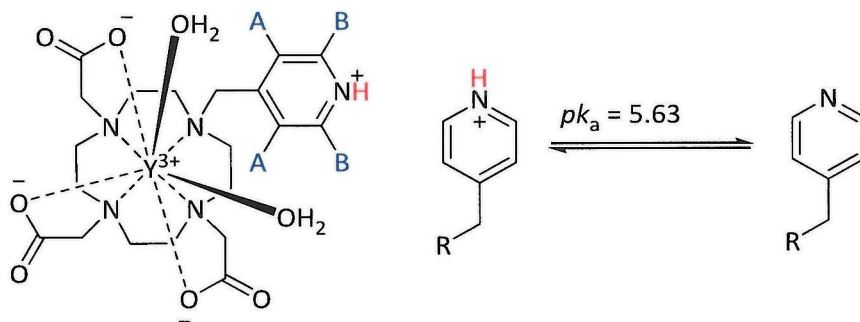


Figure 42 -  $^1\text{H}$  NMR spectrum of chelator ligand Y10 shown the effect of pD on the aromatic region.

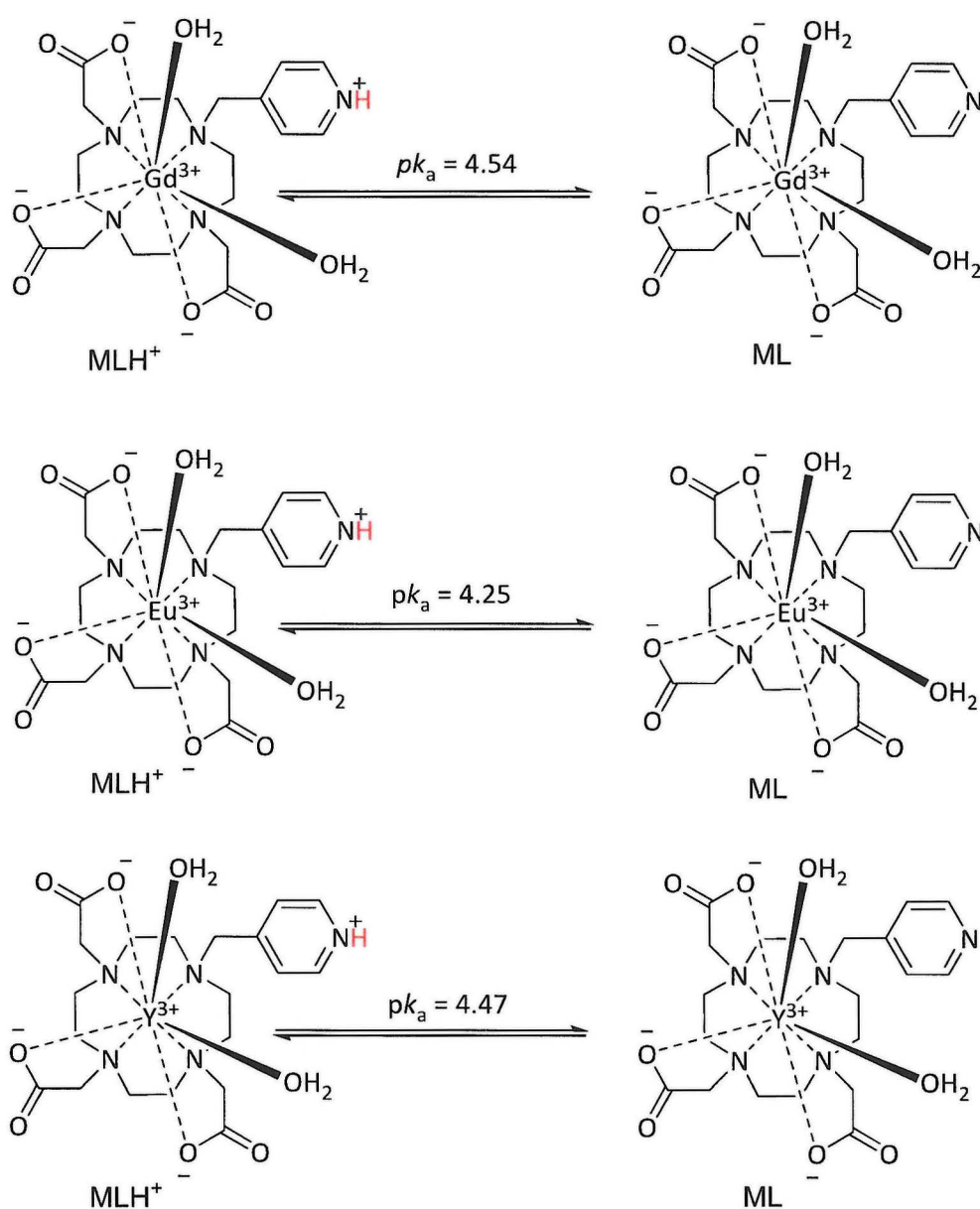
As the  $^1\text{H}$  NMR study of the ligand (10) clearly showed the presence of the pyridine ring of 10 ligand in the aromatic region, a similar aryl region for the pyridine arm was present in the  $^1\text{H}$  NMR study for Y10. The variation in NMR spectra occurred at similar pH values for the free ligand and the metal complex, see section 2.4.1.

The change that indicates the deprotonation of pyridine (N1-position) in **Y10** occurs when the pD of the sample is above 5.63. The peaks of the **A** protons, see Figure 43, present at 8.55-8.54 ppm at pD = 2.43 shifted up field to 8.43-8.42 ppm at pD = 6.43. A similar shift was observed with the peaks representing the **B** protons (at pH = 2.43 they are observed at 8.02-8.01 ppm and shift to 7.81-7.82 ppm at increased pD).



*Figure 43 - The pH effect on the 4-methylpyridine arm in Y10 complex.*

The protonation of the pyridine DO3A lanthanide complexes (**Gd10**, **Eu10**, and **Y10**) was investigated using potentiometric titration with tetramethylammonium hydroxide to determine the protonation constants of these complexes. The titration data for the lanthanide(III) complexes (**Gd10**, **Eu10**, and **Y10**) matched to the observed speciation results for the free ligand (**10**) (see section 2.4.1).



*Scheme 14 - Pyridine protonation constants of Gd10, Eu10, and Y10.*

At acidic pH (below pH 2), the formation of the pyridinium ion is observed, see Scheme 14.

The pH of deprotonation for the N1-pyridine from the potentiometric titration studies corresponds with NMR titration for Y10 and free ligand 10. The deprotonation steps appear at pH = 4.54, 4.25, and 4.47 for Gd10, Eu10, and Y10 complexes compared to pD values of 5.63 and 5.53 in <sup>1</sup>H NMR studies of the complex and ligand respectively.

The protonation constants from potentiometric titrations can be illustrated as a speciation diagram, showing which species are occurring at different pH for Gd10, Eu10, and Y10, see Figure 44.

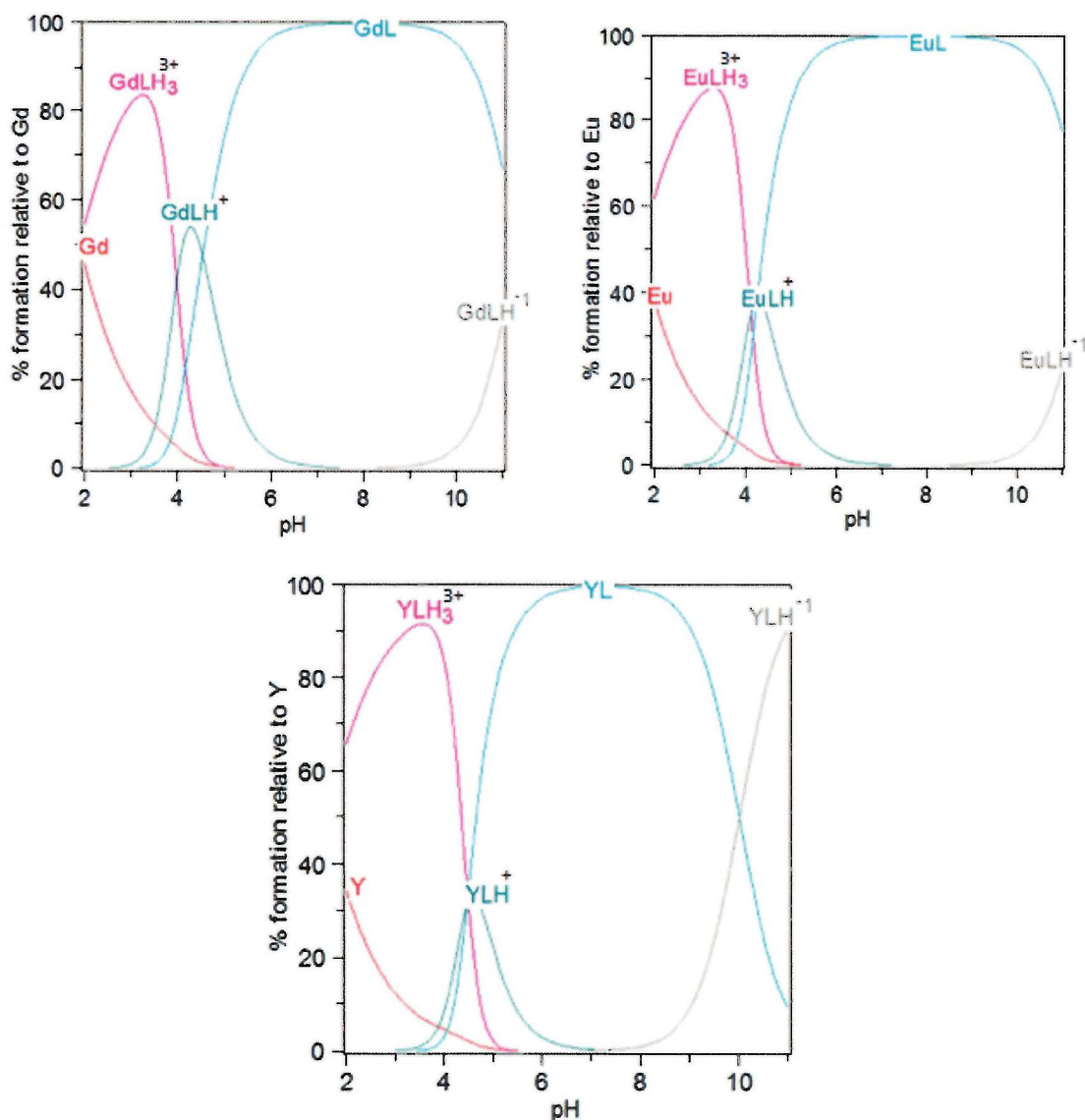


Figure 44 - Speciation diagram of Gd10, Eu10, and Y10.

The deprotonation of the pyridine in Gd10 complex, consider as attractive feature to be used as MRI contrast agents as further coordination interactions are possible to modify the relaxivity properties of the compound.

The europium complex (Eu10) could be an interesting luminescent species, because of the attached heterocycle (pyridine) unit can be coordinated or reacted (above  $pK_a = 4.25$ ) to

initiate the sensitisation process of the lanthanide luminescence. Y $\mathbf{10}$  complexes can be considered as good comparators for Eu $\mathbf{10}$  complexes in terms of the speciation as the two metals have similar properties such as ionic charge, atomic radius, and coordination characteristics. The potentiometric titrations on the Y $\mathbf{10}$  complexes clearly demonstrated the effect of changing in pH in a diamagnetic species that could also be characterised by NMR.

### 3.2.2.2 $^1\text{H}$ NMR and potentiometric titration studies for lanthanide(III) complexes of pyrimidine DO3A. [Gd11, Eu11, Y11].

$^1\text{H}$  NMR studies were also carried out on other types of yttrium(III) complex (Y11) with spectra recorded across range of pD (1.63-12.43) values, see Figure 45.

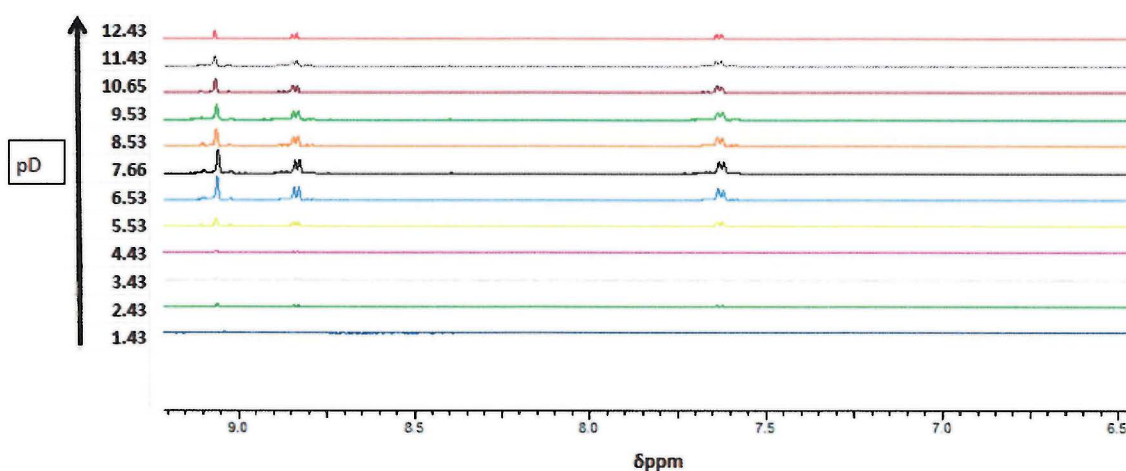


Figure 45 -  $^1\text{H}$  NMR spectrum of chelator ligand Y11 shown the effect of pD on aromatic protons

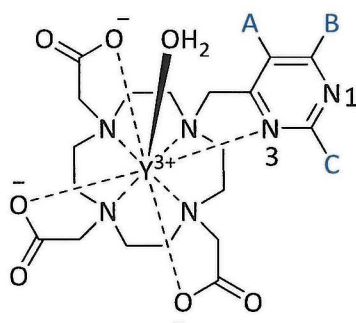
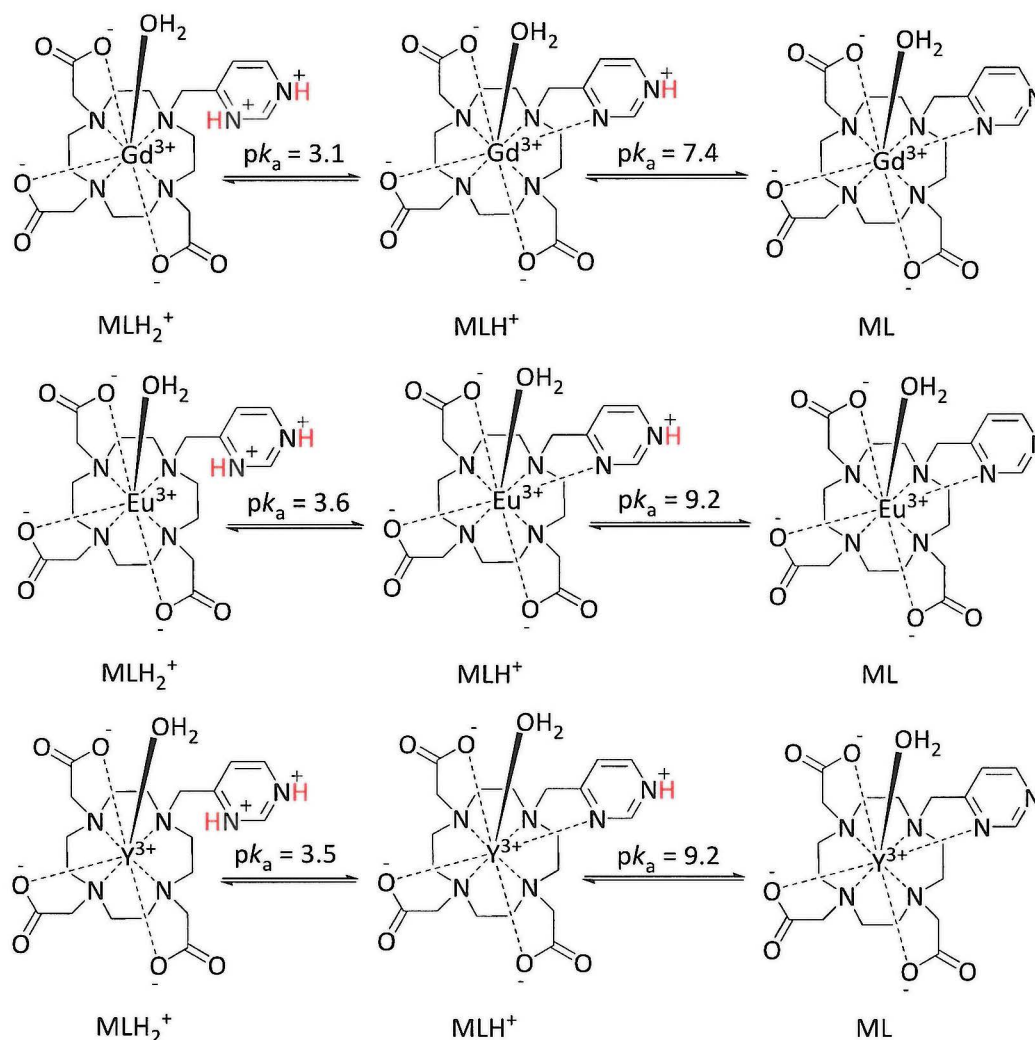


Figure 46 – Protons positions of 4-methylpyridine arm in chelator ligand (Y11).

The group of aryl peaks which appear on  $^1\text{H}$  NMR spectra represent the three different proton environments (**A**, **B**, **C**) on the heterocyclic arm (pyrimidine ring), see Figure 46. The spectra clearly show that there is no significant shift of the pyrimidine ring proton peaks. This is unexpected and indicates no change across the pH/pD range studied. It is unlikely that protonation would not occur. The two doublet peaks were assigned as **A** and **B** at (8.69 ppm for **A** and 7.49 ppm for **B**) with the singlet at 8.92 assigned to the proton at the **C** position.

Potentiometric titrations were then used to further investigate the protonation processes for a wider range of lanthanide(III) complexes. Based on the potentiometric titration data for

Gd11, Eu11, and Y11 complexes, it is useful to identify the effect of pyrimidine protonation constants on the metal coordination modes of an octacoordinate complex structure with one bound water molecule, see Scheme 15.



*Scheme 15 - Pyrimidine protonation constants of Gd11, Eu11, and Y11.*

These data may give insight into the overall thermodynamic stability of these lanthanide(III) complexes to determine if protonation of the *N*3-pyrimidine occurs which have impact on the coordination number. This could also decrease lanthanide luminescence quantum yields, because the efficiency of energy transfer is reduced and the metal centre can also be quenched more readily by coordination to free water molecule at the vacant coordination site.

The data from the potentiometric titration studies for Gd11, Eu11, and Y11 complexes matches well with the  $^1\text{H}$  NMR titration and potentiometric titration data for the free ligand. The second deprotonation step observed  $^1\text{H}$  NMR titration and potentiometric titration studies and shown to occur at *N*1-pyrimidine ring position to is at a  $\text{pK}_a = 9.38$ , and 9.13 respectively for ligand 11 by each of the techniques. The potentiometric titration of Gd11, Eu11, and Y11 complexes showed this second deprotonation step at a  $\text{pK}_a = 7.4$ , 9.2, and 9.2 respectively. That indicates a significant difference between the gadolinium and the other lanthanides which could be attributed to the size of the lanthanide ion  $\text{Eu}^{3+}$ ,  $\text{Gd}^{3+}$ ,  $\text{Tb}^{3+}$  (although not necessarily following the expected trends) and may require further investigation to fully explain.<sup>62</sup> The results from the potentiometric titrations can be depicted as a speciation diagram showing which species are occurring across the pH range, see Figure 47.

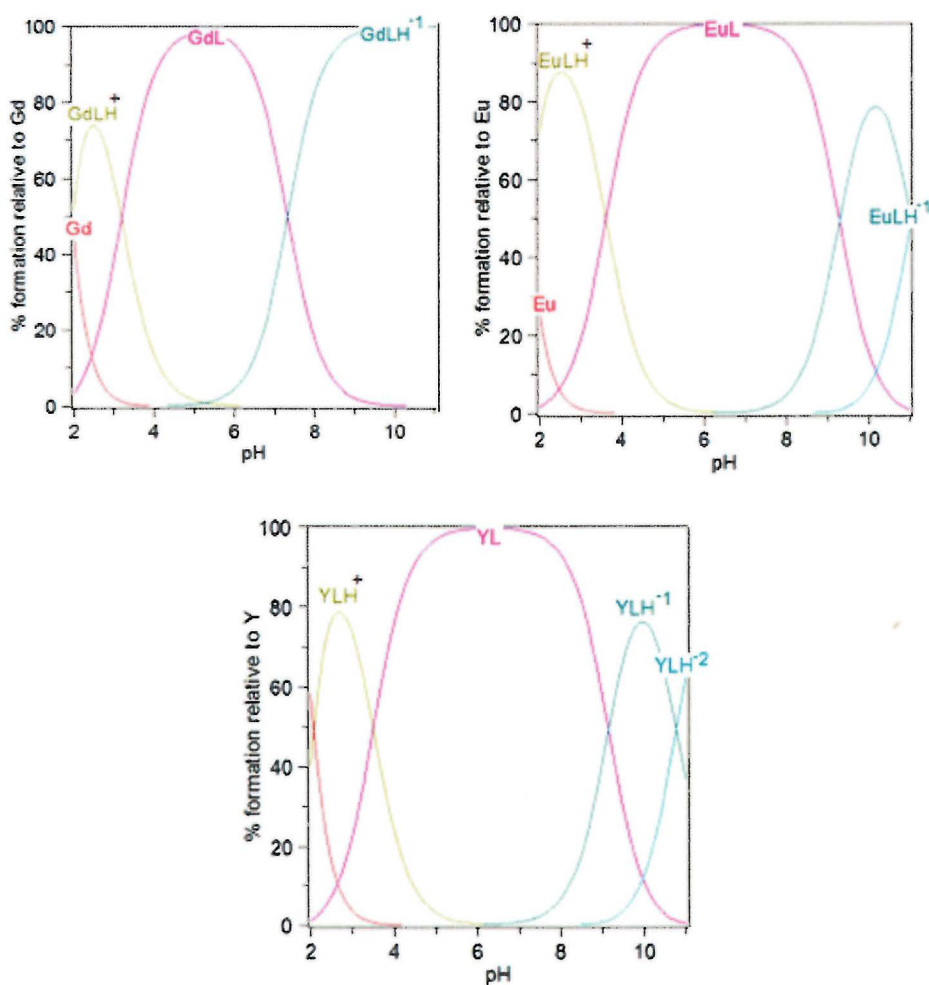


Figure 47 - Speciation diagram of Gd11, Eu11, and Y11.

### 3.2.2.3 $^1\text{H}$ NMR and potentiometric titration results for lanthanide(III) complexes of pyrazine DO3A. [Gd12, Eu12, Y12]

A  $^1\text{H}$  NMR study was carried out on the Y12 complex across a range of the pD values (1.53-12.43), see Figure 48.

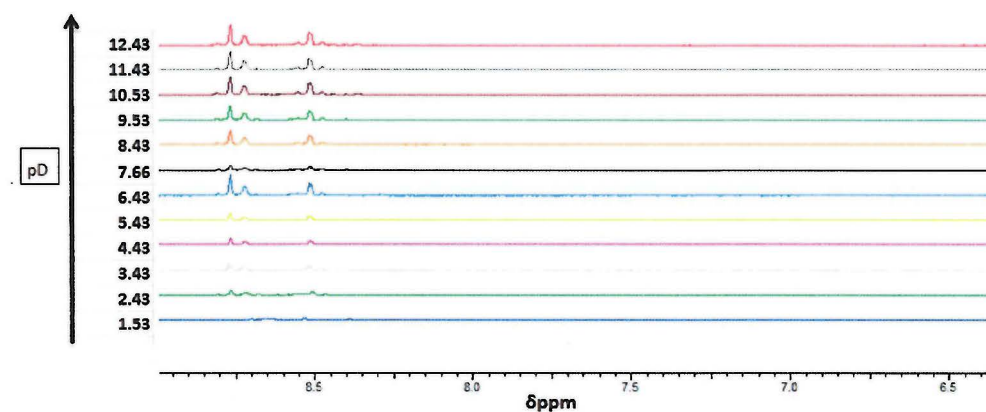


Figure 48 -  $^1\text{H}$  NMR spectrum of chelator ligand Y12 shown the effect of pD on aromatic protons

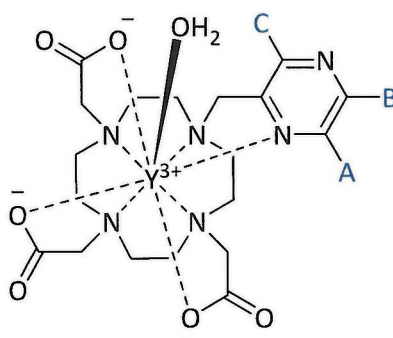


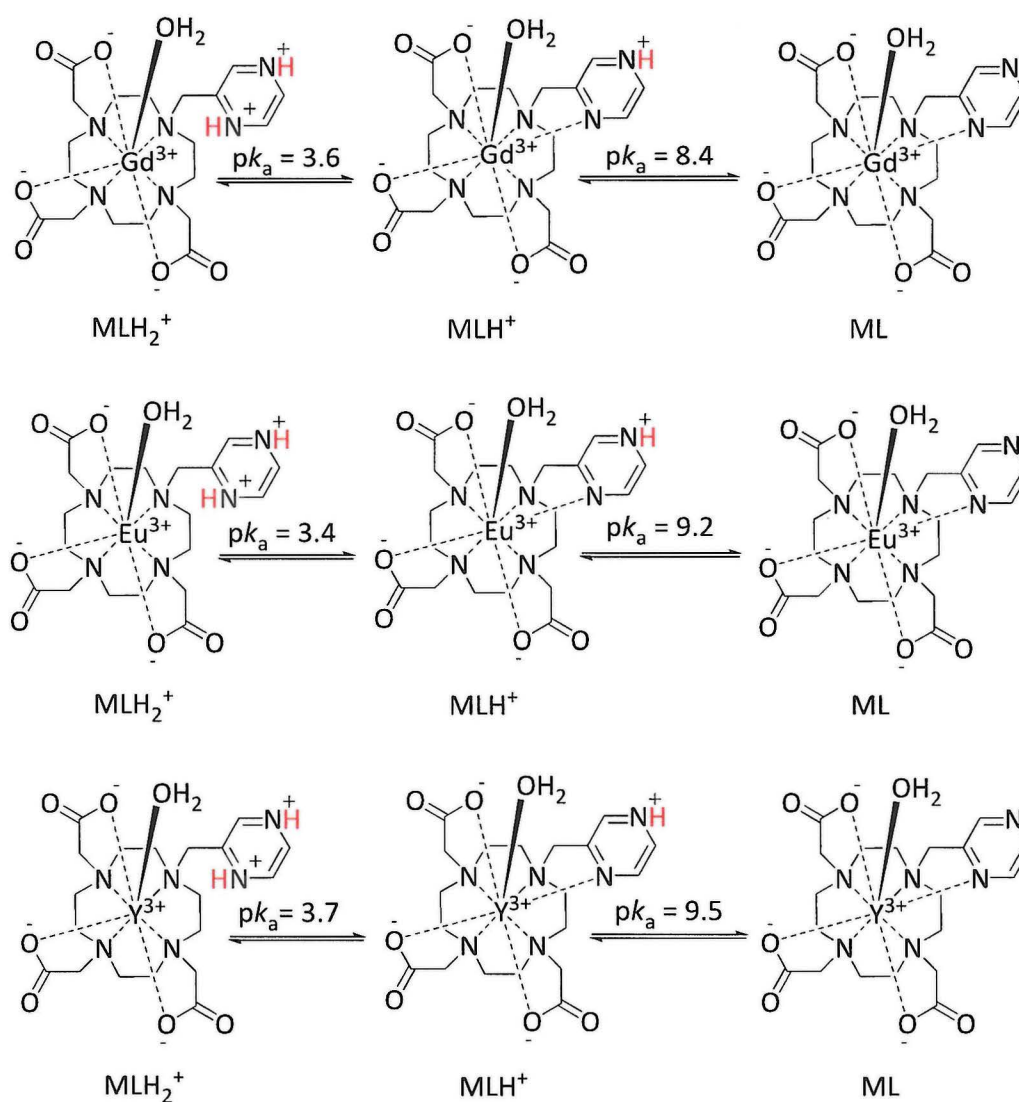
Figure 49 - Protons positions of 2-methylpyrazine arm in chelator ligand (Y12).

The  $^1\text{H}$  NMR spectra shows the three different proton environments (**A**, **B**, **C**) of the pyrazine ring, see Figure 49, with three different peak positions. The comparison among these peaks over various environment in the aromatic region confirmed that there is no major change that can be detect on the peaks of pyrazine ring two doublet peak (**A**, **B**) and one single peaks (**C**) on coordination.

The two doublet peaks (**A**, **B**) at pD = 2.43 have a chemical shift of 8.71-8.72 ppm for the **A** protons, and 8.51-8.52 ppm for the **B** protons. The peak at 8.76 ppm represents the **C** proton.

These peak positions are effectively unshifted for all three peaks (A, B, C) at pD=9.53 at 8.72, 7.52, and 8.77 ppm respectively.

Potentiometric titrations were carried out for Gd12, Eu12, and Y12 complexes to gain some insight into the protonation constants of these complexes. These studies showed the protonated form (MLH<sub>2</sub><sup>+</sup>) of the pyrazine ring can be observed to have two deprotonation steps (to form MLH<sup>+</sup>, ML), which is showed the protonation state of the pyrazine moiety and indicates the possibilities for complex formation and further reaction, see Scheme 16.



*Scheme 16 - Pyrimidine protonation constants of Gd12, Eu12, and Y12.*

The MLH<sup>+</sup> species forms at pK<sub>a</sub> = 3.6, 3.4, and 3.7 for Gd12, Eu12, and Y12 complexes respectively. By increasing the pH up to 12, the second deprotonation of the pyrazine

( $MLH^+/ML$ ) is observed at  $pK_a = 8.4, 9.2,$  and  $9.5$  for Gd12, Eu12, and Y12 respectively. Both of these deprotonation steps for the pyrazine correspond with the  $^1H$  NMR and potentiometric titration studies of free chelating ligand (12) (chapter 2), where the two deprotonation of the pyrazine occurred at  $pK_a = 2.40$  and  $8.88$  respectively. The protonation constants from the potentiometric titration can be depicted as a speciation diagram showing which species are occurring at different pH, see Figure 50.

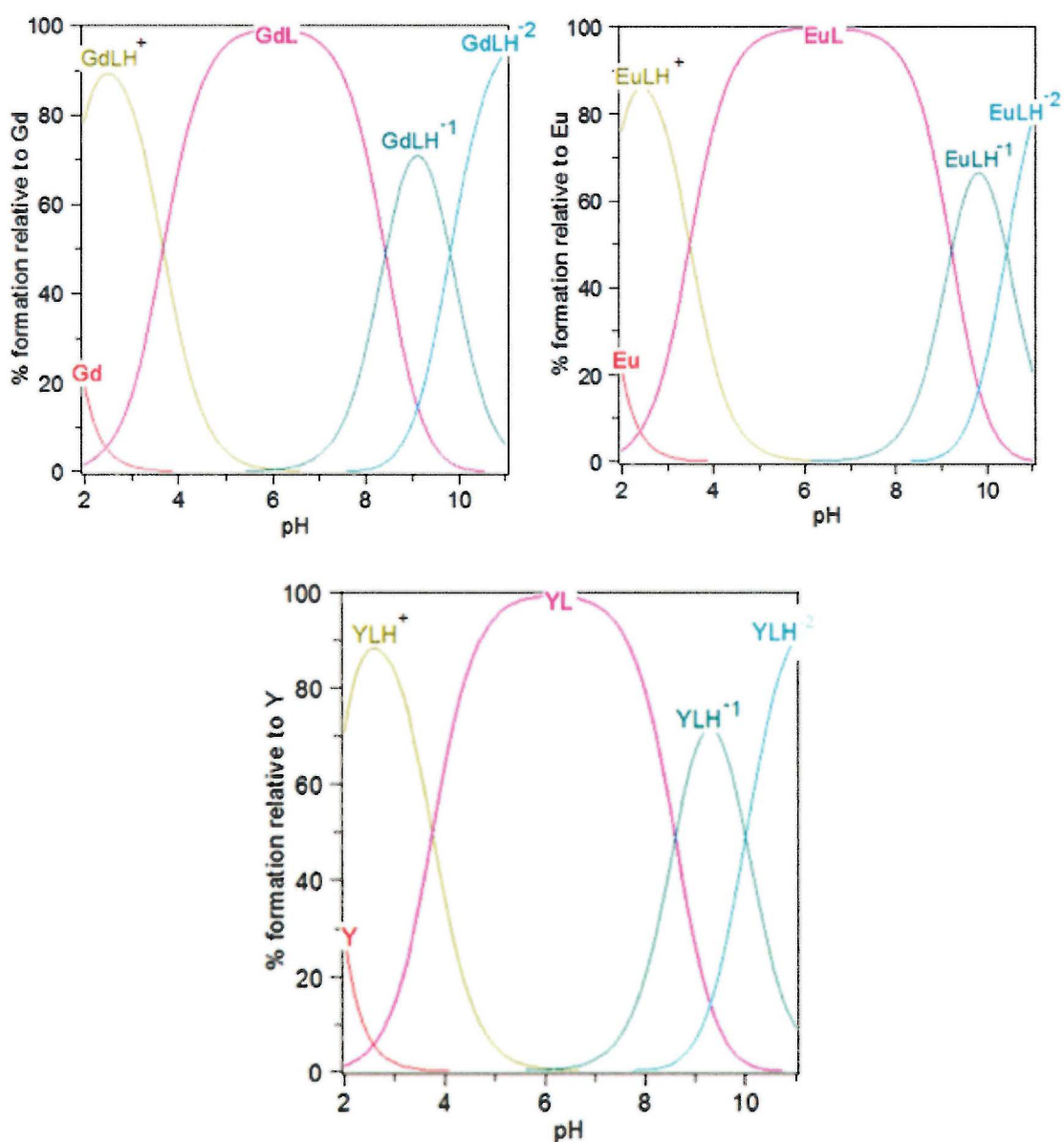


Figure 50 - Speciation diagram of Gd12, Eu12, and Y12.

Thermodynamic stability can also be assessed using this data, see Table 5. Complexation constants for gadolinium(III), europium(III) and yttrium(III) complexes of the synthesised ligands (**10**, **11**, and **12**) can be compared for stability with different macrocyclic ligands. Gd**11**, Eu**11**, and Y**11** show the higher stability in comparison to the same lanthanide(III) metal complexes of **12**. As expected, the pyridyl derivatives have significantly lower stability.

ligands	Gd(III) logK <sub>ML</sub>	Eu(III) logK <sub>ML</sub>	Y(III) logK <sub>ML</sub>	Ref.
<b>10</b>	17.0	17.3	16.4	This work
<b>11</b>	18.7	18.9	18.1	This work
<b>12</b>	17.8	17.9	17.4	This work
DOTP	20.2	20.3	20.2	2
DOTA	25.7	25.6	26.6	2

*Table 5 - Gadolinium(III), Europium(III) and yttrium(III) logK<sub>ML</sub> values for **10**, **11**, **12** and literature chelators.<sup>1</sup>*

M**10**, M**11**, and M**12** can also be compared to other common chelators on the basis of complexation constants for gadolinium(III), europium(III) and yttrium(III). Comparisons with DOTP and DOTA are of interest due to the structural similarities with **10**, **11**, and **12**.<sup>1</sup> It is observed that the tetra-acetate and tetra-phosphonate derivatives have higher stability, which is as expected but the larger difference may also reflect some inconsistencies in the experimental methods.

### 3.2.3 T<sub>1</sub> relaxation studies for Gd(III) complexes.

MRI relaxation properties for the gadolinium complexes synthesised (Gd10, Gd11, and Gd12) have been investigated, in order to demonstrate the effectiveness of these complexes as T<sub>1</sub> MRI contrast agents. T<sub>1</sub> relaxivity and subsequently r<sub>1</sub> values were measured.

The solvent longitudinal relaxation rate 1/T<sub>1</sub> for a contrast agent (CA) is linearly dependent on the concentration of the CA according to following equation

$$(1/T_1)_{\text{obsd}} = (1/T_1)_d + R_1 \times [\text{CA}]$$

Where (1/T<sub>1</sub>)<sub>obsd</sub> and (1/T<sub>1</sub>)<sub>d</sub> represent the measured relaxation rate of the solvent with or without paramagnetic species respectively, R<sub>1</sub> is the relaxivity with units of mM<sup>-1</sup> s<sup>-1</sup>, reflecting the improvement in the relaxation capability of the CA.

The T<sub>1</sub> relaxation times of the two selected complexes (Gd11, Gd12) were recorded in aqueous solutions over a range of concentrations (0.25, 0.5, 1.0, 1.5, 2.0 mM) in H<sub>2</sub>O, and measured at a field strength of 3 T. While T<sub>1</sub> relaxation of Gd10 has previously been and is reported in the literature.<sup>74</sup>

### 3.2.3.1 Relaxivity studies for Gd11

The relaxivity rate ( $r_1$ ) was recorded for the Gd11 complex. At low pH (above 2.90) it was expected that the N-positions of the attached heterocycle arms will become deprotonated and bound to the gadolinium ion. The relaxivity plot is shown for Gd11 at pH 7 in Figure 51.

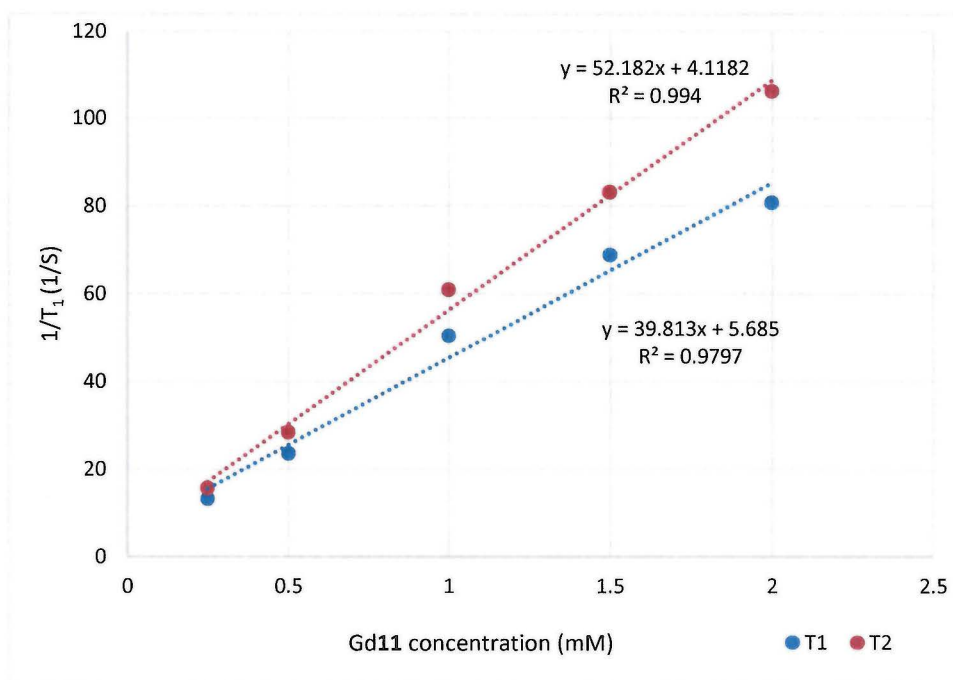


Figure 51 -Graph to show concentration vs.  $1/T$  at pH 7 for Gd11.

The data shows that the relationship between concentration and relaxation rate of the Gd11 is linear with a correlation coefficient of 0.9797 and relaxivity value of  $39.81 \text{ mM}^{-1} \text{ s}^{-1}$  for  $T_1$ . The correlation coefficient is 0.994 and the relaxivity value is  $52.18 \text{ mM}^{-1} \text{ s}^{-1}$  for  $T_2$ . For this complex, the  $T_2$  relaxivity properties of Gd11 are marginally higher than the  $T_1$  relaxivity value. Potentially it could be a contrast agent for both  $T_1$  and  $T_2$  weighted contrast applications in MRI.

### 3.2.3.1 Relaxivity studies for Gd12

The relaxation values were also determined for the gadolinium(III) complex (Gd12), across several concentration values at pH = 7. Gd12 relaxivity properties could similarly be influenced by protonation at the N-positions of the heterocycle arm and by the coordination interaction with the metal ion. The plot for Gd12 relaxivity at pH 7 is shown in Figure 52.

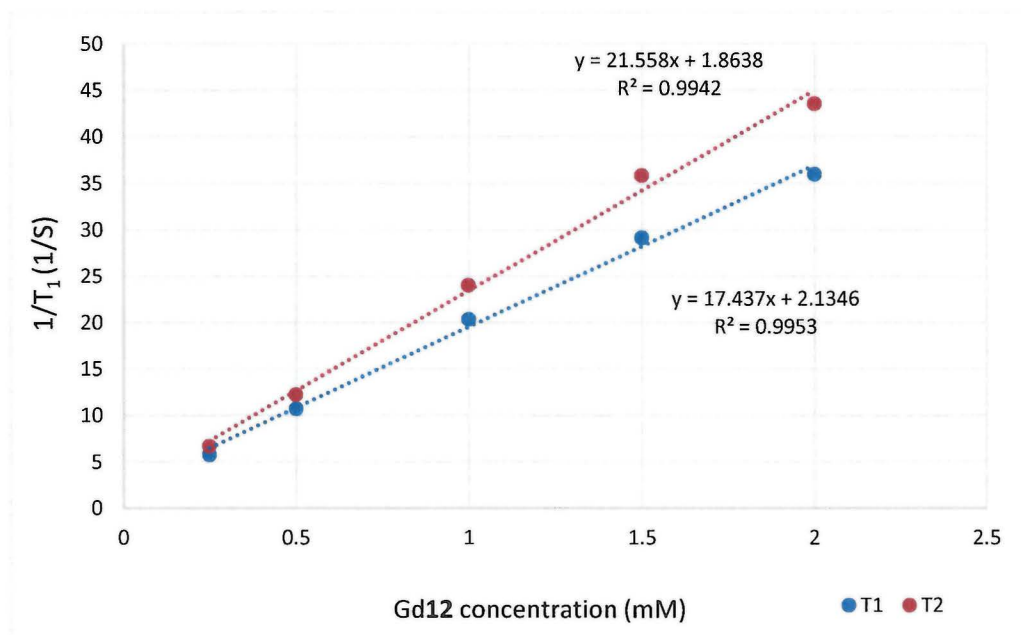


Figure 52 –Plot of concentration vs.  $1/T$  for Gd12.

The graph was plotted using the same range of sample concentrations as previously vs.  $1/T_1$  ( $r_1$ ). The correlation coefficient is 0.9953 and the relaxivity  $17.43 \text{ mM}^{-1} \text{ s}^{-1}$  for  $T_1$ . The correlation coefficient is 0.9942 and relaxivity of  $21.56 \text{ mM}^{-1} \text{ s}^{-1}$  for  $T_2$ .

Comparing the relaxivity between the two gadolinium(III) complexes (Gd11, Gd12), Gd11 has a higher relaxivity for both  $T_1$  and  $T_2$  ( $39.81, 51.81 \text{ mM}^{-1} \text{ s}^{-1}$  respectively), than Gd12 ( $17.43, 21.55 \text{ mM}^{-1} \text{ s}^{-1}$  respectively). This could be due to a higher number of water molecules bound to the higher relaxivity complex. The relaxivity of both Gd11 and Gd12 are much higher than the relaxivity of Gd-DO3Apyridine reported in the literature ( $5.83 \text{ mM}^{-1} \text{ s}^{-1}$  at 11.7 T) but this experiment has been carried out at a much higher field strength.<sup>74</sup>

In terms of comparison with gadolinium(III) complexes in the literature, the new compounds show interesting relaxivity results compared to the clinical contrast agents,<sup>80</sup> see Table 6

Gd(III) complexes	Relaxivity (mM <sup>-1</sup> s <sup>-1</sup> ) (T <sub>1</sub> )	Relaxivity (mM <sup>-1</sup> s <sup>-1</sup> ) (T <sub>2</sub> )	Field strength	References
DOTAREM®	3.5	4.9	3T	97
GADOVIST®	5.0	7.1	3T	97
Gd12	17.43	21.56	3T	This work
Gd11	39.81	52.18	3T	This work

*Table 6 - Relaxivity comparison of Gd10, Gd11 with clinical contrast agents.*

It should be noted that at high magnetic field strengths the relaxivity ( $r_1$ ) of gadolinium based contrast decrease whilst the  $r_2$  relaxivity increases. Gd12 has approximately 4 times higher relaxivity compared with commercial contrast agents (DOTAREM® & GADOVIST®) whilst Gd11 has about 8 fold higher relaxivity with the same comparison.

### 3.3 Conclusions

Twelve novel lanthanide complexes have been synthesised based on the three novel chelators (**10**, **11**, and **12**) synthesised in chapter 2. These chelators include three different heterocyclic pendent arms (pyridine, pyrazine and pyrimidine) and complexes have been formed with a selection of lanthanide ions ( $\text{Gd}^{3+}$ ,  $\text{Eu}^{3+}$ ,  $\text{Tb}^{3+}$ ,  $\text{Y}^{3+}$ ).

All of these neutral complexes were produced in reasonable yields with a high level of purity (the 3+ charge of metal ions is balanced by the three deprotonated acetate arms), see Figure 53.

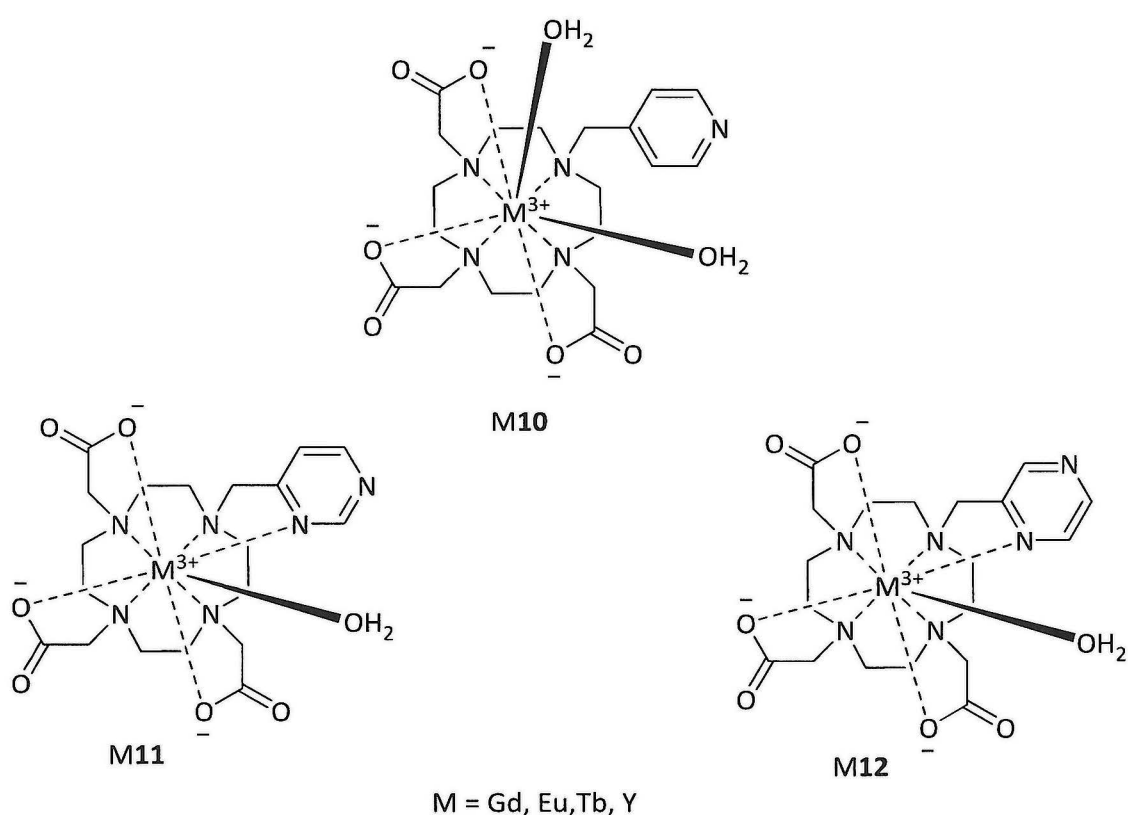


Figure 53 - Lanthanide complexes of (pyridine, pyrimidine, and pyrazine) containing tetraazamacrocycles synthesised.

The studies of  $^1\text{H}$  NMR and potentiometric titration that have been carried out on the synthesised complexes (**M10**, **M11**, and **M12**) show that at low pH the heterocyclic pendant arms can be protonated. The influence of the protonation on the coordination and relaxivity properties requires further investigation.

## **Chapter 4**

# **Towards the synthesis of multi-metallic species for potential use as imaging agents**

## 4.1 Aims

This chapter contains a report of the synthetic chemistry research attempted to combine the lanthanide(III) macrocyclic complexes described in chapter three with transition metal ions or complexes to produce multi-metal constructs for potential use as MRI, optical or multimodal MRI/optical imaging agents using two different approaches:

1. Combination of the lanthanide(III) macrocyclic complexes (M10, M11, and M12) reported in chapter three with monometallic rhenium complexes to form bimetallic constructs. These targets offer an opportunity to increase the efficiency of the luminescence or relaxivity the lanthanide(III) metals in applications such as optical or MR imaging. The production of these species can be achieved by attaching two or more metal centres via the uncoordinated N-position of the heterocycle pendant arm (pyr, pym, and pyz), see Figure 54, that will open up an energy transfer or communication pathway (conjugated system) between the metal centres which allows sensitisation of lanthanide luminescence.

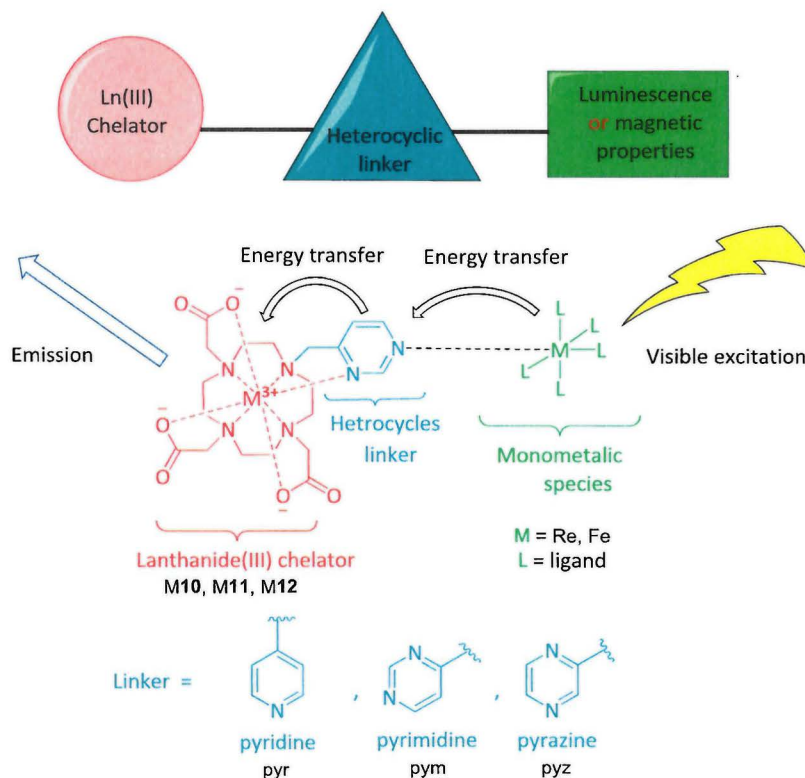


Figure 54 - Schematic representation of the combination of Ln(III) complexes with monometallic species (rhenium or iron) through the heterocyclic bridge.

2. Combining the lanthanide(III) macrocyclic complexes (M10, M11, and M12) synthesised in chapter three with multi-metallic manganese or iron species (such as a manganese(III) triangle). This molecular target offers an opportunity to increase the efficiency of magnetic properties for these complexes as MR contrast agents. Where the electronic communication pathway is open between the manganese/ iron multi-metallic species and the lanthanide(III) metal centre (again via the non-coordinated N-positions of the heterocycle linkers; pyr, pym, and pyz), see Figure 55.

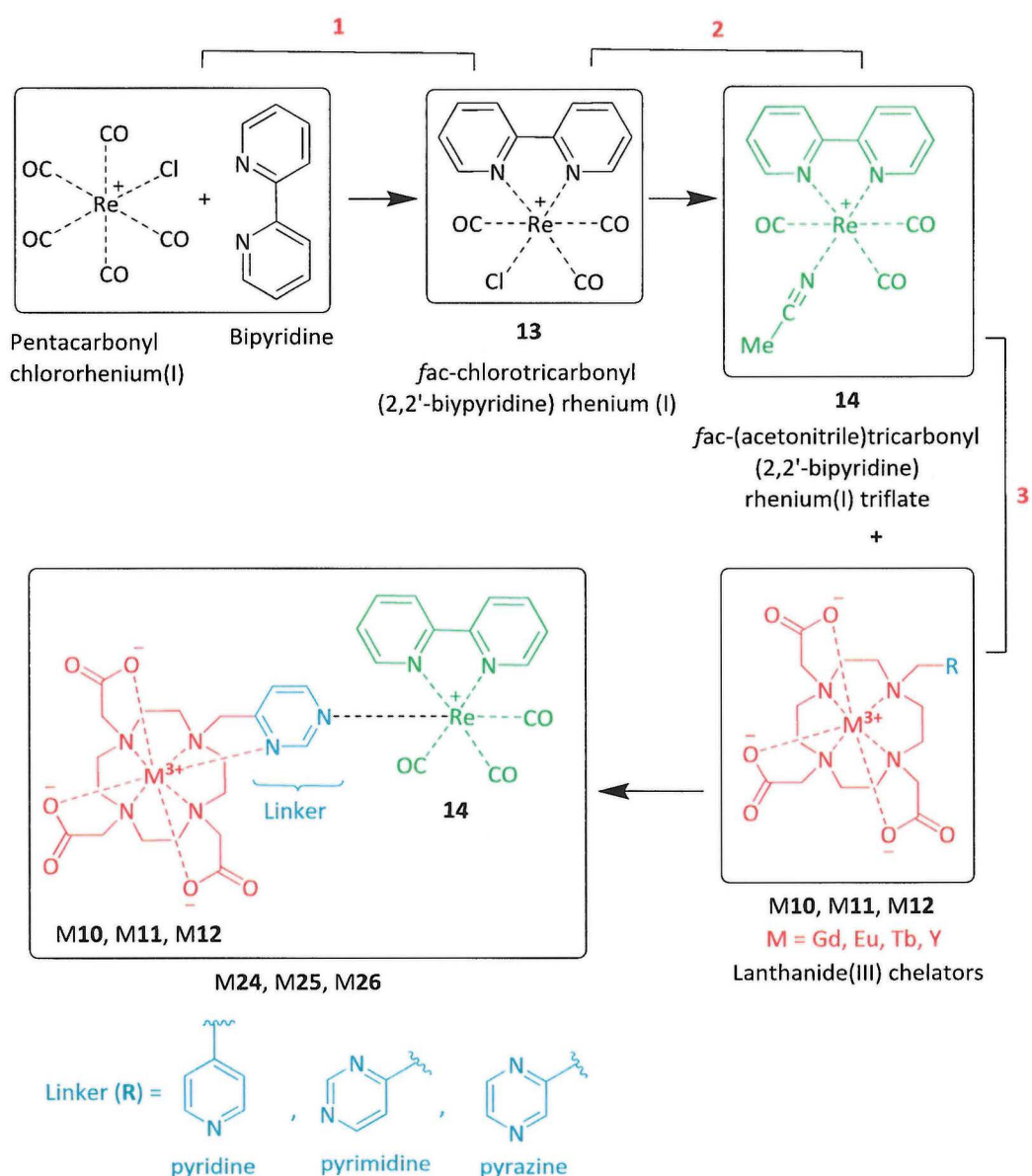


Figure 55 - Schematic representation of the combination of Ln(III) complexes with multimetallic manganese species through the heterocyclic bridge.

## 4.2 Bimetallic and multimetallic species

In this work the bimetallic species are the combination of two metal ion complexes with either similar or different properties such as paramagnetic or luminescence properties, to improve the overall properties of the construct relative to these building blocks by forming a link between the metal centres. These multimetallic species could have enhanced magnetic or luminescence properties for generating improved contrast agents for MR, optical or multimodal imaging, see Figure 56.<sup>81</sup>

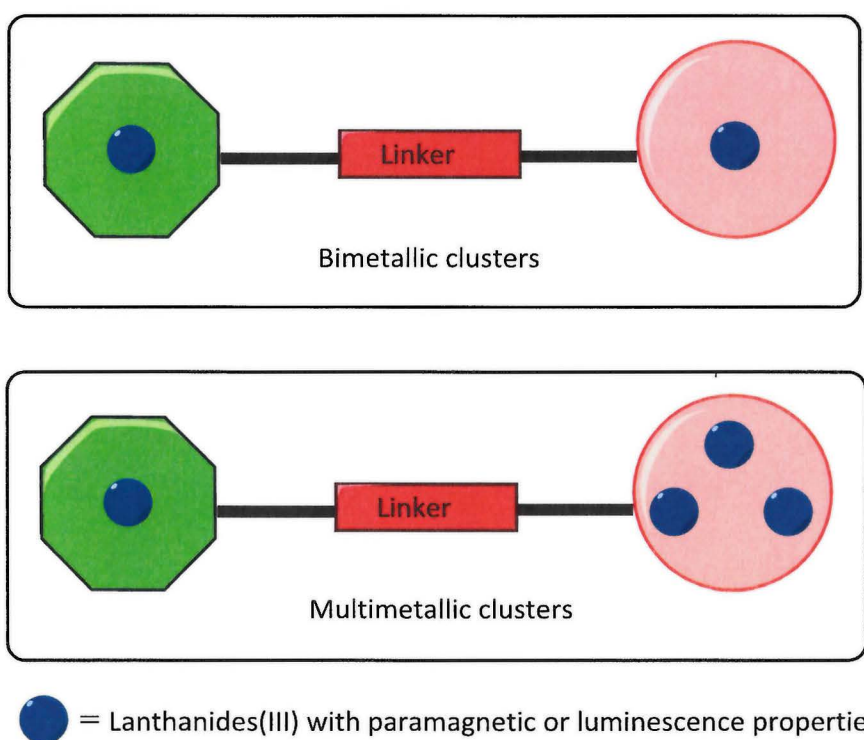


Figure 56 - Schematic representation of multimetallic species.

## 4.2.1 Gadolinium chelate based contrast agents

Multimetallic species which can be used as optical/ MRI contrast agents can be formed by linking gadolinium(III) complexes with either organic chromophores or further metal ion complexes.

### 4.2.1.1 Linking to organic chromophore agents

Methods for linking two or more molecules together to optimise physical properties has attracted increased attention in recent years from the scientific community.<sup>12</sup> For medical imaging, one of the most desirable properties for bimodal contrast agents is the ability to modulate both the relaxivity rates and the fluorescence intensities upon target detection. Using non-covalent interaction strategies to link lanthanide(III) complexes with either large or small organic chromophores can be exploited to increase the efficiency of these contrast agents. There are examples of combined species reported in the literature which have considerable potential as bimodal imaging agents (MRI, optical, MRI/optical), see Figure 57, L<sup>17</sup>, L<sup>18</sup> and L<sup>19</sup>.<sup>12</sup>

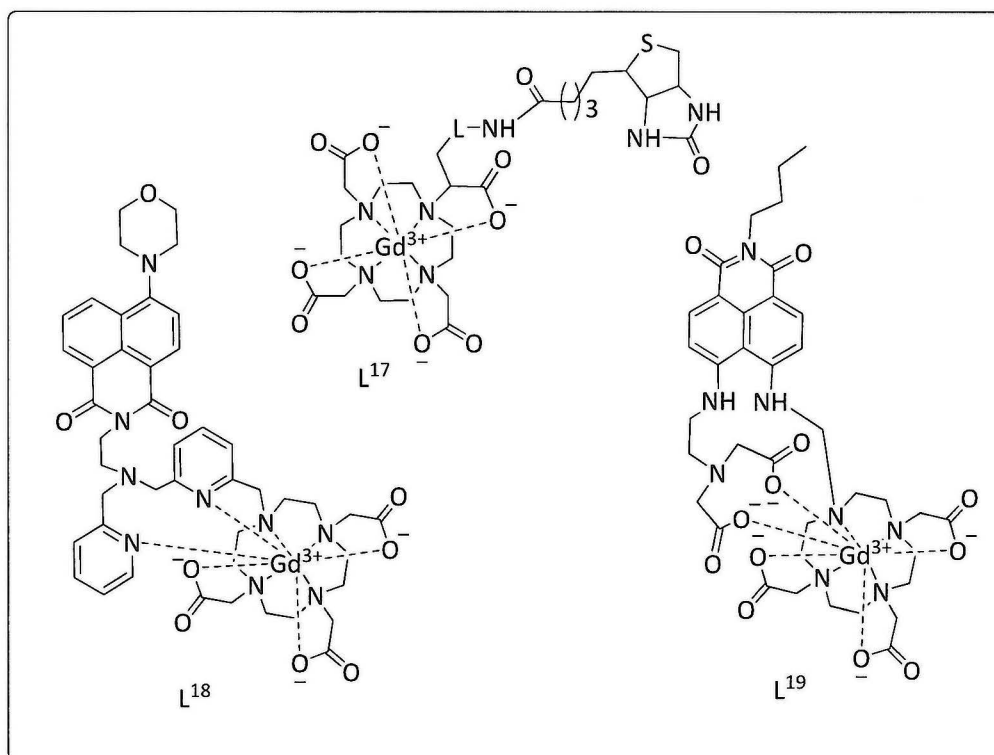


Figure 57 - Heterocyclic based GdDO3A agents.

L<sup>17</sup> is a macrocycle (DOTA) contrast agent bearing a heterocycle ligand, which shows a 36% increase in relaxation rates upon receptor binding. Although these are significant results, further toxicity studies are required to determine the applicability of in vivo bimodal imaging using constructs of this type.<sup>70,82,83</sup>

A second example was reported by Zhang *et al.*<sup>84</sup> is L<sup>18</sup> which combines a GdDO3A complex with a bis-picolyl amine component for complex formation with transition metal ions, this increases the relaxation rates and quenches fluorescence upon Cu<sup>2+</sup> ion binding. The coordination environment of the Gd<sup>3+</sup> ion consists of 9 donor atoms, four from the DO3A nitrogen atoms, three from carboxylate ligands, and two from the pyridines. The system was tested with addition of Cu<sup>2+</sup> at different concentrations; up to three equivalents shows an increase in the relaxation rate by ca. 42% from 5.53 mM<sup>-1</sup> s<sup>-1</sup> to 7.78 mM<sup>-1</sup> s<sup>-1</sup>, whilst one equivalent of Cu<sup>2+</sup> leads to a decrease in the fluorescence by 92%.

Example L<sup>19</sup> was described by Jang *et al.*<sup>85</sup> as a bimodal contrast agent exploiting similar principles to L<sup>18</sup>. This complex was also tested with addition of Cu<sup>2+</sup>, and in this case the copper(II) competes with the gadolinium(III) for the carboxylate pendant arm of an asymmetrically substituted diamionaphthalimide. On complex formation, the gadolinium(III) complex showed an increase in the relaxation rate by 100% from 2.0 mM<sup>-1</sup> s<sup>-1</sup> to 4.01 mM<sup>-1</sup> s<sup>-1</sup> at 1.4 T. An associated increase of the fluorescence (by about 56%) was observed on addition of an equimolar amount of copper(II).<sup>70,86</sup>

#### 4.2.1.2 Gd linked bimetallic/multimetallic agents

The most routinely medical diagnostic technique is magnetic resonance imaging (MRI) because of the deep tissue penetration and lack of ionizing radiation. MRI is superior in certain characteristics when compared to the other imaging techniques. However, there are limitations associated with detecting disparities in magnetic properties of tissue and organs.

Optical imaging techniques are used at cellular or sub-cellular level for detection of fluorescence or luminescence emission, however there are limitations of poor tissue penetration if used in vivo.

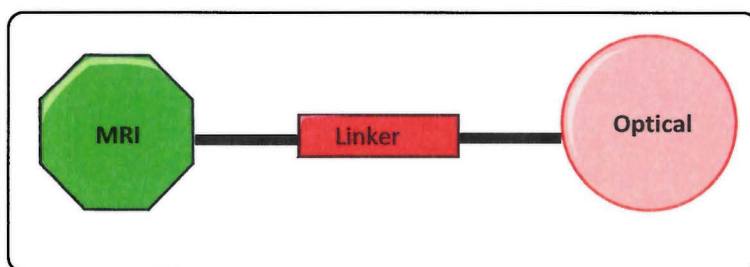


*Figure 58 - Schematic representation for MRI and optical combination of different contrast agents.*

Due to the limitations of both techniques, a combination multimodal imaging agent should open up a wider ranging applicability, see Figure 58. As demonstrated in chapter 3, gadolinium(III) based complexes are used in MRI as longitudinal relaxation ( $T_1$ ) contrast agents by relaxing water molecule protons. In addition, the use of d-block linked chromophores as antenna groups to initiate sensitized luminescence of some of the lanthanides(III) (d-f energy transfer). These d-f hybrid complexes employed many types of transition metal units selected for strong light absorbance in the visible region and the efficiency of metal to ligand charge transfer that allow it to act as an energy donor.<sup>87</sup>

These complexes exhibit intense broad absorption bands in the visible region and luminescence with tails into the NIR via one of two processes: metal to ligand charge transfer (MLCT) or ligand to metal charge transfer (LMCT).

The  $TiGd_3$  metallostar  $L^{20}$  exhibits a wide emission range (400-750 nm) with a maximum at 490 nm upon excitation at 380 nm in LMCT band and the molecular rotation enhancement increases the relaxivity rate to  $36.9 \text{ mM}^{-1} \text{ S}^{-1}$  at 0.4 T,<sup>88</sup> see Figure 59.

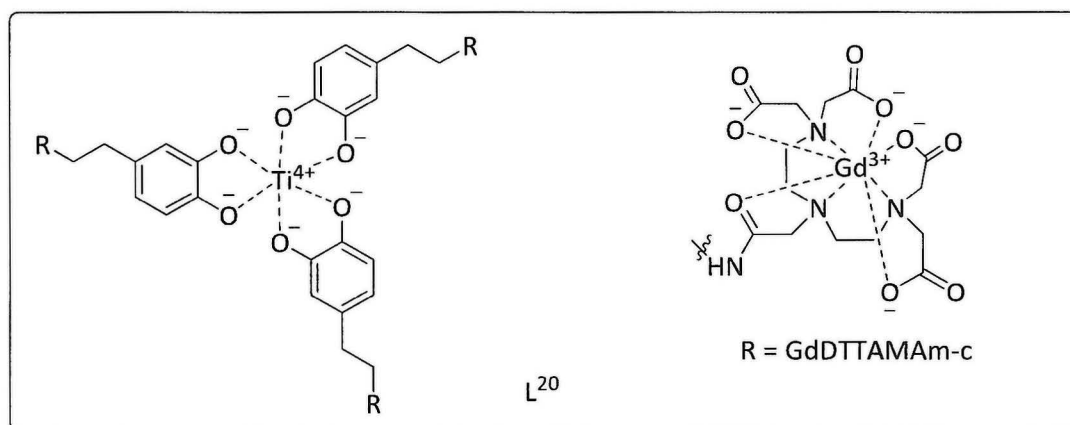


Figure 59 – Example of linking trimer Gd complexes (f-block) with chromophore based Ti metal (d-block).

Another example is the Re/Gd complex  $L^{21}$  which shows a maximum intensity at 578 nm from  $^3\text{MLCT}$  emission with tail can be reach into the NIR, upon excitation into the MLCT band at 365 nm. This complex shows a relaxivity of  $6.6 \text{ mM}^{-1} \text{ s}^{-1}$ ,<sup>89</sup> see Figure 60.

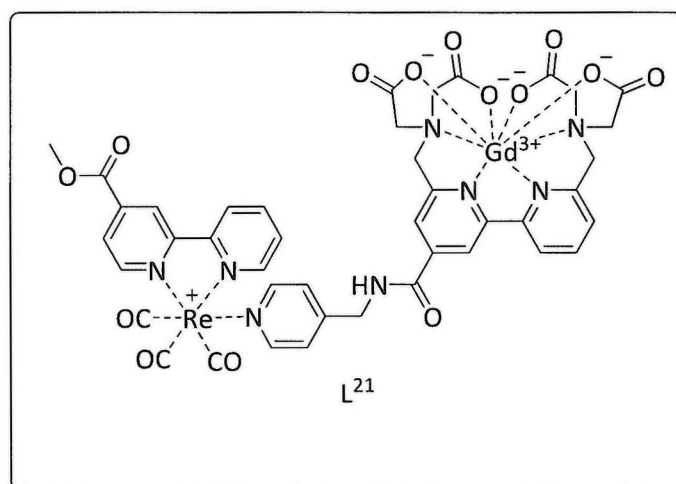


Figure 60 - Literature example for linking Gd complexes (f-block) with chromophore based Re metal (d-block).

$\text{Ru}_2\text{Gd}$  complex  $L^{22}$  shows the luminescence situated between 375 nm and 500 nm upon irradiation into the MLCT band, while abroad red emission was observed from 525 nm to reach 850 nm and a maximum at around 610 nm. The relaxivity rate of this molecule is  $7.2 \text{ mM}^{-1} \text{ s}^{-1}$  at 0.47 T,<sup>12,90</sup> see Figure 61.

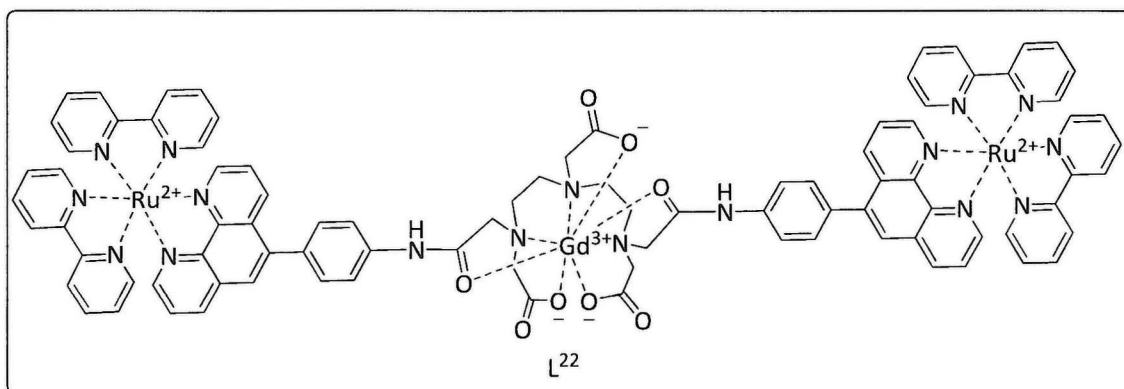


Figure 61 - Literature example for linking trimer Gd complexes (f-block) with two chromophore based on Ru metal (d-block).

Finally, a further example L<sup>23</sup> of the attachment of GdDTPA functionalises a silica nanoparticle that contains (Ru(Bipy)<sub>3</sub> species) via rigid linker. High relaxivity was reported, for this biomodal (MRI/optical) contrast agents of 30 mM<sup>-1</sup> s<sup>-1</sup> at 0.94 T,<sup>91</sup> see Figure 62.

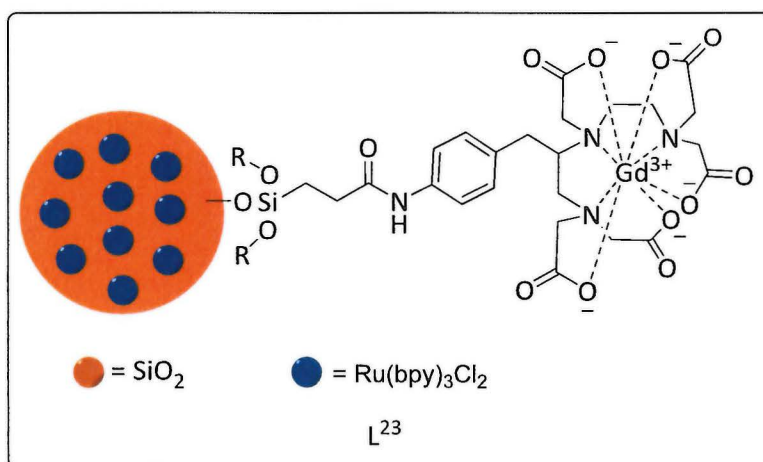


Figure 62 - Literature example for linking Gd complexes (f-block) with multimetallic species (silicone nanoparticle) included to Ru metals molecules (d-block).

### 4.3 Synthesis and characterisation of Ln-Re bimetallic species

To generate building blocks consisting of d-f hybrids bridging between the d-block and f-block metal centres is required because of the low molar absorption coefficients between lanthanide ions (f-f transition). The chromophores are used as antenna to initiate the emissive state of the lanthanides as they have large extinction coefficients.

Employing d-block transition metal (TM) complexes as sensitizers (chromophores) in what are known as d-f hybrid arrays will allow the effective energy transfer to take place, where the donor unit in the excited state of TM must lie at least  $2000\text{ cm}^{-1}$  above the Ln(III) accepting level, or thermally activated back energy transfer (ET) occurs leading to a loss of luminescence.<sup>92</sup> A number of research groups,<sup>43,78</sup> have recently demonstrated that rhenium bipyridines (chromophore) can successfully be attached to cyclen derived complexes with efficient sensitization of the lanthanide centre.

One of the aims of the work reported in this chapter is to combine rhenium bipyridine units (chromophore) with the synthesised lanthanides(III) complexes (M24, M25, and M26) in chapter 3, via heterocycle linkers (pyridine, pyrazine, and pyrimidine), see Figure 63.

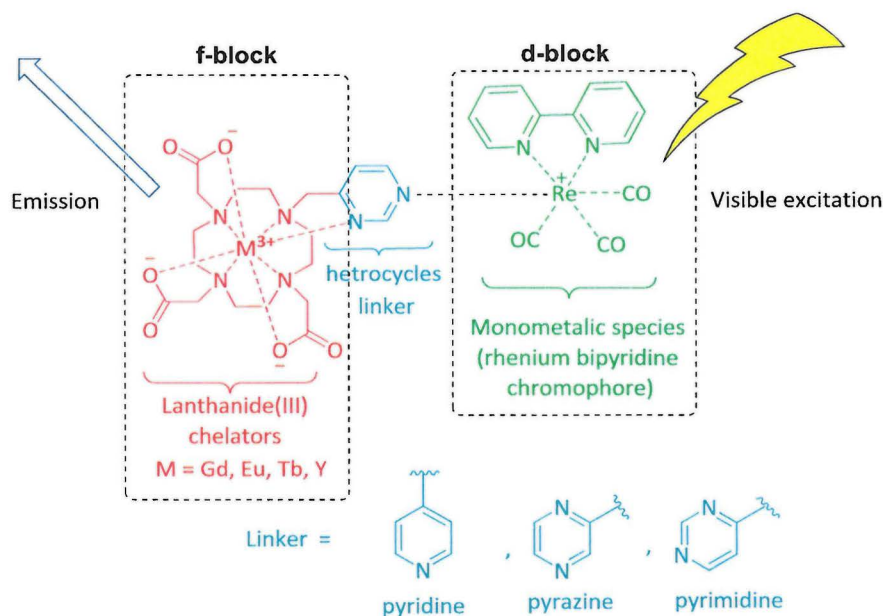


Figure 63 - Schematic representation the combination of Ln(III) complexes with monometallic species (rhenium bipyridine complex) throughout the heterocycles bridge.

### 4.3.1 Rhenium chromophore synthesis

Rhenium bipyridine derivatives have been used for many years as luminescent labels.<sup>93,94</sup> The synthesis of the desired long lived product (**rhenium bipyridine chromophore**) (**14**) which includes a d-block metal ion (rhenium) was carried out in two stages (**1**, **2**), see Figure 64. Firstly by synthesizing *fac*-chlorotricarbonyl (2,2'-bipyridine) rhenium(I) (**13**) which is then used as starting material for producing the desired chromophore *fac*-(acetonitrile) tricarbonyl (2, 2'-bipyridine) rhenium(I) triflate or (**rhenium bipyridine chromophore**) (**14**). This can be attached later to the lanthanide complexes M10, M11, and M12 to act as a sensitizer of lanthanide luminescence (**3**) via the heterocycle linkers (**R**).

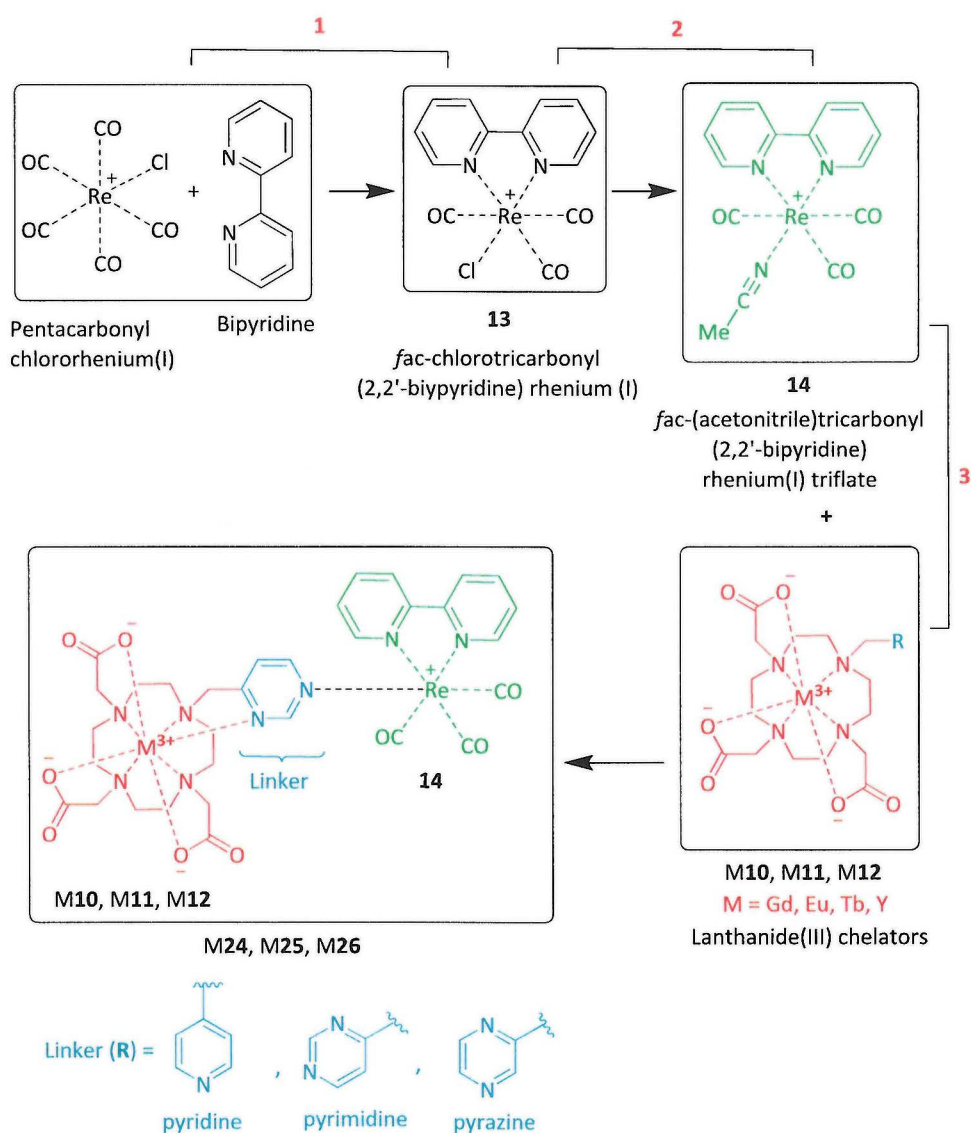
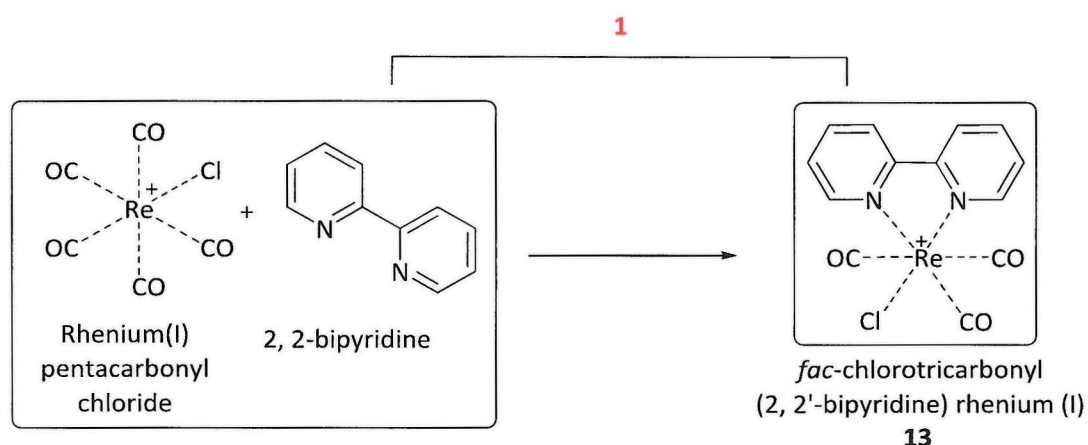


Figure 64 - Synthesis steps to produce Re-Ln compounds M24, M25, and M26.

#### 4.3.1.1 Synthesis of *fac*-chlorotricarbonyl (2, 2'-bipyridine) rhenium (I) (**13**)

By following the literature method,<sup>95</sup> the rhenium(I) chloride chromophore (**13**) was successfully synthesized. Firstly, the reaction was stirred for 1h in dry toluene and under argon using rhenium(I) pentacarbonyl chloride with equal molar of 2, 2'-bipyridine to give the crude product **13** (**1**), see Scheme 17, followed by purification via silica column chromatography to give the product in a high yield (91%). The synthesis and purity of **13** was confirmed by <sup>1</sup>H NMR, HRMS, and CHN.

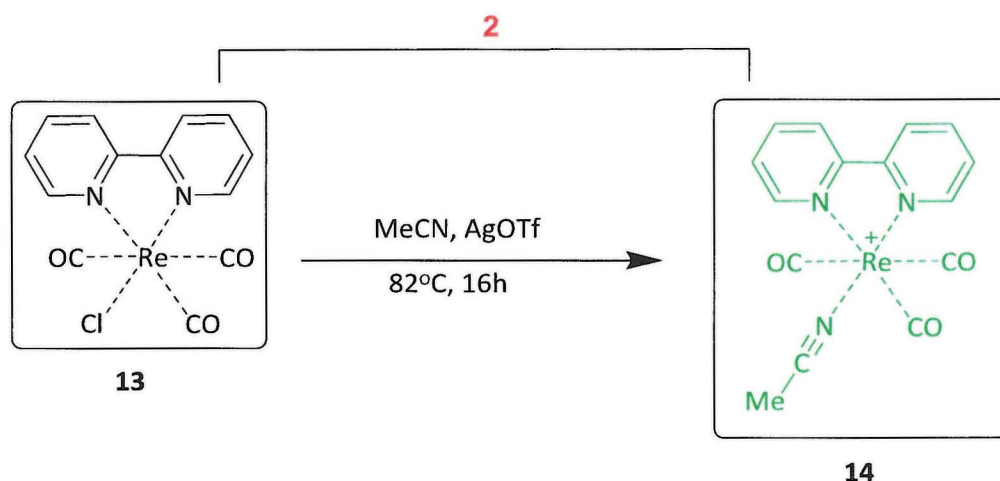


*Scheme 17 - Synthesis methods to produce a rhenium chloride complex **13** which is used in this work to attach a chromophore.*

**13** has a relatively short emissive lifetime in solution (26 ns) due to the bound chloride ion causing nonradioactive quenching of the excited state of the compound.<sup>96</sup> However, this lifetime can be improved by switching the chloride with nitrogen donor atoms of the heterocycles (linker group) of the used lanthanide(III) complexes, causing an increase of 2 orders of magnitude.<sup>96</sup> In addition, the lifetime could be also increased dependent on the lanthanide ion used, as no competitive quenching pathway are possible through the lanthanide ions.<sup>96</sup>

#### 4.3.1.2 Synthesis of *fac*-(acetonitrile)tricarbonyl(2,2'-bipyridine)rhenium(I) triflate (**14**)

Once the synthesis of **13** was completed, the acetonitrile rhenium complex (**14**) synthesis was attempted, see Scheme 18. **13** has a chloride ligand attached which is extremely labile and could possibly form rhenium complex dimers which are undesirable.



*Scheme 18 - Synthesis methods to produce the acetonitrile rhenium (I) complex **14** (chromophore) from the rhenium chloride complex **13**.*

The synthesis of **14** was produced according to modified literature methods,<sup>74</sup> in which the reaction was carried out in dark. Adding silver trifluoromethanesulfonate in THF to *fac*-chlorotricarbonyl (bipyridine) rhenium(I) (**13**) in acetonitrile under N<sub>2</sub> and stirring for 16 h, see Scheme 18. The product was then decanted and the solution filtered to remove any residual AgCl. The solvents were removed under reduced pressure and the solution of **14** was concentrated to about 20-30 ml, and recrystallized with addition of ether at -18°C to give yellow needles. The successful synthesis of **14** was confirmed by <sup>1</sup>H NMR, HRMS, CHN, and ICP.

At this stage, **14** is ready to be combined with the different synthesised lanthanides(III) complexes M10, M11, and M12, via the heterocycles linker, see section 4.3.2.1.<sup>96</sup>

### 4.3.1.3 Crystal formation of Re-Re dimer (15)

$\text{Re}(\text{bpy})(\text{CO})_3\text{Cl}$  ( $\text{bpy}=2,2'$ -bipyridine) can be used as an active catalyst in many electrocatalytic systems, and a common degradation is to produce inactive thermodynamically stable dimers.<sup>97</sup>

Additionally,  $\text{Re}(\text{bipy})(\text{CO})_3\text{Cl}$  is of interest due to its remarkable photochemical properties in several applications such as photocatalytic  $\text{CO}_2$  reduction,<sup>98</sup> pH sensor in analytical chemistry,<sup>99</sup> and, as in this work, a sensitizing chromophore for lanthanide complexes.<sup>100</sup>

An unexpected Re-Re dimer was formed during the reactions attempted in this work. It is a new hydroxide-bridged dimer of the rhenium containing triflate salt, which is similar to 5 other dimers in the CCDC database with different anions, see Figure 65.

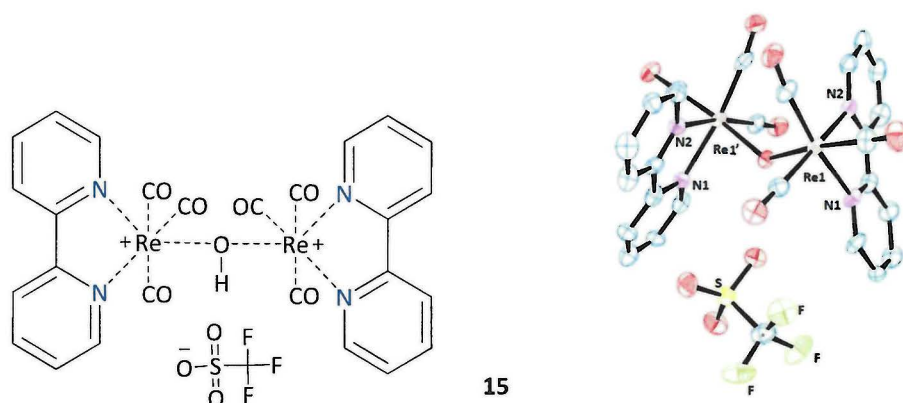
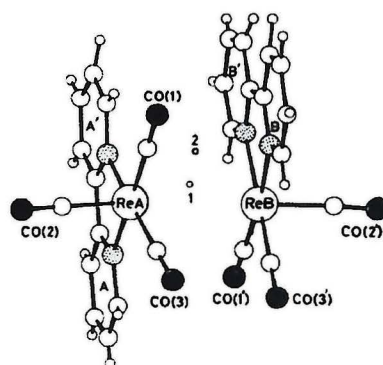


Figure 65 - Molecular structure and X-ray image of  $[\text{Re}_2(\text{bipy})_2(\text{CO})_6(\text{CF}_3\text{SO}_3^-)]$  (**15**) dimer.

The hydroxide-bridged complex  $[\text{Re}_2(\text{bipy})_2(\text{CO})_6(\mu\text{-OH})]$  (**15**) has each rhenium (I) retaining the three carbonyls and bipyridine but the hydroxide sitting between the two metal centres. All of the Re-N bond lengths are similar and there are no significant difference between the Re-CO bonds.<sup>101</sup>

Guihem *et al.*,<sup>101</sup> reported the synthesis of a hydrido rhenium(I) bipyridine species ( $\text{L}^{24}$ ) see Figure 66, the main differences compared to **15** (besides the synthetic method) is the hydrido linker instead of hydroxide in **15** and the chlorine anion instead of triflate in **15**.



$L^{24}$

Figure 66 -  $[Re_2(bipy)_2(CO)_6(\mu-H)(Cl)]$  dimer attached via hydrido bridge ( $L^{24}$ ).<sup>101</sup>

Furthermore, there are similarities between both compounds in the bond distances and angles, see Table 7.

$[Re_2(bipy)_2(CO)_6(\mu-O)(CF_3SO_3^-)]$ ( <b>15</b> )	$[Re_2(bipy)_2(CO)_6(\mu-H)(Cl)]$ ( $L^{24}$ ) <sup>101</sup>
Re(1)-C(11)= 1.926(7) Å	Re(A)-C(1)= 1.921(5) Å
Re(1)-C(12)= 1.922(8) Å	Re(A)-C(2)= 1.938(5) Å
Re(1)-C(13)= 1.925(7) Å	Re(A)-C(3)= 1.913(8) Å
Re(1)-N(1)= 2.167(5) Å	Re(A)-N(1)= 2.162(4) Å
Re(2)-C(24)= 1.919 (5) Å	Re(B)-C(1)= 1.904 (5) Å
Re(2)-N(2)= 2.189(5) Å	Re(B)-N(2)= 2.165(4) Å
C(11)-Re(1)-C(12)= 86.2(3)( $\bar{o}$ )	C(1)-Re(A)-C(2)= 90.5 ( $\bar{o}$ )
C(11)-Re(1)-C(13)= 90.6(3)( $\bar{o}$ )	C(1)-Re(A)-C(3)= 88.0 ( $\bar{o}$ )
C(13)-Re(1)-N(1)= 170.7(3)( $\bar{o}$ )	C(1)-Re(B)-N(1)= 172.0 ( $\bar{o}$ )
C(25)-Re(2)-N(4)= 171.3(3)( $\bar{o}$ )	C(1)-Re(B)-N(1)= 170.0 ( $\bar{o}$ )

Table 7 - Selected bond length and angles for (**15**) and  $[Re_2(bipy)_2(CO)_6(\mu-H)(Cl)]$  ( $L^{24}$ ) from literature.<sup>101</sup>

#### 4.3.1.4 Crystal formation of $\text{Re}(\text{bipy})(\text{C}_4\text{H}_8\text{O}_2)(\text{CO})_3(\text{CF}_3\text{SO}_3^-)(\mathbf{16})$ .

During the course of synthetic attempts, two other novel crystalline compounds were isolated. A rhenium bipyridine coordinated to ethyl acetate generated from the mixing of the species in the solvent with a triflate anion,<sup>98</sup> see Figure 67.

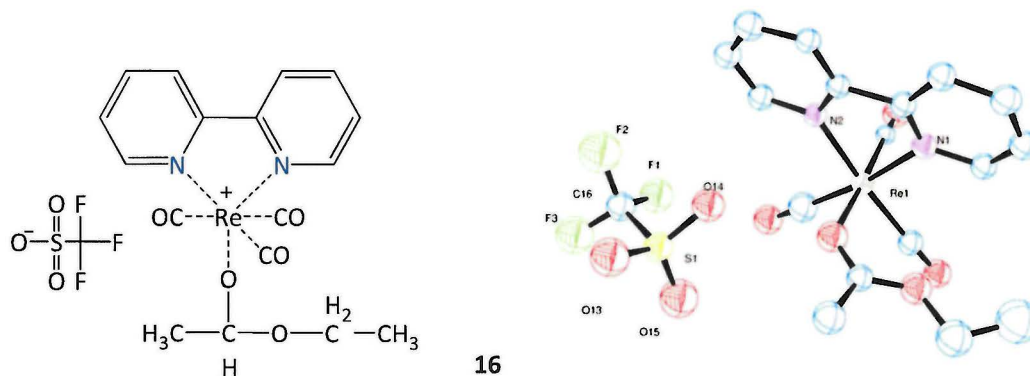


Figure 67 - Crystal structure and X-ray image of rhenium bipyridine complex coordinate ethyl acetate solvent with triflate anion

In addition, the structure of **16** showed symmetry of Re tricarbonyl bipyridine (diimine), and the three carbonyl ligands are arranged in a facial configuration at the rhenium atom. A slightly distorted octahedral geometry was observed at the rhenium atom with the bipyridine ligands.<sup>102,103</sup> The Re(1)-O(4) bond length is 2.185 Å and longer compared to the bond lengths of the rhenium to the three carbonyl groups Re(1)-C(11), Re(1)-C(12), Re(1)-C(13) which are 1.948(5), 1.930(6), 1.933(6) respectively. Gibson *et al.*,<sup>104</sup> reported very similar compound ( $\text{Re}(\text{bipy})(\text{CO})_3, \text{L}^{25}$ ) to **16**, coordinated a carboxylate, with similar properties to **16**, see Figure 68.

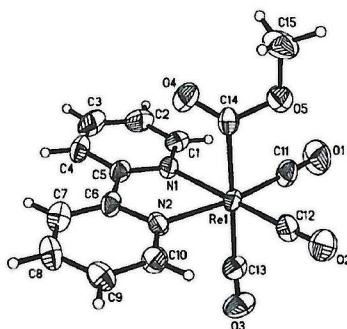


Figure 68 - *Fac-Re(bipy)(CO)3COOMe* example from literature ( $\text{L}^{25}$ ).<sup>104</sup>

In  $L^{25}$ , Re is attached to carboxylate group via carbon atom (C14), while in compound **16** the Re is attached to the ethyl acetate group through its oxygen atom. The compounds have very similar bond lengths and angles (**16** &  $L^{25}$ ), see Table 8.

Re(bipy)(C <sub>4</sub> H <sub>8</sub> O <sub>2</sub> )(CO) <sub>3</sub> (CF <sub>3</sub> SO <sub>3</sub> <sup>-</sup> ) ( <b>16</b> )	<i>fac</i> -Re(bipy)(CO) <sub>3</sub> COOMe ( $L^{25}$ ) <sup>104</sup>
Re(1)-C(11)= 1.948(5) Å	Re(1)-C(11)= 1.922(9) Å
Re(1)-C(12)= 1.930(6) Å	Re(1)-C(12)= 1.927(8) Å
Re(1)-C(13)= 1.948(6) Å	Re(1)-C(13)= 1.955(8) Å
Re(1)-O(12)= 2.185(4) Å	Re(1)-C(12)= 2.185(4) Å
Re(1)-C(11)-O(1)= 176.1(5)( $\bar{o}$ )	Re(1)-C(11)-O(1)= 178.0(8)( $\bar{o}$ )
Re(1)-C(12)-O(2)= 178.4(5)( $\bar{o}$ )	Re(1)-C(12)-O(2)= 178.4(5) ( $\bar{o}$ )
Re(1)-C(13)-O(3)= 177.1(5)( $\bar{o}$ )	Re(1)-C(13)-O(3)= 175.0(7) ( $\bar{o}$ )

Table 8 -Selected bond length and angles for **16** and *fac*-Re(bipy)(CO)<sub>3</sub>COOMe ( $L^{25}$ ).<sup>104</sup>

#### 4.3.1.5 Crystal formation of $\text{Re}(\text{bipy})(\text{C}_4\text{H}_9\text{O}_2)(\text{THF})(\text{CO})_3(\text{CF}_3\text{SO}_3^-)$ (**17**).

The second novel Re bipyridine compound generated during crystallization attempts to produce d-f building block is  $\text{Re}(\text{bipy})(\text{C}_4\text{H}_9\text{O}_2)(\text{THF})(\text{CO})_3(\text{CF}_3\text{SO}_3)$ (**17**), see Figure 69. These complexes of  $\text{ReX}(\text{diimine})(\text{CO})_3$  were recently investigated and characterised for their electrochemical and spectroscopic properties. They have been identified as convenient starting materials in several applications. Diimine ligands with the rhenium centre and aromatic rings in near planar arrangements with good leaving groups such as (Br, Cl, MeCN) will facilitate the exchange with different donor atoms or solvents in the formation of cationic complexes.<sup>100</sup>

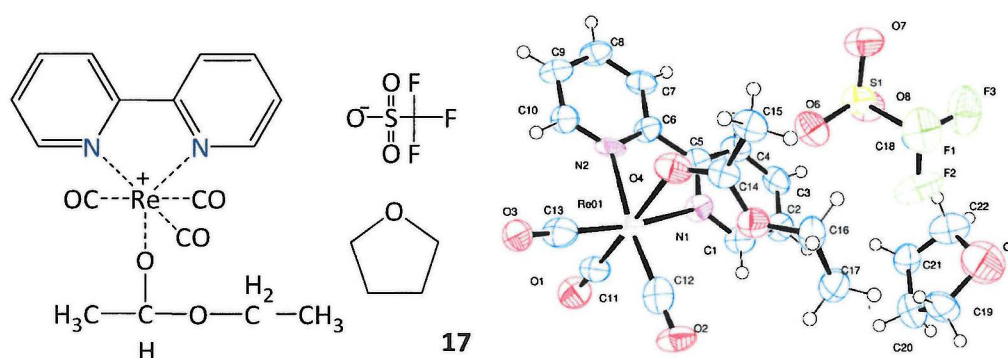


Figure 69 - Crystal structure and X-ray image of rhenium bipyridine complex coordinate ethylacetate solvent with THF ring and triflate anion.

**17** was formed during synthesis attempts to combine *fac*- $\text{Re}(\text{bipy})(\text{MeCN})(\text{CO})_3$ (**14**) with synthesised lanthanide(III) complexes (**M10**, **M11**, and **M12**) in mixture of acetonitrile/ethanol. The product was left to evaporate at room temperature which resulted in crystallisation of  $\text{Re}(\text{bipy})(\text{C}_4\text{H}_9\text{O}_2)(\text{THF})(\text{CO})_3(\text{CF}_3\text{SO}_3)$ (**17**) after one day as large yellow needles suitable for X-ray diffraction. **17** is different to the previous rhenium crystal structure (**16**) as THF is present in the compound, and the bond lengths are very similar although there is some variation in the bond angles, see Table 9.

Re(bipy)(C <sub>4</sub> H <sub>8</sub> O <sub>2</sub> )(CO) <sub>3</sub> (CF <sub>3</sub> SO <sub>3</sub> <sup>-</sup> )( <b>16</b> )	Re(bipy)(C <sub>4</sub> H <sub>8</sub> O <sub>2</sub> )(THF)(CO) <sub>3</sub> (CF <sub>3</sub> SO <sub>3</sub> <sup>-</sup> )( <b>17</b> )
Re(1)-C(11)= 1.948(5) Å	Re(1)-C(11)= 1.959(12) Å
Re(1)-C(12)= 1.930(6) Å	Re(1)-C(12)= 1.920(15) Å
Re(1)-C(13)= 1.933(6) Å	Re(1)-C(13)= 1.952(13) Å
Re(1)-O(12)= 2.185(4) Å	Re(1)-O(12)= 2.181(9) Å
Re(1)-C(11)-O(1)= 176.1(5)( $\bar{o}$ )	Re(1)-C(11)-O(1)= 178.8(11)( $\bar{o}$ )
Re(1)-C(12)-O(2)= 178.4(5)( $\bar{o}$ )	Re(1)-C(12)-O(2)= 179.8(12) ( $\bar{o}$ )
Re(1)-C(13)-O(3)= 177.1(5)( $\bar{o}$ )	Re(1)-C(13)-O(3)= 178.8(14) ( $\bar{o}$ )

Table 9- Selected bond length and angles for **16** and **17**.

The Gardiner group,<sup>105</sup> synthesised a rhenium bipyridine complex contained to THF ring (L<sup>26</sup>). Besides the three carbonyl groups, there is bromide atom attached to rhenium metal centre, this compound was prepared during the course of investigations to produce rhenium alkynyls as components of single molecule white light emitters, see Figure 70.

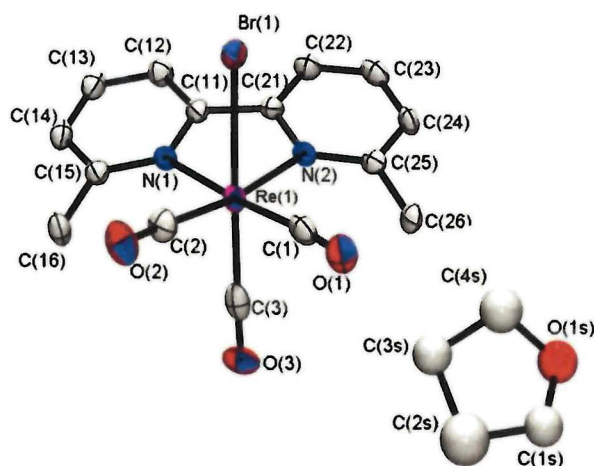


Figure 70 - Rhenium bipyridine complex contain THF ring (L<sup>26</sup>) from literature.<sup>105</sup>

In term of comparison with L<sup>26</sup>, **17** has similar bond lengths, with the exception of the bond length of Re-Br is elongated to 2.611(8) Å in contrast with Re-O bond length of **17** which is 2.181(9) Å, as would be expected for the different donor atoms. In addition, variation is observed in the bond angles for the two compounds, see Table 10.

6,6'-Me <sub>2</sub> bipy)Re(CO) <sub>3</sub> (Br).0.5 THF from literature (L <sup>26</sup> ) <sup>105</sup>	Re(bipy)(C <sub>4</sub> H <sub>8</sub> O <sub>2</sub> )(THF)(CO) <sub>3</sub> (CF <sub>3</sub> SO <sub>3</sub> <sup>-</sup> )( <b>17</b> )
Re(1)-C(1)= 1.922(5) Å	Re(1)-C(11)= 1.959(12) Å
Re(1)-C(2)= 1.925(6) Å	Re(1)-C(12)= 1.920(15) Å
Re(1)-C(3)= 1.930(6) Å	Re(1)-C(13)= 1.952(13) Å
Re(1)-Br(1)= 2.611(8) Å	Re(1)-O(12)= 2.181(9) Å
C(1)-Re(1)-C(2)= 102.3(2)( $\bar{o}$ )	C(12)-Re(1)-C(13)= 89.0(5)( $\bar{o}$ )
C(1)-Re(1)-C(3)= 88.0 (3)( $\bar{o}$ )	C(12)-Re(1)-C(11)= 88.6(5)( $\bar{o}$ )
C(2)-Re(1)-C(3)= 91.6(3)( $\bar{o}$ )	C(13)-Re(1)-C(11)= 90.1(5)( $\bar{o}$ )

Table 10 - Selected bond length and angles for **17** and 6, 6'-Me<sub>2</sub>bipy)Re(CO)<sub>3</sub>(Br).0.5 THF (L<sup>26</sup>) from literature.<sup>105</sup>

#### 4.3.1.6 Summary of rhenium chromophore synthesis and crystal formation

A rhenium bipyridine chromophore (**14**) was synthesised and purified for subsequent reaction with the previously synthesised lanthanide(III) complexes (M10, M11, and M12).

A series of crystal structures have been determined for rhenium bipyridine complexes which were produced during synthesis attempts. A rhenium bipyridine dimer (**15**), and two rhenium bipyridine compounds, one with ethyl acetate and the other with ethyl acetate and THF compound (**16** and **17**). All of these products are contained triflate salts, see Figure 71.

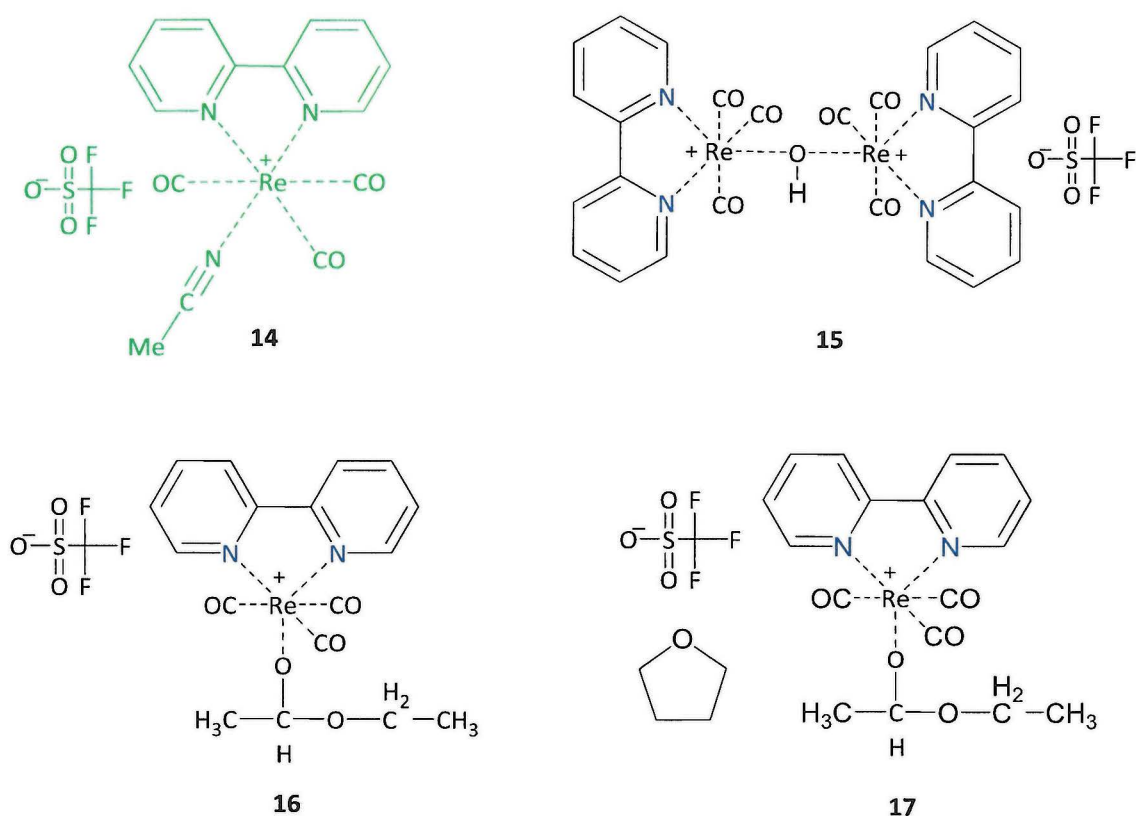
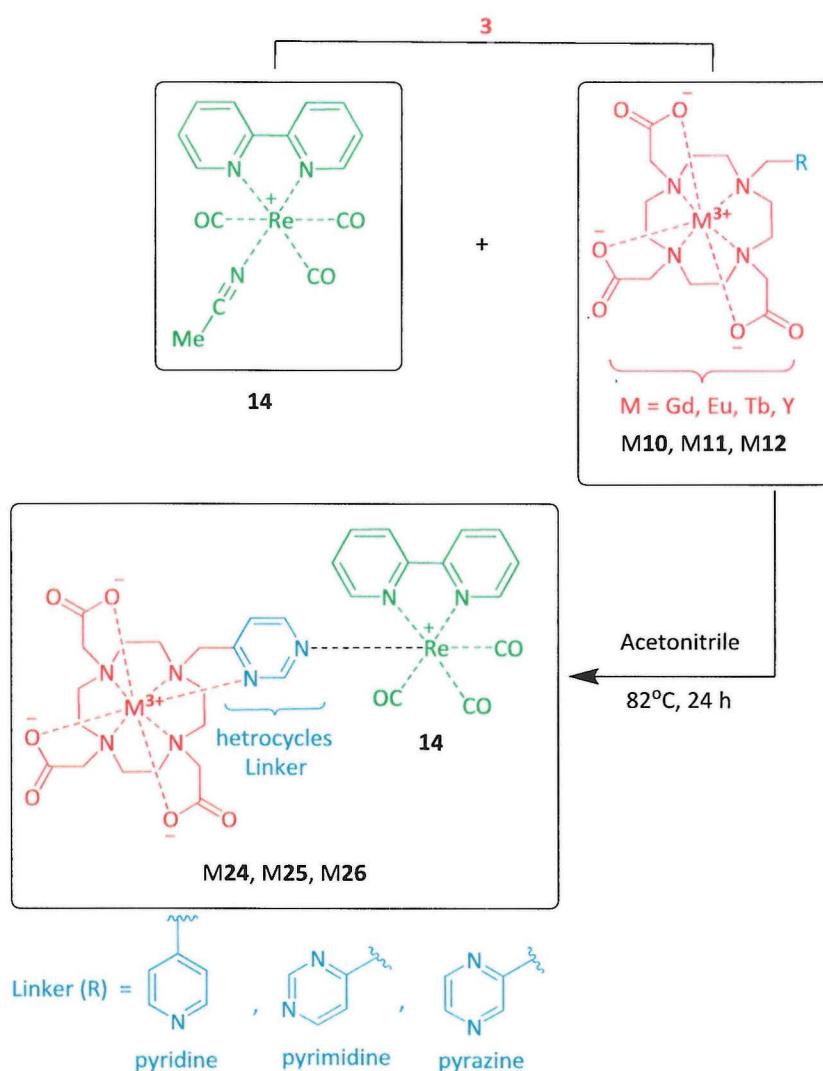


Figure 71 - Synthesised rhenium complex **14** and crystallised rhenium bipyridine complexes **15**, **16** and **17**.

### 4.3.2 Formation of combined Re-Ln(III) complexes via heterocyclic linkers.

Once the rhenium bipyridine unit (**14**) was synthesised it could be combined with the lanthanide(III) complexes (**M10**, **M11**, **M12**) synthesised in chapter 3. That combination (**M24**, **M25**, and **M26**) could offer an opportunity to increase the efficiency of the luminescence or modify the relaxivity properties of the lanthanide(III) metals for applications in optical or MR imaging.

One synthetic aim in this part of the research is to produce a linked bimetallic complex in which the rhenium chromophore complex acts as a sensitizing antenna to the lanthanide ion via the pendent heterocycle bridging between the metal ions, see Scheme 19.

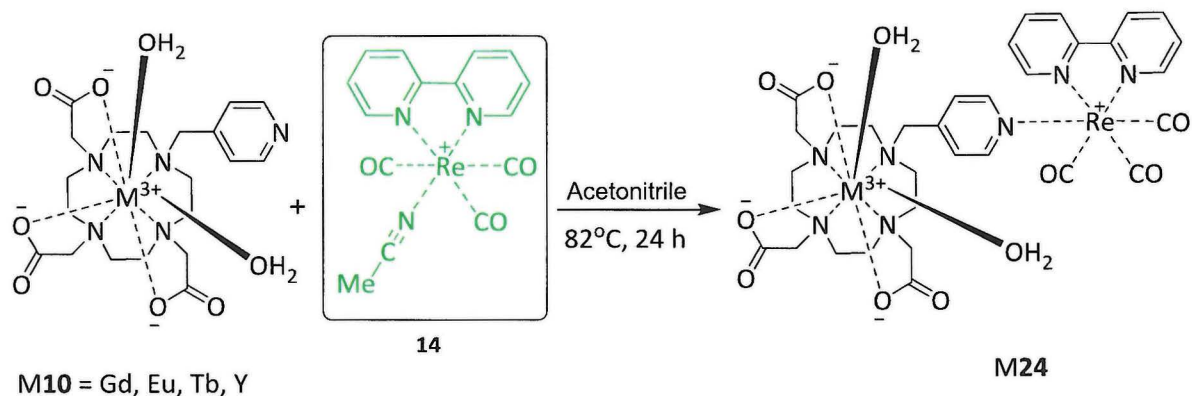


Scheme 19 – General reaction scheme to form **M24**, **M25**, and **M26**

This reaction method utilised modified version of literature procedures that had been used to synthesise related compounds.<sup>106</sup> The first step was to suspend both starting materials **M10**, **M11** or **M12** and **14** in acetonitrile and then mix and allow to react. The crude mixtures were purified via multiple precipitation steps from methanol with diethyl ether until fine yellow powders were obtained. The successful synthesis of the products (**M24**, **M25**, and **M26**) was confirmed by HRMS, CHN and ICP analysis. This method also used TLC to observe the reaction progress using DCM: MeOH 95:5 as eluent. The formation of a new yellow spot very close to the baseline indicates the formation of the products (**M24**, **M25**, and **M26**). This synthetic method was effective as clean mass spectra were obtained for synthesised products, the reaction proceeded in high yields, required few work up steps and a complicated purification method was not required.

#### 4.3.2.1 Formation of combined Re-Ln(III) complexes

The lanthanide complexes of pyridine DO3A (M10) have been combined with the rhenium bipyridine chromophore (**14**) to generate bimetallic d-f hybrid complexes (M24), where the pyridine pendent arm links to the transition metal center (Re(I)), see Scheme 20.



*Scheme 20. Reaction scheme to synthesise M24*

Faulkner and co-workers have previously synthesised the same bimetallic building blocks from lanthanide(III) complexes combined with a rhenium bipyridine chromophore also linked via pyridine ring ( $L^{27}$ ), see Figure 72.

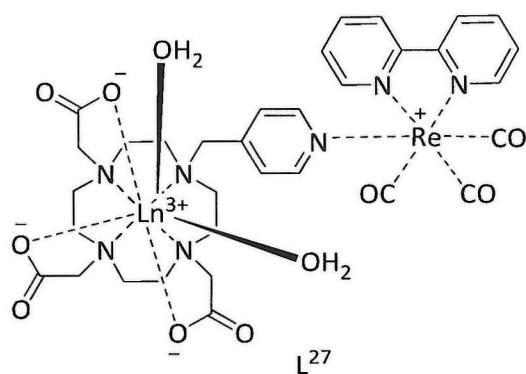
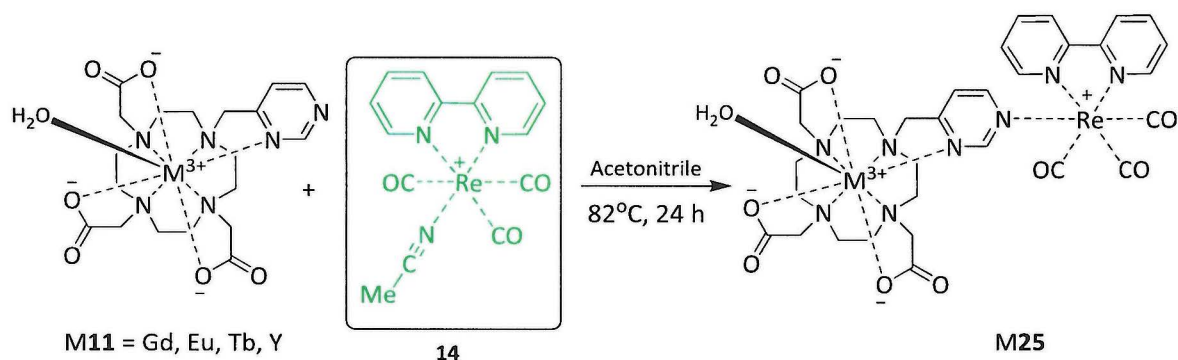


*Figure 72 - Representing example from the literature ( $L^{27}$ ), of the combining of Ln(III) complexes with rhenium bipyridine complexes through pyridine ring.*

$L^{27}$  showed interesting relaxivity properties with high relaxivity of  $8.6 \text{ mM}^{-1} \text{ s}^{-1}$  at 11.7 T for the gadolinium(III) complex. Long enough luminescence lifetimes to permit efficient gating of any fluorescent background, therefore it is a potential multimodal imaging agent. However,

as the design does not incorporate an optimal mechanism by which electrons can transfer between metals there are opportunities to modify the properties of this system.

M24 was synthesised by a different synthetic method compared to L<sup>27</sup> they are the same compound. It was resynthesized in this research work to provide a model reaction for the other synthesised building blocks M25 and M26 and a comparator where the heterocycle could not bridge between the two metal centres. Other comparable compounds were synthesised in our with the different heterocycles, consisting of a combination of synthesised lanthanide(III) complexes (M11) with rhenium bipyridine chromophore (14), including different heterocyclic linker (pyrimidine), see Scheme 21.



*Scheme 21 - Reaction scheme of synthesis of M25*

M25 could provide extra coordination bound to the Ln(III) metal centers (Gd<sup>3+</sup>, Eu<sup>3+</sup>, Tb<sup>3+</sup>, Y<sup>3+</sup>), through the additional nitrogen atom of the pyrimidine. This could lead to an energy transfer process via the conjugated  $\pi$  system between the two metal centers (Re<sup>+</sup>–Ln<sup>3+</sup>) that is not available with the M24 complexes. This could improve luminescence sensitisation of lanthanide ions. The Faulkner group synthesised an appropriate compound (L<sup>28</sup>) for comparison. As their research shows, the triazolophthalazene chromophore delivers effective sensitization to the lanthanide ions for luminescence, see Figure 73.<sup>107,108</sup>

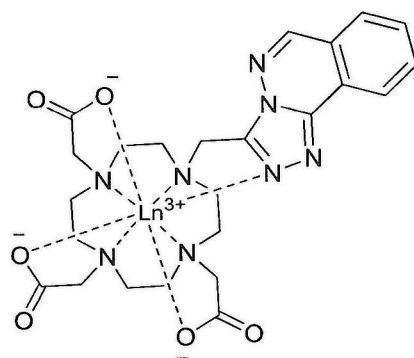
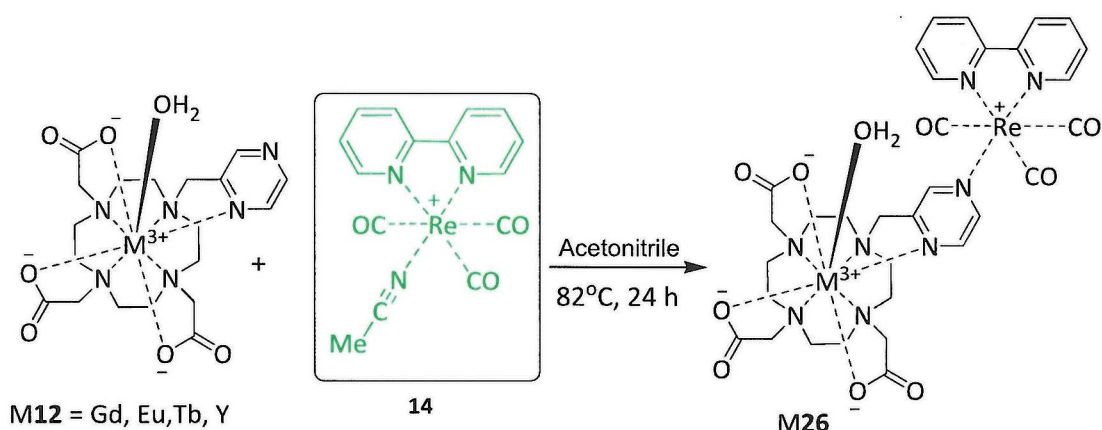


Figure 73 - Lanthanide macrocyclic complex linked with triazolophthalazene chromophore ( $L^{28}$ ).<sup>19</sup>

The third type of combined species that have been synthesised in this work is M26. Consisting of synthesised Ln(III) complexes (M12) linked to rhenium chromophore (14) via the pyrazine heterocyclic linker, see Scheme 22. The pyrazine shares the same potential properties as pyrimidine linker in M25 in terms of enhancing luminescence emission of bound lanthanide(III) ions.



Scheme 22 - Reaction scheme for the synthesis of M26

There are reports in the literature of bimetallic systems including a different heterocycle linker (triazoyl ring) ( $L^{29}$ ).<sup>106</sup> This has similar properties to the pyrazine arm in M12, in terms of containing two coordinating nitrogen positions, see Figure 74.

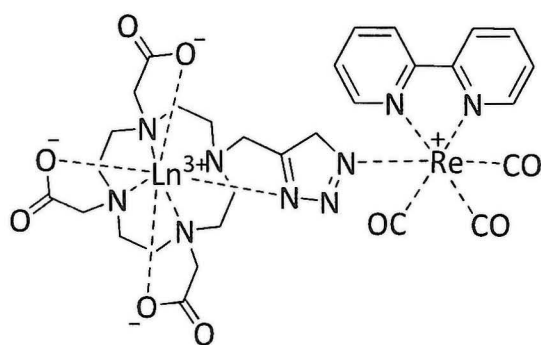


Figure 74 - Rhenium–lanthanide building blocks from the literature ( $L^{29}$ ).<sup>106</sup>

This example ( $L^{29}$ ) was produced by Faulkner's group via synthesis of bimetallic complexes from the lanthanide complexes with a rhenium chromophore, where both coordinate to the triazolyl pendent arm. Analysis of  $L^{29}$  shows that the triazole bridge facilitates the energy transfer from the rhenium chromophore to the lanthanide.  $L^{29}$  is an effective sensitizer for neodymium and ytterbium, giving emission from the ytterbium complex at 980 nm with double exponential decay kinetics.<sup>87</sup> The relaxometric studies of its gadolinium ( $L^{29}$ ) complexes demonstrate a significant effect for the combined species with a relaxivity of  $5.3 \text{ mM}^{-1} \text{ s}^{-1}$  compared to the gadolinium(III) complex on its own which has a relaxivity of  $3.4 \text{ mM}^{-1} \text{ s}^{-1}$ .<sup>44</sup>  $L^{29}$  shows that when the metal centers are held closely to each other the energy transfer will mediate most effectively,<sup>106</sup> that could point to promising future work for the building blocks (M24, M25, and M26) in this research work. Conjugated heterocycle bridged systems of this type are simple and effective with potential use in the preparation of larger luminescent assemblies.<sup>87</sup>

### 4.3.2.2 Conclusion

Three novel conjugated building blocks (M24, M25, and M26) have been synthesized which consist of a rhenium bipyridine chromophore (14) linked to the synthesised lanthanide(III) complexes (M10, M11, and M12), see Figure 75.

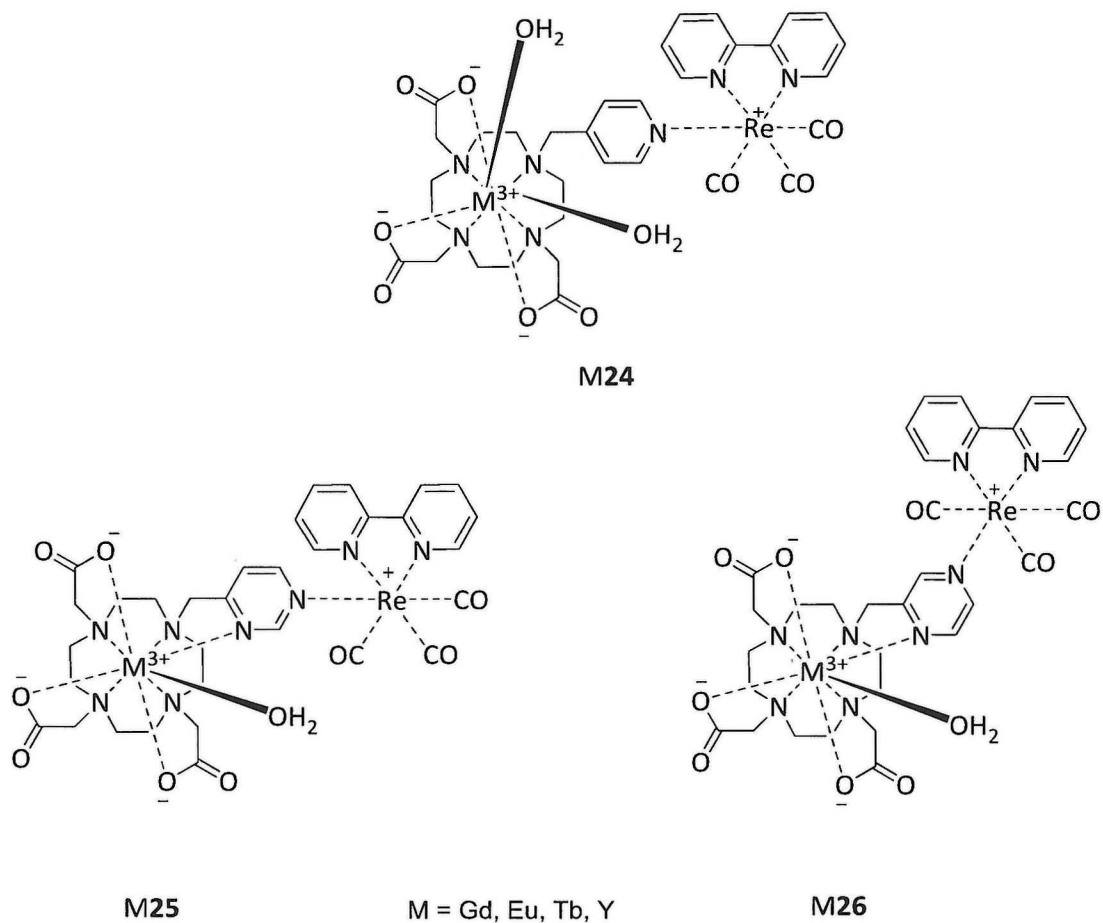


Figure 75 - Three novel combined products M24, M25, and M26.

## 4.4 Multimetallic systems

The aim of this section is to attempt to link multimetallic manganese species with the synthesised lanthanide(III) complexes (M10, M11, and M12) reported in chapter 3, via heterocyclic linkers, see Figure 76. The aim is to generate (paramagnetic) metal-metal combinations, which could offer the opportunity to alter the overall magnetic properties by combining single molecule magnets (SMMs) with lanthanide(III) complexes. The heterocycles (pyr, pym, and pyz) will act as linker units between the manganese species and the lanthanide(III) metal centres. Energy exchange can occur between the linked metal ions via the N-positions of the heterocyclic linker.

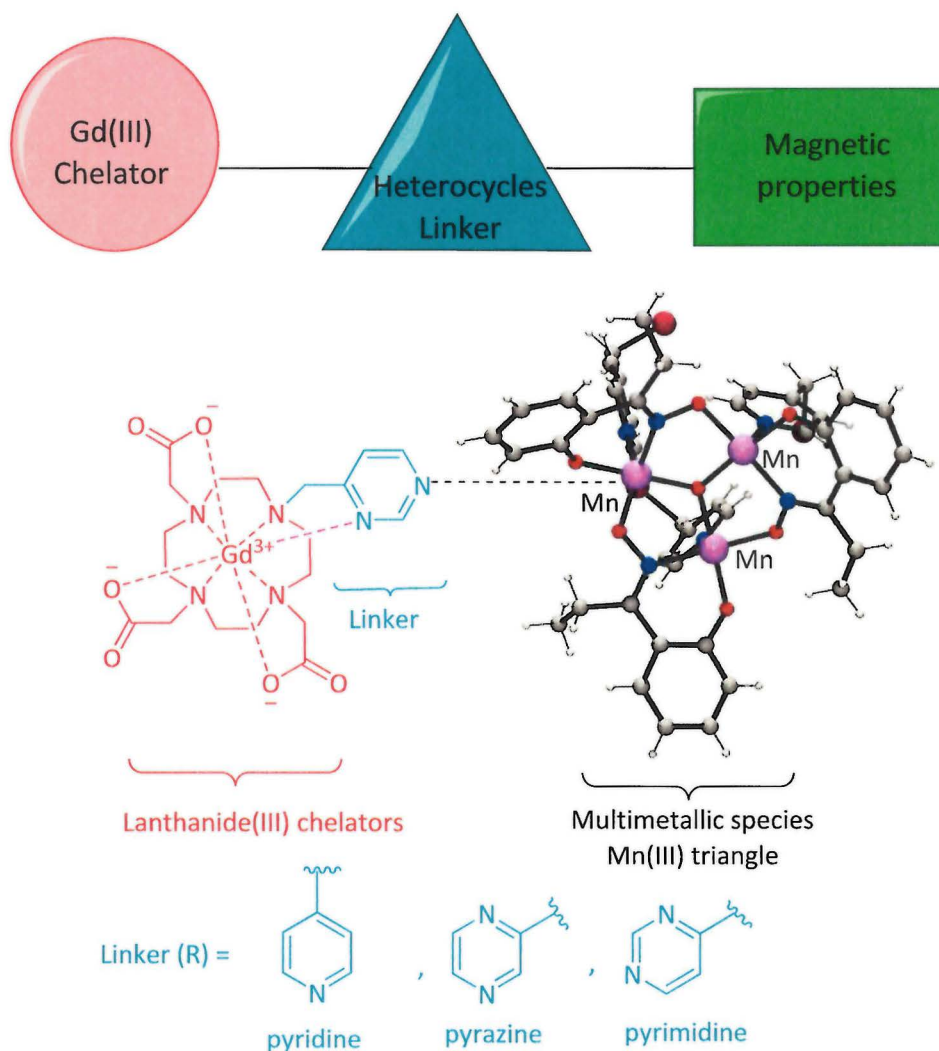


Figure 76 - Schematic representation of the combination of Gd(III) complexes with multimetallic species throughout the heterocyclic bridge. Colour code: Mn(III) (purple), O (red), N (blue) C (grey).

The same principle was used in the bimetallic system with the rhenium bipyridine complex, see section 4.3. In this case a multimetallic manganese species was used instead of the rhenium bipyridine chromophore to bind to lanthanide(III) macrocyclic complexes. These multimetallic arrays could potentially be of interest in several applications besides enhancing the relaxivity in MRI contrast experiments, such as data storage,<sup>109</sup> or as magnetic coolers.<sup>110</sup>

#### 4.4.1 Formation of multi manganese(III) systems

Multimetallic species such as manganese(III) triangles, see Figure 77, possess the ability to retain magnetization for relatively long periods of time, keeping the same properties of molecule in the absence of an applied magnetic field. These molecules often contain weak intermolecular interactions such as hydrogen bonding or  $\pi\cdots\pi$  interactions, influencing their magnetic properties, especially at low temperature.<sup>111</sup> A series of multimetallic single molecule magnets (SMMs) species have been synthesised which contained different metals such as lanthanides, transition metals, and actinides.<sup>112</sup>

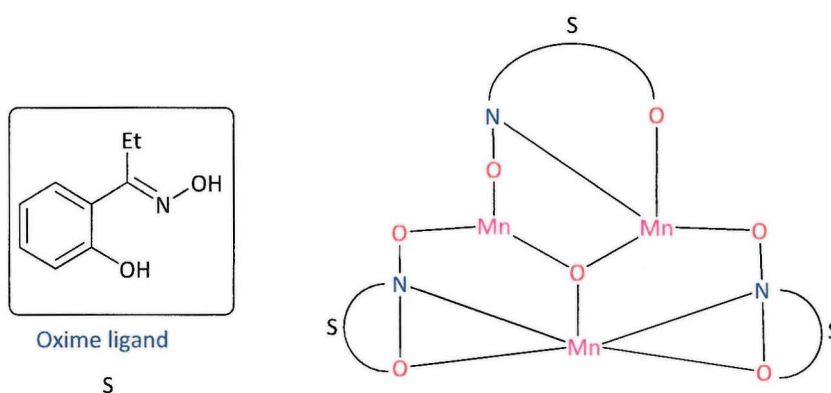
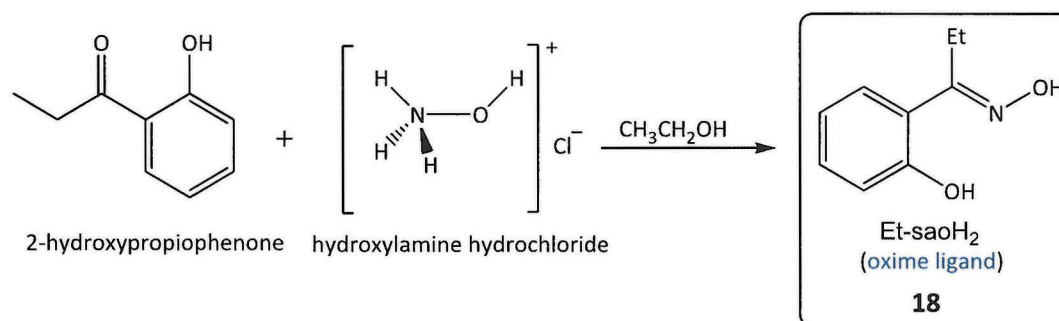


Figure 77 - Multimetallic species of Mn triangle and the positions of oxime ligands (18).

Commonly these multimetallic species use salicylaldoxime ( $\text{saoH}_2$ ) as a ligand, because it can be used under a variety of reaction conditions and is effective in producing multimetallic species. The oxime ligand ( $\text{saoH}_2$ ) is used in this work,<sup>113</sup> see Figure 77. Manganese(III) is an appropriate transition metal to be used as a core for multimetallic molecules because of the efforts to exploit it in the polymetallic SMM field, based on the Jahn–Teller of manganese(III) ion (high-spin  $d^4$ ), which is important for the magnetic anisotropy of the multimetallic species.<sup>113</sup> Moreover, the low toxicity of free manganese(III) make it preferable for biological use.

#### 4.4.1.1 Synthesis of oxime ligand (saoH<sub>2</sub>) (**18**)

The salicylaldoxime (saoH<sub>2</sub>) and its derivatives have attracted interest in coordination chemistry over last decade,<sup>114,115</sup> due to the remarkable magnetic properties of these compounds as SMMs. Two different families were formed with Mn(III), hexanuclear or trinuclear. The general formula for trinuclear species of this type is [Mn(III)O(R-sao)<sub>3</sub>(O<sub>2</sub>CR)(L)<sub>3</sub>], where R = H, Me, Et, etc., while L = solvents. In addition, the oxime (Et-saoH<sub>2</sub>) is usually used as a ligand with Mn(III) triangles (SMMs) to increase the ground spin state from S = 2 to S = 6, enhancing the effective energy barrier for magnetization of these molecules to record levels.<sup>116</sup>



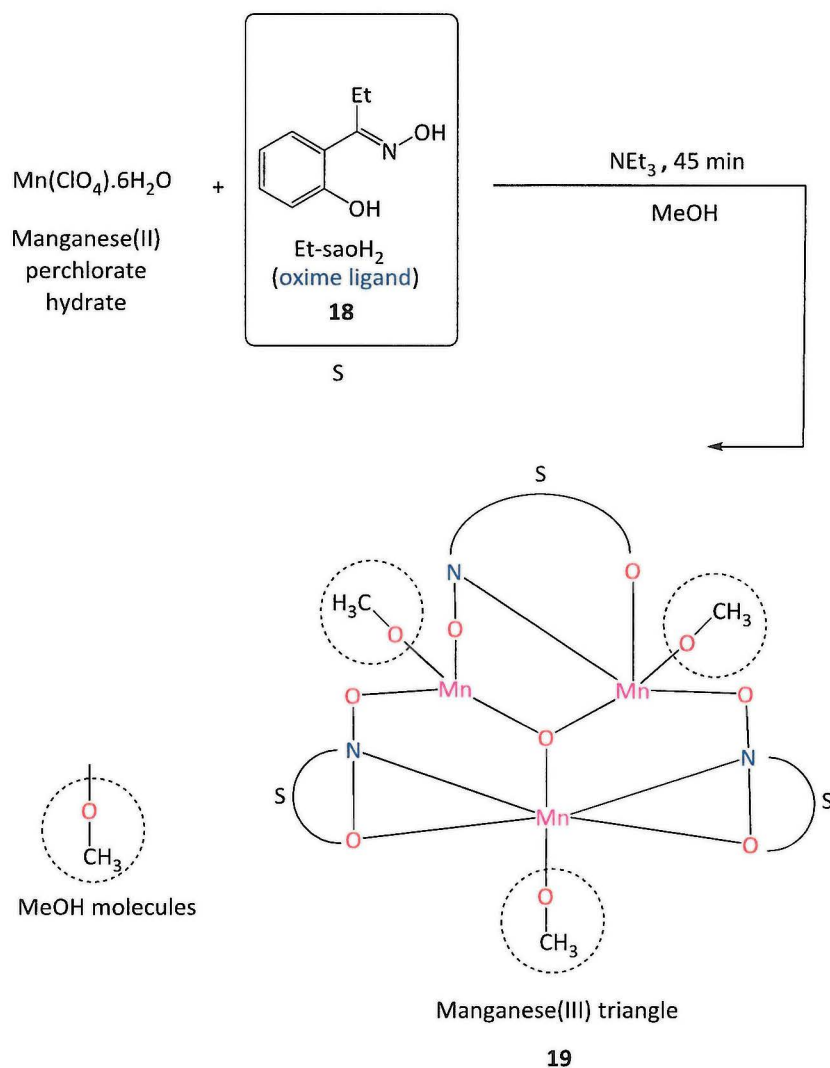
*Scheme 23 - Synthetic route to form oxime **18***

The synthetic procedures to form both the oxime and the Mn(III) triangle exactly followed literature methods,<sup>111</sup> as these are known compounds. Previous studies had succeeded in assembling the molecular triangles with a series of different heterocycles. This gave the inspiration to apply it with the heterocyclic compounds produced within this research.

The reaction to form **18** was carried out by mixing equal molar amounts of 2-hydroxypropiophenone and hydroxylamine hydrochloride in ethanol, see Scheme 23. The reaction mixture was then heated to reflux for 4 h to give a crude oil after the work up steps. Diethyl ether was used to wash the product, removing starting materials and any impurities. Drying gives a crystalline product as a white yellow solid.

#### 4.4.1.2 Synthesis of manganese triangle (19)

**18** was combined with an appropriate Mn(II) precursor to generate the desired multimetallic assemblies (Mn<sup>3+</sup> triangle, **19**) by following the reported literature method,<sup>111</sup> see Scheme 24.



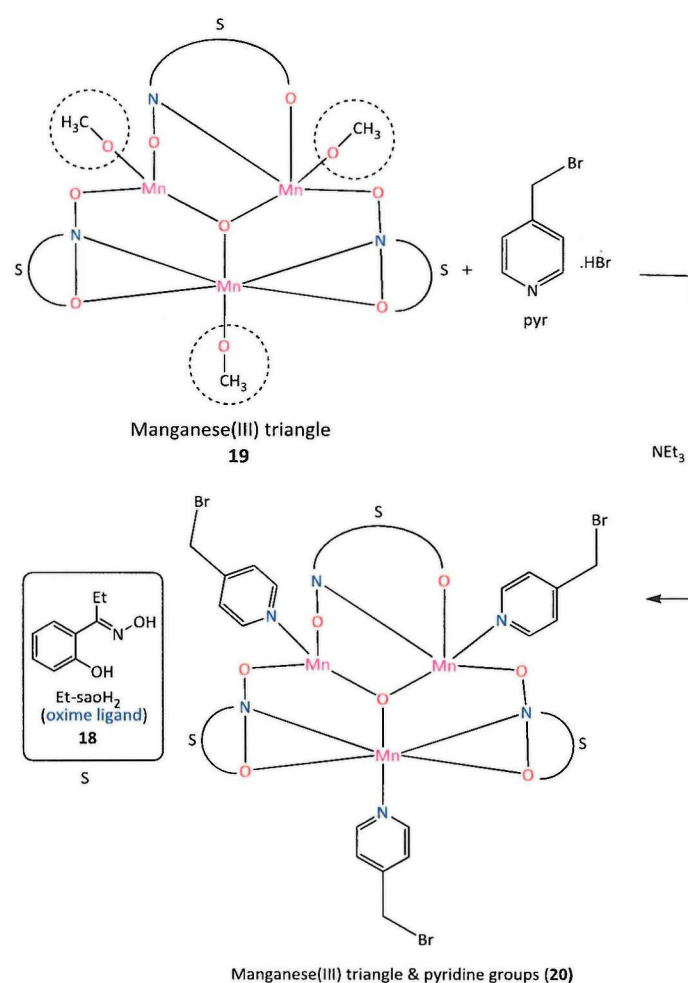
*Scheme 24 - Schematic representation of combining oxime ligand (18) with Mn(II) precursor to form a Mn(III) triangle (multimetallic species)(19).*

One equivalent of both starting materials Mn(ClO<sub>4</sub>)·6H<sub>2</sub>O and oxime ligand (**18**) were mixed in alcohol (MeOH), then base (triethylamine) was added to give a black solution,<sup>111,117</sup> in which the Mn(III) triangle is formed with the attached oxime ligand. The major advantage of this type of Mn(III) triangle is the availability of potential coordination sites on each individual Mn(III) ion which is occupied by methanol molecules in the compound synthesised<sup>118</sup> These sites are available for substitution by the heterocycle ligands.

#### 4.4.1.3 Formation of combined Mn(III) triangle (19) with pyridine heterocyclic linkers

The aim of the research work reported in this section is to combine the synthesised Mn(III) triangle (19) with a selected heterocyclic ligand (pyridine) in a model reaction. 19 was formed in a dark green solution by mixing  $\text{Mn}(\text{ClO}_4) \cdot 6\text{H}_2\text{O}$  with oxime together for 45 mins, to be then ready for simply mixing with selected heterocycles ligands (pyr) in a one-pot reaction, filtered and left without disturbing for slow diffusion at the room temperature.

The slow diffusion allowed the substitution reaction to take place between the terminally bound groups (MeOH) and 4-(bromomethyl) pyridine. Successful linking between both components (19 and pyridine) was achieved producing a supramolecular  $[\text{Mn}_3(\text{III})\text{O}(\text{Et-sao})_3(\text{pyr})_3(\text{ClO}_4)]$  (20) compound as black crystals in two days, see Scheme 25.



Scheme 25 - Schematic representation the reaction of Mn(III) triangle with pyridine (heterocycle).

This successful combination offers the proof of principle to possibly link Mn(III) triangles (**19**) with synthesised lanthanide(III) complexes **M10** via the same heterocycle (pyridine), see Figure 78, which is already successfully attached to these complexes (**M10**).<sup>111</sup>

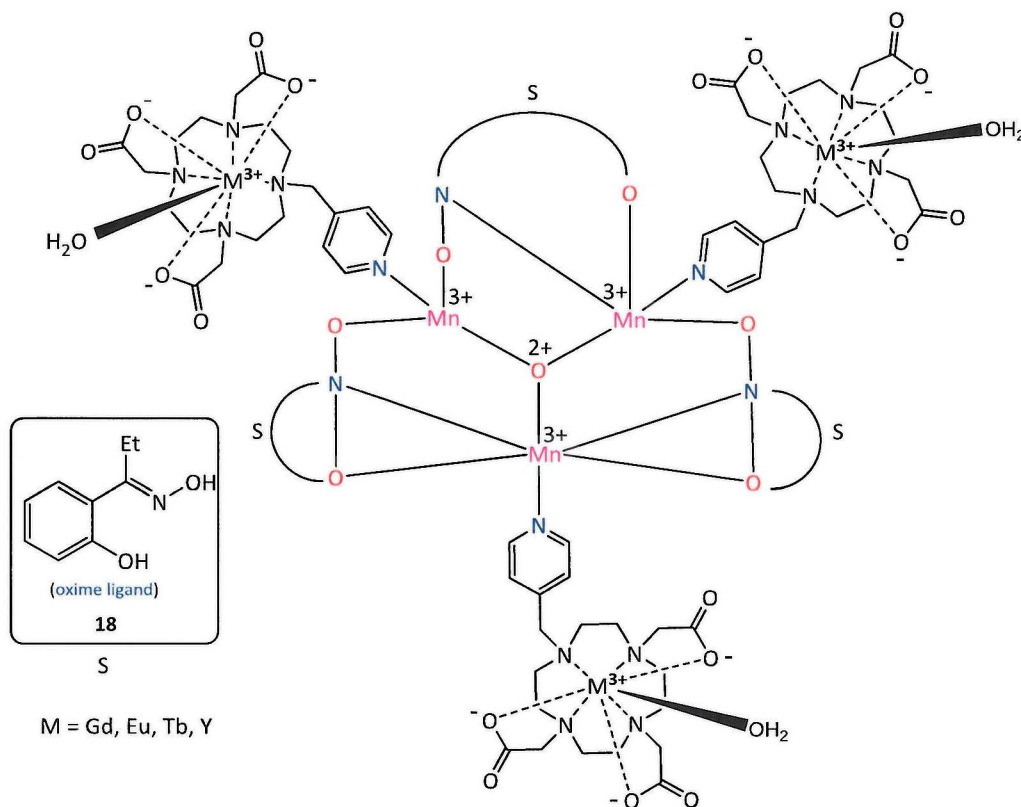


Figure 78 - Schematic representation the proposed combination of M10 complexes with Mn triangle (**19**) throughout the heterocycle bridge (pyr).

This could also be considered as model reaction to apply the same principle with **M11**, **M12** through pyrimidine or pyrazine respectively. The attachment of pyridine to the lanthanide complexes, as in the structure of **20**, shows promise as a potential method to link the components. The manganese triangle structure precursor capped from the top by  $\text{ClO}_4^-$  anion weakly coordinated to  $\text{Mn}_3$  atoms, and from the bottom each Mn(III) ion is attached to a methanol molecule which can easily be substituted by the heterocyclic group.<sup>119</sup> Brechin and co-workers,<sup>111</sup> synthesised a further similar  $\text{Mn}_3$  triangle ( $\text{L}^{30}$ ), see Figure 79, which contained the same salicylaldehyde oxime ligand (oxime). However, in this case a different substituted pyridyl ligand ( $\beta$ -picoline) was used, to give a compound with the formula  $[\text{Mn}_3(\text{III})\text{O}(\text{Et-sao})_3(\beta\text{-pic})_3(\text{ClO}_4)]$ .

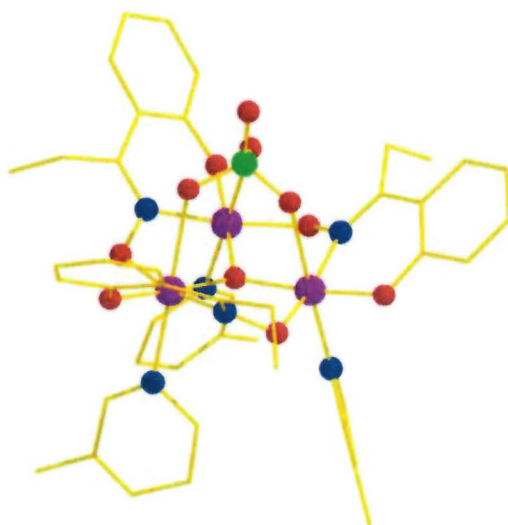


Figure 79 - Multimetallic molecule of Mn triangle attached to picoline Colour code: Mn(III) (purple), O (red), N (blue) C (yellow) Cl (green). (L<sup>30</sup>)

In terms of comparison between [Mn<sub>3</sub>(III)O(Et-sao)<sub>3</sub>(β-pic)<sub>3</sub>(ClO<sub>4</sub>)] with the novel Mn(III) triangle [Mn<sub>3</sub>(III)O(Et-sao)<sub>3</sub>(pyr)<sub>3</sub>(ClO<sub>4</sub>)] (**20**) isolated in this work, they are very similar, however some differences can be observed in their bond length and angles, see Table 11.

	[Mn <sub>3</sub> (III)O(Et-sao) <sub>3</sub> (pyr) <sub>3</sub> (ClO <sub>4</sub> )]( <b>20</b> )	[Mn <sub>3</sub> (III)O(Et-sao) <sub>3</sub> (βpic) <sub>3</sub> (ClO <sub>4</sub> )] <sup>111</sup> (L <sup>30</sup> )
Mn-(μ <sub>3</sub> -O) distance (Å) Mn <sub>1</sub> -O, Mn <sub>2</sub> -O, Mn <sub>3</sub> -O	1.867(4) ,1.858(4) ,1.896(4)	1.9007(4) ,1.899(4) ,1.9005(4)
Mn-(μ <sub>3</sub> -O)-Mn angles (°) Mn1-2, Mn2-3, Mn1-3	118.600 (2), 117.700 (2), 117.600(2)	117.917(1), 117.865(1) ,117.900(1)

Table 11- selected bond length and angles between (**20**) and similar literature compound (L<sup>30</sup>).<sup>111</sup>

A range of crystal growth experiments were carried out aimed at linking either of the other two heterocycles (pym, pyz) or the synthesised ligands (**M10**, **M11**, and **M12**) with the Mn(III) triangle (**19**) by using various molar ratios and solvents. However, all attempts failed and ended up only producing Mn(III) triangle crystals. This could be due to the solvents (alcohols) preventing any substitution reactions from occurring. Therefore further experimental work is required to join the Mn(III) triangle with pyrimidine or pyrazine and subsequently with lanthanide(III) complexes (**M10**, **M11**, and **M12**).

#### 4.4.1.4 Formation of manganese pentamer (21)

During the preparation attempts to combine heterocycles (pym, pyz) and Mn triangles under different conditions, a novel penta-manganese crystalline material was formed, see Figure 80. The structure contains five manganese atoms bridged by oxygen atoms. It has the appearance of an extended manganese triangle with an extra two manganese metal ions incorporated and the presence of two bridging oxo ligands.

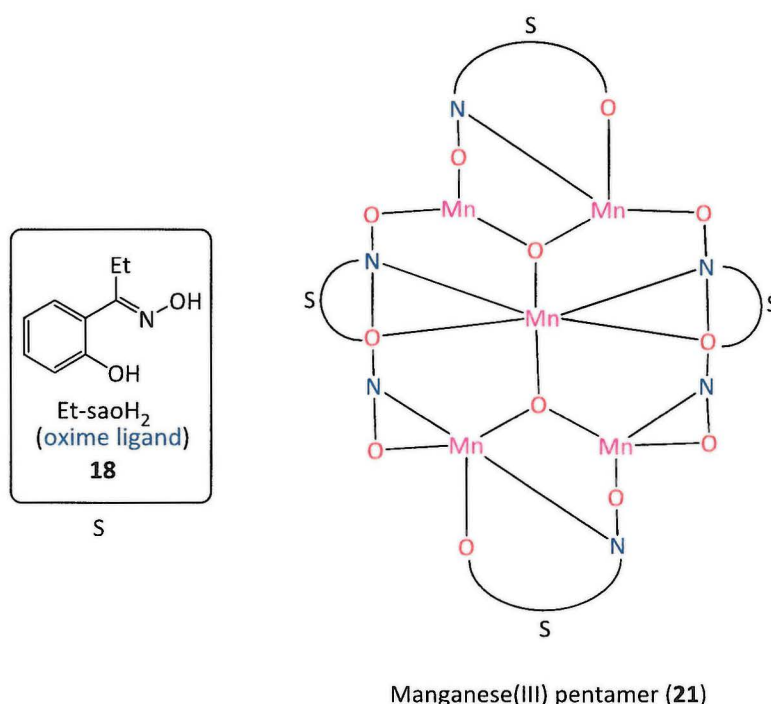
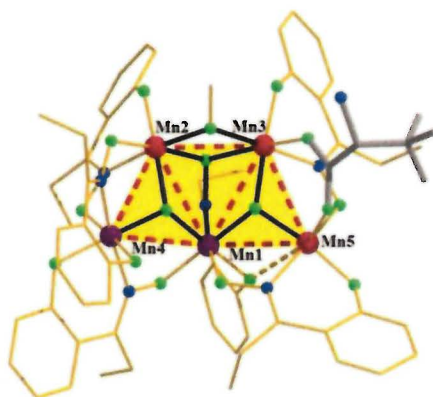


Figure 80 - X-ray crystal structure of penta-manganese **21**

The synthesis of **21** resulted from following a modified literature method,<sup>111</sup> in which the starting materials (oxime ligand **18** & Mn<sup>3+</sup>triangle **19**) and the base (triethylamine) were mixed, and stirred for 45 mins. One equivalent of **3** was added, and then the mixture was left to slowly evaporate at room temperature to give dark black crystals.

In case of the comparison between the Mn(III) triangle with pyridine (**20**) and Mn pentamer (**21**), there are significant differences in some bond angles such as 60.13° (Mn-Mn-Mn) for **20** and 117.68° (Mn-Mn-Mn) for **21**. Furthermore, there is a clear different in the bond angle (O-Mn-Mn), which is 75.74° for **20** and 122.00° in (O-Mn-Mn) for **21**.

Additionally, the perchlorate group on the top of **20** leans towards the ethyl groups in the Et-sao<sup>2-</sup> ligands is not present in **21**. Manganese pentamers in literature are rare with less than 10 examples found in the CCDC. The Brechin group,<sup>120</sup> investigated the reaction system of Mn<sup>n+</sup>/ amino acids (valine) and synthesised polynuclear manganese complexes (L<sup>31</sup>), see Figure 81, containing amino acid ligands which could be used as models for the active sites of manganese inside the enzymes.



L<sup>17</sup>

Figure 81 - The molecular structure of literature penta-manganese complex, colour code: Mn(III) = red, Mn(IV) = purple, O = green, N = blue, C = yellow, Val = grey.<sup>120,121</sup>

Significant similarities can be observed between **21** and L<sup>31</sup>, in which both have six oxygen ligands (Et-sao<sup>2-</sup>), while the amino acid manganese cluster L<sup>31</sup> has extra bridging groups ( $\mu$ -OCH<sub>3</sub><sup>-</sup>, valine carboxylate) between the Mn(III) ions compared to O<sup>2-</sup> in the penta-manganese Et-sao<sup>2-</sup> ligand compound (**21**). Selected bond angles and lengths are listed in Table 12.

[Mn <sub>5</sub> O <sub>2</sub> (Et-sao) <sub>6</sub> ]( <b>21</b> )	Bond length (Å) and angles (°)	[Mn <sub>5</sub> O <sub>2</sub> (Et-sao) <sub>6</sub> (CH <sub>3</sub> O) <sub>3</sub> (Val).1.5 H <sub>2</sub> O (L <sup>31</sup> ). <sup>120</sup>	Bond length (Å) and angles (°)
Mn(1)-O(1)	1.962 (Å)	Mn(1)-O(1)	1.880(Å)
Mn(2)-O(1)	1.900 (Å)	Mn(2)-O(1)	1.933(Å)
Mn(3)-O(18)	2.423 (Å)	Mn(3)-O(17)	2.162(Å)
Mn(4)-O(15)	1.877 (Å)	Mn(4)-O(14)	1.855(Å)
Mn(5)-O(13)	1.918 (Å)	Mn(5)-O(15)	1.995(Å)
Mn(5)-O(2)- Mn(1)	117.71(°)	Mn(5)-O(2)- Mn(1)	108.80(°)
Mn(4)-O(1)- Mn(2)	101.63 (°)	Mn(4)-O(1)- Mn(2)	108.99(°)

Table 12 - Selected bond length and angle for **20** and amino acid penta-manganese cluster from literature (L<sup>31</sup>).<sup>120,121</sup>

#### 4.4.1.5 Conclusion

The crystal structure of a novel compound has been described which consists of multimetallic species ( $\text{Mn}^{3+}$  triangle) combined with a heterocycle precursor (pyridine) (**20**). This compound is considered as a model of a potential method for linking Mn triangles with synthesised lanthanide(III) complexes (such as M**10**). Penta-manganese (**21**) was formed during the course of the reactions attempted and its crystal structure described, see Figure 82.

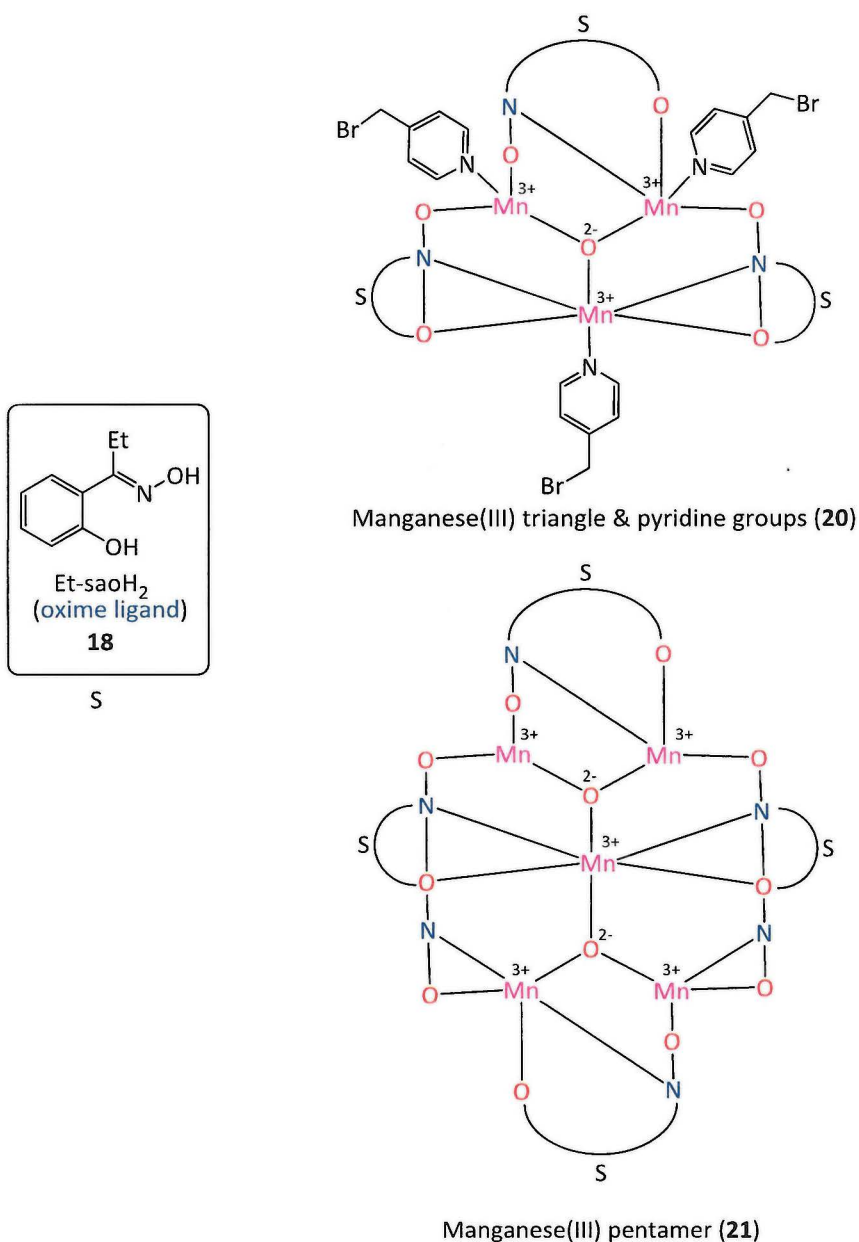
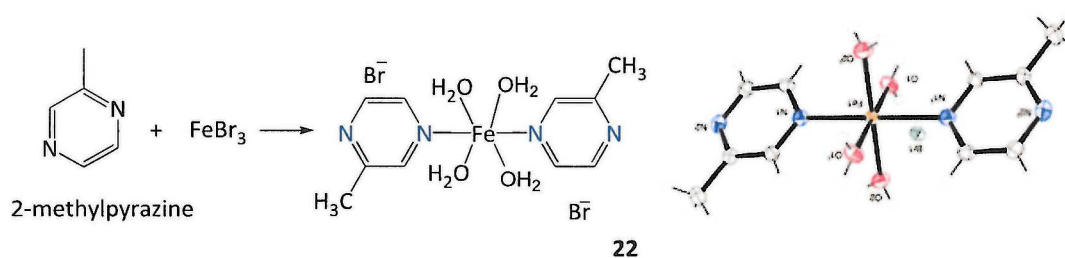


Figure 82 - The novel multimetallic (Mn triangle) with bromomethylpyridine ring attached (**20**), and formed Mn pentamer (**21**).



#### 4.4.2.1 Synthesis of $[\text{Fe}(\text{II})(\text{H}_2\text{O})_4(2\text{-methylpyrazine})_2(\text{CH}_3)_2\text{Br}_2](\mathbf{22})$

Several research groups,<sup>122,124</sup> have shown interesting magnetic properties of iron containing species. Therefore attempts to combine pyrazine rings with iron have previously succeeded in producing extensive two-dimensional networks of hydrogen bonded interactions consisting of two pyrazine rings linked via iron atoms with four water molecules coordinated to the iron,<sup>122,124</sup> see Scheme 26.



*Scheme 26- preparation reaction of crystal structure  $[\text{Fe}(\text{II})(\text{H}_2\text{O})_4(2\text{methylpyrazine})_2(\text{CH}_3)_2\text{Br}_2](\mathbf{22})$*

This reaction was carried out following modified literature methods,<sup>125,126</sup> by mixing one molar equivalent of iron(III) bromide with 2-methylpyrazine. The solution was filtered and layered with acetone to produce  $[\text{Fe}(\text{II})(\text{H}_2\text{O})_4(2\text{-methylpyrazine})_2(\text{CH}_3)_2](\mathbf{22})$  and after 3 days evaporation at room temperature yellow crystals suitable for XRD analysis were isolated. This could be considered as a model reaction towards the possibility of attaching two lanthanide complexes via the heterocycle linker (e.g. pyrazine), see Figure 84,

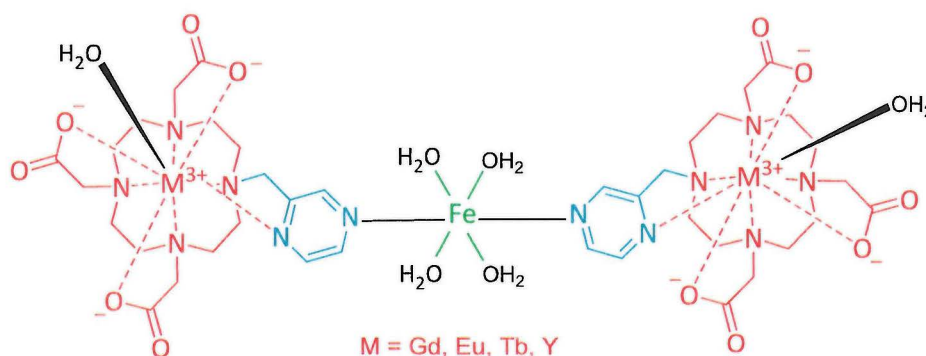


*Figure 84 – Proposed linking of two lanthanide complexes via the iron and the heterocycle linker (pyrazine).*

The structure of **22** showed an octahedral iron(III) centre which is located on an inversion centre with four water molecules coordinated to the iron atom in the equatorial plane and the two 2-methylpyrazine molecules on the perpendicular axis. **22** is very similar to compound L<sup>32</sup> reported by Stavrapoluse and co-workers,<sup>122</sup> see Figure 85.

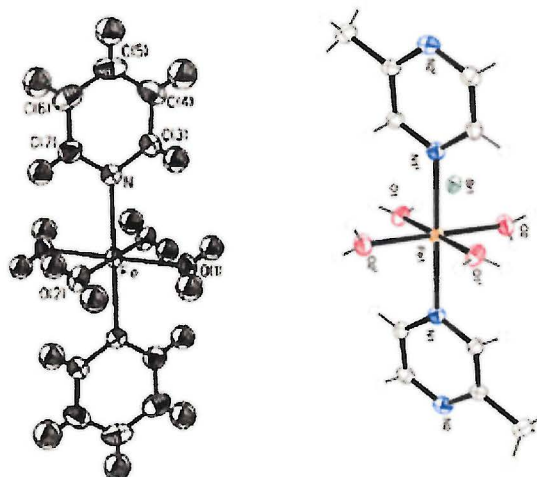


Figure 85 - Crystal structure of  $[\text{Fe}(\text{II})(\text{H}_2\text{O})_4(\text{trans-pyr})_2][\text{O}_2\text{CCH}_3]_2$  from literature (L<sup>32</sup>, eft).<sup>122</sup> Synthesised crystal **22** (right).

Nevertheless, clear differences can be observed with L<sup>32</sup>, as a different heterocycle ring has been used (pyridine) without methyl group as in **22**. Similarity can be seen between the compounds in the bonds length and angles observed, see Table 13.

$[\text{Fe}(\text{II})(\text{H}_2\text{O})_4(\text{trans-spyr})_2][\text{O}_2\text{CCH}_3]_2$ from literature (L <sup>32</sup> ). <sup>122</sup>	$[\text{Fe}(\text{II})(\text{H}_2\text{O})_4(2\text{-methylpyrazine})_2(\text{CH}_3)_2\text{Br}_2]$ <b>22</b>
Fe(1)-O(1)= 2.122(5) Å	Fe(1)-O(1)= 2.102(15) Å
Fe(1)-O(2)= 2.122(6) Å	Fe(1)-O(2)= 2.102(15) Å
Fe(1)-N(1)= 2.213(6) Å	Fe(1)-N(1)= 2.231(18) Å
O(1)-Fe(1)-O(2)= 90.32(10)(°)	O(1)-Fe(1)-O(2)= 90.23(7)(°)
O(1)- Fe (1)-N(1)= 92.82(10)(°)	O(1)- Fe (1)-N(1)= 88.33(10)(°)
O(2)- Fe (1)-N(1)= 90.67(10)(°)	O(2)- Fe (1)-N(1)= 91.67(10)(°)

Table 13 - Selected bond length and angles between **22** and similar literature compound (L<sup>32</sup>).<sup>122</sup>

The unit cell of **22** shows the packing and H-bonding interactions, see Figure 86.

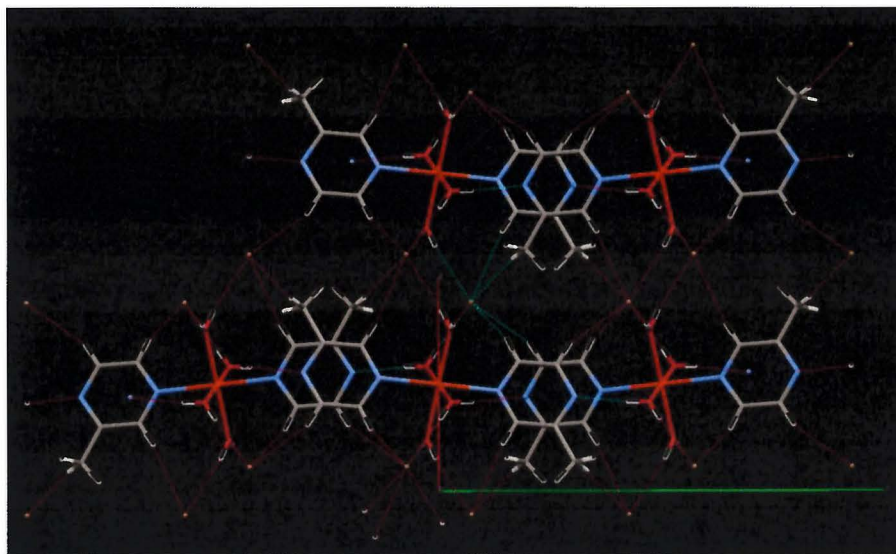
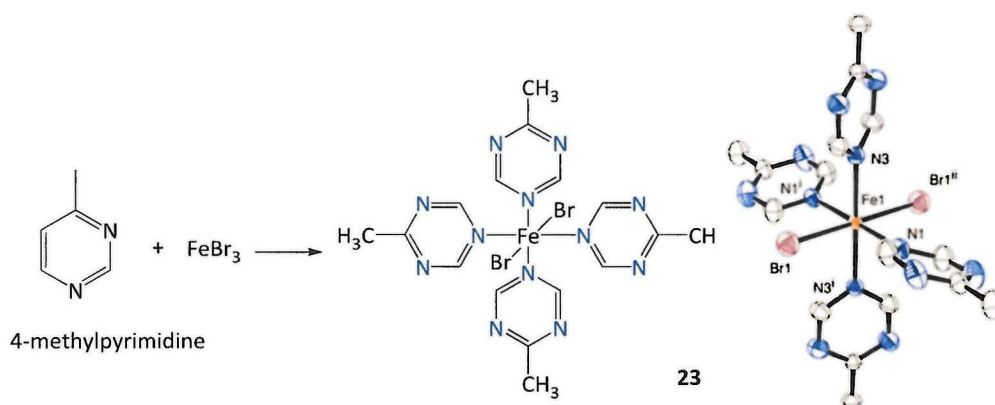


*Figure 86. Unit cell of the crystal structure of 22*

#### 4.4.2.2 Synthesis of $[\text{Fe}(\text{II})(4\text{-methylpyrimidine})_4(\text{CH}_3)_2(\text{Br}_2)](\mathbf{23})$ .

Several studies,<sup>127-131</sup> demonstrate the interesting electronic and magnetic properties of tetraheterocyclic metal halide complexes. This is due to the tetragonal symmetry of these complexes with a *trans* halide in the axial coordination sites and four heterocycle rings in equatorial positions. **23** has coordination of four pyrimidine rings (linker) via the iron metal centre, see Scheme 27.



*Scheme 27 - preparation reaction of crystal structure of  $[\text{Fe}(\text{II})(4\text{-methyl-pym})_4](\text{Br})_2(\mathbf{23})$*

Synthesis of **23** was carried out using the modified literature methods applied to the synthesis of **22**.<sup>125,126</sup> 4-Methylpyrimidine was used instead of 2-methylpyrazine as they both represent the heterocyclic bridging arms of the synthesised lanthanides(III) complexes (M11, M12). The pyrimidine ligand in **23** was partly  $\pi$ -bonded to metal via the interaction of  $t_{2g}$  orbitals in the metal, and the symmetry of the compound can be clearly observed in the distortion of Br-Fe-N and N-Fe-N bond coordination bond angles from  $90^\circ$  and  $180^\circ$  respectively.<sup>123</sup> The crystalline product **23** was isolated as blue crystals after four days. The compound consists of a *trans* bromide geometry with the four nitrogen atoms of pyrimidine rings in a plane around the metal ion (iron), see Figure 87.<sup>127</sup>

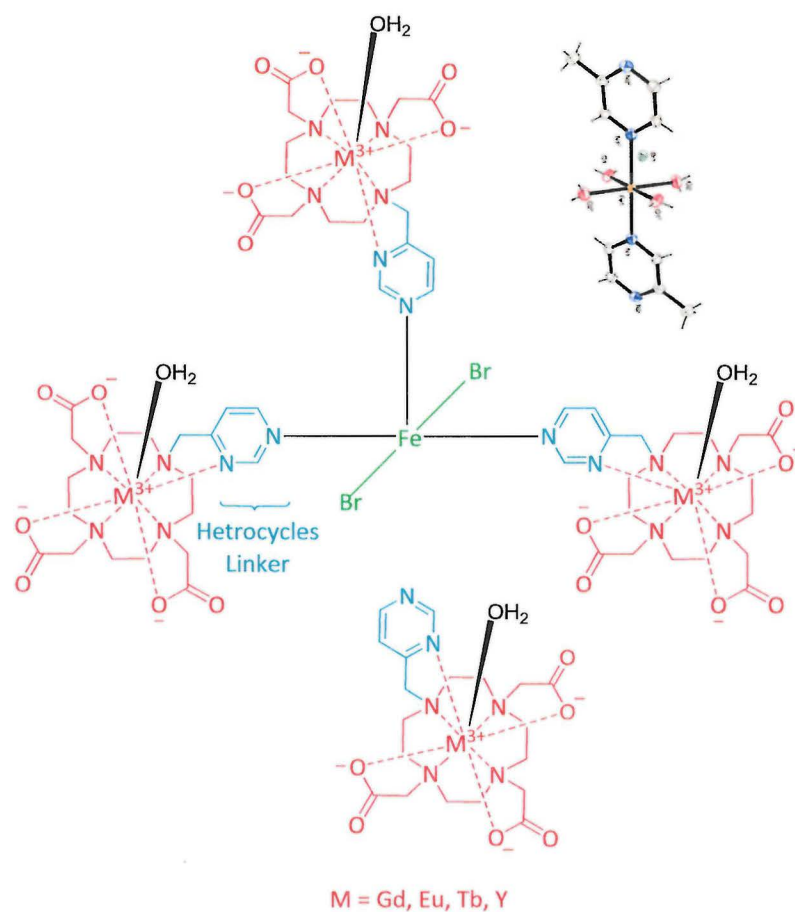


Figure 87 - Proposed combination of four lanthanide(III) complexes via iron linker.

Long *et al.* synthesised a trans compound ( $L^{33}$ ) with only two differences relative to **23**, which are the use of pyridine instead of pyrimidine and chlorine instead of bromine, see Figure 88.

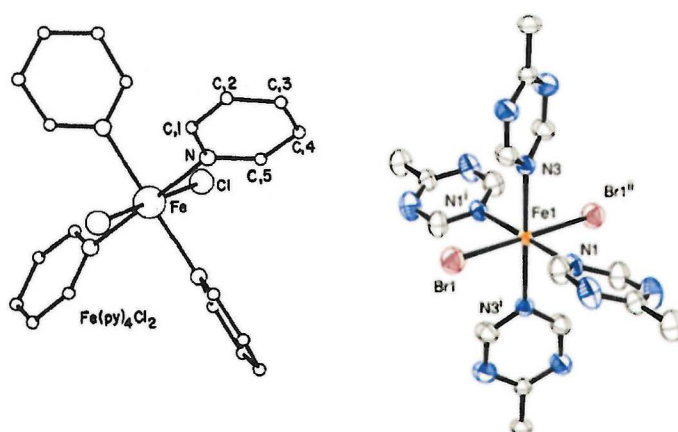


Figure 88 - crystal structure of  $[Fe(II) (trans-py)_4Cl_2]$  from literature ( $L^{33}$ , left).<sup>123</sup>Synthesised crystal **23** (right).

Similarities can be observed for the compounds in the selected bond distance and angles,<sup>123</sup> see Table 14.

[Fe(II) (4-methylpyrimidine) <sub>4</sub> ][Br] <sub>2</sub> (23)	[Fe(II) ( <i>trans</i> -py) <sub>4</sub> ][Cl] <sub>2</sub> (L <sup>33</sup> ) <sup>123</sup>
Fe(1)-Br(1)= 2.568(10)Å	Fe(1)-Br(1)= 2.444(2)Å
Fe(1)-N(3)= 2.263(6)Å	Fe(1)-N(3)= 2.183 (4)Å
Fe(1)-N(1)= 2.285(6)Å	Fe(1)-N(1)= 2.177(6)Å
N(1)-C(1)= 1.349(15)Å	N(1)-C(1)= 1.331(9)Å
N(3)-C(5)= 1.353(12)Å	N(3)-C(5)= 1.332(9)Å
N(3)- Fe(1)-N(1)= 90.1(29)( $\bar{o}$ )	N(3)- Fe(1)-N(1)= 89.90(2)( $\bar{o}$ )
N(3)- Fe(1)-Br(1)= 88.92(17)( $\bar{o}$ )	N(3)- Fe(1)-Br(1)= 90.0(14)( $\bar{o}$ )

Table 14 - Selected bond length and angles for 22 and a related literature compound.<sup>123</sup>

## 4.5 Conclusions

The main achievements reported in this chapter include the synthesis of 12 novel bimetal building blocks (M24, M25, and M26). The purity of the synthesized complexes was confirmed by HRMS and CHN analysis. Potentially the success of binding a monometallic species (rhenium bipyridine complex) (**14**) with the lanthanide(III) complexes (M10, M11, and M12) provides scope to apply these rigid multimetallic arrays (d-f hybrids) (M24, M25, and M26), see Figure 89.

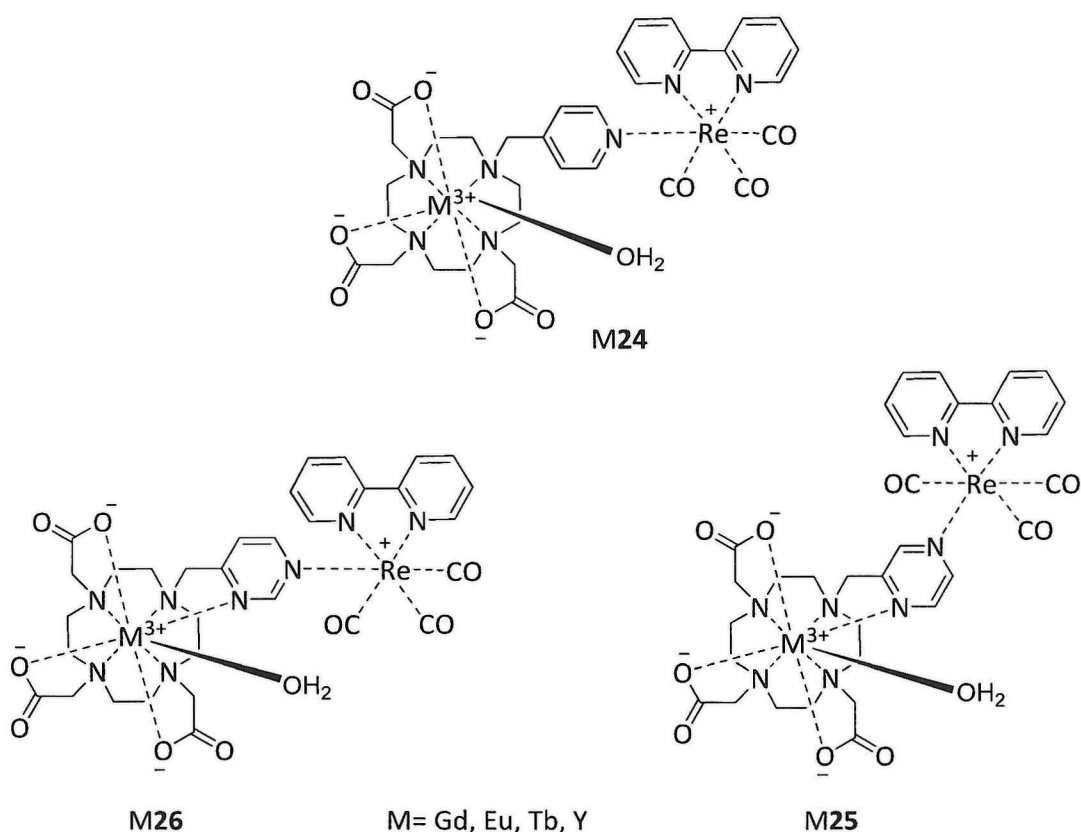
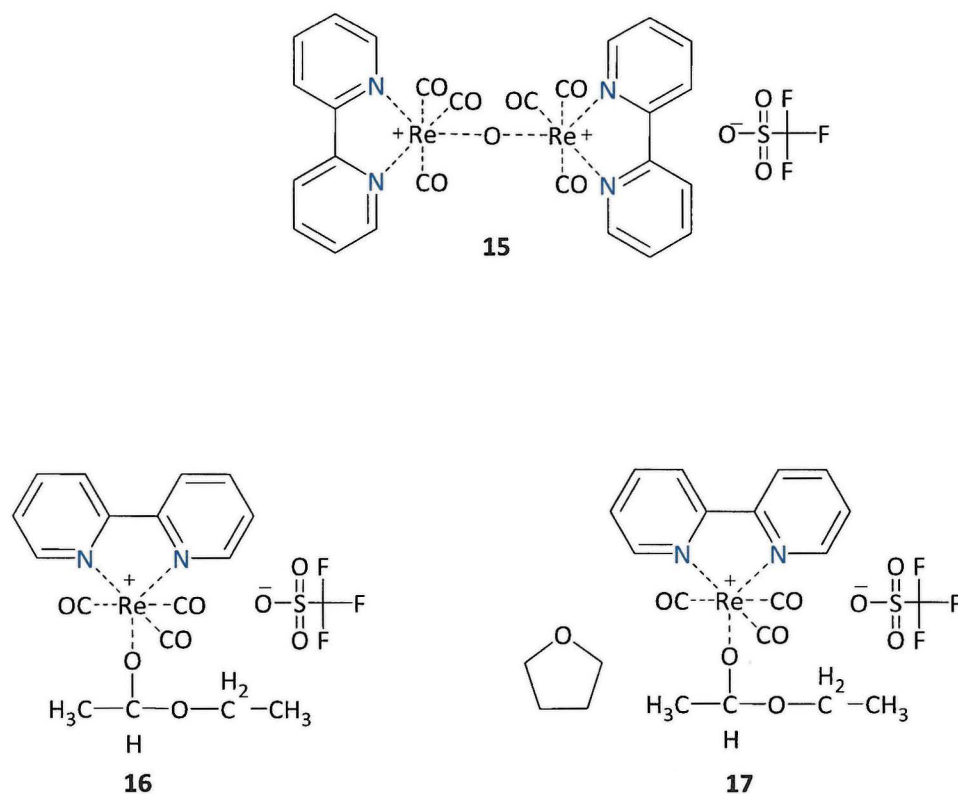


Figure 89 - three novel bimetallic building block of Re bipyridine complex with lanthanide complexes based DO3A macrocycles through three different heterocycles bridges (pyridine, pyrazine, and pyrimidine).

The chromophore can act as an antenna for the energy transfer in contrast media depending on the involved lanthanide metal ion, e.g. Eu(III) and Tb(III) complexes for luminescence imaging.

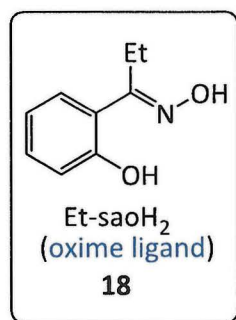
Novel crystalline compounds were produced in this work, which were isolated during the course of the attempts to develop the rhenium bipyridine chromophore (**14**) chemistry. This

resulted in the production of three novel Re bipyridine complexes; a Re bipyridine dimer (**15**) and two Re bipyridine compounds (**16** and **17**) coordinated to two different solvent systems (ethyl acetate or ethyl acetate /THF), see Figure 90.

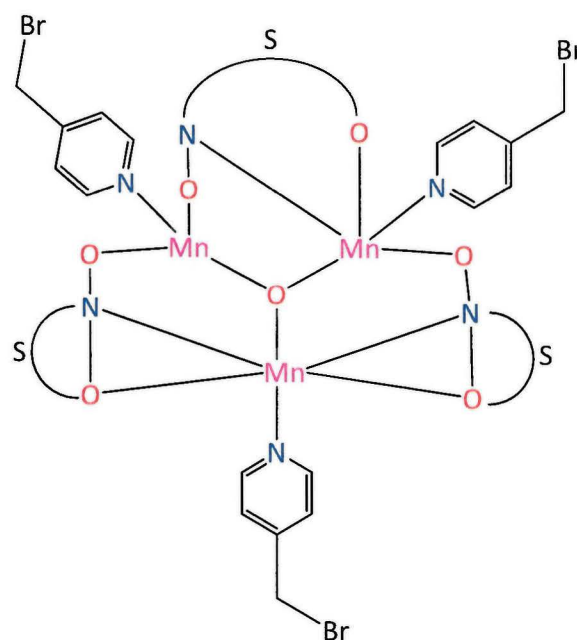


*Figure 90 - Three novel Re bipyridine complex with triflate anions; Re dimer (**15**), Re bipyridine ethyl acetate (**16**) and Re bipyridine ethyl acetate/THF (**17**).*

A second achievement reported in this chapter is the successful attachment of a novel heterocycle with a multimetallic building block ( $\text{Mn}^{3+}$  triangle), see Figure 91. This combination encourages future work, as a proof of principle for the potential to combine the synthesised lanthanide(III) complexes (**M10**, **M11**, **M12**) with  $\text{Mn}^{3+}$  triangle components.

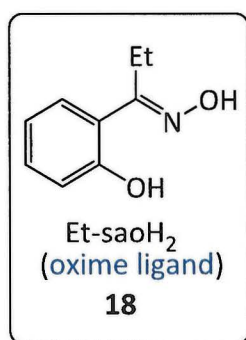


S

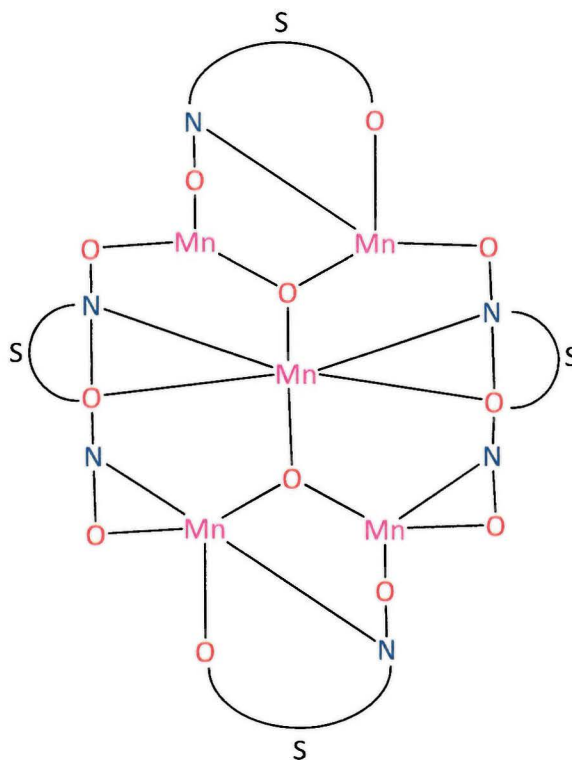


Manganese(III) triangle & pyridine groups (**20**)

Figure 91 - Novel crystal of combination of Mn(III) triangle with pyridine heterocycle (**20**).



S



Manganese(III) pentamer (**21**)

Figure 92 - Novel penta manganese single molecule magnets (**21**).

A novel crystalline compound of penta multimetallic (penta manganese) was also formed during the course of reactions to synthesise the Mn(III) triangle in combination with the heterocycles, see Figure 92.

The third achievement reported in this chapter was to attempt two model reactions, via attachment two or four of the research heterocycles around an iron ion, see Figure 93. That is a proof of principle for bridging two or four lanthanide(III) complexes (M11, M12) through analogous linkers.

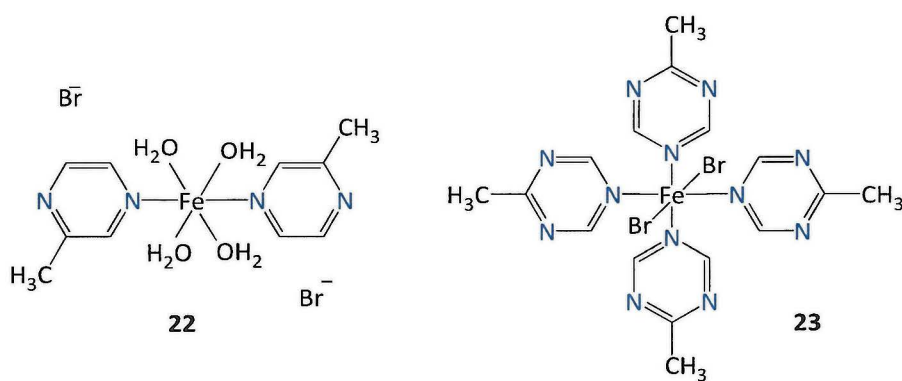


Figure 93 - Two novel mono metallic species (iron) attached to N-donors pyrazine (22) top & pyrimidine (23) bottom.

**Chapter 5**

**Concluding Remarks and Future  
Directions**

## 5.1. Conclusions

This thesis contains the reported research into the synthesis of potential dual imaging agents or to act as MRI/optical imaging agents heading towards optimizing magnetic or luminescence properties after link synthesised lanthanide(III) complexes (M10, M11, M12) with the mono or multimetallic species. This was achieved, by synthesising three chelators ligands (**10**, **11**, **12**) based on the macrocyclic backbone (DO3A) and functionalising it with heterocyclic arms of selected aromatic amine groups (pyridine, pyrimidine, pyrazine) which are offer advantages over DOTA.

The pyridyl group has a nitrogen donor for coordination apart from pyridine, keeping the chelator octadentate, at the same time including the heterocycle for another N-positions, allowing further functionalisation to take place, such as rhenium bipyridine chromophore or for bioconjugation. The pyridyl group also act as chromophores and therefore also has potential applications for lanthanide luminescence sensitisation.

On other hand, the synthesised chelators (**10**, **11**, and **12**) were complexed with a group of lanthanides (III) metal (i.e.  $Gd^{3+}$ ,  $Eu^{3+}$ ,  $Tb^{3+}$ ,  $Y^{3+}$ ) to be used in various applications depending on the included metal properties. As these lanthanides complexes (M10, M11, and M12) could act as medical imaging agents, where the gadolinium(III) complexes can be utilised as  $T_1$  MRI contrast agents, or europium(III) and terbium(III) can be used as luminescence agents, the yttrium(III) complexes could be used for study of the effects occurring on the reaction with different pH values or to monitoring the reaction progress by using  $^1H$  NMR technique because of yttrium(III) diamagnetic properties.

All these complexes that have heterocyclic arms (linkers groups) were conjugated successfully to rhenium bipyridine chromophore, and novel achievements have been done of substitution of used N-donor heterocycles (pyridine, pyrimidine and pyrazine) to mono or multimetallic species to generate building blocks to be used as MRI/Luminescence agents.

Chapter 2, presented the synthesis of alkyl halide of heterocycles (pym, pyr) to be functionalized with the macrocyclic backbone (DO3A). This was initially started by three attempted methods of halogenation (i.e. bromination, two different chlorination methods), reactions were tried to end with novel alkyl halide of pyrazine (**3**), see Figure 94, by only one of the chlorination methods.

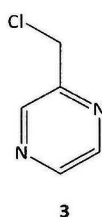


Figure 94 - Novel alkyl halide of pyrazine (3)

That success of linking reactive alkyl halide with two selected heterocycles (i.e. 4-methylpyrimidine, and 2-methyl pyrazine), was to produce two heterocycles with a good leaving group (i.e. 4-chloromethylpyrimidine, and 2-chloromethylpyrazine) along with commercially available alkyl halide heterocycle (4-methylbromopyridine hydrobromide) to enable easy coupling with the secondary amine position on macrocyclic cyclen derivatives (DO3A) chelator.

Attachment of the N-pyridyl group to *tert*-butyl protected DO3A were achieved to form macrocyclic chelators ligands with eight donor atoms and a potential site (N-heterocycles) for additional designated functionalization or bioconjugation. Synthesis of pure heterocycles-DO3A was very challenging by two stages, firstly: struggling to synthesis long term pure alkyl halide heterocycles due the high air sensitivity of these compounds. Secondly difficulty of purifying the heterocycles-DO3A ligands using column chromatography of silica gel or alumina combined with it's decomposition very rapidly even with perfect storage conditions. In an effort to overcome this, heterocycles-DO3A were successfully synthesised to results with two novel chelators ligands (**11**, and **12**), **10** was known but synthesised here differently,<sup>132</sup> see Figure 95.

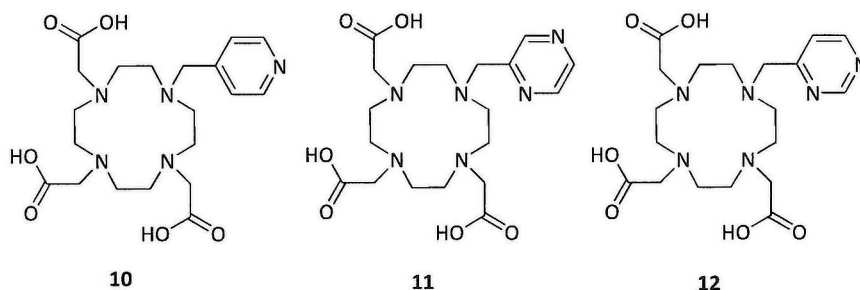


Figure 95 - Three novel chelators have been synthesised in this work

Potentiometric and NMR titrations studies were carried out in order to determine the speciation and  $pK_a$  values associated with these ligands (**10**, **11**, and **12**), with the attached

heterocycles and fully realise the effect of protonation or deprotonation states of it on the electronic or energy transfer from the attached chromophore to metal centre via the ligand, leads the sensitisation process of the lanthanides luminescence to be inhibited.

In chapter 3, the successful synthesis of the chelators ligands was followed by complexation reactions of these three ligands by following a modified strategy method.<sup>62</sup>

The preferably of these complexes was pointing towards the lanthanide(III) metals ( $Gd^{3+}$ ,  $Eu^{3+}$ ,  $Tb^{3+}$ ,  $Y^{3+}$ ) to produce 10 pure novel complexes (M10, M11, and M12), while Gd10, Eu10 were already known,<sup>132</sup> but they are synthesised here differently, see Figure 96.

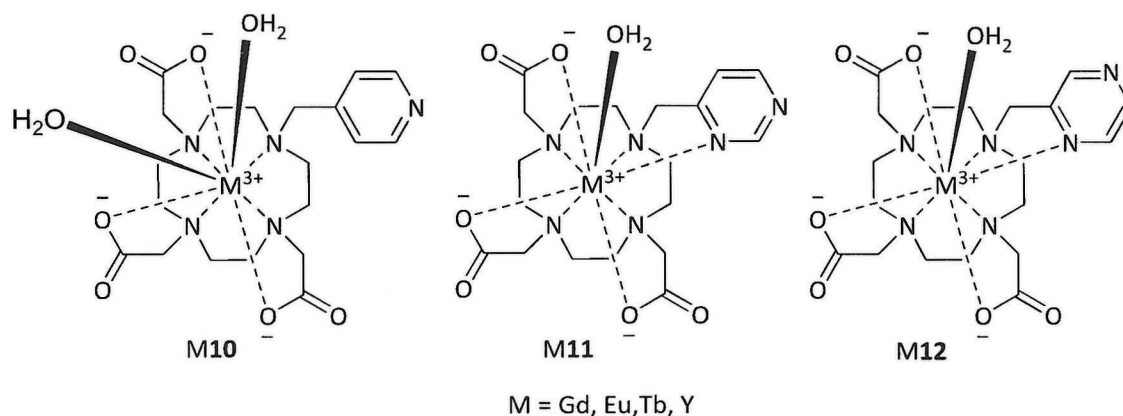


*Figure 96 –Novel lanthanide(III) complexes in this work*

These group of chelators have broader potential applications than the related DOTA due to the introduction of the heterocycles group units (**10**, **11**, and **12**) they are suggested as the lead compounds for future study as they have amine terminating groups which are ideal for multipurpose conjugations. In addition, the complexation of these ligands were very interesting due to the growing up field of similar macrocyclic complexes in the number of medical imaging techniques.

Therefore potentiometric titration study was very necessary to be done on the three lanthanides(III) metal complexes ( $Gd^{3+}$ ,  $Eu^{3+}$ ,  $Y^{3+}$ ) of each ligand to provide deeper understanding of the synthesised chelator ligands and to gain insight into the clear the effect of changing pH on the coordination modes and to fully characterise the coordination sphere of these metal complexes, which are results by matching to NMR and potentiometric titration results of the ligands and the heterocycles pendant arms.

Chapter 4, contained three parts, the first part discussed a synthesis route to produce twelve coupling species (M24, M25, M26) via combining lanthanide(III) complexes through the heterocycle arms (linker groups) with mono metallic species such as rhenium bipyridine chromophore (14) or iron(II).

The first part was began by preparation of the rhenium(I) chromophore based on the bipyridine backbone (14) which have a labile reactive group (acetonitrile) which can be substituted to couple the Re(I) complex with the heterocycles-DO3A chelators (M10, M11, M12) very easily. The final combined products (M24, M25, and M26), see Figure 97, and were obtained with high level of purity and yields.

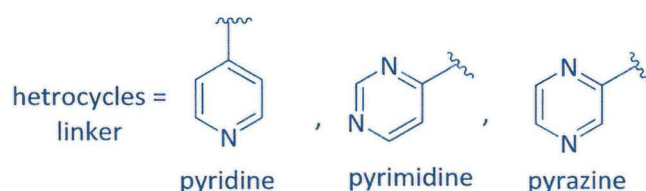
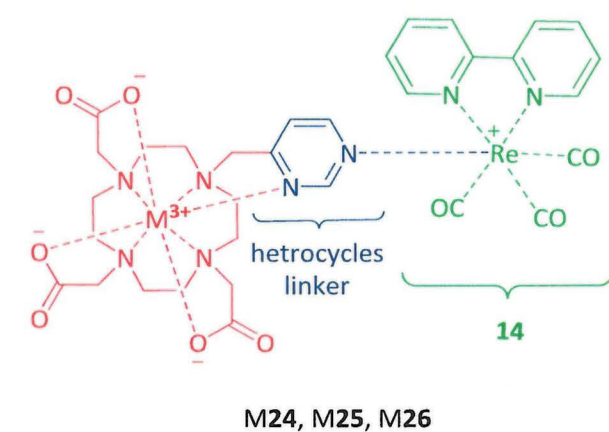


*Figure 97 -Three combined system M24, M25, M26 have been synthesised in this work.*

The second part was aiming to link the synthesised chelators (M11 & M12) together or with each other via their heterocycle arms (linker groups) and an appropriate paramagnetic metal ( $\text{Fe}^{2+}$ ). The second part was started by successful substitution of N-donor (2-methylpyrazine, 4-methylpyrimidine) to mono (iron) where efficient crystallography synthesis have been done by successful novel attachments of two pyrazine or four pyrimidine rings via mono metal [ $\text{Fe}^{2+}$ ], see Figure 98, to direct for promising future work of connecting two or four lanthanide(III) complexes with each other which have potential for different imaging applications

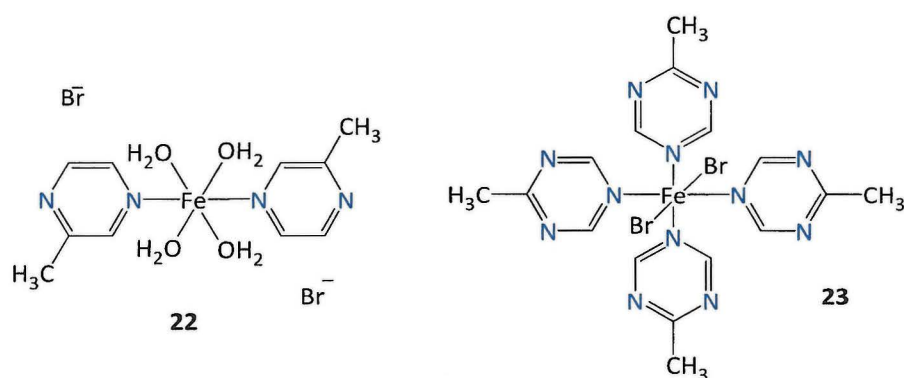


Figure 98 - Substituted of N-heterocycles with iron.

Finally a group of novel rhenium(I) bipyridine crystals have been synthesised during the course of attempting to crystalize single assembly of synthesised lanthanides(III) complexes with rhenium bipyridine chromophore. Which is consisted of a Re bipyridine dimer connected through hydroxide and three Re(I) bipyridine done with three different solvents. One with acetonitrile and two with ethyl acetate and ethyl acetate with THF respectively, see Figure 99.

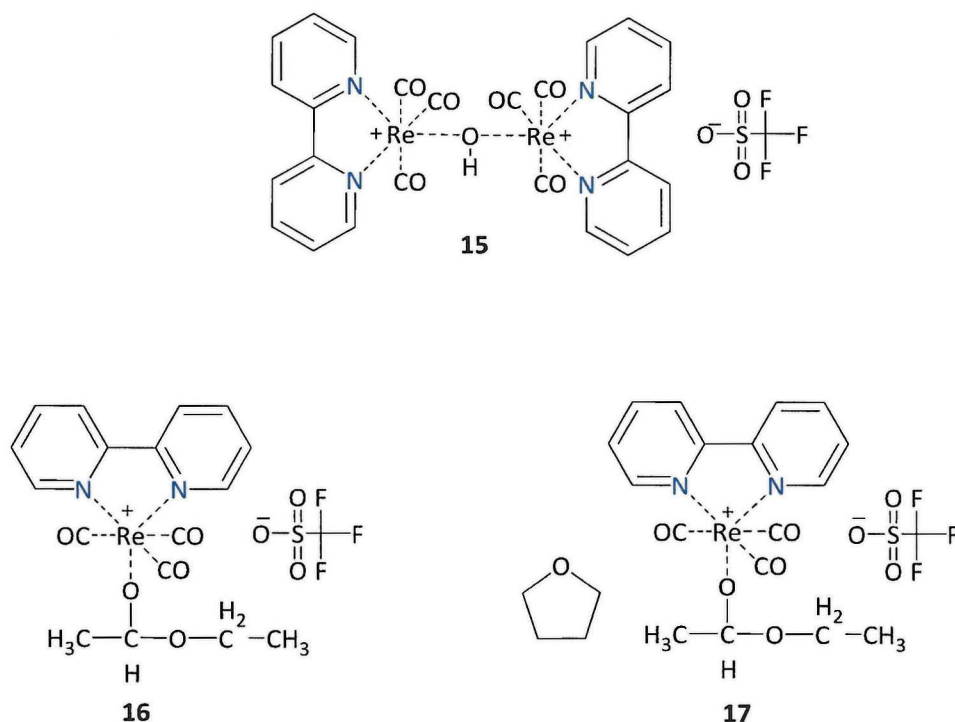
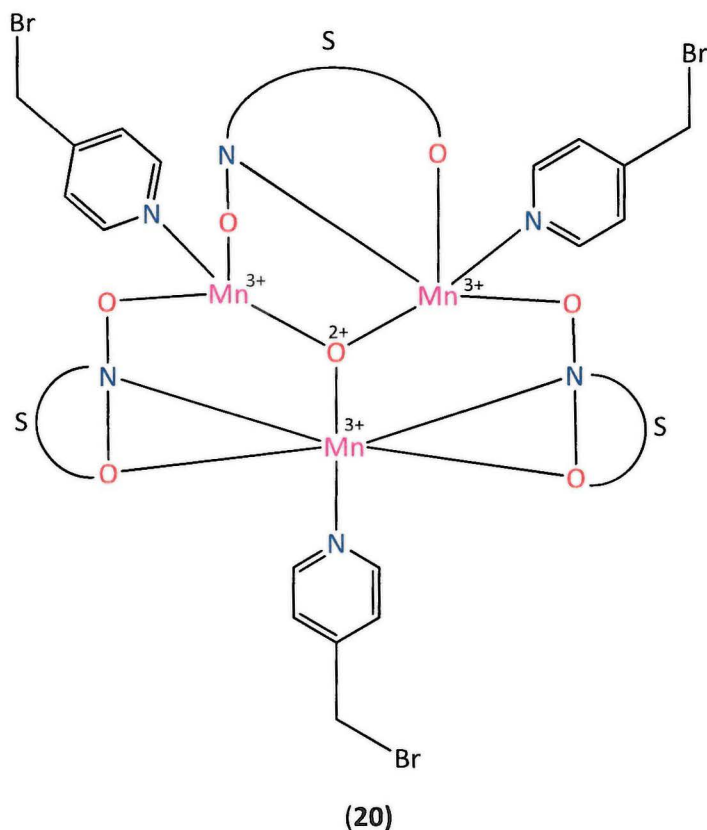


Figure 99 - Novel formation of rhenium bipyridine crystals

Fourth part, describing novel coupling was achieved by linking pyridine ring to the multi-metallic  $\text{Mn}^{3+}$  triangle, see Figure 100. To give promise further work to the production of novel

magnetic materials by combining azamacrocyclic lanthanide complexes with multi-metallic species or link more than two of them via iron a metal leading to multi metal arrays that might have unusual magnetic properties.



*Figure 100 - Manganese(III) triangle & pyridine groups*

This work enriches the current range of known macrocyclic ligands for biological use, highlighting the importance of configurational restriction and chelation of metal ions. Expanding the functionality of the macrocyclic core through attachments with chromophore containing arms demonstrates the wide scope of potential uses for macrocyclic ligands. The design and use of macrocyclic functional chelators is a relatively new field and so steps towards the synthesis of tetraazamacrocyclic-mono or multi-metallic species conjugates as targeted multi-metallic building block presents novel ideas for this field.

## 5.2. Future directions

Within this research, there is scope for further developments within many areas. This section is intended as a guide to future direction of the respective projects.

### 5.2.1 Macrocycles functional chelators – Vary metal ion, vary application

A full study in which lanthanide complexes of the chelators, most notably **10**, **11**, and **12** which with its amine functionality is ideal for multipurpose functionalization or bioconjugation, with the following metal ions and respective applications. Gadolinium(III) for MRI, europium(III)/terbium(III) for lanthanide luminescence and yttrium(III) for NMR studies. This data would validate a chelator system in which varying the metal ion gives access to the widest range of applications. More  $^1\text{H}$  NMR studies can apply with the Yttrium(III) complexes for full comprehension for any preferred reaction on the diamagnetic version of the lanthanide(III) complexes. Replication of the speciation in chapter 4 with other complexes (**Tb10**, **Tb11**, and **Tb12**) used in this work would also give an insight to the effect of pyridyl group N-functionalisation on the coordination environment and the result of that on the sensitisation on the lanthanide luminescence and for future luminescence lifetimes studies needed for complete full analysis.

### 5.2.2 Bearing of lanthanide(III) and rhenium complexes future work

Once the coupling species have been successfully prepared by linking the synthesised lanthanide(III) complexes with mono-metallic chromophore (rhenium bipyridine complexes **14**), a number of studies can be undertaken for further work which help to investigate the properties of these coupling products (**M24**, **M25**, **M26**) to utilise from it the appropriate applications according to the contained metal properties. Where many studies can be applied on these types of building blocks such as a fluorescence study on the europium(III) and terbium(III) complexes with various pH environment and observing the effect of the pH on the emission of these complexes, moreover potentiometric and NMR titrations can be a possibility also to search in different pH values and noting the effect of that on the coordination modes or the protonation state on the whole coupling blocks. Finally pH studies of  $q$  values could be examined for watching any change in the number of bound waters in these complexes at lower pH.

### 5.2.3 Substitution of N-donor (pyridine) future work

A very promising route was shown up after successful crystallography achievements of attaching the used pyridine heterocycles arm with single molecule magnets (Mn triangle), along with functionalization of the same arm with macrocyclic base cyclen (DO3A). More effort must now focus on this area to develop this system by attachment of the synthesised gadolinium(III) complexes through the same arm (pyridine) to potentially increase the magnetic properties of the whole building block to exchange the properties of it as a MRI contrast agent. This principle could also apply to the other used gadolinium(III) complexes of different arms (pyrimidine, pyrazine).

### 5.2.4 Substitution of N-donor (pyrimidine, pyrazine) future work

Another interesting future work arising from the important achievements of successfully linking the research heterocycles rings (pyrimidine, pyrazine) together via iron(II). It would be consider as approved theory of linking different macrocycles ligands (**10**, **11**, and **12**) or their lanthanide(III) complexes (**M10**, **M11**, and **M12**) with each other through the Fe(II) such as two complexes in the case of the pyrazine heterocycles pendant arm and four in term of pyrimidine arm. That is will offer potentially amazing properties especially with gadolinium(III) complexes toward increasing the relaxivity of proposed MRI contrast agents. All these promising future work can be likely apply on the third heterocycles (pyridine) or the chelators and complexes that include it.

# **Chapter 6**

## **Experimental**

## 6.1 General notes

Bulk solvent was removed by rotary evaporation on a Buchi RE 111 evaporator equipped with a diaphragm vacuum pump, trace solvent was removed on a Schlenk line equipped with an oil pump. Reactions were performed at room temperature (RT) unless otherwise stated. Speciation, stability, and luminescence studies, were carried out by Prof. Raphael Tripier. 71 experiments were carried out by Alicja Kownacka. Optical emission ICP was carried out by Dr. Bob Knight.

## 6.2 Materials

Solvents were used as received, except when dry solvents were required. Solvents were dried over activated (oven dried at 200 °C for 14 hours) 20 angstrom molecular sieves following literature method.<sup>133</sup> Chemicals were purchased from Sigma-Aldrich, Fisher, Acros, TCI, Chematech, and Strem. Chemicals were used as commercially obtained without any further purification.

## 6.3 Instrumentation

### 6.3.1. NMR spectroscopy

<sup>1</sup>H NMR and <sup>13</sup>C NMR were obtained using a Jeol JNM-LA400 spectrometer at 400 MHz for <sup>1</sup>H and 100 MHz for <sup>13</sup>C in the solvents indicated, referenced against standard internal TMS or residual non deuterated solvent signal. Chemical shifts ( $\delta$ ) are quoted in parts per million (ppm). Splitting patterns are designated as s (singlet), d (doublet), t (triplet), q (quartet), quin (quintet), m (multiplet) and br (broad). Deuterated solvents were purchased from either Goss chemicals Ltd or Cambridge Isotopes Ltd.

### 6.3.2 MS

Electrospray MS was performed at the University of Hull using a Finnegan MAT 900 XLT system. Accurate mass spectrometry measurements (HRMS) were recorded at the EPSRC National Mass Spectrometry Service Centre at the University of Swansea using a LQT Orbitrap XL.

### 6.3.3 CHN

CHN analysis was performed using a CHN analyser EA1108 (Carlo Erba). Most compounds

### 6.3.4 ICP-OES

Inductively Coupled Optical Emission Spectroscopy (ICP-OES) analysis was carried out using a Perkin Elmer Optima 5300 DV. All the samples were in solid state, digested with aqua regia in glass sample vials on a hotplate. Calibration standards were prepared at 1 and 10 ppm from 1000 ppm concentrates of gadolinium, europium, terbium, yttrium, and rhenium, which were purchased from Romil UK.

### 6.3.5 Potentiometric titrations

Potentiometric titrations were carried out with an automatic titrator composed of a microprocessor burette Metrohm Dosimat 665 and a Metrohm 713 pH meter, connected to a computer. All measurements were performed within a thermoregulated cell at  $25.0 \pm 0.1$  °C under an argon stream to prevent dissolution of the carbon dioxide. The ionic strength was adjusted to 0.1 with NMe<sub>4</sub>Cl. The combined Type "U" glass Metrohm electrode used, had a very low alkaline error.

### 6.3.6 X-ray crystallography

Single crystal X-ray diffraction data sets were collected on a Stöe IPDS-II imaging plate diffractometer, using MoK $\alpha$  X-rays of  $\lambda$  0.71073 Å. Crystals were cooled to 150 K during data collection, with the temperature controlled by an Oxford Systems Cryostream Cooler. Diffraction data were solved using direct methods or Patterson syntheses (ShelXS), 174 and the refinement was by the full-matrix least squares against  $F^2$  (ShelXL-97)<sup>175</sup> method. The WinGX program<sup>176</sup> was used for refinement and production of data tables, and the ORTEP-3 program<sup>134</sup> used for structure visualisation.

### 6.3.7 <sup>1</sup>H-NMR titration

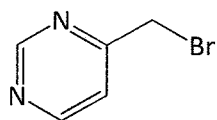
All yttrium(III) complexes (Y10, Y11, Y12) were prepared for <sup>1</sup>H NMR analysis by using only deuterium solvents, were dissolved in D<sub>2</sub>O and titrated with NaOD and DCl solvents which are commercially available from sigma Aldrich by using Jenway 3510 pH Meter.

### **6.3.8 Relaxivity measurements**

Magnetic resonance imaging and relaxivity studies were carried out using a wide bore vertical 11.7 T MR scanner (Bruker, Germany). For  $T_1$  relaxation study, FISP  $T_1 + T_2$  map sequence protocol was used with used parameters: FOV = 4.0 cm, FA = 60 dg, TR = 3.0 ms, TE = 1.5 ms, TA = 5 min 20 s, TI = 65 ms.  $T_2$  relaxivity data was collected using a MSME sequence protocol (Bruker MSME-T2-map) where FOV = 4.0 cm, FA = 180 dg, TR = 2000 ms, TE = 10 ms, TA = 6 min 24 s.

## 6.4 Synthesis of heterocycle functionalised tetraazamacrocyclic chelators.

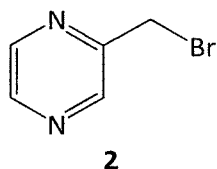
### 6.4.1 Attempted synthesis of 4-(bromomethyl) pyrimidine.



**1**

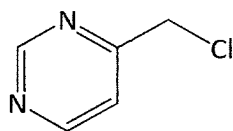
Following to modified literature method,<sup>48</sup> 2,2-Azobisisobutylnitrile (AIBN) (0.348 g, 0.0021 mmol) was added to solution of 4-methylpyrimidine (2 g, 0.021 mmol) and N-bromosuccinimide (NBS) (3.78 g, 0.021 mmol) in  $\text{CCl}_4$  (30 ml), the mixture was a few minutes under Ar bubbling through the solution, heat to reflux 18-24h with stirring and the Ar across the condenser in light. After cooling in ice bath, the mixture filtered and solvent evaporated under reduced pressure, to yield dark yellow solid. The desired product was not isolated using this synthetic procedure. Analytical data indicates that the desired product was not obtained.

#### 6.4.2 Attempted synthesis of 2-(bromomethyl) pyrazine.



Following to modified literature method,<sup>48</sup> 2,2-Azobisisobutylnitrile (AIBN) (0.348 g, 0.0021 mmol) was added to solution of 2-methylpyrazine (2 g, 0.021 mmol) and N-bromosuccinimide (NBS) (3.78 g, 0.021 mmol) in CCl<sub>4</sub> (30 ml), the mixture was a few minutes under Ar bubbling through the solution, heat to reflux 18-24 h with stirring and the Ar across the condenser in light. After cooling in ice bath, the mixture filtered and the solvent evaporated under reduced pressure, to yield black sticky solid. Analytical data indicates that the desired product was not obtained.

### 6.4.3 Synthesis of 4-chloromethyl pyrimidine.



3

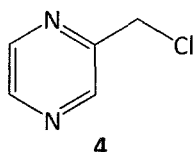
#### **Method 1 (Preferred)**

Following to literature method,<sup>52</sup> to a solution of 4-methylpyrimidine (2.00 g, 21.25 mmol) in  $\text{CHCl}_3$  (30 ml) was added trichloroisocyanuric acid (1.98 g, 8.50 mmol) in one portion at room temperature and the reaction mixture was heated to reflux for 9 h. The reaction mixture was then allowed to reach room temperature and filtered through a small plug of celite. The precipitate was rinsed with DCM (30 ml) and the filtrate was washed with aqueous 1 M NaOH (1 x 50 ml) and brine (1 x 50 ml). The organic phase was dried over  $\text{MgSO}_4$ , concentrated under reduced pressure and the residue was purified by flash column chromatography (hexane/EtOAc 2:1) to yield a redish liquid (1.40 g, 48%). TLC:  $R_f$  0.21 (hexane/EtOAc 2:1, UV).  $^1\text{H-NMR}$  (400 MHz,  $\text{CDCl}_3$ )  $\delta$ : 9.15 (d, 1H,  $J=1.3$  Hz), 8.76 (d, 1H,  $J=5.3$  Hz), 7.53 (dm, 1H,  $J=5.3$  Hz), 4.60 (s, 2H).  $^{13}\text{C-NMR}$  (100 MHz,  $\text{CDCl}_3$ )  $\delta$ : 165.3, 155.1, 157.2, 119.3, 44.9. GCMS (EI): calcd for  $\text{C}_5\text{H}_5\text{ClN}_2$   $[\text{M}]^+$  128 found 128, Retention time= 3.23 min, purity= 95.19%.

#### **Method 2**

Following to modified literature method.<sup>51</sup> Thionyl chloride (10 ml) was added to 4-(hydroxyl methyl) pyrimidine (0.5 g, 4.5 mmol) in dropwise and the reaction stirred under argon for 24 h. Thionyl chloride was evaporated under reduced pressure. The solid was redissolved in a minimum amount of MeOH and precipitated using excess diethyl ether, which was left to settle then decanted to leave brown solid. Analytical data indicates that the desired product was not obtained.

#### 6.4.4 Synthesis 2-chloromethyl pyrazine



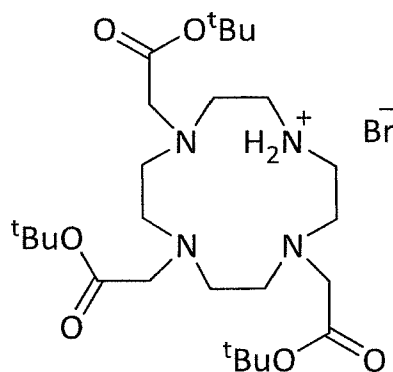
##### Method 1 (Preferred)

Following to modified literature method,<sup>52</sup> to a solution of 2-methylpyrazine (2.00 g, 21.25 mmol) in  $\text{CHCl}_3$  (30 ml) was added trichloroisocyanuric acid (1.98 g, 8.50 mmol) in one portion at room temperature and the reaction mixture was heated to reflux for 9 h. The reaction mixture was then allowed to reach room temperature and filtered through a small plug of celite. The precipitate was rinsed with DCM (30 ml) and the filtrate was washed with aqueous 1 M NaOH (1 x 50 ml) and brine (1 x 50 ml). The organic phase was dried over  $\text{MgSO}_4$ , concentrated under reduced pressure and the residue was purified by flash column chromatography (hexane/EtOAc 2:1) to yield a black liquid (1.22 g, 45%). TLC:  $R_f$  0.21 (hexane/EtOAc 2:1, UV).  $^1\text{H}$  NMR (400 MHz,  $\text{CDCl}_3$ )  $\delta$ : 9.22 (d, 1H,  $J=1.3$  Hz), 8.75 (s, 1H,  $J=1.3$  Hz), 8.55 (m, 2H,  $J=2.4$  Hz), 4.69 (s, 2H).  $^{13}\text{C}$  NMR (100 MHz,  $\text{CDCl}_3$ )  $\delta$ : 164.2, 154.3, 158.9, 118.7, 45.8. GCMS calcd. for  $\text{C}_5\text{H}_5\text{ClN}_2$   $[\text{M}]^+$  128 found 128, Retention time= 7.01, purity= 93.71%.

##### Method 2

Following to modified literature method.<sup>51</sup> Thionyl chloride (10 ml) was added to 2-(hydroxyl methyl) pyrazine (0.5 g, 4.5 mmol) in dropwise and the reaction stirred under argon for 24h. Thionyl chloride was removed in *vacuo*. The solid was redissolved in a minimum amount of MeOH and precipitated using excess diethyl ether, which was left to settle then decanted to leave a dark black solid, the desired product was not isolated using this synthetic procedure. Analytical data indicates that the desired product was not obtained.

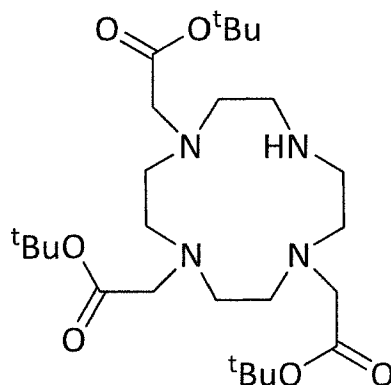
#### 6.4.5 Synthesis of 1, 4, 7-tris (tert-butoxycarbonylmethyl)-1, 4, 7, 10-tetraazacyclododecane hydrobromide.



5

Following literature method,<sup>59</sup> to a suspension of cyclen (5.00 g, 29 mmol) and sodium acetate (7.86 g, 96 mmol) in *N,N*-dimethylacetamide (DMA, 60 ml) at -20 °C was added a solution of *tert*-butyl bromoacetate (18.7 g, 14.1 ml, 96 mmol) in DMA (20 ml) dropwise over a period of (0.5 h). The temperature was maintained at -20 °C during the addition, after which the reaction mixture was allowed to come to room temperature. After 24 h of vigorous stirring, the reaction mixture was poured into water (300 ml) to give a clear solution solid  $\text{KHCO}_3$  (15 g, 150 mmol) was added portion wise, and intermediate compound precipitated as a white solid. The precipitate was collected by filtration and dissolved in  $\text{CHCl}_3$  (250 ml). The solution was washed with water (100 ml), dried ( $\text{MgSO}_4$ ), filtered, and concentrated to about 20-30 ml. Ether (250 ml) was added, **5** was crystallised as a white fluffy solid. (12.7g, 73%).  $^1\text{H}$  NMR (400 MHz,  $\text{CDCl}_3$ )  $\delta$ : 1.42 (s, 9H,  $\text{C}(\underline{\text{C}}\text{H}_3)_3$ ), 1.43 (s, 18H,  $\text{C}(\underline{\text{C}}\text{H}_3)_2$ ), 2.85-2.94 (m, 12H, N- $\text{CH}_2$ ), 3.20 (m, 4H, N- $\text{CH}_2$ ), 3.30 (s, 2H, N- $\text{CH}_2$ -C=O), 3.55 (s, 4H, N- $\text{CH}_2$ -C=O), 10.02 (br s, 1H, NH),  $^{13}\text{C}$  NMR (100 MHz,  $\text{CDCl}_3$ )  $\delta$ : 28.16  $\text{C}(\underline{\text{C}}\text{H}_3)_3$ , 28.20 ( $\text{C}(\underline{\text{C}}\text{H}_3)_3$ ), 47.57( $\text{C}(\underline{\text{C}}\text{H}_3)_3$ ), 49.23 (N- $\text{CH}_2$ ), 51.33 (N- $\text{CH}_2$ ), 51.21 (N- $\text{CH}_2$ ), 58.24 (N- $\text{CH}_2$ ), 76.84 ( $\underline{\text{C}}(\text{CH}_3)$ ), 77.1 ( $\underline{\text{C}}(\text{CH}_3)$ ), 169.61 (C=O), 170.46 (C=O). Elemental analysis for  $\text{C}_{26}\text{H}_{51}\text{BrN}_4\text{O}_6$ . calcd. C, 52.43; H, 8.63; N, 9.41. Found: C, 52.30; H, 8.75; N, 9.18. MS-ESI: 515  $[\text{M}-\text{Br}]^+$ .

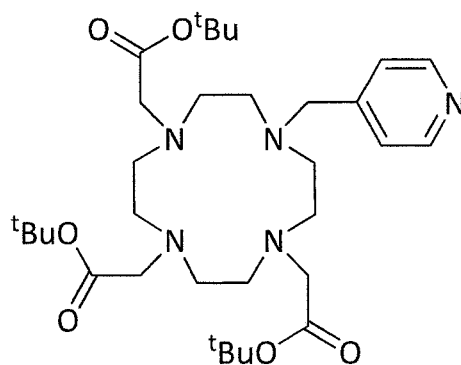
#### 6.4.6 Synthesis of 1, 4, 7-Tris (tert-butoxycarbonylmethyl)-1, 4, 7, 10-tetraazacyclododecane (*t*Bu-DO3A).



6

Following to modified literature method,<sup>59</sup> Hydrobromide (**5**) (5.00 g, 8.40 mmol) was dissolved in water (250 ml) at 70°C. The solution was allowed to cool to 40°C, after which 10% aqueous KOH solution (9.4 ml, 16.8 mmol) was added the reaction mixture was stirred for 15 min then filtered to yield a white solid. (4.20 g, 97%). <sup>1</sup>H NMR (400 MHz, CDCl<sub>3</sub>) δ: 1.42 (m, 27H, C(CH<sub>3</sub>)<sub>3</sub>), 2.55-2.59 (m, 4H, N-CH<sub>2</sub>), 2.75-2.86 (m, 12H, N-CH<sub>2</sub>), 3.30 (s, 6H, N-CH<sub>2</sub>-CO). <sup>13</sup>C NMR (100, MHz, CDCl<sub>3</sub>) δ: 28.39 (C(CH<sub>3</sub>)<sub>3</sub>), 28.33 (C(CH<sub>3</sub>)<sub>3</sub>), 47.64(C(CH<sub>3</sub>)<sub>3</sub>), 50.91(N-CH<sub>2</sub>), 52.33 (N-CH<sub>2</sub>), 52.41 (N-CH<sub>2</sub>), 53.11 (N-CH<sub>2</sub>), 57.12 (N-CH<sub>2</sub>), 79.87 (N-CH<sub>2</sub>-CO), 80.92 (N-CH<sub>2</sub>-CO), 171.12 (C=O), 171.21 (C=O). MS-ESI calcd for C<sub>26</sub>H<sub>50</sub>BrN<sub>4</sub>O<sub>6</sub> [M+H]<sup>+</sup> 514.obsd 515. Elemental analysis for C<sub>26</sub>H<sub>50</sub>N<sub>4</sub>O<sub>6</sub>·1.7H<sub>2</sub>O: calcd. C, 57.26, H, 9.87, N, 10.27.Found: C, 57.47; H, 9.54, N, 10.05.

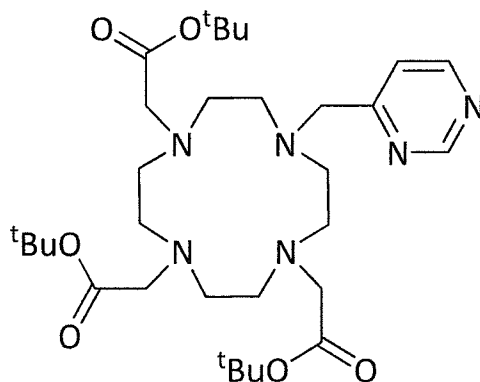
### 6.4.7 Synthesis of tri-tert-butyl 2, 2, 2-10-(4-methylpyridyl) 14,7,10 tetraazacyclododecane-1, 4, 7-triyl) triacetate



7

Following to modified literature methods,<sup>62</sup> *tert*-butyl DO3A (**6**)(100 mg, 0.19 mmol) was dissolved in dry MeCN (100 ml) 4-bromo methylpyridine hydrobromide (45 mg, 0.19 mmol) and caesium carbonate (298 mg, 0.91 mmol) was added and the reaction was stirred for 18 h. Concentrated in *vacuo* to yield dark yellow solid (109 mg, 94%). <sup>1</sup>H NMR (400 MHz, CD<sub>3</sub>OD)  $\delta$ : 1.41-1.51 (s, 27H, C(CH<sub>3</sub>)<sub>3</sub>), 1.91-3.93 (br m, 24H, CH<sub>2</sub>-N), 7.58 (d, 2H, J=5.7Hz, CH-Ar), 8.50 (d, 2H, J=5.7Hz, CH-Ar). <sup>13</sup>C NMR (100 MHz, CD<sub>3</sub>OD)  $\delta$ : 27.14 (C(CH<sub>3</sub>)<sub>3</sub>), 27.97 (C(CH<sub>3</sub>)<sub>3</sub>), 28.14 (C(CH<sub>3</sub>)<sub>3</sub>), 32.52 (N-CH<sub>2</sub>), 50.85 (N-CH<sub>2</sub>), 53.74(N-CH<sub>2</sub>), 54.64 (N-CH<sub>2</sub>-C=O), 56.14 (N-CH<sub>2</sub>-C=O), 59.56 (N-CH<sub>2</sub>-C=O), 80.40 (C(CH<sub>3</sub>)<sub>3</sub>), 82.92 (C(CH<sub>3</sub>)<sub>3</sub>), 123.85 (CH-Ar), 147.44 (CH-Ar), 149.07 (C-Ar), 172.67 (C=O), 173.61(C=O). HRMS-ESI calcd for C<sub>32</sub>H<sub>55</sub>N<sub>5</sub>NaO<sub>6</sub> [M+Na]<sup>+</sup> 628.403.obsd 628.404. Elemental analysis for C<sub>32</sub>H<sub>55</sub>N<sub>5</sub>O<sub>6</sub> Calcd. C, 63.44, H 9.15, N, 11.56.Found: C, 63.29, H, 8.71, N, 11.22.

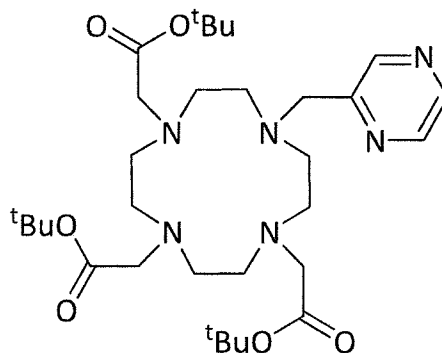
#### 6.4.8 Synthesis of tri-tert-butyl 2, 2', 2''-(10(4-methyl pyrimidyl)-1, 4, 7, 10-tetraazacyclododecane-1, 4, 7-triyl) triacetate.



8

Following to modified literature methods,<sup>62</sup> *tert*-butyl DO3A (**6**) (100 mg, 0.19 mmol) was dissolved in dry MeCN (1 L) 4-chloromethyl pyrimidine (24 mg, 0.19 mmol) and caesium carbonate (298 mg, 0.91 mmol) was added and the reaction was stirred for 18 h. Concentrated in vacuo to yield a brown solid (108 mg, 93%).<sup>1</sup>H NMR (400 MHz, CD<sub>3</sub>OD)  $\delta$ : 1.48-1.52 (s, 27H, C(CH<sub>3</sub>)<sub>3</sub>), 2.44-3.13 (m, CH<sub>2</sub>, 14H), 3.25-3.34 (s, 11H, CH<sub>2</sub>-N), 4.25-4.47 (s, 2H, CH<sub>2</sub>-pym), 8.33-8.34 (dd, J=2.6, 1H, CH-pym), 8.50-8.51 (d, J=2.4, 1H, CH-pym), 8.58-8.59 (d, J=1.2, 1H, CH-pym). <sup>13</sup>C NMR (100 MHz, CD<sub>3</sub>OD)  $\delta$ : 27.14 (C(CH<sub>3</sub>)<sub>3</sub>), 47.48 (N-CH<sub>2</sub>), 47.69 (N-CH<sub>2</sub>), 48.11 (N-CH<sub>2</sub>), 48.32 (N-CH<sub>2</sub>), 55.14 (N-CH<sub>2</sub>-Ar), 142.73 (CH<sub>2</sub>-Ar), 143.44 (C-Ar), 144.96 (C-Ar), 155.42 (C=O). HRMS-ESI calcd for C<sub>31</sub>H<sub>54</sub>N<sub>6</sub>O<sub>6</sub>Na [M+Na]<sup>+</sup> 629.398. obsd 629.399 Elemental analysis for C<sub>31</sub>H<sub>54</sub>N<sub>6</sub>O<sub>6</sub>, calcd. C, 61.36; H, 8.97; N, 13.85. Found C, 60.98; H, 8.67; N, 14.12.

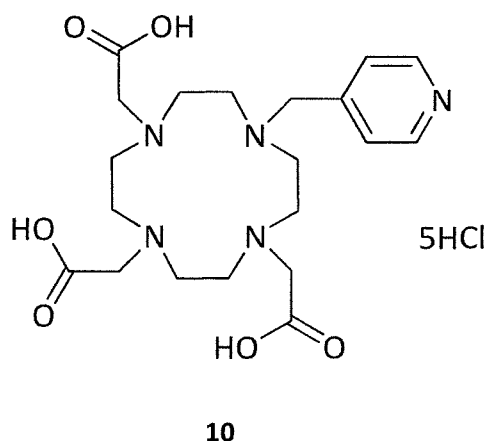
#### 6.4.9 Synthesis of tri-*tert*-butyl 2, 2', 2''-(10-(2-methyl pyrazine)-1, 4, 7, 10-tetraazacyclododecane-1, 4, 7-triyl) triacetate.



9

Following to modified literature methods,<sup>62</sup> *tert*-butyl DO3A (**6**) (100 mg, 0.19 mmol) was dissolved in dry MeCN (1 L) 2-chloromethyl pyrazine (24 mg, 0.19 mmol) and caesium carbonate (298 mg, 0.91 mmol) was added and the reaction was stirred for 18 h. Concentrated in *vacuo* to yield dark brown solid (105 mg, 91%). <sup>1</sup>H NMR (400 MHz, CD<sub>3</sub>OD)  $\delta$ : 1.47 (s, 27H, C(CH<sub>3</sub>)<sub>3</sub>), 2.11-3.32 (br m, 22H, CH<sub>2</sub>-N), 4.41 (s, 2H, CH<sub>2</sub>-Ar), 7.92 (d, 1H, J=1.4 Hz, CH-Ar), 8.68-8.69 (d, 1H, J=1.4 Hz, CH-Ar), 8.85-8.86 (d, 1H, J=2.5 Hz, CH-Ar). <sup>13</sup>C NMR (100 MHz, CD<sub>3</sub>OD)  $\delta$ : 28.43 (C(CH<sub>3</sub>)<sub>3</sub>), 43.55 (N-CH<sub>2</sub>), 50.15 (N-CH<sub>2</sub>), 57.6 (N-CH<sub>2</sub>-C=O), 57.91 (N-CH<sub>2</sub>-C=O), 80.83 (C(CH<sub>3</sub>)<sub>3</sub>), 156.46 (CH-Ar), 157.46 (C-Ar), 158.45 (C-Ar), 172.55 (C=O), 174.51 (C=O). HRMS-ESI calcd for C<sub>31</sub>H<sub>54</sub>N<sub>6</sub> NaO<sub>6</sub> [M+Na]<sup>+</sup>. 629.41. obsd 629.22. Elemental analysis for C<sub>31</sub>H<sub>54</sub>N<sub>6</sub>O<sub>6</sub>, calcd. C, 61.36; H, 8.97; N, 13.85. Found C, 61.10; H, 9.23; N, 13.52.

**6.4.10 (10-(4-methyl pyridyl)-1, 4, 7, 10-tetraazacyclododecane-1, 4, 7-triyl) triacetic acid**



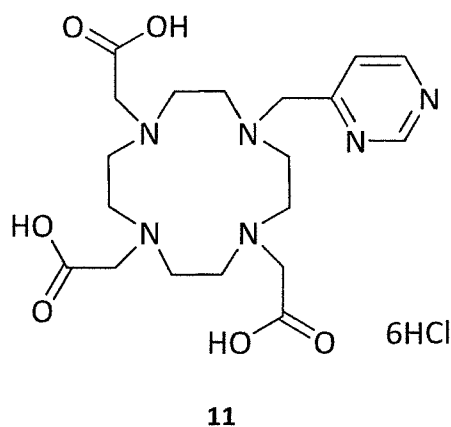
**Method 1 (preferred)**

Following to modified literature methods,<sup>62</sup> tri-*tert*-butyl 2,2,2-10-(4-methylpyridine)14,7,10 tetraazacyclododecane-1,4,7-triyl triacetate (**7**) (100 g, 0.16 mmol) was dissolved in 6M HCl (50 ml) in microwave (temp. =120 °C, pressure =182 psi, power =182 w, ramp time = 02.00 min) for 15 min, the reaction was then concentrated *in vacuo* to yield a light brown solid (97 mg, 97%). <sup>1</sup>H NMR (400 MHz, D<sub>2</sub>O) δ: 2.62-4.65 (s, 24H, CH<sub>2</sub>-N) 7.86-7.88 (d, 2H, J=8.1Hz CH-Ar), 8.41-8.42 (d, 2H, J=8.1Hz, CH-Ar). <sup>13</sup>C NMR (100 MHz, D<sub>2</sub>O) δ: 48.18 (CH<sub>2</sub>-N), 48.38 (CH<sub>2</sub>-N), 50.84 (CH<sub>2</sub>-N), 52.36 (CH<sub>2</sub>-N), 53.31 (CH<sub>2</sub>-N), 128.25 (CH-Ar), 141.36 (CH-Ar), 158.38 (C-Ar), 168.71 (C=O), 171.91 (C=O), MS-ESI calcd for C<sub>20</sub>H<sub>31</sub>N<sub>5</sub>O<sub>6</sub> [M+H]<sup>+</sup> 437. obsd 438 .Elemental analysis for C<sub>20</sub>H<sub>31</sub>N<sub>5</sub>O<sub>6</sub>·5.5HCl·0.1H<sub>2</sub>O calcd. C, 38.76, H, 5.85, N, 11.30. Found: C, 38.78, H, 5.58, N, 10.93.

## Method 2

Following to modified literature methods,<sup>62</sup> tri-tert-butyl 2,2,2-10-(4-methylpyridine)14,7,10 tetraazacyclododecane-1,4,7-triyl triacetate (7) (100 mg, 0.16 mmol) was dissolved in 6M HCl (50 ml) and heated under reflux for 18 h. The reaction was then concentrated in vacuo and diethyl ether (3 × 100 ml) was added and decanted off to remove any impurities to yield a light brown solid (87 mg, 87%). <sup>1</sup>H NMR (400 MHz, D<sub>2</sub>O) δ: 2.62-4.65 (s, 24H, CH<sub>2</sub>-N), 7.86-7.88 (d, 2H, J=8.1Hz, CH-Ar), 8.41-8.42 (d, 2H, J=8.1Hz, CH-Ar). <sup>13</sup>C NMR (100 MHz, D<sub>2</sub>O) δ: 48.18 (CH<sub>2</sub>-N), 48.38 (CH<sub>2</sub>-N), 50.84 (CH<sub>2</sub>-N), 52.36 (CH<sub>2</sub>-N), 53.31 (CH<sub>2</sub>-N), 128.25 (CH-Ar), 141.36 (CH-Ar), 158.38 (C-Ar), 168.71 (C=O), 171.91 (C=O).

#### 6.4.11 Synthesis of 2,2',2''-(10-(4-methyl pyrimidyl)-1,4,7,10-tetraazacyclododecane-1,4,7-triyl)triacetic acid.



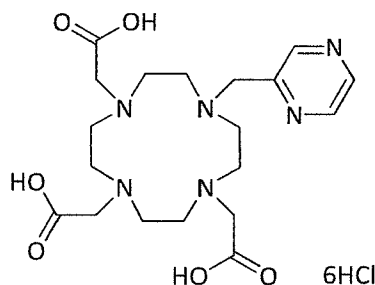
##### **Method 1 (Preferred)**

Following to modified literature methods,<sup>62</sup> tri-*tert*-buty2,2,2-10-(4-methylpyrimidine) 14,7,10 tetraazacyclododecane-1,4,7-triyl) triacetate (**9**) (100 mg, 0.16 mmol) was dissolved in 6 M HCl (25 ml) and heated in microwave for 15 min. (temp. =120°C, pressure =182 psi, power =182 w, ramp time=02.00 min), then concentrated *in vacuo* to yield a light yellow solid (96 mg, 96%). <sup>1</sup>H NMR (400 MHz, D<sub>2</sub>O) δ: 1.92-4.29 (m, 24H, CH<sub>2</sub>-N), 7.71-8.91 (m, 3H, CH-Ar).<sup>13</sup>C NMR (400 MHz, D<sub>2</sub>O) δ: 52.14 (N-CH<sub>2</sub>), 53.08 (N-CH<sub>2</sub>), 56.76 (N-CH<sub>2</sub>), 122.10 (CH-Ar), 139.22 (CH-Ar), 155.78 (C-Ar), 174.43 (C=O), 177.53 (C=O). MS-ESI calcd for C<sub>19</sub>H<sub>30</sub>N<sub>6</sub>O<sub>6</sub> [M+Na]<sup>+</sup> 438 obsd 460 Elemental analysis for C<sub>19</sub>H<sub>36</sub>Cl<sub>6</sub> N<sub>6</sub>O<sub>6</sub>. 6HCl1.2H<sub>2</sub>O calcd. C, 33.62, H, 5.73, N, 12.38, Found C, 33.56, H, 6.17, N, 12.75.

##### **Method 2**

Following modified literature methods,<sup>62</sup> tri-*tert*-buty2,2,2-10-(4-methylpyrimidine) 14,7,10tetraazacyclododecane-1,4,7-triyl) triacetate (**9**) (100 mg, 0.16 mmol) was dissolved in 6M HCl (25 ml)and heated under reflux for 18 h. The reaction was then concentrated *in vacuo* and diethyl ether (3×100 ml) was added, then decanted off to remove any impurities to yield golden yellow solid (84 mg, 84%).<sup>1</sup>H NMR (400 MHz, D<sub>2</sub>O) δ: 1.92-4.29 (m, 24H, CH<sub>2</sub>-N), 7.71-8.91 (m, 3H, CH-Ar).<sup>13</sup>C NMR (400 MHz, D<sub>2</sub>O) δ: 52.14 (N-CH<sub>2</sub>), 53.08 (N-CH<sub>2</sub>), 56.76 (N-CH<sub>2</sub>), 122.10 (CH-Ar), 139.22 (CH-Ar), 155.78 (C-Ar), 174.43 (C=O), 177.53 (C=O).

#### 6.4.12 Synthesis of 1, 4, 7-tris (tert-butoxycarbonylmethyl)-10-(2-methylpyrazine) tetraazadodecane.



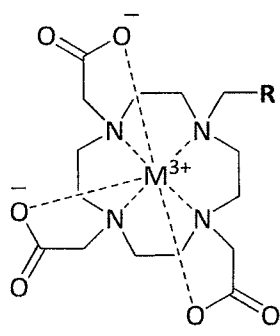
##### Method 1(Preferred)

Following modified literature methods,<sup>62</sup> tri-*tert*-buty2,2,2-10-(2-methylpyrazine) 14,7,10tetraazacyclododecane-1,4,7-triyl) triacetate (**8**) (100 mg, 0.16 mmol) was dissolved in 6M HCl (25 ml) and heated in microwave (temp. =120 °C, pressure =182 psi, power =182 w, ramp time=02.00 min.) for 15 min., then concentrated *in vacuo* to yield a black solid (98 mg, 98%).<sup>1</sup>H NMR (400 MHz, D<sub>2</sub>O) δ: 2.22-4.55 (m, 24H, CH<sub>2</sub>-N), 8.38-8.40 (d, 1H, J=2.1Hz, CH-Ar), 8.45-8.50 (d, 2H, J=2.1Hz, CH-Ar).<sup>13</sup>C NMR (100 MHz, D<sub>2</sub>O) δ: 47.68 (CH<sub>2</sub>-N), 49.28 (CH<sub>2</sub>-N), 51.45 (CH<sub>2</sub>-N), 52.14 (CH<sub>2</sub>-N), 53.55 (CH<sub>2</sub>-N), 55.33 (CH<sub>2</sub>-N), 140.04 (CH-Ar), 143.15 (CH-Ar), 145.45 (C-Ar), 172.76 (C=O), 175.24 (C=O). MS-ESI calcd for C<sub>20</sub>H<sub>31</sub>N<sub>5</sub>O<sub>6</sub> [M+Na]<sup>+</sup> 438. obsd 460 Elemental analysis for C<sub>19</sub>H<sub>35</sub>Cl<sub>6</sub> N<sub>6</sub>O<sub>6</sub>.6HCl<sub>3</sub>.5H<sub>2</sub>O calcd. C, 31.68, H, 6.02, N, 11.76. Found C, 31.20, H, 6.12, N, 12.23.

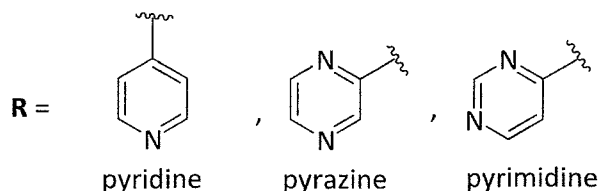
##### Method 2

Following modified literature methods,<sup>62</sup> tri-*tert*-buty2,2,2-10-(2-methylpyrazine) 14,7,10 tetraazacyclododecane-1, 4,7-triyl) triacetate (**8**) (100 mg, 0.15 mmol) was dissolved in 6M HCl (200 ml) and heated under reflux for 18 h. The reaction was then concentrated *in vacuo* and diethyl ether (3×100ml) was added and decanted off to remove any impurities to yield a light brown solid (86 mg, 86%).<sup>1</sup>H NMR (400 MHz, D<sub>2</sub>O) δ: 2.22-4.55 (m, 24H, CH<sub>2</sub>-N), 8.38-8.40 (d, 1H, J=2.1Hz, CH-Ar), 8.45-8,50 (d, 2H, J=2.1Hz, CH-Ar).<sup>13</sup>C NMR (100 MHz, D<sub>2</sub>O) δ: 47.68 (CH<sub>2</sub>-N), 49.28 (CH<sub>2</sub>-N), 51.45 (CH<sub>2</sub>-N), 52.14 (CH<sub>2</sub>-N), 53.55 (CH<sub>2</sub>-N), 55.33 (CH<sub>2</sub>-N), 140.04 (CH-Ar), 143.15 (CH-Ar), 145.45 (C-Ar), 172.76 (C=O), 175.24 (C=O).

### 6.4.13 Attempted method of synthesis metal(III) complexes of 1, 4, 7-tris (tert-butoxycarbonyl)-10-[pyr, pyz, pym] tetraazadodecane.



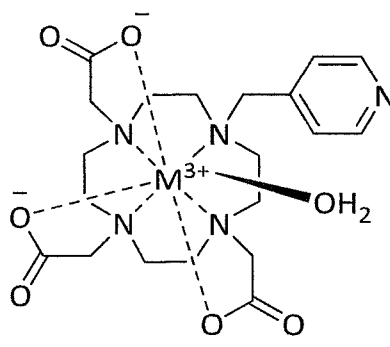
M10, M11, M12  
M = Gd, Eu, Tb, Y



#### Method 1 (preferred)

Following modified literature methods,<sup>62</sup> deprotected ligands (**10**) (**11**) (**12**) (500 mg) was dissolved in ammonium acetate buffer (0.2 M, pH 5, 25 ml). To this, metal (III) salt in ammonium acetate buffer (0.2M, pH 5, 25 ml) was added, the reaction was heated under reflux for 18 h then concentrated *in vacuo*. The crude solid was redissolved in water (20 ml) and purified using an Amberlite XAD16N column, eluting with water (300 ml) then methanol (250 ml), the solvents were then removed under reduced pressure to yield as solid product. Analytical data indicates that the desired product was successfully achieved by using this synthetic procedure.

**6.4.14 synthesis of metal(III) complex of 1, 4, 7-tris (tert-butoxycarbonylmethyl)-10-(4-methylpyridyl) tetraazadodecane.**



**M10**

M= Gd, Eu, Tb, Y

**6.4.15 Synthesis of gadolinium (III) complex of 1, 4, 7-tris (tert-butoxycarbonylmethyl)-10-(4-methylpyridyl)tetraazadodecane. (Gd10)**

Amounts: gadolinium(III) chloride hexahydrate (299 mg, 0.80 mmol) to yield a dark yellow solid (184 mg, 39%). HRMS calc. 592.1355 found 592.9965 [M+H]<sup>+</sup>. Elemental analysis for C<sub>20</sub>H<sub>28</sub>GdN<sub>5</sub>O<sub>6</sub> (M + H<sub>2</sub>O + MeOH), calcd. C, 38.86 H, 5.40 N, 10.79. Found C: 38.95 H, 5.76 N, 10.41.

**6.4.16 Synthesis of europium(III) complex of 1, 4, 7-tris (tert-butoxycarbonylmethyl)-10-(4-methylpyridyl) tetraazadodecane. (Eu10)**

Amounts: europium(III) trifluoromethanesulfonate (483 mg, 0.80 mmol) to yield a dark yellow solid (192 mg, 40%). HRMS calc. 588.1326 found 588.1318 [M+H]<sup>+</sup>. Elemental analysis for C<sub>20</sub>H<sub>28</sub>N<sub>5</sub>O<sub>6</sub>Eu (M + H<sub>2</sub>O + MeOH), calcd. C, 39.07 H, 5.47 N, 10.85. Found C, 39.11 H, 5.53 N, 10.63.

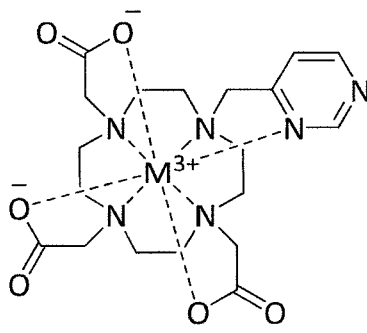
**6.4.17 Synthesis of terbium(III) complex of 1, 4, 7-tris (tert-butoxycarbonylmethyl)-10-(4-methylpyridyl) tetraazadodecane. (Tb10)**

Amounts: terbium(III) trifluoromethanesulfonate (484 mg, 0.80 mmol) to yield a dark yellow solid (181 mg, 35%). HRMS calc. 616.1185 found 616.1177 [M+Na]<sup>+</sup>. Elemental analysis for C<sub>20</sub>H<sub>28</sub>N<sub>5</sub>O<sub>6</sub>Tb (M + H<sub>2</sub>O + MeOH), calcd. C: 38.65 H: 5.68 N: 10.73. Found C: 38.59 H: 5.58 N: 10.50.

**6.4.18 Synthesis of yttrium(III) complex of 1, 4, 7-tris (tert-butoxycarbonylmethyl)-10-(4-methylpyridyl) tetraazadodecane. (Y10)**

Amounts: yttrium(III) trifluoromethanesulfonate (428 mg, 0.80 mmol) to yield a dark yellow solid (177 mg, 43%). HRMS calc. 546.0990 found 546.0981  $[M+Na]^+$ .  $^1H$  NMR (400 MHz,  $D_2O$ )  $\delta$ : 2.62-4.65 (s, 24H,  $CH_2-N$ ) 7.81-7.82 (d, 2H,  $J=8.1Hz$  CH-Ar), 8.42-8.43(d, 2H,  $J=8.1Hz$ , CH-Ar).Elemental analysis for  $C_{20}H_{28}N_5O_6Y$  (M +  $H_2O$ + MeOH), calcd. C: 44.42 H: 6.54 N: 11.77. Found C: 44.42 H: 6.84 N: 12.00.

**6.4.19 Synthesis of metal(III) complexes of 1, 4, 7-tris (tert-butoxycarboxymethyl)-10-(4-methylpyrimidyl) tetraazadodecane.**



**M11**

M = Gd, Eu, Tb, Y

**6.4.20 Synthesis of gadolinium(III) complexes of 1, 4, 7-tris (tert-butoxycarboxymethyl)-10-(4-methylpyrimidyl)tetraazadodecane. (Gd11)**

Amounts: gadolinium(III) chloride hexahydrate (265 mg, 0.71 mmol) to yield a golden solid (141 mg, 33%). HRMS calc. 615.1051 found 615.1163 [M+Na]<sup>+</sup>. Elemental analysis for C<sub>19</sub>H<sub>27</sub>GdN<sub>6</sub>O<sub>6</sub> (M + H<sub>2</sub>O + MeOH), calcd. C: 38.31 H: 5.39 N: 12.76. Found C: 38.46 H: 5.55 N: 12.44.

**6.4.21 Synthesis of europium(III) complex of 1, 4, 7-tris (tert-butoxycarboxymethyl)-10-(4-methylpyrimidyl)tetraazadodecane. (Eu11)**

Amounts: europium(III) trifluoromethanesulfonate (425 mg, 0.71 mmol) to yield a yellow solid (142 mg, 34%). HRMS calc. 610.1145 found 610.1133 [M+H]<sup>+</sup>. Elemental analysis for C<sub>19</sub>H<sub>27</sub>N<sub>6</sub>O<sub>6</sub>Eu (M + H<sub>2</sub>O + MeOH), calcd. C: 38.85 H: 4.63 N: 14.31. Found C: 38.48 H: 4.67 N: 14.22.

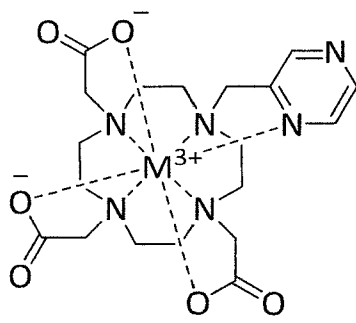
**6.4.22 Synthesis of terbium(III) complex of 1, 4, 7-tris (tert-butoxycarboxymethyl)-10-(4-methylpyrimidyl) tetraazadodecane. (Tb11)**

Amounts: terbium(III) trifluoromethanesulfonate (430 mg, 0.71 mmol) to yield a black solid (154 mg, 36%). HRMS calc. 617.1138 found 617.1131 [M+H]<sup>+</sup>. Elemental analysis for C<sub>19</sub>H<sub>27</sub>N<sub>6</sub>O<sub>6</sub>Tb (M + H<sub>2</sub>O + MeOH), calc. C: 38.39 H: 4.58 N: 14.14. Found C: 38.37 H: 4.83 N: 13.74.

**6.4.23 Synthesis of yttrium (III) complex of 1, 4, 7-tris (tert-butoxycarboxymethyl)-10-(4-methylpyrimidyl) tetraazadodecane. (Y11)**

Amounts: yttrium(III) trifluoromethanesulfonate (375mg, 0.71 mmol) to yield a black solid (137 mg, 40%). HRMS calc. 524.1045 found 524.1161 [M]<sup>+</sup>. <sup>1</sup>H NMR (400 MHz, D<sub>2</sub>O) δ: 1.92-4.29 (m, 24H, CH<sub>2</sub>-N), 7.49 (d, 1H, CH-Ar), 8.69 (d, 1H, CH-Ar), 8.92 (s, 1H, CH-Ar). Elemental analysis for C<sub>19</sub>H<sub>27</sub>N<sub>6</sub>O<sub>6</sub>Y (M+ H<sub>2</sub>O+MeOH), calc. C: 37.15 H: 5.98 N: 13.13. Found C: 37.35.42 H: 5.50 N: 13.24.

**6.4.24 Synthesis of metal (III) complex of 1, 4, 7-tris (tert-butoxycarbonylmethyl)-10-(2-methylpyrazine) tetraazadodecane.**



**M12**

M = Gd, Eu, Tb, Y

**6.4.25 Synthesis of gadolinium(III) complex of 1, 4, 7-tris (tert-butoxycarbonylmethyl)-10-(2-methylpyrazine) tetraazadodecane. (Gd12)**

Amounts: gadolinium(III) chloride hexahydrate (293 mg, 0.78 mmol) to yield a black solid (187 mg, 40%). HRMS calc. 615.1051 found 615.1163 [M+Na]<sup>+</sup>. Elemental analysis for C<sub>19</sub>H<sub>27</sub>GdN<sub>6</sub>O<sub>6</sub> (M +H<sub>2</sub>O+3MeOH), calcd. C, 38.36 H, 5.71 N, 12.20. Found C, 38.53 H, 5.99 N, 12.22.

**6.4.26 Synthesis of europium(III) complex of 1, 4, 7-tris (tert-butoxycarbonylmethyl)-10-(2-methylpyrazine)tetraazadodecane. (Eu12)**

Amounts: europium(III) trifluoromethanesulfonate (467 mg, 0.78 mmol) to yield a yellow solid (188 mg, 41%). HRMS calc. 588.1326 found 588.8150 [M+H]<sup>+</sup>. Elemental analysis for C<sub>19</sub>H<sub>27</sub>N<sub>6</sub>O<sub>6</sub>Eu (M +H<sub>2</sub>O+3MeOH), calcd. C, 39.49 H, 6.20 N, 12.01. Found C, 39.19 H, 6.12 N, 12.08.

**6.4.27 Synthesis of terbium(III) complex of 1, 4, 7-tris (tert-butoxycarbonylmethyl)-10-(2-methylpyrazine)tetraazadodecane. (Tb12)**

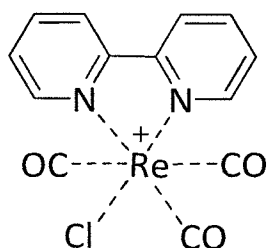
Amounts: terbium(III) trifluoromethanesulfonate (473 mg, 0.78 mmol) to yield a black solid (178 mg, 38%). HRMS calc. 617.1138 found 617.1131 [M+Na]<sup>+</sup>. Elemental analysis for C<sub>19</sub>H<sub>27</sub>N<sub>6</sub>O<sub>6</sub>Tb (M+ H<sub>2</sub>O+3MeOH), calcd. C, 38.18 H, 5.71 N, 12.14. Found C, 38.37 H, 5.65 N, 12.06

#### 6.4.28 Synthesis of yttrium(III) complex of 1, 4, 7-tris(tert-butoxycarbonylmethyl)-10-(2-methylpyrazine)tetraazadodecane. (Y12)

Amounts: yttrium(III) trifluoromethanesulfonate (415 mg, 0.78 mmol) to yield a black solid (148 mg, 30%). HRMS calc. 525.1123 found 525.1117 [M+H]<sup>+</sup>. <sup>1</sup>H NMR (400 MHz, D<sub>2</sub>O)  $\delta$ : 2.22-4.55 (m, 24H, CH<sub>2</sub>-N), 8.51-8.52 (d, 1H, J=2.1Hz, CH-Ar), 8.71-8.72 (s, 2H, J=2.1Hz, CH-Ar). 8.77 (s, 2H, J=2.2Hz, CH-Ar). Elemental analysis for C<sub>20</sub>H<sub>28</sub>N<sub>5</sub>O<sub>6</sub>Y (M+ H<sub>2</sub>O +3MeOH), calcd. C, 42.47 H, 6.35 N, 13.51. Found C, 42.22 H, 6.52 N, 13.36.

## 6.5 Synthesis of Multi-metallic species

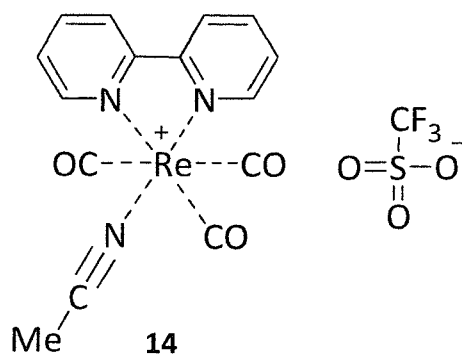
### 6.5.1 *fac*-chlorotricarbonyl (bipyridine) rhenium(I).



13

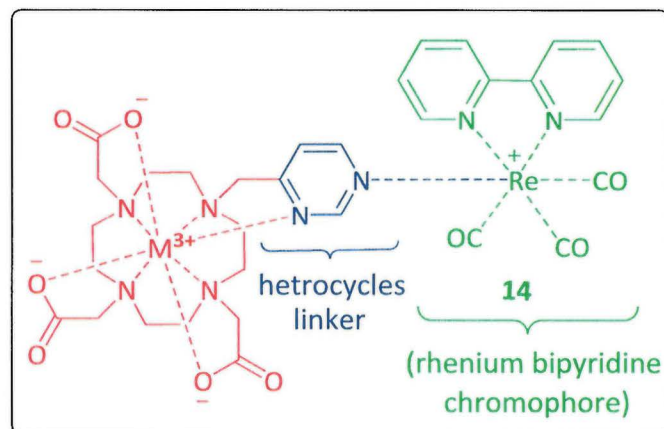
Following to modified literature method,<sup>95</sup>  $\text{Re}(\text{CO})_5\text{Cl}$  (30 mg, 0.08 mmol) and 2,2'-bipyridine (13 mg, 0.08 mmol) were dissolved in dry toluene and heated to 110°C, the mixture was stirred under Ar for 1 h. The solvent was then removed under reduced pressure, and the product was obtained as a light yellow solid by column chromatography (silica gel,  $\text{CH}_2\text{Cl}_2:\text{CH}_3\text{OH} = 100:1$ ) (31 mg, 91%).  $^1\text{H}$  NMR (400 MHz,  $\text{CDCl}_3$ )  $\delta$ : 9.08 (d, 2H,  $J=5.5$  Hz), 8.20 (d, 2H,  $J= 8.1$  Hz), 8.07 (t, 2H,  $J= 15.7\text{Hz}$ ), 7.58 (t, 2H,  $J= 13.1\text{Hz}$ ). HRMS calc. 427.0087 found 427.001  $[\text{M}+\text{H}]^+$ . Elemental analysis for  $\text{C}_{13}\text{H}_{11}\text{ClN}_2\text{O}_3\text{Re}$ : Calcd. C, 33.59; H, 2.38; N, 6.03; Found C, 34.06; H, 1.90; N, 5.98.

### 6.5.2 *fac*-(acetonitrile) tricarbonyl (2, 2'-bypyridine) rhenium (I) triflate.

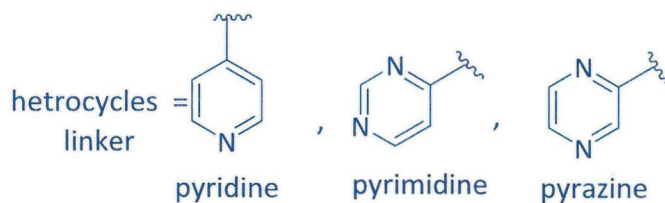


Following to modified literature method,<sup>74</sup> a solution of AgOTf (0.256 g, 1.00 mmol) in 5 cm<sup>3</sup> of THF was added to a solution of *fac*-chlorotricarbonyl(bypyridine)rhenium(I) (**13**) (0.48 g, 1.00 mmol) in 50 ml of acetonitrile in the dark under N<sub>2</sub> for 16 h. The reaction was then allowed to settle and the supernatant decanted from the salts and filtered through a pad of celite to eliminate any residual AgCl. All volatiles were removed under reduced pressure and the crude product recrystallized from CHCl<sub>3</sub>/Et<sub>2</sub>O at -18°C to yield the title compound as yellow needles <sup>1</sup>H NMR (0.42 g, 65%)(400 MHz,CDCl<sub>3</sub>) δ: 8.93 (dt, 2H, J=5.5 Hz, J=0.7(2) Hz), 8.67 (d, 2H, J=8.4Hz), 8.28 (td, 2H, J=8.0 (2) Hz, J=1.6 Hz), 7.56 (td, 2H, J=7.5 Hz, J=5.5 Hz, J=1.2 Hz). ESI-MS calc. 468.0 found 468.0 [M+H]<sup>+</sup>. Elemental analysis for C<sub>16</sub>H<sub>11</sub>N<sub>3</sub>O<sub>6</sub>F<sub>3</sub>SRe.0.009CHCl<sub>3</sub>, Calcd. C, 31.17, H, 1.80, N, 6.82. Found C, 31.49, H, 1.33, N, 6.68.

### 6.5.3 Combined complexes (rhenium-lanthanide).



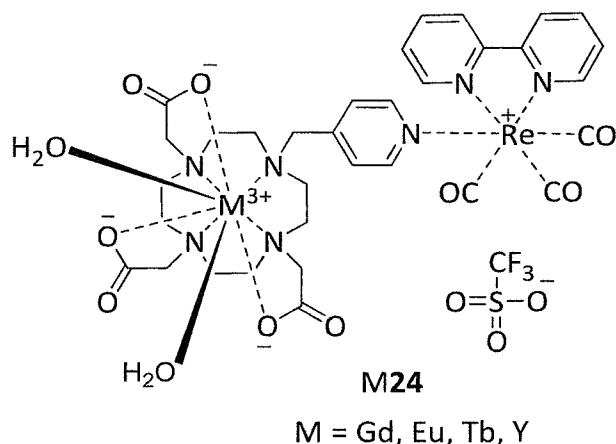
M24, M25, M26



#### General procedure

Following to modified literature method,<sup>106</sup> Ln(III) complexes (M10, M11, M12) (1 eq.) and Re(bipy)(CO)<sub>3</sub>(OTf) (1.5 eq.) were suspended in acetonitrile and heated to reflux for 24 h. TLC (DCM-MeOH 95:5) showed the development of a new yellow spot on the baseline indicating the formation of the product as confirmed also by HRMS and CHN. Once the reaction cooled to room temperature the solvent was removed and the crude mixture was redissolved in methanol and precipitated with diethyl ether decanting the solvents and repeating this process several time until a fine yellow powder was obtained.

#### 6.5.4 Combined complexes (rhenium-lanthanide). (Pyridyl linker)



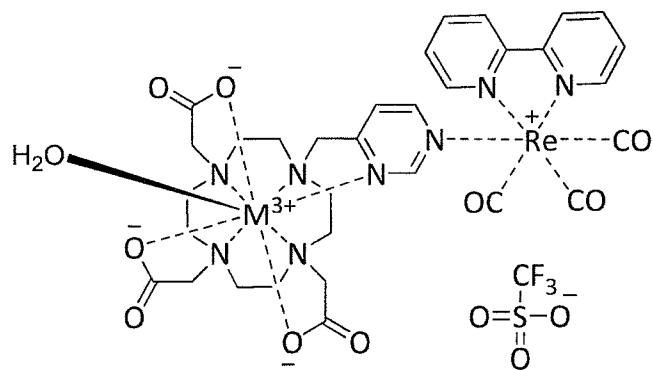
Amounts: a solution of 1,4,7,10-tetraazacyclododecane-(4-methylpyridyl) 4,7,10-tris(carboxymethyl)-gadolinium (100 mg, 0.15 mmol) in ethanol and solution of  $\text{Re}(\text{bipy})(\text{CO})_3(\text{MeCN})\cdot\text{OTf}$  (139 mg, 0.22 mmol) in acetonitrile (20 ml) to yield as yellow solid (114 mg, 74%). HRMS calc. 1019.1374 found 1019.1365  $[\text{M}+\text{OTf}]^+$ . Elemental analysis for  $\text{C}_{33}\text{H}_{36}\text{GdN}_7\text{O}_9\text{Re}\cdot\text{OTf}$ , calcd. C, 34.99 H, 3.11 N, 8.40. Found C, 34.69 H, 3.34 N, 8.32.

Amounts: a solution of 1,4,7,10-tetraazacyclododecane-(4-methylpyridyl) 4,7,10-tris(carboxymethyl)-europium (100 mg, 0.15 mmol) in ethanol (20 ml), and solution of  $\text{Re}(\text{bipy})(\text{CO})_3(\text{MeCN})\cdot\text{OTf}$  (139 mg, 0.22 mmol) in acetonitrile (20 ml) to yield as yellow solid (120 mg, 78%). HRMS calc. 1012.1320 found 1012.1320  $[\text{M}]^+$ . Elemental analysis for  $\text{C}_{33}\text{H}_{36}\text{EuN}_7\text{O}_9\text{Re}\cdot\text{OTf}$ , calcd. C, 35.15 H, 3.12 N, 8.44. Found C, 35.32 H, 3.48 N, 8.60.

Amounts: a solution of 1,4,7,10-tetraazacyclododecane-(4-methylpyridyl) 4,7,10-tris(carboxymethyl)-terbium (100 mg, 0.14 mmol) in ethanol (20 ml) , and solution of  $\text{Re}(\text{bipy})(\text{CO})_3(\text{MeCN})\cdot\text{OTf}$  (130 mg, 0.21 mmol) in acetonitrile (20 ml) to yield as yellow solid (122 mg, 85%). HRMS calc. 1020.1381 found 1020.1375  $[\text{M}+\text{OTf}]^+$ . Elemental analysis for  $\text{C}_{33}\text{H}_{36}\text{TbN}_7\text{O}_9\text{Re}\cdot\text{OTf}$ , calcd. C, 34.94 H, 3.10 N, 8.39. Found C, 35.15 H, 3.38 N, 8.69.

Amounts: a solution of 1,4,7,10-tetraazacyclododecane-(4-methylpyridyl) 4,7,10-tris(carboxymethyl)-yttrium (100 mg, 0.14 mmol) in ethanol (20 ml) and solution of  $\text{Re}(\text{bipy})(\text{CO})_3(\text{MeCN})\cdot\text{OTf}$  (130 mg, 0.21 mmol) in acetonitrile (20 ml) to yield as yellow solid (109g, 82%). HRMS calc. 950.1186 found 950.1208  $[\text{M}+\text{OTf}]^+$ . Elemental analysis for  $\text{C}_{33}\text{H}_{36}\text{YN}_7\text{O}_9\text{Re}\cdot\text{OTf}$ , calcd. C, 37.16 H, 3.30 N, 8.92. Found C, 37.51 H, 3.41 N, 9.17.

### 6.5.5 Combined complexes (rhenium-lanthanide). (Pyrimidyl linker)



**M25**

M = Gd, Eu, Tb, Y

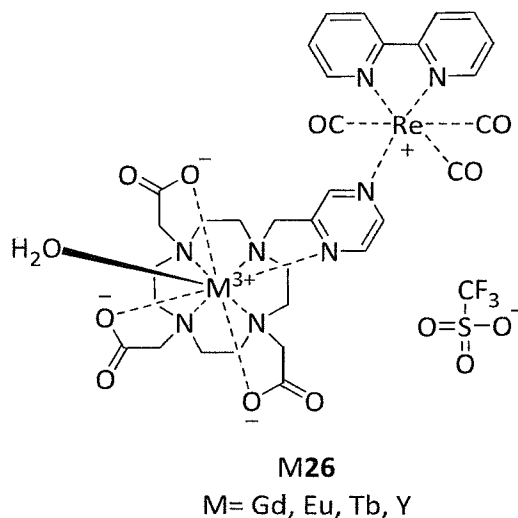
**Amounts:** a solution of 4,7,10-tris(carboxymethyl)(4-methylpyrimidyl)-1,4,7,10-tetraazacyclododecane-gadolinium (100 mg, 0.15 mmol) in ethanol (20 ml) and solution of Re(bipy)(CO)<sub>3</sub>(MeCN).OTf (139 mg, 0.22 mmol) in acetonitrile (20 ml) to yield as light yellow solid (111 mg, 72 %). HRMS calc. 1020.1381 found 1020.1326 [M]<sup>+</sup>. Elemental analysis for C<sub>32</sub>H<sub>35</sub>GdN<sub>8</sub>O<sub>9</sub>Re.OTf, calcd. C, 33.93 H, 3.02 N, 9.59. Found C, 34.23 H, 3.24 N, 9.71.

**Amounts:** a solution of 4,7,10-tris(carboxymethyl)(4-methylpyrimidyl)-1,4,7,10-tetraazacyclododecane-europium (100 mg, 0.16 mmol) in ethanol (20 ml) and solution of Re(bipy)(CO)<sub>3</sub>(MeCN).OTf (148 mg, 0.24 mmol) in acetonitrile (20 ml) to yield as light yellow solid (135 mg, 83 %). HRMS calc. 1014.0611 found 1014.0620 [M+H]<sup>+</sup>. Elemental analysis for C<sub>32</sub>H<sub>35</sub>EuN<sub>8</sub>O<sub>9</sub>Re.OTf, calcd. C, 34.08 H, 3.03 N, 9.69. Found C, 34.35 H, 3.18 N, 9.83.

**Amounts:** a solution of 4,7,10-tris(carboxymethyl)(4-methylpyrimidyl)-1,4,7,10-tetraazacyclododecane-terbium (100 mg, 0.16 mmol) in ethanol (20 ml) and solution of Re(bipy)(CO)<sub>3</sub>(MeCN).OTf (148 mg, 0.24 mmol) in acetonitrile (20 ml) to yield as light yellow solid (129 mg, 79%). HRMS calc. 1021.1334 found 1021.1332 [M+H]<sup>+</sup>. Elemental analysis for C<sub>32</sub>H<sub>35</sub>TbN<sub>8</sub>O<sub>9</sub>Re.OTf, calcd. C, 33.88 H, 3.02 N, 9.58. Found C, 34.12 H, 3.43 N, 9.77.

**Amounts:** a solution of 4,7,10-tris(carboxymethyl)(4-methylpyrimidyl)-1,4,7,10-tetraazacyclododecane-yttrium (100 mg, 0.14 mmol) in ethanol (20 ml) and solution of Re(bipy)(CO)<sub>3</sub>(MeCN).OTf (130 mg, 0.21 mmol) in acetonitrile (20 ml) to yield as light yellow solid (109 g, 81%). HRMS calc. 950.1122 found 950.1214 [M]<sup>+</sup>. Elemental analysis for C<sub>32</sub>H<sub>35</sub>YN<sub>8</sub>O<sub>9</sub>Re.OTf, calcd. C, 36.04 H, 3.21 N, 10.19. Found C, 36.51 H, 3.42 N, 10.52.

### 6.5.6 Combined complexes (rhenium-lanthanide). (Pyrazine linker)



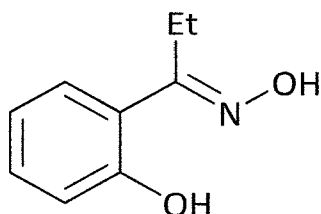
**Amounts:** a solution of 4,7,10-tris(carboxymethyl)(2-methylpyrazine)1,4,7,10-tetraazacyclododecane-gadolinium (100 mg, 0.14 mmol) in ethanol (20 ml) and a solution of Re(bipy)(CO)<sub>3</sub>(MeCN).OTf (130 mg, 0.21 mmol) in acetonitrile (20 ml) to yield as brown solid (117 g, 81%). HRMS calc. 1020.1273 found 1020.1256 [M+H]<sup>+</sup>. Elemental analysis for C<sub>32</sub>H<sub>35</sub>GdN<sub>8</sub>O<sub>9</sub>Re.OTf, calcd. C, 33.93 H, 3.02 N, 9.59. Found C, 34.31 H, 3.32 N, 9.65.

**Amounts:** a solution of 4,7,10-tris(carboxymethyl)(2-methylpyrazine)1,4,7,10-tetraazacyclododecane-europium (100 mg, 0.14 mmol) in ethanol (20 ml) and solution of Re(bipy)(CO)<sub>3</sub>(MeCN).OTf (130 mg, 0.21 mmol) in acetonitrile (20 ml) to yield as brown solid (105 mg, 73%). HRMS calc. 1013.1521 found 1013.1511 [M]<sup>+</sup>. Elemental analysis for C<sub>32</sub>H<sub>35</sub>EuN<sub>8</sub>O<sub>9</sub>Re.OTf, calcd. C, 34.08 H, 3.03 N, 9.69. Found C, 34.51 H, 3.45 N, 9.73.

**Amounts:** a solution of 4,7,10-tris(carboxymethyl)(2-methylpyrazine)1,4,7,10-tetraazacyclododecane-terbium (100 mg, 0.16 mmol) in ethanol (20 ml) was adjusted to pH 8 by the addition of NaHCO<sub>3</sub>, a solution of Re(bipy)(CO)<sub>3</sub>(MeCN).OTf (148 mg, 0.24 mmol) in acetonitrile (20 ml) to yield as brown solid (124 mg, 76%). HRMS calc. 1020.1338 found 1020.1316 [M]<sup>+</sup>. Elemental analysis for C<sub>32</sub>H<sub>35</sub>TbN<sub>8</sub>O<sub>9</sub>Re.OTf, calcd. C, 33.88 H, 3.02 N, 9.58. Found C, 34.31 H, 3.25 N, 9.42.

Amounts: a solution of 4,7,10-tris(carboxymethyl)(2-methylpyrazine)1,4,7,10-tetraazacyclododecane-yttrium (100 mg, 0.16 mmol) in ethanol (20 ml) and a solution of Re(bipy)(CO)<sub>3</sub>(MeCN).OTf (148 mg, 0.24 mmol) in acetonitrile (20 ml) to yield as brown solid (127 mg, 83%). HRMS calc. 950.1296 found 950.1233 [M]<sup>+</sup>. Elemental analysis for C<sub>32</sub>H<sub>35</sub>YN<sub>8</sub>O<sub>9</sub>Re.OTf, calcd. C, 36.04 H, 3.21 N, 10.19. Found C, 36.22 H, 3.36 N, 10.43.

### 6.5.7 Oxime synthesis: Et-saoH<sub>2</sub>

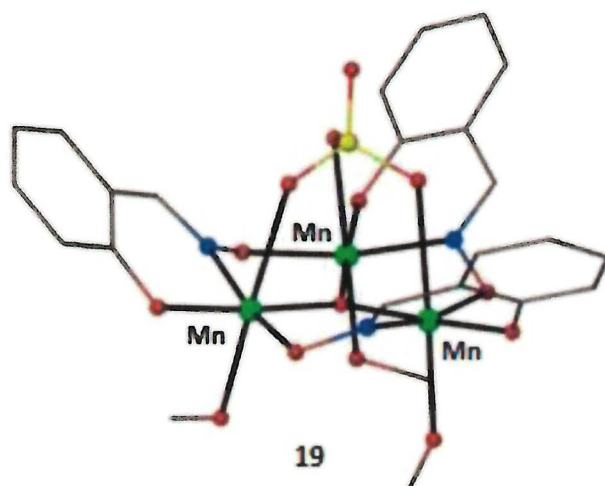


Et-saoH<sub>2</sub>

**18**

According to a literature procedure,<sup>111</sup> 2-hydroxypropiophenone (25 g, 0.17 mol) and hydroxylamine hydrochloride (11.57 g, 0.17 mol) were dissolved in ethanol (200 ml) before adding sodium acetate (13.66 g, 0.17 mol) and with constant stirring, heated to reflux for 4 h. The precipitated salt was filtered off and the solvent was removed on a rotary evaporator until an oily substance appeared. After washing with Et<sub>2</sub>O the reaction flask was evacuated on a Schlenk line until the white/yellow crystalline product was completely dry to yield (25.8 g, 92%). <sup>1</sup>H NMR (400 MHz, CD<sub>3</sub>OH) δ: 1.14-1.11 (t, 3H, CH<sub>2</sub>CH<sub>3</sub>) 2.83-2.89 (q, 2H, CH<sub>2</sub>CH<sub>3</sub>), 6.84-6.90 (m, 2H, CH-Ar), 7.17-7.21 (m, 1H, CH-Ar), 7.43-7.45 (m, 1H, CH-Ar) <sup>13</sup>C NMR (400 MHz, CD<sub>3</sub>OH) δ: 10.20 (Et), 17.35 (CH<sub>2</sub>-Et), 116.68 (C-Ar), 127.10 (CH-Ar), 129.84 (CH-Ar), 158.09 (Ar-C=N), 162.60 (Ar-OH). GC-MS (EI): calculated for C<sub>9</sub>H<sub>11</sub>NO<sub>2</sub> [M]<sup>+</sup> 165.08 found 165.33. Retention time = 11.41 min, purity= 98.5%

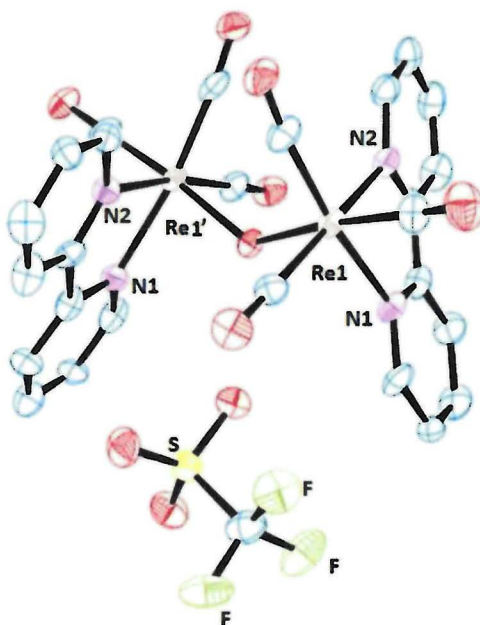
### 6.5.8 Synthesis manganese (III) triangle (19)



Following a modified literature method,<sup>111</sup>  $\text{Mn}(\text{ClO}_4)_2 \cdot 6\text{H}_2\text{O}$  (362 mg, 1mmol), Et-saoH<sub>2</sub> (165 mg, 1mmol) (**18**) and  $\text{NEt}_3$  (101 mg, 1mmol) in MeOH (25 ml) was allowed to stir for 45 minutes at RT. Colour code: Mn(III) (green), O (red), N (blue) C (grey)

## 6.6 Single crystal X-ray diffractometer data

### 6.6.1 Data for 15



According to a literature procedure,<sup>74</sup> a solution of Eu(III) complex (Eu10)(100 mg) in ethanol (20 ml) was adjusted to pH 8 by the addition of NaHCO<sub>3</sub>. A solution of Re(bipy)(CO)<sub>3</sub>(MeCN).triflate (100 mg)(14) in acetonitrile (20 ml) was then added to this solution and the reaction mixture heated to 50°C and stirred for 17 h. The solvents were then removed under reduced pressure and the solid washed with water to remove any unreacted starting materials, after removal of the water by evaporation, the complex was dissolved in a minimal volume of THF, followed by filtration slow diffusion of hexane into this solution afforded. Yellow colour blocks were separated in two days from the solvent and a suitable crystal was selected and mounted on a glass fibre using perfluoropolyether oil.

Crystal data and structure refinement for 15

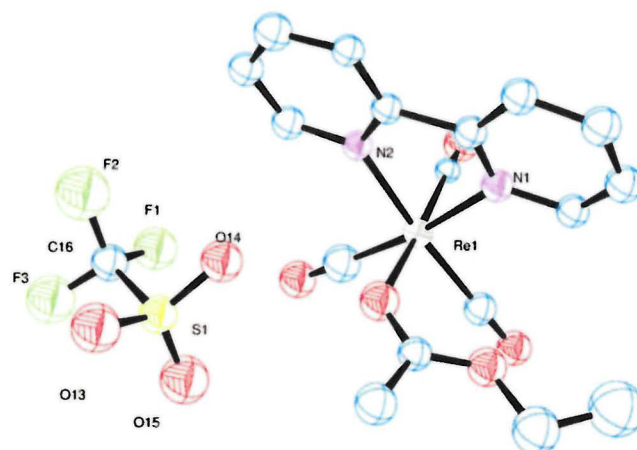
Identification code	shelx
Empirical formula	C <sub>27</sub> H <sub>16</sub> F <sub>3</sub> N <sub>4</sub> O <sub>10</sub> Re <sub>2</sub> S
Formula weight	1017.89
Temperature	150(2) K
Wavelength	0.71073 Å
Crystal system	Triclinic
Space group	P -1
Unit cell dimensions	
a	9.1900(7) Å
b	10.7478(10) Å
c	15.5136(13) Å
α	80.223(7)°
β	85.846(7)°
γ	90°
Volume	1484.8(2) Å <sup>3</sup>
Z	2
Density (calculated)	2.277 Mg/m <sup>3</sup>
Absorption coefficient	8.299 mm <sup>-1</sup>
F(000)	958
Crystal size	0.120 x 0.100 x 0.100 mm <sup>3</sup>
Theta range for data collection	1.925 to 29.217°
Index ranges	-12 ≤ h ≤ 12, -14 ≤ k ≤ 14, -21 ≤ l ≤ 21
Reflections collected	15372
Independent reflections	7825 [R(int) = 0.0592]
Completeness to theta =	25.242° 98.7 %
Absorption correction	Semi-empirical from equivalents
Max. and min. transmission	0.869 and 0.644
Refinement method	Full-matrix least-squares on F <sup>2</sup>
Data / restraints / parameters	7825 / 2 / 427
Goodness-of-fit on F <sup>2</sup>	0.899
Final R indices [I > 2σ(I)]	R1 = 0.0388, wR2 = 0.0862
R indices (all data)	R1 = 0.0650, wR2 = 0.0941
Extinction coefficient	n/a
Largest diff. peak and hole	1.750 and -2.218 e.Å <sup>-3</sup>

Bond lengths [Å] and angles [°] for 15			
Re(1)-C(12)	1.922(8)	C(20)-C(21)	1.379(13)
Re(1)-C(13)	1.925(7)	C(20)-H(20)	0.9500
Re(1)-C(11)	1.926(7)	C(21)-C(22)	1.366(13)
Re(1)-O(4)	2.139(4)	C(21)-H(21)	0.9500
Re(1)-N(1)	2.167(5)	C(22)-C(23)	1.391(11)
Re(1)-N(2)	2.189(5)	C(22)-H(22)	0.9500
Re(2)-C(24)	1.919(7)	C(23)-N(4)	1.345(10)
Re(2)-C(26)	1.927(8)	C(23)-H(23)	0.9500
Re(2)-C(25)	1.940(8)	C(24)-O(5)	1.152(9)
Re(2)-N(4)	2.168(6)	C(25)-O(6)	1.142(9)
Re(2)-O(4)	2.173(4)	C(26)-O(7)	1.131(9)
Re(2)-N(3)	2.179(6)	O(8)-S(1)	1.460(6)
O(4)-H(4A)	0.911(17)	O(9)-S(1)	1.438(6)
C(1)-N(1)	1.354(8)	O(10)-S(1)	1.459(6)
C(1)-C(2)	1.368(10)	S(1)-C(30)	1.791(9)
C(1)-H(1)	0.9500	C(30)-F(3)	1.328(10)
C(2)-C(3)	1.386(11)	C(30)-F(2)	1.339(10)
C(2)-H(2)	0.9500	C(30)-F(1)	1.343(10)
C(3)-C(4)	1.380(10)		
C(3)-H(3)	0.9500	C(12)-Re(1)-C(13)	88.4(3)
C(4)-C(5)	1.388(10)	C(12)-Re(1)-C(11)	86.2(3)
C(4)-H(4)	0.9500	C(13)-Re(1)-C(11)	90.6(3)
C(5)-N(1)	1.354(9)	C(12)-Re(1)-O(4)	98.1(3)
C(5)-C(6)	1.485(10)	C(13)-Re(1)-O(4)	89.2(2)
C(6)-N(2)	1.363(9)	C(11)-Re(1)-O(4)	175.7(2)
C(6)-C(7)	1.376(10)	C(12)-Re(1)-N(1)	97.7(3)
C(7)-C(8)	1.394(10)	C(13)-Re(1)-N(1)	170.7(3)
C(7)-H(7)	0.9500	C(11)-Re(1)-N(1)	96.9(2)
C(8)-C(9)	1.379(11)	O(4)-Re(1)-N(1)	82.90(19)
C(8)-H(8)	0.9500	C(12)-Re(1)-N(2)	170.8(2)
C(9)-C(10)	1.380(10)	C(13)-Re(1)-N(2)	100.1(3)
C(9)-H(9)	0.9500	C(11)-Re(1)-N(2)	90.0(3)
C(10)-N(2)	1.354(9)	O(4)-Re(1)-N(2)	85.8(2)
C(10)-H(10)	0.9500	N(1)-Re(1)-N(2)	74.5(2)
C(11)-O(1)	1.148(9)	C(24)-Re(2)-C(26)	85.2(3)
C(12)-O(2)	1.153(9)	C(24)-Re(2)-C(25)	88.7(3)
C(13)-O(3)	1.148(8)	C(26)-Re(2)-C(25)	90.6(3)
C(14)-N(3)	1.352(10)	C(24)-Re(2)-N(4)	96.0(3)
C(14)-C(15)	1.396(11)	C(26)-Re(2)-N(4)	97.1(3)
C(15)-C(16)	1.392(13)	C(25)-Re(2)-N(4)	171.3(3)
C(15)-H(15)	0.9500	C(24)-Re(2)-O(4)	100.1(3)
C(16)-C(17)	1.380(13)	C(26)-Re(2)-O(4)	174.7(3)
C(16)-H(16)	0.9500	C(25)-Re(2)-O(4)	89.5(3)
C(17)-C(18)	1.399(10)	N(4)-Re(2)-O(4)	82.46(19)
C(17)-H(17)	0.9500	C(24)-Re(2)-N(3)	170.6(3)
C(18)-N(3)	1.368(9)	C(26)-Re(2)-N(3)	93.9(3)
C(18)-C(19)	1.465(11)	C(25)-Re(2)-N(3)	100.6(3)
C(19)-N(4)	1.350(9)	N(4)-Re(2)-N(3)	74.9(2)
C(19)-C(20)	1.421(10)	O(4)-Re(2)-N(3)	80.9(2)

## Bond angles [°] for 15

Re(1)-O(4)-Re(2)	135.0(2)	C(21)-C(20)-H(20)	120.5
Re(1)-O(4)-H(4A)	124(5)	C(19)-C(20)-H(20)	120.5
Re(2)-O(4)-H(4A)	93(5)	C(22)-C(21)-C(20)	119.7(8)
N(1)-C(1)-C(2)	123.2(7)	C(22)-C(21)-H(21)	120.1
C(2)-C(1)-H(1)	118.4	C(20)-C(21)-H(21)	120.1
C(1)-C(2)-C(3)	119.1(7)	C(21)-C(22)-C(23)	119.5(8)
C(1)-C(2)-H(2)	120.5	C(21)-C(22)-H(22)	120.2
C(3)-C(2)-H(2)	120.5	C(23)-C(22)-H(22)	120.2
C(4)-C(3)-C(2)	118.8(7)	N(4)-C(23)-C(22)	121.6(8)
C(4)-C(3)-H(3)	120.6	N(4)-C(23)-H(23)	119.2
C(2)-C(3)-H(3)	120.6	C(22)-C(23)-H(23)	119.2
C(3)-C(4)-C(5)	119.5(7)	O(5)-C(24)-Re(2)	176.5(7)
C(3)-C(4)-H(4)	120.2	O(6)-C(25)-Re(2)	177.4(7)
C(5)-C(4)-H(4)	120.2	O(7)-C(26)-Re(2)	179.0(8)
N(1)-C(5)-C(4)	121.9(6)	C(1)-N(1)-C(5)	117.6(6)
N(1)-C(5)-C(6)	114.9(6)	C(1)-N(1)-Re(1)	124.2(5)
C(4)-C(5)-C(6)	123.1(7)	C(5)-N(1)-Re(1)	117.7(4)
N(2)-C(6)-C(7)	121.3(6)	C(10)-N(2)-C(6)	118.5(6)
N(2)-C(6)-C(5)	114.9(6)	C(10)-N(2)-Re(1)	124.1(5)
C(7)-C(6)-C(5)	123.8(6)	C(6)-N(2)-Re(1)	117.0(4)
C(6)-C(7)-C(8)	119.5(7)	C(14)-N(3)-C(18)	118.8(6)
C(6)-C(7)-H(7)	120.3	C(14)-N(3)-Re(2)	125.0(5)
C(8)-C(7)-H(7)	120.3	C(18)-N(3)-Re(2)	116.1(5)
C(9)-C(8)-C(7)	119.4(7)	C(23)-N(4)-C(19)	119.8(6)
C(9)-C(8)-H(8)	120.3	C(23)-N(4)-Re(2)	124.0(5)
C(7)-C(8)-H(8)	120.3	C(19)-N(4)-Re(2)	115.9(5)
C(8)-C(9)-C(10)	118.6(7)	O(9)-S(1)-O(10)	114.5(4)
C(8)-C(9)-H(9)	120.7	O(9)-S(1)-O(8)	115.4(4)
N(2)-C(10)-H(10)	118.7	O(10)-S(1)-O(8)	112.4(3)
C(9)-C(10)-H(10)	118.7	O(9)-S(1)-C(30)	105.2(4)
O(1)-C(11)-Re(1)	178.8(7)	O(10)-S(1)-C(30)	103.1(4)
O(2)-C(12)-Re(1)	175.3(6)	O(8)-S(1)-C(30)	108.0(7)
O(3)-C(13)-Re(1)	176.4(7)	F(3)-C(30)-F(2)	107.0(7)
N(3)-C(14)-C(15)	121.9(8)	F(3)-C(30)-F(1)	105.9(7)
C(16)-C(15)-C(14)	118.9(8)	F(2)-C(30)-F(1)	111.7(6)
C(16)-C(15)-H(15)	120.5	F(3)-C(30)-S(1)	112.3(6)
C(14)-C(15)-H(15)	120.5	F(2)-C(30)-S(1)	111.6(6)
C(17)-C(16)-C(15)	119.7(7)	F(1)-C(30)-S(1)	123.2(7)
C(17)-C(16)-H(16)	120.1	C(20)-C(19)-C(18)	124.5(4)
C(15)-C(16)-H(16)	120.1		
C(16)-C(17)-C(18)	119.1(8)		
C(16)-C(17)-H(17)	120.5		
C(18)-C(17)-H(17)	120.5		
N(3)-C(18)-C(17)	121.5(7)		
N(3)-C(18)-C(19)	114.8(6)		
C(17)-C(18)-C(19)	123.7(7)		
N(4)-C(19)-C(20)	120.2(7)		
N(4)-C(19)-C(18)	116.5(6)		

## 6.6.2 Data for 16



According to a literature procedure,<sup>74</sup> a solution of (Tb10) (100 mg) in ethanol (20 ml) was adjusted to pH 8 by the addition of NaHCO<sub>3</sub>. A solution of Re(bipy)(CO)<sub>3</sub>(MeCN). triflate (100 mg)(14) in acetonitrile (20 ml) was then added to this solution and the reaction mixture heated to 50°C and stirred for 17 h. The solvents were then removed under reduced pressure and the solid washed with water to remove any unreacted starting materials, after removal of the water by evaporation, the complex was dissolved in a minimal volume of THF, followed by filtration slow diffusion of hexane into this solution afforded. Yellow colour blocks were separated from the solvent in two days and a suitable crystal was selected and mounted on a glass fibre using perfluoropolyether oil.

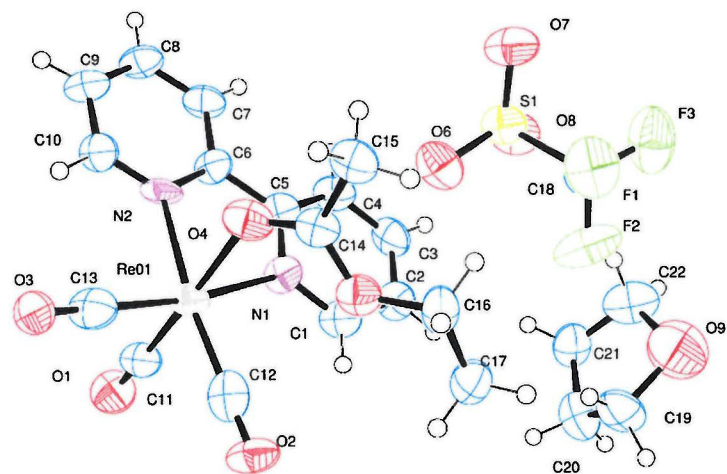
Crystal data and structure refinement for **16**

Identification code	shelx
Empirical formula	C <sub>38</sub> H <sub>32</sub> F <sub>6</sub> N <sub>4</sub> O <sub>17</sub> Re <sub>2</sub> S <sub>2</sub>
Formula weight	1367.19
Temperature	150(2) K
Wavelength	0.71073 Å
Crystal system	Triclinic
Space group	P -1
Unit cell dimensions	
a	8.3582(7) Å
b	11.5768(11) Å
c	13.4193(11) Å
α	91.659(7)°.
β	101.253(6)°.
γ	108.744(7)°.
Volume	1200.08(19) Å <sup>3</sup>
Z	1
Density (calculated)	1.892 Mg/m <sup>3</sup>
Absorption coefficient	5.221 mm <sup>-1</sup>
F(000)	660
Crystal size	0.400 x 0.350 x 0.280 mm <sup>3</sup>
Theta range for data collection	1.555 to 29.229°.
Index ranges	-11<=h<=11, -14<=k<=15, -18<=l<=18
Reflections collected	12419
Independent reflections	6363 [R(int) = 0.0364]
Completeness to theta =	25.242° 98.9 %
Absorption correction	Semi-empirical from equivalents
Max. and min. transmission	0.530 and 0.416
Refinement method	Full-matrix least-squares on F <sup>2</sup>
Data / restraints / parameters	6363 / 0 / 325
Goodness-of-fit on F <sup>2</sup>	0.966
Final R indices [I>2σ(I)]	R1 = 0.0393, wR2 = 0.0980
R indices (all data)	R1 = 0.0498, wR2 = 0.1008
Extinction coefficient	n/a
Largest diff. peak and hole	2.257 and -2.681 e.Å <sup>-3</sup>

Bond lengths [Å] and angles [°] for 16			
N(1)-C(1)	1.347(7)	C(10)-N(2)-Re(1)	124.4(4)
N(1)-C(5)	1.361(7)	C(6)-N(2)-Re(1)	117.2(4)
N(1)-Re(1)	2.176(4)	O(2)-C(12)-Re(1)	178.4(5)
C(4)-C(3)	1.384(9)	C(7)-C(8)-C(9)	118.8(5)
C(4)-C(5)	1.396(7)	N(2)-C(6)-C(7)	121.3(5)
C(1)-C(2)	1.393(8)	N(2)-C(6)-C(5)	114.6(5)
C(3)-C(2)	1.378(9)	C(7)-C(6)-C(5)	124.0(5)
N(2)-C(10)	1.354(7)	C(10)-C(9)-C(8)	118.9(6)
N(2)-C(6)	1.359(6)	N(2)-C(10)-C(9)	122.8(5)
N(2)-Re(1)	2.171(5)	N(1)-C(5)-C(4)	120.5(5)
O(2)-C(12)	1.144(8)	N(1)-C(5)-C(6)	116.1(4)
C(12)-Re(1)	1.930(6)	C(4)-C(5)-C(6)	123.4(5)
O(1)-C(11)	1.112(6)	O(3)-C(13)-Re(1)	177.1(5)
C(8)-C(7)	1.378(9)	C(14)-O(5)-C(16)	120.8(5)
C(8)-C(9)	1.394(9)	O(4)-C(14)-O(5)	116.8(5)
C(6)-C(7)	1.386(8)	O(4)-C(14)-C(15)	123.3(6)
C(6)-C(5)	1.482(8)	O(5)-C(14)-C(15)	119.9(5)
C(9)-C(10)	1.371(9)	O(8)-S(1)-O(7)	115.9(4)
O(3)-C(13)	1.139(7)	O(8)-S(1)-O(6)	115.4(3)
C(13)-Re(1)	1.933(6)	O(7)-S(1)-O(6)	113.7(3)
O(5)-C(14)	1.334(7)	O(8)-S(1)-C(18)	102.1(3)
O(5)-C(16)	1.458(7)	O(7)-S(1)-C(18)	102.7(3)
C(14)-O(4)	1.282(7)	O(6)-S(1)-C(18)	104.5(3)
C(14)-C(15)	1.500(8)	C(8)-C(7)-C(6)	119.9(5)
S(1)-O(8)	1.427(5)	C(17)-C(16)-O(5)	106.8(7)
S(1)-O(7)	1.438(5)	F(3)-C(18)-F(2)	108.3(6)
S(1)-O(6)	1.446(5)	F(3)-C(18)-F(1)	107.6(6)
S(1)-C(18)	1.810(7)	F(2)-C(18)-F(1)	106.8(6)
C(16)-C(17)	1.390(14)	F(3)-C(18)-S(1)	110.7(5)
F(3)-C(18)	1.316(8)	F(2)-C(18)-S(1)	111.6(5)
F(1)-C(18)	1.341(7)	F(1)-C(18)-S(1)	111.7(5)
F(2)-C(18)	1.328(9)	O(20)-C(21)-C(22)	119.6(12)
C(21)-O(20)	1.358(14)	O(20)-C(21)-C(22)	135.3(7)
C(21)-C(22)	1.404(18)	C(22)-C(21)-C(22)	187.8(10)
C(21)-C(22)#1	1.95(2)	C(22)#1-O(20)-C(21)	101.6(13)
O(20)-C(22)#1	1.148(19)	O(20)#1-C(22)-C(21)	43.1(9)
C(22)-O(20)#1	1.148(19)	C(21)-C(22)-C(21)	92.2(10)
C(22)-C(21)#1	1.95(2)	C(12)-Re(1)-C(13)	91.6(3)
Re(1)-C(11)	1.948(5)	C(12)-Re(1)-C(11)	89.1(2)
Re(1)-O(4)	2.185(4)	C(13)-Re(1)-C(11)	88.1(2)
		C(12)-Re(1)-N(2)	171.61(19)
C(1)-N(1)-C(5)	119.3(4)	C(13)-Re(1)-N(2)	96.3(2)
C(1)-N(1)-Re(1)	124.3(4)	C(11)-Re(1)-N(2)	94.1(2)
C(5)-N(1)-Re(1)	116.2(3)	C(12)-Re(1)-N(1)	97.0(2)
C(3)-C(4)-C(5)	120.0(5)	C(13)-Re(1)-N(1)	170.7(2)
N(1)-C(1)-C(2)	122.0(5)	C(11)-Re(1)-N(1)	95.6(2)
C(2)-C(3)-C(4)	119.0(5)	N(2)-Re(1)-N(1)	74.99(17)
C(3)-C(2)-C(1)	119.2(6)	C(12)-Re(1)-O(4)	94.7(2)
C(10)-N(2)-C(6)	118.2(5)	C(13)-Re(1)-O(4)	92.9(2)

Bond angles [°] for 16	
C(11)-Re(1)-O(4)	176.0(2)
N(2)-Re(1)-O(4)	81.93(17)
N(1)-Re(1)-O(4)	82.77(16)
O(1)-C(11)-Re(1)	176.1(5)
C(14)-O(4)-Re(1)	130.0(4)

### 6.6.3 Data for 17



Following to modified literature method,<sup>74</sup> a solution of Gd(III) complex (Gd11) in ethanol (20 ml) was adjusted to pH 8 by the addition of NaHCO<sub>3</sub>. A solution of Re(bipy)(CO)<sub>3</sub>(MeCN) triflate (**14**) in acetonitrile (20 ml) was then added to this solution and the reaction mixture heated to 50°C and stirred for 17 h. The solvents were then removed under reduced pressure and the solid washed with water to remove any unreacted starting materials, after removal of the water by evaporation, the complex was dissolved in a minimal volume of THF, followed by filtration slow diffusion of hexane into this solution afforded.

Crystal data and structure refinement for 17

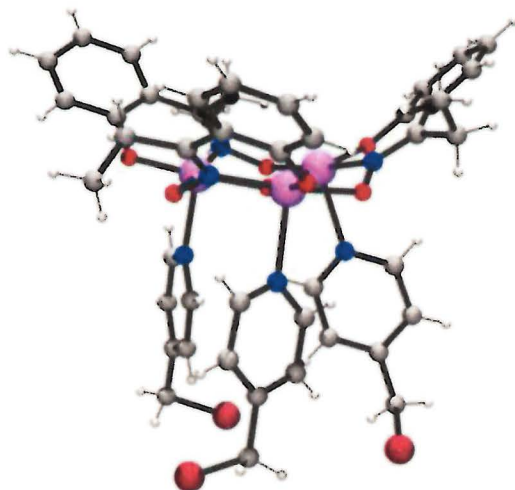
Identification code	Shelx
Empirical formula	C <sub>22</sub> H <sub>24</sub> F <sub>3</sub> N <sub>2</sub> O <sub>9</sub> Re S
Formula weight	735.69
Temperature	150(2) K
Wavelength	0.71073 Å
Crystal system	Triclinic
Space group	P -1
Unit cell dimensions	
a =	8.4399(10) Å
b =	12.6873(17) Å
c =	13.4476(16) Å
α =	104.756(10)°.
β =	93.396(9)°.
γ =	108.744(7)°.
Volume	1306.9(3) Å <sup>3</sup>
Z	2
Density (calculated)	1.870 Mg/m <sup>3</sup>
Absorption coefficient	4.803 mm <sup>-1</sup>
F(000)	720
Crystal size	0.370 x 0.330 x 0.250 mm <sup>3</sup>
Theta range for data collection	1.584 to 29.486°.
Index ranges	-9<=h<=11, -17<=k<=17, -18<=l<=18
Reflections collected	13235
Independent reflections	6924 [R(int) = 0.1018]
Completeness to theta =	25.242° 98.8 %
Absorption correction	Semi-empirical from equivalents
Max. and min. transmission	0.905 and 0.482
Refinement method	Full-matrix least-squares on F <sup>2</sup>
Data / restraints / parameters	6924 / 0 / 344
Goodness-of-fit on F <sup>2</sup>	0.994
Final R indices [I>2sigma(I)]	R1 = 0.0798, wR2 = 0.2013
R indices (all data)	R1 = 0.1102, wR2 = 0.2318
Extinction coefficient	n/a
Largest diff. peak and hole	2.288 and -5.119 e.Å <sup>-3</sup>

## Bond lengths [Å] and angles [°] for 17

C(1)-N(1)	1.326(15)	C(7)-C(6)-C(5)	122.0(10)
C(1)-C(2)	1.393(16)	C(8)-C(7)-C(6)	119.1(10)
C(2)-C(3)	1.390(17)	C(9)-C(8)-C(7)	118.3(10)
C(3)-C(4)	1.373(18)	C(10)-C(9)-C(8)	119.1(12)
C(4)-C(5)	1.403(16)	N(2)-C(10)-C(9)	123.6(11)
C(5)-N(1)	1.353(13)	O(1)-C(11)-Re(01)	178.8(11)
C(5)-C(6)	1.485(16)	O(2)-C(12)-Re(01)	179.4(12)
C(6)-N(2)	1.357(13)	O(3)-C(13)-Re(01)	178.8(14)
C(6)-C(7)	1.388(14)	O(4)-C(14)-O(5)	116.9(10)
C(7)-C(8)	1.381(17)	O(4)-C(14)-C(15)	123.0(10)
C(8)-C(9)	1.381(17)	O(5)-C(14)-C(15)	120.0(11)
C(9)-C(10)	1.375(15)	O(5)-C(16)-C(17)	106.5(10)
C(10)-N(2)	1.307(15)	F(3)-C(18)-F(2)	109.8(12)
C(11)-O(1)	1.139(15)	F(3)-C(18)-F(1)	106.7(12)
C(11)-Re(01)	1.959(12)	F(2)-C(18)-F(1)	105.6(11)
C(12)-O(2)	1.152(16)	F(3)-C(18)-S(1)	111.7(10)
C(12)-Re(01)	1.920(15)	F(2)-C(18)-S(1)	111.8(11)
C(13)-O(3)	1.104(15)	F(1)-C(18)-S(1)	111.1(9)
C(13)-Re(01)	1.952(13)	C(20)-C(19)-O(9)	103.6(12)
C(14)-O(4)	1.278(15)	C(21)-C(20)-C(19)	105.0(12)
C(14)-O(5)	1.333(13)	C(20)-C(21)-C(22)	109.2(12)
C(14)-C(15)	1.500(15)	C(21)-C(22)-O(9)x	109.2(12)
C(16)-O(5)	1.431(14)	C(1)-N(1)-C(5)	119.1(9)
C(16)-C(17)	1.510(18)	C(1)-N(1)-Re(01)	123.9(7)
C(18)-F(3)	1.313(17)	C(5)-N(1)-Re(01)	116.9(7)
C(18)-F(2)	1.317(16)	C(10)-N(2)-C(6)	118.2(9)
C(18)-F(1)	1.341(14)	C(10)-N(2)-Re(01)	125.4(7)
C(18)-S(1)	1.811(15)	C(6)-N(2)-Re(01)	116.4(7)
C(19)-C(20)	1.449(19)	C(14)-O(4)-Re(01)	130.2(8)
C(19)-O(9)	1.57(2)	C(14)-O(5)-C(16)	121.3(9)
C(20)-C(21)	1.44(2)	C(22)-O(9)-C(19)	100.5(13)
C(21)-C(22)	1.45(2)	O(6)-S(1)-O(8)	117.1(6)
C(22)-O(9)	1.53(2)	O(6)-S(1)-O(7)	114.5(6)
N(1)-Re(01)	2.186(8)	O(8)-S(1)-O(7)	113.4(6)
N(2)-Re(01)	2.183(8)	O(6)-S(1)-C(18)	103.9(6)
O(4)-Re(01)	2.181(9)	O(8)-S(1)-C(18)	102.8(6)
O(6)-S(1)	1.433(10)	O(7)-S(1)-C(18)	102.7(7)
O(7)-S(1)	1.451(10)	C(12)-Re(01)-C(13)	89.1(5)
O(8)-S(1)	1.440(8)	C(12)-Re(01)-C(11)	88.6(5)
	123.1(11)	C(13)-Re(01)-C(11)	90.1(5)
N(1)-C(1)-C(2)	118.4(11)	N(2)-C(6)-C(5)	116.2(9)
C(3)-C(2)-C(1)	118.8(11)	C(11)-Re(01)-N(1)	92.1(4)
C(4)-C(3)-C(2)	120.0(10)	O(4)-Re(01)-N(1)	85.4(4)
C(3)-C(4)-C(5)	120.6(10)	N(2)-Re(01)-N(1)	75.1(3)
N(1)-C(5)-C(4)	115.3(9)	C(13)-Re(01)-N(1)	172.2(4)
N(1)-C(5)-C(6)	124.1(10)		
C(4)-C(5)-C(6)	121.7(10)		
N(2)-C(6)-C(7)			

Bond angles [°] for 17	
C(12)-Re(01)-N(2)	172.8(4)
C(13)-Re(01)-N(2)	97.3(5)
C(11)-Re(01)-N(2)	94.6(4)
O(4)-Re(01)-N(2)	81.8(3)
C(12)-Re(01)-N(1)	98.4(4)
C(12)-Re(01)-O(4)	94.7(4)
C(13)-Re(01)-O(4)	91.9(5)
C(11)-Re(01)-O(4)	176.1(4)

#### 6.6.4 Data for 20



Following a modified literature method,<sup>111</sup>  $\text{Mn}(\text{ClO}_4)_2 \cdot 6\text{H}_2\text{O}$  (362 mg, 1mmol), Et-saoH<sub>2</sub> (165 mg, 1mmol) (**18**) and  $\text{NEt}_3$  (101 mg, 1mmol) in MeOH (25 ml) was allowed to stir for 45 minutes at RT. The resulting dark green solution 4-bromomethyl pyridine hydrobromide (196 mg, 1 mmol) was added followed by filtration. The solution was left not moved to slowly evaporate at room temperature. Black colour blocks were separated from the solvent and a suitable crystal was selected and mounted on a glass fibre using perfluoropolyether oil. Colour code: Mn(III) (purple), O (red), N (blue) C (grey)

Crystal data and structure refinement for 20

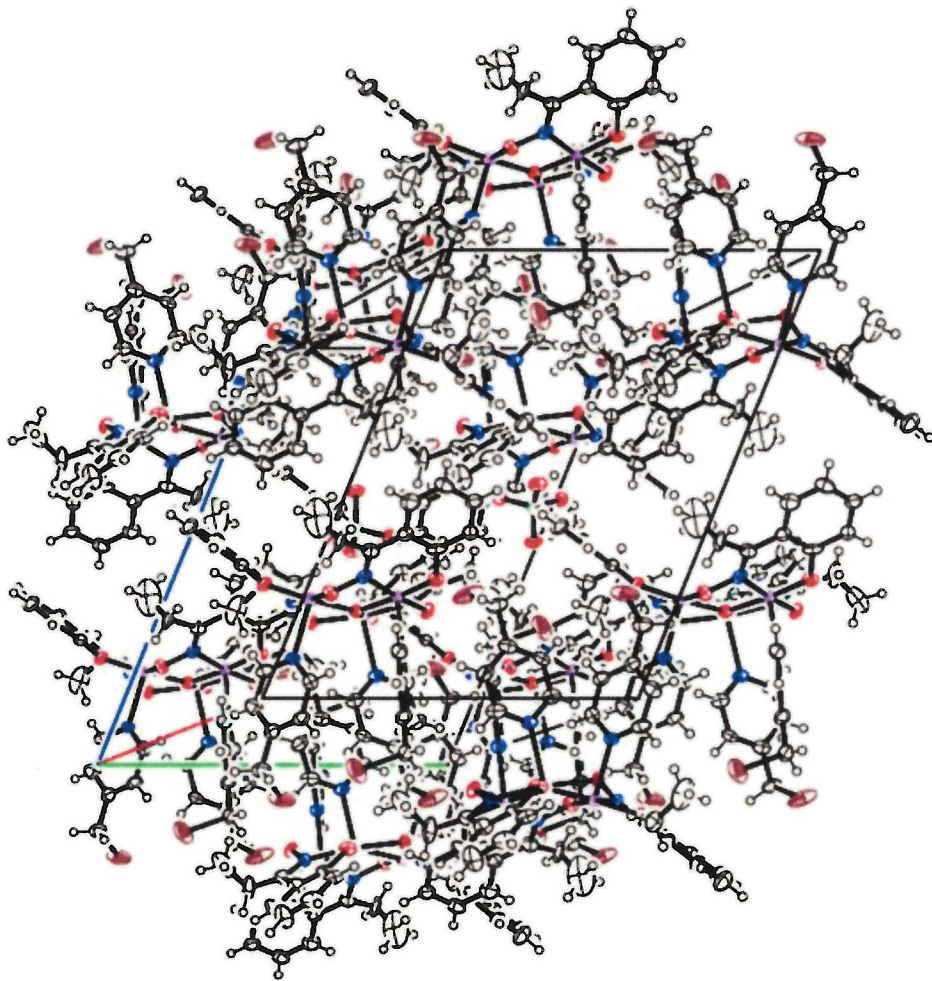
Identification code	sj19_12
Empirical formula	C45 H45 Br3 Cl Mn3 N6 O11
Formula weight	1285.87
Temperature	293(2) K
Wavelength	0.71073 Å
Crystal system	Triclinic
Space group	P-1
Unit cell dimensions	
a =	13.549(2) Å
b =	13.772(2) Å
c =	17.630(3) Å
α =	67.848(11)°.
β =	67.626(11)°.
γ =	60.228(11)°.
Volume	2567.2(7) Å <sup>3</sup>
Z	2
Density (calculated)	1.664 Mg/m <sup>3</sup>
Absorption coefficient	3.175 mm <sup>-1</sup>
F(000)	1284
Crystal size	0.2 x 0.2 x 0.2 mm <sup>3</sup>
Theta range for data collection	2.57 to 34.84°.
Index ranges	-19<=h<=21, -20<=k<=22, 0<=l<=28
Reflections collected	21160
Independent reflections	21160 [R(int) = 0.0000]
Completeness to theta =	34.84° 94.7 %
Refinement method	Full-matrix least-squares on F <sup>2</sup>
Data / restraints / parameters	21160 / 0 / 617
Goodness-of-fit on F <sup>2</sup>	0.545
Final R indices [I>2sigma(I)]	R1 = 0.0591, wR2 = 0.1069
R indices (all data)	R1 = 0.2893, wR2 = 0.1521
Largest diff. peak and hole	0.906 and -0.872 e.Å <sup>-3</sup>

Bond lengths [Å] for 20			
C(1)-N(1)	1.308(8)	C(39)-Br(2)	1.924(7)
C(1)-C(2)	1.462(9)	C(40)-N(6)	1.321(9)
C(1)-C(8)	1.499(9)	C(40)-C(41)	1.395(10)
C(2)-C(3)	1.421(9)	C(41)-C(42)	1.384(9)
C(2)-C(7)	1.426(9)	C(42)-C(43)	1.384(10)
C(3)-O(2)	1.337(7)	C(42)-C(45)	1.478(10)
C(3)-C(4)	1.401(9)	C(43)-C(44)	1.381(9)
C(4)-C(5)	1.375(9)	C(44)-N(6)	1.323(8)
C(5)-C(6)	1.373(10)	C(45)-Br(3)	1.923(7)
C(6)-C(7)	1.379(10)	N(1)-O(3)	1.354(6)
C(8)-C(9)	1.428(12)	N(1)-Mn(9)	1.989(5)
C(10)-N(2)	1.297(8)	N(2)-O(5)	1.386(7)
C(10)-C(11)	1.420(10)	N(2)-Mn(8)	1.994(5)
C(10)-C(17)	1.591(12)	N(3)-O(7)	1.385(6)
C(11)-C(16)	1.406(10)	N(3)-Mn(10)	1.987(6)
C(11)-C(12)	1.409(9)	N(4)-Mn(10)	2.292(5)
C(12)-O(4)	1.328(7)	N(5)-Mn(8)	2.287(5)
C(12)-C(13)	1.405(10)	N(6)-Mn(9)	2.300(5)
C(13)-C(14)	1.381(9)	Mn(8)-O(4)	1.856(5)
C(14)-C(15)	1.361(10)	Mn(8)-O(1)	1.887(4)
C(15)-C(16)	1.387(11)	Mn(8)-O(7)	1.913(4)
C(17)-C(18)	1.318(15)	Mn(8)-O(9)	2.519(4)
C(19)-N(3)	1.305(9)		
C(19)-C(26)	1.494(11)	Mn(8)-Mn(10)	3.2362(15)
C(19)-C(20)	1.495(9)	Mn(9)-O(2)	1.858(4)
C(20)-C(21)	1.350(10)	Mn(9)-O(1)	1.884(4)
C(20)-C(25)	1.427(10)	Mn(9)-O(5)	1.918(4)
C(21)-O(6)	1.370(8)	Mn(9)-O(10)	2.505(4)
C(21)-C(22)	1.406(8)	Mn(9)-Mn(10)	3.2343(15)
C(22)-C(23)	1.376(10)	Mn(10)-O(6)	1.864(4)
C(23)-C(24)	1.378(12)	Mn(10)-O(1)	1.896(4)
C(24)-C(25)	1.399(10)	Mn(10)-O(3)	1.927(4)
C(26)-C(27)	1.431(12)	Mn(10)-O(11)	2.515(4)
C(28)-N(4)	1.335(8)	O(8)-Cl(1)	1.426(4)
C(28)-C(29)	1.383(9)	O(9)-Cl(1)	1.459(5)
C(29)-C(30)	1.377(9)	O(10)-Cl(1)	1.453(4)
C(30)-C(31)	1.364(10)	O(11)-Cl(1)	1.451(5)
C(30)-C(33)	1.492(9)	C(36)-C(39)	1.499(9)
C(31)-C(32)	1.386(9)	C(37)-C(38)	1.397(9)
C(32)-N(4)	1.335(8)	C(38)-N(5)	1.329(8)
C(33)-Br(1)	1.916(7)		
C(34)-N(5)	1.328(8)		
C(34)-C(35)	1.408(9)		
C(35)-C(36)	1.348(9)		
C(36)-C(37)	1.375(9)		

## Bond angles [°] for 20

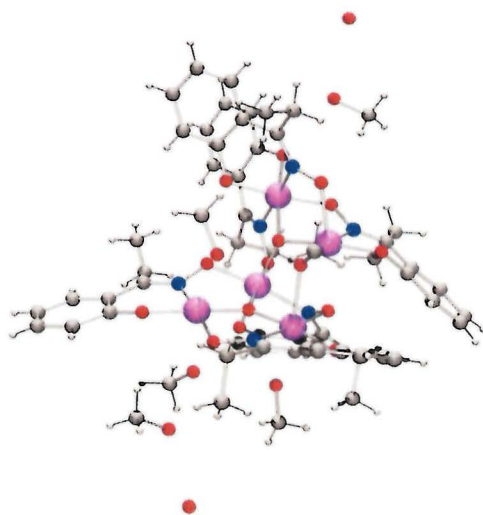
N(1)-C(1)-C(2)	119.3(6)	C(30)-C(31)-C(32)	121.0(7)
N(1)-C(1)-C(8)	120.1(6)	N(4)-C(32)-C(31)	110.5(5)
C(2)-C(1)-C(8)	120.5(6)	C(30)-C(33)-Br(1)	110.5(5)
C(3)-C(2)-C(7)	117.3(6)	N(5)-C(34)-C(35)	123.1(6)
C(3)-C(2)-C(1)	122.9(6)	C(36)-C(35)-C(34)	119.8(6)
C(7)-C(2)-C(1)	119.4(6)	C(35)-C(36)-C(37)	118.0(6)
O(2)-C(3)-C(4)	116.5(6)	C(35)-C(36)-C(39)	123.0(7)
O(2)-C(3)-C(2)	124.1(6)	C(37)-C(36)-C(39)	119.0(7)
C(4)-C(3)-C(2)	119.4(6)	C(36)-C(37)-C(38)	119.1(6)
C(5)-C(4)-C(3)	121.0(7)	N(5)-C(38)-C(37)	123.5(6)
C(6)-C(5)-C(4)	121.0(7)	C(36)-C(39)-Br(2)	110.7(5)
C(5)-C(6)-C(7)	119.6(7)	N(6)-C(40)-C(41)	122.6(6)
C(6)-C(7)-C(2)	121.7(7)	C(42)-C(41)-C(40)	119.9(7)
C(9)-C(8)-C(1)	109.2(7)	C(43)-C(42)-C(41)	116.4(7)
N(2)-C(10)-C(11)	120.8(6)	C(41)-C(42)-C(45)	123.2(7)
N(2)-C(10)-C(17)	119.9(7)	C(44)-C(43)-C(42)	120.1(6)
C(11)-C(10)-C(17)	119.0(6)	N(6)-C(44)-C(43)	123.1(6)
C(16)-C(11)-C(12)	117.5(7)	C(42)-C(45)-Br(3)	111.9(5)
C(16)-C(11)-C(10)	120.1(7)	(1)-N(1)-O(3)	115.8(5)
C(12)-C(11)-C(10)	122.3(6)	C(1)-N(1)-Mn(9)	129.3(4)
O(4)-C(12)-C(13)	116.4(6)	O(3)-N(1)-Mn(9)	114.8(3)
O(4)-C(12)-C(11)	124.5(7)	C(10)-N(2)-O(5)	117.4(5)
C(13)-C(12)-C(11)	119.1(6)	C(10)-N(2)-Mn(8)	129.3(5)
C(14)-C(13)-C(12)	121.1(7)	O(5)-N(2)-Mn(8)	113.4(4)
C(15)-C(14)-C(13)	120.6(8)	C(19)-N(3)-O(7)	115.1(5)
C(14)-C(15)-C(16)	119.2(7)	C(19)-N(3)-Mn(10)	130.8(5)
C(15)-C(16)-C(11)	122.4(7)	O(7)-N(3)-Mn(10)	114.0(4)
C(18)-C(17)-C(10)	104.0(11)	C(28)-N(4)-C(32)	117.2(6)
N(3)-C(19)-C(26)	120.3(6)	C(28)-N(4)-Mn(10)	123.1(4)
N(3)-C(19)-C(20)	115.7(7)	C(34)-N(5)-C(38)	116.4(6)
C(26)-C(19)-C(20)	124.0(7)	C(34)-N(5)-Mn(8)	119.5(4)
C(21)-C(20)-C(25)	117.4(6)	C(38)-N(5)-Mn(8)	123.9(4)
C(21)-C(20)-C(19)	125.8(6)	C(40)-N(6)-C(44)	117.9(6)
C(25)-C(20)-C(19)	116.4(7)	C(40)-N(6)-Mn(9)	118.7(4)
C(20)-C(21)-O(6)	123.5(6)	C(44)-N(6)-Mn(9)	123.4(5)
C(20)-C(21)-C(22)	122.9(6)	O(4)-Mn(8)-O(1)	175.56(18)
O(6)-C(21)-C(22)	113.6(6)	O(4)-Mn(8)-O(7)	91.98(19)
C(23)-C(22)-C(21)	119.6(7)	O(1)-Mn(8)-O(7)	90.29(18)
C(22)-C(23)-C(24)	119.2(7)	O(4)-Mn(8)-N(2)	88.1(2)
C(23)-C(24)-C(25)	121.0(7)	O(1)-Mn(8)-N(2)	89.2(2)
C(24)-C(25)-C(20)	119.8(8)	O(7)-Mn(8)-N(2)	173.2(2)
C(27)-C(26)-C(19)	105.0(8)	O(4)-Mn(8)-N(5)	88.44(19)
N(4)-C(28)-C(29)	122.7(7)	O(1)-Mn(8)-N(5)	95.13(19)
C(30)-C(29)-C(28)	120.3(7)	O(7)-Mn(8)-N(5)	95.63(18)
C(31)-C(30)-C(29)	116.5(6)	N(2)-Mn(8)-N(5)	91.1(2)
C(31)-C(30)-C(33)	121.7(7)	O(4)-Mn(8)-O(9)	90.60(17)
C(29)-C(30)-C(33)	121.8(7)	O(1)-Mn(8)-O(9)	85.66(16)

Bond angles [°] for 20			
O(7)-Mn(8)-O(9)	88.26(16)	O(3)-Mn(10)-Mn(9)	60.58(12)
N(2)-Mn(8)-O(9)	84.96(18)	N(3)-Mn(10)-Mn(9)	116.71(17)
N(5)-Mn(8)-O(9)	176.02(17)	N(4)-Mn(10)-Mn(9)	107.05(14)
O(4)-Mn(8)-Mn(10)	149.38(14)	O(11)-Mn(10)-Mn(9)	75.88(10)
O(1)-Mn(8)-Mn(10)	31.27(12)	O(6)-Mn(10)-Mn(8)	146.21(16)
O(7)-Mn(8)-Mn(10)	60.85(13)	O(1)-Mn(10)-Mn(8)	31.10(13)
N(2)-Mn(8)-Mn(10)	117.10(18)	O(3)-Mn(10)-Mn(8)	120.46(13)
N(5)-Mn(8)-Mn(10)	106.89(14)	N(3)-Mn(10)-Mn(8)	58.11(16)
O(9)-Mn(8)-Mn(10)	75.74(11)	N(4)-Mn(10)-Mn(8)	95.52(13)
O(2)-Mn(9)-O(1)	175.42(18)	O(11)-Mn(10)-Mn(8)	83.11(10)
O(2)-Mn(9)-O(5)	92.23(19)	Mn(9)-Mn(10)-Mn(8)	60.13(3)
O(1)-Mv(9)-O(5)	89.39(18)	Mn(9)-O(1)-Mn(8)	118.6(2)
O(2)-Mv(9)-N(1)	88.9(2)	Mn(9)-O(1)-Mn(10)	117.7(2)
O(1)-Mv(9)-N(1)	89.00(19)	Mn(8)-O(1)-Mn(10)	117.6(2)
O(5)-Mv(9)-N(1)	173.3(2)	C(3)-O(2)-Mn(9)	127.0(4)
O(2)-Mv(9)-N(6)	89.47(19)	N(1)-O(3)-Mn(10)	112.6(3)
O(1)-Mv(9)-N(6)	94.64(18)	C(12)-O(4)-Mn(8)	126.6(4)
O(5)-Mn(9)-N(6)	95.44(19)	N(2)-O(5)-Mn(9)	113.6(3)
N(1)-Mn(9)-N(6)	91.2(2)	C(21)-O(6)-Mn(10)	125.2(4)
O(2)-Mn(9)-O(10)	89.45(17)	N(3)-O(7)-Mn(8)	112.7(3)
O(1)-Mn(9)-O(10)	86.29(16)	Cl(1)-O(9)-Mn(8)	120.2(3)
O(5)-Mn(9)-O(10)	89.16(17)	Cl(1)-O(10)-Mn(9)	120.0(2)
N(1)-Mn(9)-O(10)	84.23(18)	Cl(1)-O(11)-Mn(10)	119.9(2)
N(6)-Mn(9)-O(10)	175.31(18)	O(8)-Cl(1)-O(11)	109.7(3)
O(2)-Mn(9)-Mn(10)	146.28(14)	O(8)-Cl(1)-O(10)	109.9(3)
O(1)-Mn(9)-Mn(10)	31.27(12)	O(11)-Cl(1)-O(10)	109.0(3)
O(5)-Mn(9)-Mn(10)	120.29(14)	O(8)-Cl(1)-O(9)	109.8(3)
N(1)-Mn(9)-Mn(10)	57.75(14)	O(11)-Cl(1)-O(9)	109.0(3)
N(6)-Mn(9)-Mn(10)	95.53(13)	O(10)-Cl(1)-O(9)	109.4(3)
O(10)-Mn(9)-Mn(10)	82.87(10)		
O(6)-Mn(10)-O(1)	176.2(2)		
O(6)-Mn(10)-O(3)	92.3(2)		
O(1)-Mn(10)-O(3)	89.77(18)		
O(6)-Mn(10)-N(3)	88.3(2)		
O(1)-Mn(10)-N(3)	89.2(2)		
O(3)-Mn(10)-N(3)	172.3(2)		
O(6)-Mn(10)-N(4)	88.05(18)		
O(1)-Mn(10)-N(4)	94.92(18)		
O(3)-Mn(10)-N(4)	96.35(19)		
N(3)-Mn(10)-N(4)	91.3(2)		
O(6)-Mn(10)-O(11)	90.81(16)		
O(1)-Mn(10)-O(11)	86.05(15)		
O(3)-Mn(10)-O(11)	87.88(17)		
N(3)-Mn(10)-O(11)	84.44(19)		
N(4)-Mn(10)-O(11)	175.65(19)		
O(6)-Mn(10)-Mn(9)	149.69(15)		
O(1)-Mn(10)-Mn(9)	31.05(13)		



Triclinic unit cell for 20

### 6.6.5 Data for 21



**21**

According to a literature procedure,<sup>111</sup> Mn(ClO<sub>4</sub>)<sub>2</sub>·6H<sub>2</sub>O (362 mg, 1mmol), Et-saoH<sub>2</sub> (165 mg, 1mmol) (**18**) and NEt<sub>3</sub> (101 mg, 1mmol) in MeOH (25 ml) was allowed to stir for 45 minutes at RT. The resulting dark green solution 4-chloromethyl pyrimidine (200 mg, 1mmol ) was added followed by paper filtration. The solution was left undisturbed to slowly evaporate at room temperature. Black colour blocks were separated from the solvent and a suitable crystal was selected and mounted on a glass fibre using perfluoropolyether oil. Colour code: Mn(III) (purple), O (red), N (blue) C (grey).

Crystal data and structure refinement for 21	
Identification code	shelxl
Empirical formula	C60 H72 Mn5 N6 O21
Formula weight	1487.94
Temperature	150(2) K
Wavelength	0.71073 Å
Crystal system Space group	Triclinic
Unit cell dimensions	P-1
a =	
b =	11.5555(14) Å
c =	16.412(3) Å
$\alpha$ =	18.419(3) Å
B =	99.688(12)°
$\gamma$ =	95.415(11)°
Volume	103.037(11)°
Z	3322.6(8) Å <sup>3</sup>
Density (calculated)	2
Absorption coefficient	1.487 Mg/m <sup>3</sup>
F(000)	1.001 mm <sup>-1</sup>
Crystal size	1534
Theta range for data collection	? x ? x ? mm <sup>3</sup>
Index ranges	1.83 to 29.54°
Reflections collected	- 15<=h<=15, -22<=k<=22, -22<=l<=25
Independent reflections	28779
Completeness to theta =	15834 [R(int) = 0.0911]
Refinement method	29.54° 85.2 %
Data / restraints / parameters	Full-matrix least-squares on F <sup>2</sup>
Goodness-of-fit on F <sup>2</sup>	15834 / 0 / 870
Final R indices [I>2sigma(I)]	0.621
R indices (all data)	R1 = 0.0455, wR2 = 0.0927
Largest diff. peak and hole	R1 = 0.1475, wR2 = 0.1199 0.704 and -0.774 e.Å <sup>-3</sup>

## Bond lengths [Å] and angles [°] for 21

C(1)-N(1)	1.304(6)	C(41)-C(42)	1.383(8)
C(1)-C(2)	1.462(7)	C(43)-N(5)	1.286(6)
C(1)-C(8)	1.511(7)	C(43)-C(44)	1.518(7)
C(2)-C(7)	1.411(7)	C(44)-C(45)	1.516(8)
C(2)-C(3)	1.421(7)	C(46)-N(6)	1.304(6)
C(3)-O(8)	1.347(6)	C(46)-C(47)	1.453(7)
C(3)-C(4)	1.379(6)	C(46)-C(53)	1.494(6)
C(4)-C(5)	1.404(7)	C(47)-C(52)	1.408(7)
C(5)-C(6)	1.364(8)	C(47)-C(48)	1.426(6)
C(6)-C(7)	1.364(7)	C(48)-O(14)	1.338(6)
C(8)-C(9)	1.509(7)	C(48)-C(49)	1.375(7)
C(10)-N(2)	1.304(6)	C(49)-C(50)	1.377(7)
C(10)-C(11)	1.456(7)	C(50)-C(51)	1.381(7)
C(10)-C(17)	1.504(7)	C(51)-C(52)	1.385(7)
C(11)-C(16)	1.411(7)	C(53)-C(54)	1.517(7)
C(11)-C(12)	1.423(7)	C(55)-O(15)	1.441(5)
C(12)-O(4)	1.327(5)	C(56)-O(16)	1.444(6)
C(12)-C(13)	1.396(7)	C(57)-O(17)	1.426(6)
C(13)-C(14)	1.393(7)	C(58)-O(18)	1.383(8)
C(14)-C(15)	1.386(8)	C(59)-O(19)	1.405(11)
C(15)-C(16)	1.382(8)	C(60)-O(20)	1.435(8)
C(17)-C(18)	1.511(7)	N(1)-O(3)	1.379(5)
C(20)-C(25)	1.390(7)	N(1)-Mn(1)	1.979(4)
C(20)-C(21)	1.440(7)	N(2)-O(5)	1.369(5)
C(20)-C(19)	1.462(7)	N(2)-Mn(2)	2.022(4)
C(21)-O(6)	1.309(6)	N(3)-C(19)	1.300(6)
C(21)-C(22)	1.415(7)	N(3)-O(7)	1.377(4)
C(22)-C(23)	1.369(8)	N(3)-Mn(3)	1.994(4)
C(23)-C(24)	1.385(8)	N(4)-O(9)	1.360(5)
C(24)-C(25)	1.376(7)	N(4)-Mn(5)	2.007(4)
C(28)-N(4)	1.281(6)	N(5)-O(12)	1.348(5)
C(28)-C(29)	1.477(7)	N(5)-Mn(5)	1.986(4)
C(28)-C(35)	1.503(7)	N(6)-O(13)	1.368(5)
C(29)-C(34)	1.406(8)	N(6)-Mn(4)	1.975(4)
C(29)-C(30)	1.415(7)	Mn(1)-O(1)	1.877(3)
C(30)-O(11)	1.347(6)	Mn(1)-O(7)	1.888(3)
C(30)-C(31)	1.370(7)	Mn(1)-O(9)	1.893(3)
C(31)-C(32)	1.347(7)	Mn(1)-O(8)	1.894(3)
C(32)-C(33)	1.396(7)	Mn(1)-O(2)	1.902(3)
C(33)-C(34)	1.363(7)	Mn(1)-Mn(3)	3.2399(10)
C(35)-C(36)	1.500(9)	Mn(2)-O(4)	1.855(4)
C(37)-C(42)	1.408(7)	Mn(2)-O(1)	1.900(3)
C(37)-C(38)	1.417(6)	Mn(2)-O(3)	1.978(3)
C(37)-C(43)	1.462(7)	Mn(2)-O(15)	2.211(3)
C(38)-O(10)	1.337(6)	Mn(2)-O(17)	2.292(3)
C(38)-C(39)	1.405(7)	Mn(2)-Mn(4)	3.2107(11)
C(39)-C(40)	1.378(7)	Mn(3)-O(6)	1.861(3)
C(40)-C(41)	1.379(7)	Mn(3)-O(1)	1.875(3)

Bond angles [°] for 21			
N(1)-C(1)-C(2)	117.3(5)	C(31)-C(32)-C(33)	119.6(5)
N(1)-C(1)-C(8)	122.3(4)	C(34)-C(33)-C(32)	122.5(5)
C(2)-C(1)-C(8)	120.1(4)	C(33)-C(34)-C(29)	122.5(5)
C(7)-C(2)-C(3)	117.2(5)	C(36)-C(35)-C(28)	111.5(5)
C(7)-C(2)-C(1)	121.6(5)	C(42)-C(37)-C(38)	116.9(4)
C(3)-C(2)-C(1)	121.0(4)	C(42)-C(37)-C(43)	121.6(4)
O(8)-C(3)-C(4)	118.9(5)	C(38)-C(37)-C(43)	121.2(4)
O(8)-C(3)-C(2)	120.3(4)	O(10)-C(38)-C(39)	117.8(4)
C(4)-C(3)-C(2)	120.8(4)	O(10)-C(38)-C(37)	121.8(4)
C(3)-C(4)-C(5)	119.2(5)	C(39)-C(38)-C(37)	120.4(5)
C(6)-C(5)-C(4)	121.0(5)	C(40)-C(39)-C(38)	120.6(5)
C(5)-C(6)-C(7)	120.1(5)	C(39)-C(40)-C(41)	119.9(5)
C(6)-C(7)-C(2)	121.6(5)	C(40)-C(41)-C(42)	120.3(5)
C(9)-C(8)-C(1)	112.6(4)	C(41)-C(42)-C(37)	121.9(5)
N(2)-C(10)-C(11)	120.6(4)	N(5)-C(43)-C(37)	120.3(4)
N(2)-C(10)-C(17)	118.5(5)	N(5)-C(43)-C(44)	119.9(4)
C(11)-C(10)-C(17)	120.9(4)	C(37)-C(43)-C(44)	119.7(4)
C(16)-C(11)-C(12)	117.1(5)	C(45)-C(44)-C(43)	112.8(4)
C(16)-C(11)-C(10)	119.8(5)	N(6)-C(46)-C(47)	118.2(4)
C(12)-C(11)-C(10)	123.0(4)	N(6)-C(46)-C(53)	118.9(4)
O(4)-C(12)-C(13)	117.5(4)	C(46)-C(53)-C(54)	110.3(4)
O(4)-C(12)-C(11)	123.3(5)	C(1)-N(1)-O(3)	119.0(4)
C(13)-C(12)-C(11)	119.2(4)	C(1)-N(1)-Mn(1)	127.5(3)
C(14)-C(13)-C(12)	121.8(5)	O(3)-N(1)-Mn(1)	112.9(3)
C(15)-C(14)-C(13)	119.8(5)	C(10)-N(2)-O(5)	117.0(4)
C(16)-C(15)-C(14)	118.9(5)	C(10)-N(2)-Mn(2)	128.2(3)
C(15)-C(16)-C(11)	123.2(5)	O(5)-N(2)-Mn(2)	114.8(2)
C(10)-C(17)-C(18)	112.0(4)	C(19)-N(3)-O(7)	114.7(4)
C(25)-C(20)-C(21)	119.4(4)	C(19)-N(3)-Mn(3)	130.5(3)
C(25)-C(20)-C(19)	119.5(5)	O(7)-N(3)-Mn(3)	114.8(3)
C(21)-C(20)-C(19)	121.0(5)	C(28)-N(4)-O(9)	116.0(4)
O(6)-C(21)-C(22)	118.0(5)	C(28)-N(4)-Mn(5)	129.5(4)
O(6)-C(21)-C(20)	125.4(4)	O(9)-N(4)-Mn(5)	114.3(3)
C(22)-C(21)-C(20)	116.6(5)	C(43)-N(5)-O(12)	120.3(4)
C(23)-C(22)-C(21)	121.6(5)	C(43)-N(5)-Mn(5)	124.1(3)
C(22)-C(23)-C(24)	121.6(5)	O(12)-N(5)-Mn(5)	115.5(3)
C(22)-C(23)-C(24)	121.6(5)	C(46)-N(6)-O(13)	117.2(4)
C(25)-C(24)-C(23)	118.3(5)	C(46)-N(6)-Mn(4)	128.6(3)
C(24)-C(25)-C(20)	122.5(5)	O(13)-N(6)-Mn(4)	114.2(3)
N(4)-C(28)-C(29)	118.8(5)	O(1)-Mn(1)-O(7)	91.00(13)
N(4)-C(28)-C(35)	119.1(5)	O(1)-Mn(1)-O(9)	177.62(15)
C(29)-C(28)-C(35)	122.0(4)	O(7)-Mn(1)-O(9)	91.36(14)
C(34)-C(29)-C(30)	116.8(5)	O(1)-Mn(1)-O(8)	92.74(13)
C(34)-C(29)-C(28)	119.9(5)	O(7)-Mn(1)-O(8)	91.97(15)
C(30)-C(29)-C(28)	123.3(5)	O(9)-Mn(1)-O(8)	86.84(13)
O(11)-C(30)-C(31)	119.6(5)	O(1)-Mn(1)-O(2)	91.46(13)
O(11)-C(30)-C(29)	121.1(4)	O(7)-Mn(1)-O(2)	90.39(14)
C(31)-C(30)-C(29)	119.3(5)	O(9)-Mn(1)-O(2)	88.86(12)

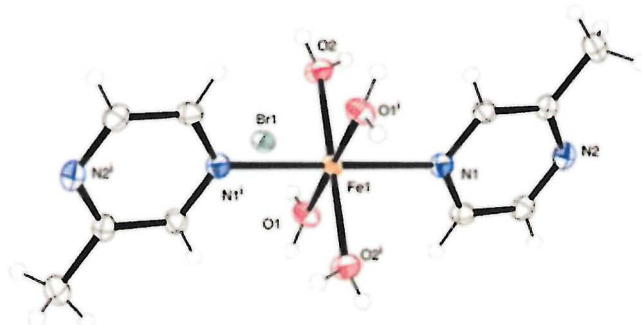
## Bond angles [°] for 21

O(7)-Mn(1)-N(1)	174.64(14)	O(5)-Mn(3)-Mn(1)	121.87(10)
O(9)-Mn(1)-N(1)	92.86(14)	N(3)-Mn(3)-Mn(1)	58.68(11)
O(8)-Mn(1)-N(1)	84.96(16)	O(16)-Mn(3)-Mn(1)	85.16(9)
O(2)-Mn(1)-N(1)	93.00(15)	O(18)-Mn(3)-Mn(1)	85.67(11)
O(1)-Mn(1)-Mn(3)	30.28(10)	O(14)-Mn(4)-O(15)	94.62(14)
O(7)-Mn(1)-Mn(3)	61.23(9)	O(14)-Mn(4)-O(2)	168.69(14)
O(9)-Mn(1)-Mn(3)	151.98(11)	O(15)-Mn(4)-O(2)	90.90(13)
O(8)-Mn(1)-Mn(3)	88.31(9)	O(14)-Mn(4)-N(6)	87.94(15)
O(2)-Mn(1)-Mn(3)	96.54(9)	O(15)-Mn(4)-N(6)	170.71(15)
N(1)-Mn(1)-Mn(3)	114.18(10)	O(2)-Mn(4)-N(6)	85.12(14)
O(4)-Mn(2)-O(1)	173.50(15)	O(14)-Mn(4)-O(12)	100.49(13)
O(4)-Mn(2)-O(3)	94.08(14)	O(15)-Mn(4)-O(12)	99.28(13)
O(1)-Mn(2)-O(3)	87.74(13)	O(2)-Mn(4)-O(12)	88.32(13)
O(4)-Mn(2)-N(2)	88.56(15)	N(6)-Mn(4)-O(12)	89.01(14)
O(1)-Mn(2)-N(2)	90.07(15)	O(14)-Mn(4)-O(3)	86.40(13)
O(3)-Mn(2)-N(2)	175.35(16)	O(15)-Mn(4)-O(3)	79.93(12)
O(4)-Mn(2)-O(15)	98.42(14)	O(2)-Mn(4)-O(3)	84.86(12)
O(1)-Mn(2)-O(15)	87.97(13)	N(6)-Mn(4)-O(3)	91.34(14)
O(3)-Mn(2)-O(15)	84.23(12)	O(12)-Mn(4)-O(3)	173.11(12)
N(2)-Mn(2)-O(15)	91.60(14)	O(15)-Mn(4)-Mn(5)	117.05(11)
O(4)-Mn(2)-O(17)	92.92(15)	O(2)-Mn(4)-Mn(5)	35.20(9)
O(1)-Mn(2)-O(17)	80.73(14)	N(6)-Mn(4)-Mn(5)	63.17(12)
O(3)-Mn(2)-O(17)	93.68(13)	O(12)-Mn(4)-Mn(5)	62.62(9)
N(2)-Mn(2)-O(17)	90.01(14)	O(3)-Mn(4)-Mn(5)	111.54(8)
O(15)-Mn(2)-O(17)	168.58(14)	O(14)-Mn(4)-Mn(2)	94.94(10)
O(4)-Mn(2)-Mn(4)	103.54(10)	O(15)-Mn(4)-Mn(2)	42.41(9)
O(1)-Mn(2)-Mn(4)	82.33(9)	O(2)-Mn(4)-Mn(2)	82.50(9)
O(3)-Mn(2)-Mn(4)	48.73(10)	N(6)-Mn(4)-Mn(2)	128.52(11)
N(2)-Mn(2)-Mn(4)	126.88(12)	O(12)-Mn(4)-Mn(2)	139.97(9)
O(15)-Mn(2)-Mn(4)	35.95(8)	O(3)-Mn(4)-Mn(2)	37.95(7)
O(17)-Mn(2)-Mn(4)	139.21(9)	Mn(5)-Mn(4)-Mn(2)	117.68(3)
O(6)-Mn(3)-O(1)	175.81(15)	O(10)-Mn(5)-O(11)	89.81(14)
O(6)-Mn(3)-O(5)	90.58(14)	O(10)-Mn(5)-O(2)	97.99(13)
O(1)-Mn(3)-O(5)	91.60(14)	O(11)-Mn(5)-O(2)	170.90(14)
O(6)-Mn(3)-N(3)	88.55(16)	O(10)-Mn(5)-O(13)	173.26(14)
O(1)-Mn(3)-N(3)	88.90(15)	O(11)-Mn(5)-O(13)	83.63(14)
O(5)-Mn(3)-N(3)	173.86(16)	O(2)-Mn(5)-O(13)	88.67(13)
O(6)-Mn(3)-O(16)	100.15(14)	O(10)-Mn(5)-N(5)	86.53(15)
O(1)-Mn(3)-O(16)	83.40(13)	O(11)-Mn(5)-N(5)	96.88(14)
O(5)-Mn(3)-O(16)	90.83(14)	O(2)-Mn(5)-N(5)	88.30(14)
N(3)-Mn(3)-O(16)	95.30(15)	O(13)-Mn(5)-N(5)	92.69(15)
O(6)-Mn(3)-O(18)	93.80(16)	O(10)-Mn(5)-N(4)	89.51(15)
O(1)-Mn(3)-O(18)	82.86(14)	O(11)-Mn(5)-N(4)	87.01(14)
O(5)-Mn(3)-O(18)	84.26(16)	O(2)-Mn(5)-N(4)	88.38(14)
N(3)-Mn(3)-O(18)	89.73(17)	O(13)-Mn(5)-N(4)	91.70(15)
O(16)-Mn(3)-O(18)	165.27(15)	N(5)-Mn(5)-N(4)	174.43(15)
O(6)-Mn(3)-Mn(1)	147.21(11)	O(10)-Mn(5)-Mn(4)	122.00(10)
O(1)-Mn(3)-Mn(1)	30.30(10)	O(11)-Mn(5)-Mn(4)	140.62(10)

## Bond angles [°] for 21

O(2)-Mn(5)-Mn(4)	36.27(9)	Mn(5)-O(2)	1.887(3)
O(13)-Mn(5)-Mn(4)	63.41(10)	Mn(5)-O(13)	1.918(3)
N(5)-Mn(5)-Mn(4)	65.79(11)	O(21)-O(22)	11.34(2)
N(4)-Mn(5)-Mn(4)	113.39(11)	O(22)-O(21)2	1.34(2)
Mn(3)-O(1)-Mn(1)	119.43(18)	C(19)-C(26A)	1.504(18)
Mn(3)-O(1)-Mn(2)	118.62(16)	C(19)-C(26B)	1.525(13)
Mn(1)-O(1)-Mn(2)	121.06(16)	C(26A)-C(27A)	1.57(2)
Mn(5)-O(2)-Mn(1)	117.71(15)	C(26B)-C(27B)	1.506(16)
Mn(5)-O(2)-Mn(4)	108.54(13)		
Mn(1)-O(2)-Mn(4)	121.30(17)		
N(1)-O(3)-Mn(2)	111.9(2)		
N(1)-O(3)-Mn(4)	106.1(2)		
Mn(2)-O(3)-Mn(4)	93.31(13)		
C(12)-O(4)-Mn(2)	127.8(3)		
N(2)-O(5)-Mn(3)	117.4(2)		
C(21)-O(6)-Mn(3)	128.5(3)		
N(3)-O(7)-Mn(1)	116.2(3)		
C(3)-O(8)-Mn(1)	117.8(3)		
N(4)-O(9)-Mn(1)	114.1(2)		
C(38)-O(10)-Mn(5)	119.3(3)		
C(30)-O(11)-Mn(5)	123.8(3)		
N(5)-O(12)-Mn(4)	113.1(2)		
N(6)-O(13)-Mn(5)	117.8(2)		
C(48)-O(14)-Mn(4)	119.8(3)		
C(55)-O(15)-Mn(4)	116.4(3)		
C(55)-O(15)-Mn(2)	126.1(3)		
Mn(4)-O(15)-Mn(2)	101.63(13)		
C(56)-O(16)-Mn(3)	126.5(3)		
C(57)-O(17)-Mn(2)	122.2(3)		
C(58)-O(18)-Mn(3)	131.3(4)		
N(3)-C(19)-C(20)	120.4(5)		
N(3)-C(19)-C(26A)	115.7(8)		
C(20)-C(19)-C(26A)	121.6(8)		
N(3)-C(19)-C(26B)	117.9(6)		
C(20)-C(19)-C(26B)	120.6(6)		
C(26A)-C(19)-C(26B)	25.8(5)		
C(19)-C(26A)-C(27A)	104.4(13)		
C(27B)-C(26B)-C(19)	108.6(10)		
Mn(3)-O(5) 1.921(3)			
Mn(3)-O(16) 2.239(3)			
Mn(3)-O(18) 2.423(4)			
Mn(4)-O(14) 1.877(3)			
Mn(4)-O(15) 1.925(3)			
Mn(4)-O(2) 1.937(3)			
Mn(4)-O(12) 2.115(3)			
Mn(4)-O(3) 2.417(3)			
Mn(4)-Mn(5) 3.1041(11)			
Mn(5)-O(10) 1.871(3)			
Mn(5)-O(11) 1.885(3)			

### 6.6.6 Data for 22



Following to modified literature method,<sup>134</sup> FeBr<sub>3</sub> (500 mg, 3.38 mmol) was added to 2-methylpyridazine (10 ml) and stirred for 30 mins, the solution was filtered and layered with acetone producing complex [Fe(II)(H<sub>2</sub>O)<sub>4</sub>(*trans*-pyz)<sub>2</sub>(CH<sub>3</sub>)<sub>2</sub>Br] after evaporation at room temperature in 3 days as yellow crystal, and mounted on a glass fibre using perfluoropolyether oil.

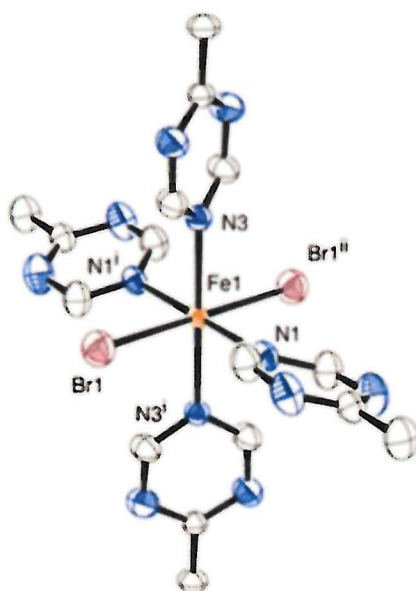
Crystal data and structure refinement for **22**

Identification code	shelx
Empirical formula	C <sub>10</sub> H <sub>20</sub> Br <sub>2</sub> Fe N <sub>4</sub> O <sub>4</sub>
Formula weight	475.97
Temperature	150(2) K
Wavelength	0.71073 Å
Crystal system	Monoclinic
Space group	P 21/c
Unit cell dimensions	
a =	8.3260(7) Å
b =	16.1146(15) Å
c =	7.1437(7) Å
α =	90°.
β =	113.455(6)°.
γ =	90°.
Volume	879.28(14) Å <sup>3</sup>
Z	2
Density (calculated)	1.798 Mg/m <sup>3</sup>
Absorption coefficient	5.419 mm <sup>-1</sup>
F(000)	472
Crystal size	0.210 × 0.200 × 0.180 mm <sup>3</sup>
Theta range for data collection	2.528 to 29.168°.
Index ranges	-9 ≤ h ≤ 11, -20 ≤ k ≤ 22, -9 ≤ l ≤ 9
Reflections collected	6695
Independent reflections	2364 [R(int) = 0.0347]
Completeness to theta =	25.242° 99.8 %
Refinement method	Full-matrix least-squares on F <sup>2</sup>
Data / restraints / parameters	2364 / 9 / 116
Goodness-of-fit on F <sup>2</sup>	0.919
Final R indices [I > 2σ(I)]	R1 = 0.0246, wR2 = 0.0569
R indices (all data)	R1 = 0.0333, wR2 = 0.0590
Extinction coefficient	None
Largest diff. peak and hole	0.488 and -0.630 e.Å <sup>-3</sup>

Bond lengths [Å] and angles [°] for **22**

C(1)-N(1)	1.343(3)	N(1)-C(4)-H(4)	119.4
C(1)-C(2)	1.394(3)	C(3)-C(4)-H(4)	119.4
C(1)-H(1)	0.94(2)	C(2)-C(5)-H(5A)	109.5
C(2)-N(2)	1.343(3)	C(2)-C(5)-H(5B)	109.5
C(2)-C(5)	1.503(3)	H(5A)-C(5)-H(5B)	109.5
C(3)-N(2)	1.336(3)	C(2)-C(5)-H(5C)	109.5
C(3)-C(4)	1.386(3)	H(5A)-C(5)-H(5C)	109.5
C(3)-H(3)	0.95(2)	H(5B)-C(5)-H(5C)	109.5
C(4)-N(1)	1.338(3)	C(4)-N(1)-C(1)	116.78(18)
C(4)-H(4)	0.93(2)	C(4)-N(1)-Fe(1)	121.19(14)
C(5)-H(5A)	0.9800	C(1)-N(1)-Fe(1)	121.56(13)
C(5)-H(5B)	0.9800	C(3)-N(2)-C(2)	117.20(18)
C(5)-H(5C)	0.9800	Fe(1)-O(1)-H(1A)	119(2)
N(1)-Fe(1)	2.2312(18)	Fe(1)-O(1)-H(1B)	126(2)
O(1)-Fe(1)	2.1056(15)	H(1A)-O(1)-H(1B)	106(3)
O(1)-H(1A)	0.78(2)	Fe(1)-O(2)-H(2A)	126(2)
O(1)-H(1B)	0.79(2)	Fe(1)-O(2)-H(2B)	122(2)
O(2)-Fe(1)	2.1024(15)	H(2A)-O(2)-H(2B)	106(2)
O(2)-H(2A)	0.80(2)	O(2)#1-Fe(1)-O(2)	180.0
O(2)-H(2B)	0.79(2)	O(2)#1-Fe(1)-O(1)	90.23(7)
Fe(1)-O(2)#1	2.1023(15)	O(2)-Fe(1)-O(1)	89.77(7)
Fe(1)-O(1)#1	2.1056(16)	O(2)#1-Fe(1)-O(1)#1	89.77(7)
Fe(1)-N(1)#1	2.2313(18)	O(2)-Fe(1)-O(1)#1	90.23(7)
		O(1)-Fe(1)-O(1)#1	180.0
N(1)-C(1)-C(2)	122.26(19)	O(2)#1-Fe(1)-N(1)	91.67(6)
N(1)-C(1)-H(1)	118.9	O(2)-Fe(1)-N(1)	88.33(6)
C(2)-C(1)-H(1)	118.9	O(1)-Fe(1)-N(1)	88.12(6)
N(2)-C(2)-C(1)	120.37(19)	O(1)#1-Fe(1)-N(1)	91.88(6)
N(2)-C(2)-C(5)	118.0(2)	O(2)#1-Fe(1)-N(1)#1	88.33(6)
C(1)-C(2)-C(5)	121.7(2)	O(2)-Fe(1)-N(1)#1	91.67(6)
N(2)-C(3)-C(4)	122.25(19)	O(1)-Fe(1)-N(1)#1	91.88(6)
N(2)-C(3)-H(3)	118.9	O(1)#1-Fe(1)-N(1)#1	88.12(6)
C(4)-C(3)-H(3)	118.9	N(1)-Fe(1)-N(1)#1	180.0
N(1)-C(4)-C(3)	121.11(19)		

### 6.6.7 Data for 23



Following a modified literature method,<sup>134</sup> FeBr<sub>3</sub> (500 mg, 3.38 mmol) was added to 4-methylpyrimidine (10 ml) and stirred for 30 mins, the solution was filtered and layered with acetone producing complex [Fe(II)(pyrimidine)<sub>4</sub>(CH<sub>3</sub>)<sub>2</sub>(Br<sub>2</sub>)] after evaporation at RT blue crystals were isolated in 5 days, and mounted on a glass fibre using perfluoropolyether oil.

Crystal data and structure refinement for **23**

Identification code	shelx
Empirical formula	C <sub>24</sub> H <sub>28</sub> Br <sub>2</sub> FeN <sub>4</sub>
Formula weight	588.17
Temperature	150(2) K
Wavelength	0.71073 Å
Crystal system	Monoclinic
Space group	I 2/m
Unit cell dimensions	
a =	10.9709(13) Å
b =	9.7769(8) Å
c =	10.8286(12) Å
α =	90°
β =	90°.434(9)°
γ =	90°
Volume	1161.5(2) Å <sup>3</sup>
Z	2
Density (calculated)	1.682 Mg/m <sup>3</sup>
Absorption coefficient	4.109 mm <sup>-1</sup>
F(000)	592
Crystal size	0.250 × 0.150 × 0.150 mm <sup>3</sup>
Theta range for data collection	2.633 to 29.285°
Index ranges	-12 ≤ h ≤ 15, -13 ≤ k ≤ 12, -14 ≤ l ≤ 14
Reflections collected	4279
Independent reflections	1642 [R(int) = 0.0510]
Completeness to theta =	25.242° 99.2 %
Refinement method	Full-matrix least-squares on F <sup>2</sup>
Data / restraints / parameters	1642 / 0 / 96
Goodness-of-fit on F <sup>2</sup>	1.000
Final R indices [ >2sigma(I)]	R1 = 0.0726, wR2 = 0.2163
R indices (all data)	R1 = 0.0998, wR2 = 0.2394
Extinction coefficient	none
Largest diff. peak and hole	1.377 and -1.255 e.Å <sup>-3</sup>

## Bond lengths [Å] and angles [°] for 23

C(1A)-N(1)	1.319(17)	C(3)-C(2A)-C(1A)	120.3(14)
C(1A)-C(2A)	1.39(2)	C(3)-C(2A)-H(2A)	119.8
C(1A)-H(1A)	0.9500	C(1A)-C(2A)-H(2A)	119.8
C(2A)-C(3)	1.324(16)	C(2B)-C(1B)-N(1)	126.3(15)
C(2A)-H(2A)	0.9500	C(2B)-C(1B)-H(1B)	116.8
C(1B)-C(2B)	1.33(2)	N(1)-C(1B)-H(1B)	116.8
C(1B)-N(1)	1.343(17)	C(1B)-C(2B)-C(3)	117.1(13)
C(1B)-H(1B)	0.9500	C(1B)-C(2B)-H(2B)	121.5
C(2B)-C(3)	1.352(15)	C(3)-C(2B)-H(2B)	121.5
C(2B)-H(2B)	0.9500	C(2A)#1-C(3)-C(2A)	108.8(14)
C(3)-C(2A)#1	1.324(16)	C(2B)-C(3)-C(2B)#	1112.9(14)
C(3)-C(2B)#1	1.352(16)	C(2A)#1-C(3)-C(4)	121.4(8)
C(3)-C(4)	1.514(12)	C(2A)-C(3)-C(4)	121.4(8)
C(4)-H(4A)	0.9800	C(2B)-C(3)-C(4)	119.1(7)
C(4)-H(4B)	0.9800	C(2B)#1-C(3)-C(4)	119.1(7)
C(4)-H(4C)	0.9800	C(3)-C(4)-H(4A)	109.5
C(5A)-N(2)	1.315(14)	C(3)-C(4)-H(4B)	109.5
C(5A)-C(6A)	1.369(16)	H(4A)-C(4)-H(4B)	109.5
C(5A)-C(5A)#1	2.00(3)	C(3)-C(4)-H(4C)	109.5
C(5A)-H(5A)	0.9500	H(4A)-C(4)-H(4C)	109.5
C(6A)-C(7)	1.345(13)	H(4B)-C(4)-H(4C)	109.5
C(6A)-H(6A)	0.9500	N(2)-C(5A)-C(6A)	123.7(12)
C(5B)-N(2)	1.350(14)	N(2)-C(5A)-C(5A)#	140.4(6)
C(5B)-C(6B)	1.354(16)	C(6A)-C(5A)-C(5A)#	192.0(8)
C(5B)-H(5B)	0.9500	N(2)-C(5A)-H(5A)	118.1
C(6B)-C(7)	1.324(12)	C(6A)-C(5A)-H(5A)	118.1
C(6B)-H(6B)	0.9500	C(5A)#1-C(5A)-H(5A)	140.4
C(7)-C(6B)#1	1.324(12)	C(7)-C(6A)-C(5A)	118.5(11)
C(7)-C(6A)#1	1.345(13)	C(7)-C(6A)-H(6A)	120.7
C(7)-C(8)	1.496(10)	C(5A)-C(6A)-H(6A)	120.7
C(8)-H(8A)	0.9800	N(2)-C(5B)-C(6B)	125.0(12)
C(8)-H(8B)	0.9800	N(2)-C(5B)-H(5B)	117.5
C(8)-H(8C)	0.9800	C(6B)-C(5B)-H(5B)	117.5
Br(1)-Fe(1)	2.5694(11)	C(7)-C(6B)-H(6B)	121.2
Fe(1)-N(2)	2.265(6)	C(5B)-C(6B)-H(6B)	121.2
Fe(1)-N(2)#2	2.265(6)	C(6B)#1-C(7)-C(6B)	106.3(11)
Fe(1)-N(1)	2.286(7)	C(6A)#1-C(7)-C(6A)	102.3(12)
Fe(1)-N(1)#2	2.286(7)	C(6B)#1-C(7)-C(8)	118.4(6)
Fe(1)-Br(1)#2	2.5694(11)	C(6B)-C(7)-C(8)	118.4(6)
N(1)-C(1A)#1	1.319(17)	C(6A)#1-C(7)-C(8)	121.0(6)
N(1)-C(1B)#1	1.343(17)	C(6A)-C(7)-C(8)	121.0(6)
N(2)-C(5A)#1	1.315(14)	N(2)-Fe(1)-N(2)#	2180.0
N(2)-C(5B)#1	1.350(14)	N(2)-Fe(1)-N(1)	90.2(2)
		N(2)#2-Fe(1)-N(1)	89.8(2)
C(6A)#1-C(7)-C(8)	121.0(6)	N(2)-Fe(1)-N(1)#	289.8(2)
C(6A)-C(7)-C(8)	121.0(6)	N(2)#2-Fe(1)-N(1)#	290.2(2)
C(7)-C(8)-H(8A)	109.5	N(1)-Fe(1)-N(1)#	2180.0
H(8A)-C(8)-H(8C)	109.5	C(7)-C(8)-H(8A)	109.5
H(8B)-C(8)-H(8C)	109.5	C(7)-C(8)-H(8B)	109.5

Bond angles [°] for <b>23</b>	
N(1)-Fe(1)-N(1)#2	180.0
N(2)-Fe(1)-Br(1)	90.0
N(2)#2-Fe(1)-Br(1)	90.0
N(1)-Fe(1)-Br(1)	90.0
N(1)#2-Fe(1)-Br(1)	90.0
N(2)-Fe(1)-Br(1)#2	90.0
N(2)#2-Fe(1)-Br(1)#2	90.0
N(1)-Fe(1)-Br(1)#2	90.0
N(1)#2-Fe(1)-Br(1)#2	90.0
Br(1)-Fe(1)-Br(1)#2	180.0
C(1A)#1-N(1)-C(1A)	104.8(14)
C(1B)#1-N(1)-C(1B)	105.0(14)
C(1A)#1-N(1)-Fe(1)	121.3(8)
C(1A)-N(1)-Fe(1)	121.3(8)
C(1B)#1-N(1)-Fe(1)	123.7(7)
C(1B)-N(1)-Fe(1)	123.7(7)
C(5A)#1-N(2)-C(5A)	99.1(12)
C(5B)-N(2)-C(5B)#1	99.6(12)
C(5A)#1-N(2)-Fe(1)	122.3(6)
C(5A)-N(2)-Fe(1)	122.3(6)
C(5B)-N(2)-Fe(1)	122.3(6)

## References

- (1) Mewis, R. E.; Archibald, S. J. *Coord. Chem. Rev.* **2010**, 254, 1686.
- (2) Polikarpov, Y. M.; Bodrin, G. V. *Zh. Neorg. Khim.* **1980**, 25, 2355.
- (3) Plutnar, J.; Havlickova, J.; Kotek, J.; Hermann, P.; Lukes, I. *New J. Chem.* **008**, 32, 496.
- (4) Martell, A. E.; *Coord. Chem. A Century of Progress*; 1994; Vol. 565, p 240.
- (5) Ryan Edward Mewis; university of Hull: 2009, university of Hull.
- (6) Major, J. L.; Boiteau, R. M.; Meade, T. J. *Inorg. Chem.* **2008**, 47, 10788.
- (7) Dhingra, K.; Maier, M. E.; Logothetis, N. K. *Chem. Commun.* **2008**, 3444.
- (8) Li, W.S.; Luo, J.; Jiang, F.; Chen, Z. *N. Dalton Trans.* **2012**, 41, 9405.
- (9) Willmann, J. K.; Gambhir, S. S. *Nat. Rev. Drug Discov.* **2008**, 7, 591.
- (10) <http://www.magnetic-resonance-imaging/3t-mri-scanner/magnetom-skyra>.
- (11) Aime, S.; Botta, M.; Terreno, E. *ADV. Inorg. Chem. Vol 57* **2005**, 57, 173.
- (12) Verwilt, P.; Park, S.; Yoon, B.; Kim, J. S. *Chem. Soc. Rev.* **2015**, 44, 1791.
- (13) Costa, J.; Toth, E.; Helm, L.; Merbach, A. E. *Inorg. Chem.* **2005**, 44, 4747.
- (14) Brown, M. A. S., R. C. *MRI Basic Principles and Applications*; John Wiley & Sons, 2003.
- (15) Sharma, H. A. *Acta Neuropsychiatrica* **2009**, 21, 200.
- (16) Westbrook, C. K., C. *MRI In Practice*; Blackwell Publishing: Blackwell Publishing, 1998.
- (17) Brown, M. A. S., R. C. *MRI Basic Principles and Applications*; **2003**.
- (18) Hall, J.; Haner, R.; Aime, S.; Faulkner, S.; Parker, D.; *New J. Chem.* **1998**, 22, 627.
- (19) Que, E. L.; Chang, C. J. *Chem. Soc. Rev.* **2010**, 39, 51.
- (20) Accardo, A.; Barnert, S.; Schubert, R.; Morelli, G. *Chem. Mater.* **2013**, 1, 617.
- (21) Semelka, R. C.; Hernandez, M.; Castillo, M. *Mater. Res. IM.* **2013**, 31, 96.
- (22) Zhou, Z.; Lu, W.I.R.E.s. *Nanomedicine and Nanobiotechnology.* **2013**, 5, 1.
- (23) Huber, M.; Jorge, M.; Pecara, E. *Mol. Biol. of the Cell* **1998**, 9, 220A.
- (24) van Tilborg, G. A. F.; Strijkers, G. J. *Bioconjug. Chem.* **2006**, 17, 865.
- (25) Corot, C.; Idee, J. M.; B.; Meyer, D. *J. Magn. Reson.* **1998**, 8, 695.
- (26) Morcos, S. K. *Eur. J. Radiol.* **2008**, 66, 175.
- (27) Balogh, E.; Tripiet, R.; Ruloff, R.; Toth, E. *Dalton Trans.* **2005**, 1058.
- (28) Marckmann, P.; Skov, L.; M. B.; Thomsen, H. S. *J. Am. Soc. Nephrol.* **2006**, 17, 2359.
- (29) Tung, C.-H.; Quinti, L.; Jaffer, F. A.; Weissleder, R. *Mol. Pharm.* **2005**, 2, 92.
- (30) Gross, S.; Piwnica, Worms, D. *Cancer Cell* **2005**, 7, 5.
- (31) Caravan, P.; Parigi, G.; S. A.; Spiller, M.; McMurry, T. J. *Inorg. Chem.* **2007**, 46, 6632.
- (32) Elmore, S. P.; Nishimura, Y.; Lemasters, J. *Arch. Biochem. Biophys.* **2004**, 422, 145.
- (33) Scaduto, R. C.; Grotjohann, L. W. *Biophys. J.* **1999**, 76, 469.
- (34) Bunzli, J. C. G.; Pigué, C. *Chem. Soc. Rev.* **2005**, 34, 1048.
- (35) Gunnlaugsson, T. *Abstr. Pap. Am. Chem. Soc.* **2005**, 230, U3011.
- (36) Gunnlaugsson, T.; Leonard, J. P. *Chem. Commun.* **2005**, 3114.
- (37) Faulkner, S.; Pope, S. J. A.; Burton Pye, B. P. *Appl. Spectrosc. Rev.* **2005**, 40, 1.
- (38) Beeby, A.; Bushby, L. M.; Williams, J. A. G. *J. Chem. Soc., Dalton Trans.* **2002**, 48.
- (39) Clayden, J. G. N. W. S. G. *Org. Chem.*; Oxford University Press: Oxford; New York, **2012**.
- (40) Yam, V. W.-W.; Wong, K. M. C. *Chem. Commun.* **2011**, 47, 11579.
- (41) Zhao, J.; Ji, S.; Wu, W.; Wu, W.; Huang, L. *RSC Adv.* **2012**, 2, 1712.
- (42) Kennedy, F.; Koullourou, T.; J. C.; Faulkner, S.; Ward, M. D. *Dalton Trans.* **2007**, 1492.
- (43) Pope, S. J. A.; Coe, B. J.; Faulkner, S. *Chem. Commun.* **2004**, 1550.
- (44) Perry, W. S.; Pope, S. J. A.; Faulkner, S. *Dalton Trans.* **2010**, 39, 10974.
- (45) Wadsak, W.; Mitterhauser, M. *Eur. J. Radiol.* **2010**, 73, 461.
- (46) Volkert, W. A.; Hoffman, T. J. *Chem. Rev.* **1999**, 99, 2269.
- (47) Jamous, M.; Haberkorn, U.; Mier, W. *Molecules* **2013**, 18, 3379.
- (48) Sasaki, K.; Sugou, K.; Tsubouchi, S.; Kuroda, Y. *Org. Biomol. Chem.* **2004**, 2, 2852.
- (49) Segura, J. L.; Gomez, R.; Martin, N.; Guldi, D. M. *Org. Lett.* **2001**, 3, 2645.
- (50) Karlin, K. D.; Kaderli, S.; Zuberbuhler, A. D. *J. Am. Chem. Soc.* **1994**, 116, 1324.
- (51) Sparke, A. E.; Mewis, R. E.; Archibald, S. J. *Tetrahedron Lett.* **2010**, 51, 4723.

- (52) Schiess, R.; Gertsch, J.; Schweizer, W. B.; Altmann, K.H. *Org. Lett.* **2011**, *13*, 1436.
- (53) Mendonca, G. F.; Bastos, A. R.; Boltz, M.; *Appl. Catal. A. Applied* . **2013**, *460*, 46.
- (54) Juenge, E. C.; Beal, D. A.; Duncan, W. P. *J. Org. Chem.* **1970**, *35*, 719.
- (55) Rohovec, J.; Gyepes, R.; Cisarova, I.; Lukes, I. *Tetrahedron Lett.* **2000**, *41*, 1249.
- (56) Weisman, G. R.; Ho, S. C. H.; Johnson, V. *Tetrahedron Lett.* **1980**, *21*, 335.
- (57) Sparke, A. E. 'PhD thesis', University of Hull, 2008.
- (58) Fisher, C. M. 'PhD thesis', University of Hull, 2005.
- (59) Jagadish, B.; Brickert, A., E. A.; Raghunand, N. *Tetrahedron Lett.* **2011**, *52*, 2058.
- (60) Bianchi, A.; Micheloni, M.; Paoletti, P. *Coord. Chem. Rev.* **1991**, *110*, 17.
- (61) Monfort, M.; Resino, I.; M.; Stoeckli-Evans, H. *New J. Chem.* **2002**, *26*, 1601.
- (62) Fisher, C. M.; Burke, B. P.; Faulkner, S.; Archibald, S. J. *Dalton Trans.* **2014**, *43*, 9567.
- (63) Burke, B. 'PhD thesis, University of Hull, 2013.
- (64) Avila-Flores, R.; Medellin, R. A. *J. Mammal.* **2004**, *85*, 675.
- (65) Kim, H.; Gao, J.; Burgess, D. J. *Int. J. Pharm.* **2009**, *377*, 105.
- (66) Jiang, W.; Lumata, L.; Chen, W.; Zhang, S.; Khemtong, C. *Sci. Rep.* **2015**, *5*.
- (67) Kenwright, A. M.; Parker, D.; Pandya, S. U.; Smith, D. G. *Chem. Commun.* **2008**, 2514.
- (68) Lippert, B.; Gupta, D. *Dalton Trans.* **2009**, 4619.
- (69) Arranz-Mascaros, P.; Lopez-Leon, M. D.; Stoeckli-Evans, H. *Polym.* **2008**, *27*, 623.
- (70) Sorensen, T. J.; Kenwright, A. M.; Faulkner, S. *Chem. Sci.* **2015**, *6*, 2054.
- (71) Ammar, R. A.; Nafady, A.; Amin, M. F.; *Int. J. Electrochem. Sci.* **2013**, *8*, 1501.
- (72) Crutchley, R. J.; Kress, N.; Lever, A. B. P. *J. Am. Chem. Soc.* **1983**, *105*, 1170.
- (73) Barlin, G. B. *Aust. J. Chem.* **1982**, *35*, 2299.
- (74) Koullourou, T.; Natrajan, L. S.; Faulkner, S. *J. Am. Chem. Soc.* **2008**, *130*, 2178.
- (75) Heralut, D.; Aelvoet, K.; Blatch, A. J.; Whiting, A. *J. Org. Chem.* **2007**, *72*, 71.
- (76) Raban, M.; Chang, H.; Craine, L.; Hortelano, E. *J. Org. Chem.* **1985**, *50*, 2205.
- (77) Tilney, J. A.; Sorensen, T. J.; Faulkner, S. *Dalton Trans.* **2011**, *40*, 12063.
- (78) Charbonniere, L. J.; Faulkner, S.; Platas-Iglesias, C.; M. *Dalton Trans.* **2013**, *42*, 3667.
- (79) Gempf, K. L.; Butler, S. J.; Funk, A. M.; Parker, D. *Chem. Commun.* **2013**, *49*, 9104.
- (80) Rohrer, M.; Bauer, H.; Mintonovitch, J.; Requardt, M.; *Invest. Radiol.* **2005**, *40*, 715.
- (81) Zhao, J.; Huang, X.; Jin, P.; Chen, Z. *Coord. Chem. Rev.* **2015**, *289*, 315.
- (82) Sim, N.; Gottschalk, S.; Pal, R.; Engelmann, J.; *A. Chem. Sci.* **2013**, *4*, 3148.
- (83) Mishra, A.; Mishra, R.; Gottschalk, S.; *ACS Chem. Neurosci.* **2014**, *5*, 128.
- (84) Gong, T.; Zhang, X.; Bai, T.; Zhang, Q.; Zhang, L. *Ind. Eng. Chem. Res.* **2012**, *51*, 13589.
- (85) Jang, J. H.; Bhuniya, S.; Kang, J.; Yeom, A.; Hong, J. S. *Org. Lett.* **2013**, *15*, 4702.
- (86) Zhang, X.; Jing, X.; Liu, T.; Han, G.; Li, H.; Duan, C. *Inorg. Chem.* **2012**, *51*, 2325.
- (87) Lazarides, T.; Sykes, D.; Faulkner, S.; Barbieri, A.; *Chem. Eur. J.* **2008**, *14*, 9389.
- (88) Dehaen, G.; Eliseeva, S. V.; Kimpe, K.; Laurent, S.; *Chem. Eur. J.* **2012**, *18*, 293.
- (89) Boulay, A.; Laine, S.; Leygue, N.; Picard, C. *Tetrahedron Lett.* **2013**, *54*, 5395.
- (90) Dehaen, G.; Verwilst, P.; De Parac-Vogt, T. N. *Inorg. Chem.* **2011**, *50*, 10005.
- (91) Lipani, E.; Laurent, S.; Surin, M.; Muller, R. N. *Langmuir* **2013**, *29*, 3419.
- (92) Faulkner, S.; Natrajan, L. S.; Perry, W. S.; Sykes, D. *Dalton Trans.* **2009**, 3890.
- (93) Hill, L. R.; Blackburn, O. A.; Faulkner, S. *Dalton Trans.* **2013**, *42*, 16255.
- (94) Havas, F.; Leygue, N.; Danel, M.; Picard, C. *Tetrahedron Lett.* **2009**, *65*, 7673.
- (95) Yi, X.; Zhao, J.; Sun, J.; Guo, S.; Zhang, H. *Dalton Trans.* **2013**, *42*, 2062.
- (96) Pope, S. J. A.; Coe, B. J.; Faulkner, S.; Douglas, K. T. *J. Am. Chem. Soc.* **2004**, *126*, 9490.
- (97) Bronner, C.; Wenger, O. S. *Inorg. Chem.* **2012**, *51*, 8275.
- (98) Kurz, P.; Probst, B.; Spingler, B.; Alberto, R. *Eur. J. Inorg. Chem.* **2006**, 2966.
- (99) Cattaneo, M.; Fagalde, F.; Borsarelli, C. D.; Katz, N. E. *Inorg. Chem.* **2009**, *48*, 3012.
- (100) Pfennig, B. W.; Chen, P. Y.; Meyer, T. J. *Inorg. Chem.* **1996**, *35*, 2898.
- (101) Guilhem, J.; Pascard, C.; Lehn, J. M.; Ziessel, R. *J. Chem. Soc., Dalton Trans.* **1989**, 1449.
- (102) Costa, I.; Montalti, M.; Pallavicini, P.; Zaccheroni, J. *Organomet. Chem.* **2000**, *593*, 267.

- (103) Smieja, J. M.; Kubiak, C. P. *Inorganic Chemistry* **2010**, *49*, 9283.
- (104) Gibson, D. H.; Sleadd, B. A.; Vij, A. *Journal of Chemical Crystallography* **1999**, *29*, 619.
- (105) Liddle, B. J.; Lindeman, S. V.; Reger, D. L.; Gardinier, J. R. *Inorg. Chem.* **2007**, *46*, 8484.
- (106) Tropiano, M.; Record, C. J.; Faulkner, S. *J. Organomet. Chem.* **2012**, *31*, 5673.
- (107) Burton-Pye, B. P.; Heath, S. L.; Faulkner, S. *Dalton Trans.* **2005**, 146.
- (108) Koshitani, J.; Hassen, W.; Rawashdeh, O. M. A. *Abst. Pap. Am. Chem. Soc.* **2014**, 248.
- (109) Ho, K.; Kane, M. H.; Lairson, B. M.; Kim, Y. K. *Trans. Magn.* **1997**, *33*, 2538.
- (110) Manoli, M.; Collins, A.; Parsons, S.; Brechin, E. K. *J. Am. Chem. Soc.* **2008**, *130*, 11129.
- (111) Inglis, R.; Katsenis, A. D.; Brechin, E. K. *Cryst. Eng. Comm.* **2010**, *12*, 2064.
- (112) Pedersen, K. S.; Bendix, J.; Clerac, R. *Chem. Commun.* **2014**, *50*, 4396.
- (113) Wernsdorfer, W.; Aliaga-Alcalde, N.; Christou, G. *Nat.* **2002**, *416*, 406.
- (114) Inglis, R.; Brechin, E. K.; Papaefstathiou, G. S. *Chem. Commun.* **2011**, *47*, 3090.
- (115) Kotzabasaki, V.; Inglis, R.; Brechin, E. K.; Milios, C. J. *Dalton Trans.* **2011**, *40*, 1693.
- (116) Birnara, C.; Kessler, V. G.; Papaefstathiou, G. S. *Polym.* **2009**, *28*, 3291.
- (117) Datta, S.; Bolin, E.; Inglis, R.; Milios, C. J.; Brechin, E. K.; Hill, S. *Polym.* **2009**, *28*, 1788.
- (118) Inglis, R.; Milios, C. J.; Jones, L. F.; Brechin, E. K. *Chem. Commun.* **2012**, *48*, 181.
- (119) Inglis, R.; Taylor, S. M.; Jones, L. F.; Brechin, E. K. *Dalton Trans.* **2009**, 9157.
- (120) Kozoni, C.; Brechin, E. K.; Milios, C. J. *Dalton Trans.* **2010**, *39*, 7943.
- (121) Kozoni, C.; Siczek, M.; Lis, T.; Brechin, E. K.; Milios, C. J. *Dalton Trans.* **2009**, 9117.
- (122) Singh, B.; Long, J. R.; de Biani, F. F.; Stavropoulos, P. *J. Am. Chem. Soc.* **1997**, *119*, 7030.
- (123) Long, G. J.; Clarke, P. J. *Inorg. Chem.* **1978**, *17*, 1394.
- (124) Hoser, A.; Pietrzak, J.; Glowiak, T. *Acta. Cryst. Commun.* **1983**, *39*, 1039.
- (125) Gass, I. A.; Milios, C. J.; M.; Perlepes, S. P.; Brechin, E. K. *Dalton Trans.* **2008**, 2043.
- (126) Vecchini, C.; M.; Gass, I. A.; Brechin, E. K.; Moze, O. *Phys. Rev. B* **2008**, *77*.
- (127) Little, B. F.; Long, G. J. *Inorg. Chem.* **1978**, *17*, 3401.
- (128) Takeda, M.; Tominaga, T.; Saito, N. *J. Inorg. Nucl. Chem.* **1974**, *36*, 2459.
- (129) Merrithew, P.; Rasmussen, P.; Vincent, D. H. *Inorg. Chem.* **1971**, *10*, 1401.
- (130) Reiff, W. M.; Long, G. J.; Little, B. F. *Inorg. Nucl. Chem. Lett.* **1976**, *12*, 405.
- (131) Gerloch, M.; McMeeking, R. F.; White, A. M. *J. Chem. Soc., Dalton Trans.* **1976**, 655.
- (132) Koullourou, T.; Natrajan, L. S.; Faulkner, S. *J. Am. Chem. Soc.* **2008**, *130*, 2178.
- (133) Bradley, D.; Williams, G.; Lawton, M. *J. Org. Chem.* **2010**, *75*, 8351.
- (134) Gass, I. A.; Milios, C. J.; Collison, D.; Parsons, S.; Brechin, E. K. *Polym.* **2007**, *26*, 1835.